HELICOBACTER PYLORI BOTH ACTIVATES AND SUPPRESSES INNATE IMMUNE NUCLEIC ACID SENSORS

By

Samuel Douglas Reiff Dooyema

Dissertation
Submitted to the Faculty of the
Graduate School of Vanderbilt University
in partial fulfillment of the requirements
for the degree of

DOCTOR OF PHILOSOPHY
in
Microbe-Host Interactions
May 13th, 2022
Nashville, Tennessee

Approved:

James E. Cassat, M.D., Ph.D.

Manuel Ascano, Jr., Ph.D.

Maria Hadjifrangiskou, Ph.D.

Eric P. Skaar, Ph.D., M.P.H

Richard M. Peek Jr., M.D.

In loving memory of Hannah Violet Dooyema and Dewey Dooyema

and

To my dear wife Jackie,

Who accompanied me every step of the way

With her never ceasing love and encouragement.

ACKNOWLEDGEMENTS

When the inevitable small-talk question arises of “what do you do?” I would often instinctively answer “graduate student.” To an unknowing audience, they likely picture a grown adult sitting in a lecture hall or pouring over books in a library. We are lifelong learners after all. However, this depiction is not of course entirely accurate, and understates the hard work we all put in as students in our fields. The response of “I am pursing a Ph.D.” more appropriately embodies the long journey to degree completion. Like anything in life worth experiencing, this journey is more than just a task to be completed but full of experiences and people that make it worthwhile. It’s the people past and present that have helped make this thesis a reality.

First, I would like to thank my mentor Dr. Rick Peek. He graciously welcomed me into his laboratory and always allowed me freedom to pursue both my scientific and professional interests. Rick has always been patient with me, while demanding me to “keep moving forward”. I am thankful to have a caring and understanding mentor during the hardest moments of this journey. Thanks “boss.”

To my colleagues in the Peek Laboratory, I cannot thank you enough for your friendship, kindness, generosity, experimental instruction, thoughtful questions, and valuable suggestions over the years. Uma Krishna, thank you for adopting me as your third son. I will cherish the laughs and deep conversations we shared in our little lab bay. Lydia Wroblewski, thank you for providing much needed liveliness in the post-COVID lab normal and for putting up with my countless organoid questions. I am grateful for the experimental skills I learned from you, but will more importantly, our time shared as lab neighbors that made coming to work fun. Jenny Noto, thank you for your scrupulous attention to detail in all aspects of life. My work was much more

comprehensive and precise because of your questions, editing, and proofreading. I always enjoyed our early evening conversations catching up when everyone else had gone home. Giovanni Suarez, your scientific advice, worth ethic, are a huge reason why I've been able to earn this degree. You always challenged me with hard questions and your technical expertise is unrivaled. I couldn't have done it without you. I thank Judy Romero for the laughs we shared and her extraordinary expert animal skills that made my infection models possible. I would also like to acknowledge Dawn Israel and my former student Julia An for all their help and support in completing this work. Thus, to all the Peek Laboratory members past and present, thank you for being colleagues that made going to the lab enjoyable. Even more so, a special thank you for caring for me and my family in the lowest moments. I am so thankful to call you as friends as well.

I want to acknowledge all the people outside of our laboratory that made this work possible as well. A special thank you to Blanca Piazuelo for scoring what likely seemed like never-ending histology slides. Without her and Alberto Delgado's diligent work, these studies would not be as compelling. A sincere thank you to Tim Cover and his laboratory, namely John Loh, and Sai Lin, for collaborating on two different projects. I thank my thesis committee as well, Dr. Jim Cassat, Dr. Manny Ascano, Dr. Maria Hadjifrangiskou, and Dr. Eric Skaar. I sincerely appreciate their flexibility and understanding of personal hardships. They challenged me scientifically by asking tough questions and demanding thorough answers. I am very appreciative to the growth I experienced under their tutelage. Their expertise and advice were invaluable to my studies. Finally, a thank you for my funding sources. During my training I was supported by NIH grants T32AI112541-02, R01CA077955-21, and P30DK058404.

Prior to my time at Vanderbilt, I honed my scientific chops as a research technician at Sanford Research in Sioux Falls, South Dakota. I am forever thankful for that job and the

friendships I cultivated. The skills and relationships gained there have served me well in graduate school and many techniques performed in this work were first mastered at Sanford. I especially want to thank my OG mentor Dr. Haotian Zhao for his patience in training me, and his sincere and honest advice. Thank you for your constant reminders to slow down and think before I perform my experiments; it's a skill I'm still perfecting. Also thank you to Dr. Jill Weimer for her instruction and support in my pursuit of a Ph.D. Thank you for encouraging me to reach higher and never settle. Similarly, to my USF mentor Dr. Cliff Lewis, thank you for challenging me to apply to the best schools in the country like Vanderbilt, and believing that I could succeed there.

The nature of laboratory benchwork (especially in a COVID-ruled world) can be very isolating. To remedy this throughout my graduate career, as well as maintain my sanity, I will be forever grateful to a multitude of family and friends. These people provided love, encouragement, support, and prayers. They also provided welcome distractions, listening ears, professional advice, and everything in between. This thesis couldn't have been completed without you.

Thank you to Ben and Mackenzie Coleman, Mike Doyle, Clare Laut, Kevin Kramer, Ariana von Lersner, Nate Klopfenstein, and all my other friends with whom I've shared so many memories. Thanks for indulging this diehard football fan by attending so many tailgates and games, even when the play on the field meant you could've been, and we all should've been, elsewhere. Vanderbilt brought our hodgepodge group together from across the country to form lifelong friendships. I loved learning about where everyone was from and am excited about where the next stage of life will bring us so I can visit.

Vanderbilt has also provided me two instrumental people in developing my career goals in Kate Stuart and Ashley Brady through their tireless work with the ASPIRE program in the BRET office. Thank you for introducing me to so many career options, cultivating my non-scientific

skills, and growing my professional network. I am indebted to you for your advice and support to navigate the post-graduation workforce. Thank you for listening to my dreams, my career aspirations, and personal needs. I am thankful for your work but also for your friendship.

Off West End, my church family at The Gospel Church was instrumental to completing this work. These brothers and sisters in Christ, quickly became more than friends, they became family 1,000 miles away from my own family. Thank you to Jason and Ondee Whitman, Ty and Suzette Laws, and Laura Katherine Wood who graciously opened their homes and quickly adopted my wife and I when we first sought a church home. I will forever cherish our Thursday night dinners and passionate discussions. Your prayers and support as I slogged through the doldrums of a Ph.D. were just what I needed at the time. I need to especially thank Phil and Susan Perdue, Trey and Carly Powell, Colleen and David Gensheimer, George and Sara Lin, Jackie and Will Pierce, Aaron Yang, and Mike Harder. Thank you for loving me and my family at our lowest and darkest moments. We could not have experienced what we experienced without your love, prayers, wisdom, support, and sometimes simply, some much-needed food. I could write another dissertation on the impact these people had in my personal and spiritual life, but I will simply say again, thank you. Thank you for being the hands and feet of Jesus.

Thank you to my own wonderfully large family, my parents Doug and Pam, my dear eight siblings Andrew, Katie, Amanda, Kelsey, Eli, Naomi, Jeremiah, and Jed, my in-laws Brad, Jordan, and Jake, and all my nieces and nephews. I want to thank you for your constant love and prayers. Thank you for providing a goal to always see the end, and remembering that Earthly things are temporary, and faith and family are forever. Thank you to my in-laws Curt and Shelly, as well as Krista, Adam, and Mitch for welcoming me into your family from the start. I am thankful for your constant love, support, and prayers. Curt and Shelly, I especially thank you for not batting an eye

when I said I wanted to bring your daughter halfway across the country so I could pursue my dream of earning a Ph.D. In addition, your seemingly never-ending supply of canned goods and fresh-caught fish sustained the writing of the dissertation. I also want to thank my grandpa Dewey, one of my biggest champions and cheerleaders before his passing. Thank you for asking me so many questions which forced me to explain my work in a comprehensible manner. While it breaks my heart knowing how close you were to physically hold my diploma, just know, your grandson isn't "gonna be a doctor" anymore, he is one.

Finally, I cannot say thank you enough to my dear wife Jackie. I had put in my final graduate school application hours before our first date. Ten schools across the country, all greater than 500 miles away from home and you never once said I was crazy. You supported me from the very beginning and that's how I knew you'd be with me forever. When you brought me to Nashville to start this dream you simply reminded me "I wasn't meant to do it alone." This section says as much, but you deserve the most thanks of any one person. I love you so much and couldn't have done this without you. I am so grateful I got to come home to you when my experiments didn't work or after a long, arduous timepoint. You never ceasing love sustained me on the darkest days and cheered with me on the brightest days. You thanklessly ran our home when studying, writing, or experiments overwhelmed me. You motivated me, impressed me, surprised me, cared for me, laughed with me, cried with me, and cheered with me. We started this journey as young lovers and finished it as parents of two children. We walked through the indescribable loss of our baby girl Hannah, just when the end of this Ph.D. journey seemed tangible. That abrupt reminder that God's timing is not our own is a testament to his everlasting love and faithfulness. We made it this far with all the obstacles. "...Thanks be to God! He gives us the victory through our Lord Jesus Christ" (1 Cor. 15:57). Amen.

TABLE OF CONTENTS

LIST OF FIGURES

LIST OF TABLES

LIST OF ABBREVIATIONS

AIM2 ..... absent in melanoma 2
ANOVA ..... analysis of variance
AP ..... adaptor protein
APC ..... antigen presenting cell
ATP ..... adenosine triphosphate
BB ..... Brucella broth
BMDC ..... bone marrow-derived dendritic cells
BrdU ..... bromodeoxyuridine
cag ..... cytotoxin-associated gene
CD ..... Cluster of Differentiation
CEACAM ..... carcinoembryonic antigen-related cell adhesion molecule
cGAMP ..... cyclic GMP-AMP
cGAS ..... cyclic GMP-AMP synthase
CFU ..... colony forming units
Cox ..... cyclooxygenase
CpG ..... 5'-cytosine-phosphate-guanine-3'
CRE ..... cyclic-AMP response element
CREB ..... cyclic-AMP response element binding protein
CXCL ..... C-X-C motif chemokine ligand
DAI ..... DNA-dependent activator of IRFs
DC ..... dendritic cell
DE ..... differentially expressed
DMEM ..... Dulbecco's Modified Eagle Medium
DSS ..... dextran sodium sulfate
DUF ..... domain of unknown function
EBV ..... Epstein-Barr virus
ELISA ..... enzyme linked immunosorbent assay
ER ..... endoplasmic reticulum
ERK ..... extracellular regulated kinase
FBS ..... fetal bovine serum
GAPDH ..... glyceraldehyde-3-phosphate dehydrogenase
GM-CSF ..... granulocyte macrophage colony stimulating factor
HBP heptose-1,7-bisphosphate
HCMV ..... human cytomegalovirus
HEK ..... human embryonic kidney
HI ..... heat inactivated
Hop ..... *Helicobacter* outer membrane protein
HPF ..... high-power field
HPV ..... human papillomavirus
HSV ..... herpes simplex virus
IFI16 ..... interferon-inducible protein 16
IFN ..... interferon
IFNAR1 ..... interferon alpha/beta receptor 1
IκB ..... inhibitor of κB

IL ..... interleukin
IRAK ..... IL-1 receptor-associated kinase
IPA ..... Ingenuity Pathway Analysis
IP-10 ..... Interferon-γ Induced Protein 10
IRF ..... interferon regulatory factor
ISG ..... interferon stimulated gene
JAK ..... Janus kinase
JNK ..... c-Jun N-terminal kinase
KSHV ..... Kaposi's sarcoma-associated herpesvirus
LC3 ..... microtubule-associated protein 1A/1B-light chain 3
LGP2 ..... laboratory of genetics and physiology 2
LPS ..... lipopolysaccharide
LRO ..... lysosome related organelle
LRR ..... leucine rich repeat
MAPK ..... mitogen-activated protein kinase
MAVS ..... mitochondrial antiviral-signaling protein
MCL-1 ..... myeloid cell leukemia 1
MDA5 ..... melanoma differentiation-associated protein
MIP ..... macrophage inflammatory protein
MOI ..... multiplicity of infection
MyD88 ..... myeloid differentiation primary response protein
MPO ..... myeloperoxidase
mtDNA ..... mitochondrial DNA
NF-κB ..... nuclear factor-κB
NFAT ..... nuclear factor of activated T-cell
NLR ..... NOD-like receptor
NLRP ..... NOD-, LRR- and pyrin domain-containing protein
NOD ..... nucleotide-binding oligomerization domain
OD ..... optical density
OMP ..... outer membrane protein
PAI ..... pathogenicity island
PAMP ..... pathogen associated molecular pattern
PBS ..... phosphate buffered saline
PRR ..... pattern recognition receptor
PVDF ..... polyvinylidene difluoride
RIG-I ..... retinoic acid-inducible gene I
RIP-2 ..... receptor-interacting protein 2
RIPA ..... radio immunoprecipitation assay
RPMI ..... Royal Park Memorial Institute
SDS-PAGE ..... sodium dodecyl sulfate polyacrylamide gel electrophoresis
SEM ..... standard error of the mean
SHP-2 ..... Src homology phosphatase-2
SNP ..... single nucleotide polymorphism
STAT ..... signal transducer and activator of transcription
STING ..... stimulator of interferon genes
T3SS ..... type III secretion system

T4SS.....type IV secretion system
TAB.....TAK1 binding protein
TAK1 ..... transforming growth factor-activated kinase 1
TBK1.....TANK-binding kinase 1
TGF-β..... transforming growth factor β
Th ..... T helper
TIFA..... TRAF-interacting protein with FHA domain
TIR .....toll/IL-1 receptor
TLR .....toll-like receptor
TNF .....tumor necrosis factor
TRAF ..... TNF receptor associated factor
TSA .....tryptic soy agar
TRIF ..... TIR-domain-containing adapter-inducing interferon-β
TRIM.....tripartite motif-containing
TYK2 ..... tyrosine kinase 2
UI .....uninfected
VacA .....vacuolating cytotoxin A
WT ..... wild-type

CHAPTER I

INTRODUCTION

1.1. The discovery of *Helicobacter pylori*

The well characterized bacterium known today as *Helicobacter pylori* is relatively young by microbial standards. The discovery of *Escherichia coli* and *Staphylococcus aureus* dates back to the 1880s and 90s [1-4], whereas the genus *Helicobacter* came into existence just over 30 years ago [5]. In a sense, *H. pylori* is a 'Millennial' microbe compared to the 'Lost Generation' bacteria that predate the 20th century. Although its known history is more recent, *H. pylori* has been colonizing humans for thousands of years while silently avoiding detection. The earliest known reports date back to 1875 when German physicians identified spiral shaped bacteria in the linings of human stomachs [6]. However, their inability to culture the bacteria allowed *H. pylori* to be quickly forgotten and avoid human detection for nearly 25 more years. A Polish physician named Walery Jaworski in 1899 again observed spiral shaped bacteria in the residues from washed stomachs biopsies and named it *Vibrio rugula* [7]. While the new organism was deemed the causative agent of gastric diseases in his book entitled "Handbook of Gastric Diseases" [8], the observations went mostly unnoticed. It would be another four decades until spiral shaped bacteria were again observed and documented in the gastric mucosa of patients [9, 10]. In less than 15 years, these observations would be overshadowed by a large-scale study in 1954 that found no spiral shaped bacteria in over 1,000 gastric biopsy specimens displaying gastritis [11]. For much of the 20th century, because of this study, it was believed that the stomach is a sterile organ and that any observed bacteria were oral contaminants.

By the early 1980s though, a spiral shaped bacteria was identified once again in gastric tissue biopsies taken from patients with gastritis and duodenal ulcers by two Australian researchers Barry Marshall and Robin Warren, which they named *Campylobacter pyloridis* [12]. It would take an additional two years to successfully culture their new bacterium [13]. However, the field of gastroenterology remained skeptical of their discovery, hesitant to accept the concept that a bacterium alone could be the causative agent of ulcers and gastritis. Marshall even would recall, "It was a campaign, everyone was against me. But I knew I was right... And when I was criticized by gastroenterologists, I knew that they were mostly making their living doing endoscopies on ulcer patients... A few years from now you'll be saying, 'Hey! Where did all those endoscopies go to' And it will be because I was treating ulcers with antibiotics [14]." To definitively prove that *Campylobacter pyloridis* was the causative agent of gastritis and duodenal ulceration, Marshall consumed a culture of the isolated bacterium, and tracked his disease progression by serial endoscopy over the course of weeks [15]. He had established a baseline prior to his inoculation that his stomach was normal. His boss who performed the endoscopy remarked, "Barry, I'm not sure why you asked me to do this endoscopy, and I don't want you to tell me." [16] Within a few days he felt ill along with classical symptoms of gastritis, vomiting and bad breath. A follow-up endoscopy confirmed the presence of the spiral-shaped bacterium, demonstrating a healthy person could be infected. Marshall then treated his self-inflicted infection with antibiotics, as he had wisely tested *C. pyloridis's* response to antibiotics prior to his ingestion of it, and again monitored his progression as he returned to health [15]. By fulfilling Koch's postulates, Marshall and Warren proved beyond a doubt that their 'new' bacterium could colonize the gastric mucosa and induce disease [17]. This pivotal finding was corroborated by a subsequent study in 1988, which demonstrated that in a prospective double blind trial of duodenal ulcer relapse, 92% of patients

who were successfully cleared of *C. pyloridis* infection by antibiotic treatment showed signs of ulcer healing and only 21% displayed signs of relapse within the 12 month follow-up period [18].

In 1989 16S ribosomal gene sequencing and additional morphological differences such as being multi- not uni-flagellated, revealed that *C. pyloridis* was not actually a member of the enteropathogenic *Campylobacter* genus, but merited its own category and was termed *Helicobacter* instead [5, 19]. By this time, a second, independent, team of investigators were able to replicate Marshall and Warren findings in 1990 and concluded that *H. pylori* eradication cures duodenal ulcer disease [20]. The field of *Helicobacter* research has expanded exponentially in the past 30 years. Marshall and Warren, after numerous studies further validating their work, ultimately won the 2005 Nobel Prize for their groundbreaking discovery. While *H. pylori* got a 100-year head start on avoiding human detection at a macro level, the research field of *H. pylori* has now blossomed to over 47,000 publications to date and averages nearly 2,000 new publications per year. Its ability to persist and evade detection at a molecular level continues, and as such, *H. pylori* remains a major human health problem.

1.2. Prevalence and Epidemiology of *H. pylori*

Due to high acidity, the stomach was long believed to be sterile but *H. pylori* has succeeded in colonizing the human stomach over thousands of years [21]. *H. pylori* has been so successful that greater than 50% of the world's population is currently infected [22]. The *H. pylori* phylogeographic distribution pattern is very similar to corresponding patterns of its human host due to coexisting with each other for thousands of years and *H. pylori*'s typical intrafamilial transmission [23, 24]. This has allowed *H. pylori* to serve as a marker for tracing demographic events in human prehistory [23, 25, 26] including the sequencing of a *H. pylori* strain extracted

from a 5,000 year old Iceman mummy that has helped clarify the timeline of human migration from Asia into Europe [27]. The exact mode of transmission is somewhat surprisingly poorly understood, even with such a long history with its human host. Epidemiological studies have suggested that lower socioeconomic status, often accompanied with poor sanitation and higher population density facilitate *H. pylori* transmission, generally from mother-to-child or spouse-to-spouse [28-30]. These observations correlate with prevalence data that demonstrate high rates of infection (70-90%) in developing countries, often in Africa, South American, and Western Asia **(Figure 1A)**. Much lower prevalence (19-37%) is observed in developed countries in Europe and North America [22]. *H. pylori* colonization is on the decline worldwide, a trend that appears to continue provided that living conditions can continue to improve across the developing world [31].

1.3. Risks Associated with *H. pylori* Infection

While the worldwide prevalence of *H. pylori* infection remains high and persists for the lifetime of the host, the vast majority of infected patients (90%) remain asymptomatic [32, 33]. While superficial chronic gastritis is the most common response to *H. pylori* infection, only a portion of infected individuals will progress beyond superficial gastritis and among infected individuals. Approximately 10% develop peptic ulcer disease, 1-3% develop gastric adenocarcinoma, and <0.1% develop mucosa-associated lymphoid tissue (MALT) lymphoma [33-35]. Persistent inflammation caused by *H. pylori* infection is accompanied by chronic oxidative stress, DNA damage, and accumulation of genetic and epigenetic changes in gastric tissue, which lead to genomic instability during cell divisions and can force neoplastic transformation [36].

A multitude of environmental, host, and microbial factors impact the degree of injury in infected persons that can lead to gastric carcinoma **(Figure 2),** which is driven by local and

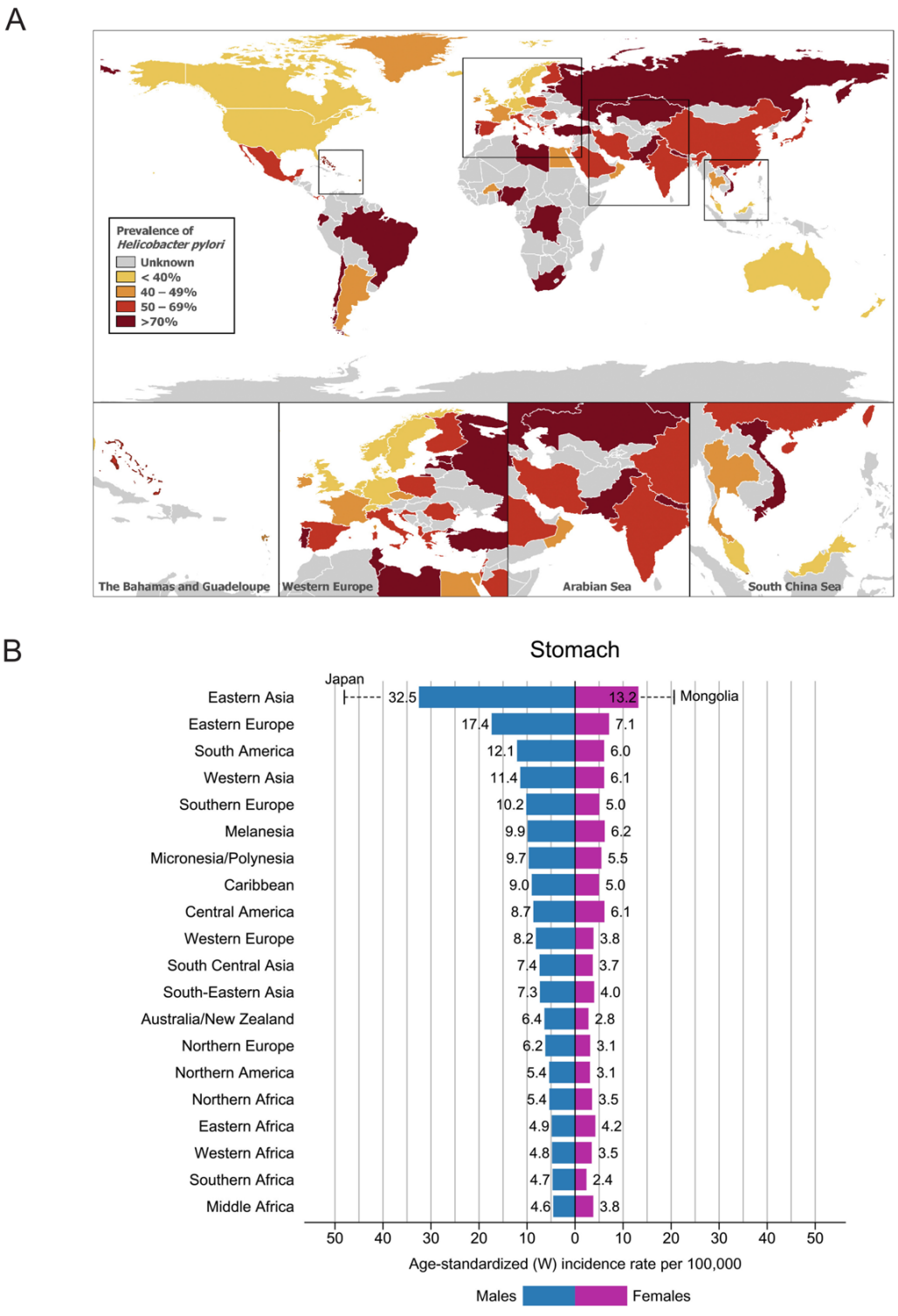

Figure 1. Global prevalence of *H. pylori* and worldwide gastric cancer incidence rates. (A) Global prevalence of *H. pylori* infection choropleth map. Certain regions are magnified to better display the smaller countries. Reprinted from [22], under the terms of the Creative Commons Attribution 4.0 license. **(B)** Region-specific incidence age-standardized rates by sex for stomach cancer in 2020. Rates are shown in descending order of the world (W) age-standardized rate among men, and the highest national rates among men and women are superimposed. Reprinted with permission from [37].

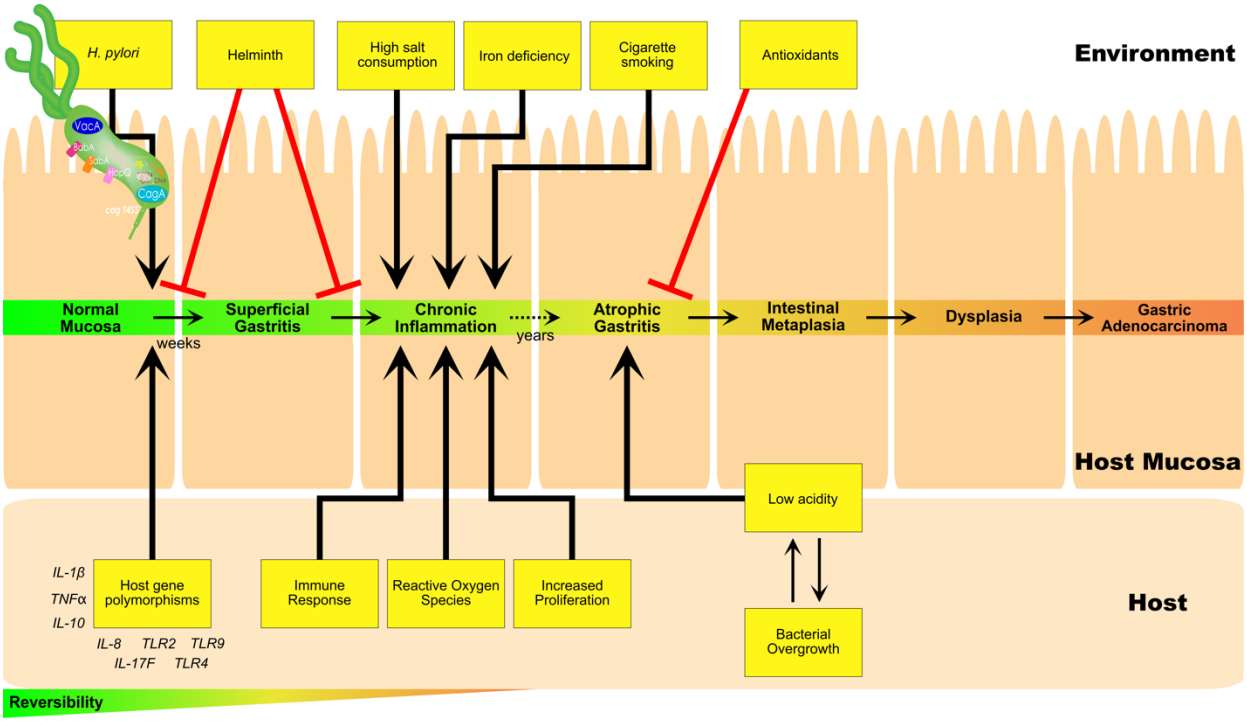

Figure 2. Multifactorial pathway leading to gastric carcinoma. Many host, bacterial, and environmental factors act in combination to contribute to the precancerous cascade leading to development of gastric cancer.

systemic immune responses induced by *H. pylori.* Recognition of *H. pylori* by the innate immune system is generally mediated by epithelial cell pattern recognition receptors (PRRs), antigen presenting cells (APCs), such as dendritic cells (DCs) and macrophages, which in turn drive adaptive immune mediated responses [38-41]. The adaptive immune response is primarily T-helper cell type 1 (Th1) [42-44] and type 17 (Th17) [45, 46], which can consequently lead to atrophy and metaplasia [47, 48]. Localization of inflammation within the stomach in concert with the type and severity of immune response dictates disease outcome [49]. Chronic antral-predominant inflammation can produce hyperchlorhydria and increased risk for duodenal ulceration; however, corpus-predominant or pangastritis can lead to hypochlorhydria and a predisposition for gastric adenocarcinoma [49, 50].

Although less than 5% of individuals colonized with *H. pylori* will go on to develop gastric cancer [33], gastric adenocarcinoma is the fourth leading cause of cancer-related death worldwide accounting for 769,000 deaths annually (equating to one in every 13 deaths globally) [37, 51, 52]. Chronic infection with *Helicobacter pylori* remains the highest known risk for this disease [37, 53]. *H. pylori* seropositivity is associated with a significantly increased risk of gastric cancer ranging from 2.1–16.7-fold greater than in seronegative persons [32]. Consequently, *H. pylori* was specified a Class I carcinogen in 1994 by the World Health Organization just a decade after its discovery [54]. Unsurprisingly then, gastric cancer incidence reasonably correlates with *H. pylori* geographic variation **(Figure 1B)**. This disease is the leading cause of cancer death in several South Central Asian countries, including Iran, Afghanistan, and Kyrgyzstan and incidence rates are highest in Eastern Asia, such as Japan and Mongolia (the countries with the highest incidence in men and women, respectively), Eastern Europe, and some Latin American countries [37].

Due to the wide variation in etiological and epidemiological factors, gastric cancers are typically classified anatomically as cardia (proximal) and non-cardia (distal) (**Figure 3A)** [55]. Non-cardia cancers are much more common (~73%) and the vast majority worldwide are caused by *H. pylori* infection [56, 57]. Of these non-cardia cancers, there are two categories, 1) diffuse-type and 2) the more common intestinal-type. Diffuse-type gastric adenocarcinoma commonly affects younger persons, occurs equally in males and females, and is typically composed of individually infiltrating neoplastic cells that fail to form glandular structures and are independent of intestinal metaplasia [58]. In contrast, intestinal-type (named after the islands of intestinal epithelium found within the gastric mucosa) affects males at greater rates, occurs in areas with high gastric cancer incidence, and progresses through a series of well-defined preneoplastic steps as defined by Dr. Pelayo Correa in 1975 **(Figure 3B)** [59]. The model of initiation and progression

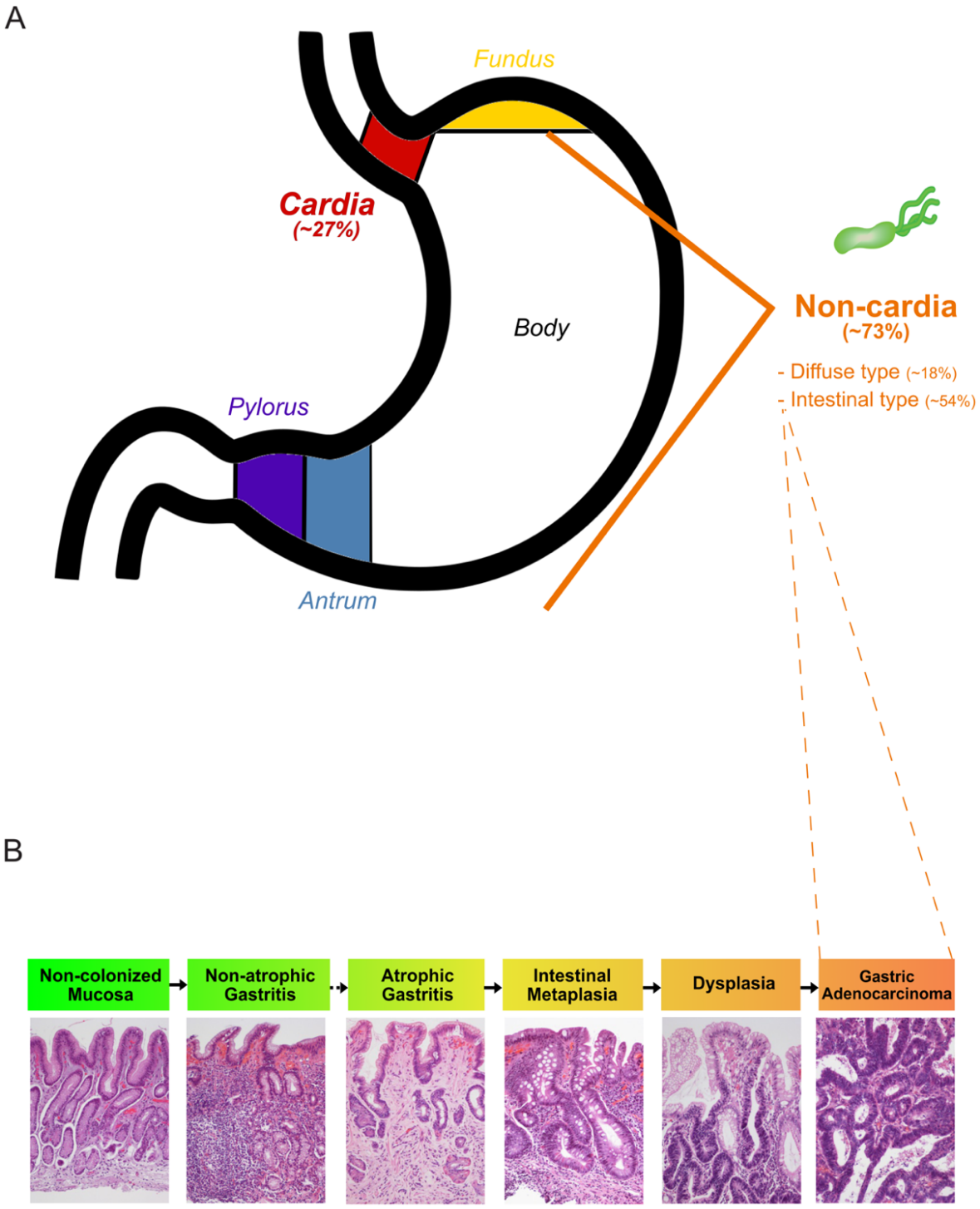

Figure 3. Gastric cancer histological classification. (A) Historically, histologic classification of gastric carcinoma is largely based on Lauren's criteria [55], in which intestinal type and diffuse type adenocarcinoma are the two major histologic subtypes of non-cardia cancers. The relative frequencies of each type relative to the overall global gastric cancer burden are displayed [60]. **(B)** The Correa cascade characterizes the progression of intestinal-type gastric adenocarcinoma through a well-defined series of steps [59]. Representative images of hematoxylin and eosin stains (H&E) are shown below each of the steps.

of gastric cancer proposed by Correa and colleagues was centered on atrophic changes developing from chronic gastritis, which over time increases the risk of intestinal metaplasia as well as gastric cancer within 30–50 years of development [59, 61]. Correa's astute observations would be corroborated in the early 1980s with Warren and Marshall's *H. pylori* discovery work [12, 13], which demonstrated the role of *H. pylori* infection as the initial step in the gastric carcinogenesis cascade. Large-scale associations between *H. pylori* eradication and diminished gastric cancer incidence have been confirmed within the past six years [62].

While *H. pylori* is the strongest recognized risk factor for the development of gastric cancer, the vast majority of infected persons never develop this malignancy. This large discrepancy between the number of individuals infected with *H. pylori* compared to those who develop gastric cancer suggests there are a variety of factors that have distinct interactions that enhance cancer risk **(Figure 4)**. These include specific bacterial factors, host genetic differences, age of infection acquisition, and environmental factors or dietary constituents that may alter the delicate equilibrium between pathogen and host **(Figure 2)** [63-66]. *H. pylori*'s long evolutionary history with humans and the recognition that most infected individuals remain asymptomatic suggest that *H. pylori* is not a pathogen at all but may be simply a commensal organism with carcinogenic potential. Evidence is also mounting that *H. pylori* infection is inversely related to the risk of developing Barrett's esophagus, esophageal adenocarcinoma, and other inflammatory diseases such as hay fever, asthma, and atopic eczema [67-75]. These advantages to infection have greatly obscured the role between *H. pylori* functioning as a commensal versus a pathogen. Additionally, *H. pylori* DNA has been shown to mitigate the inflammatory responses resultant from dextran sulfate sodium (DSS)-induced colitis in a murine model [76, 77]. In conclusion, these data suggest that a more complete picture of *H. pylori*-host interactions is essential for balancing the benefits

and risks of eradication and the potential for gastric carcinogenesis.

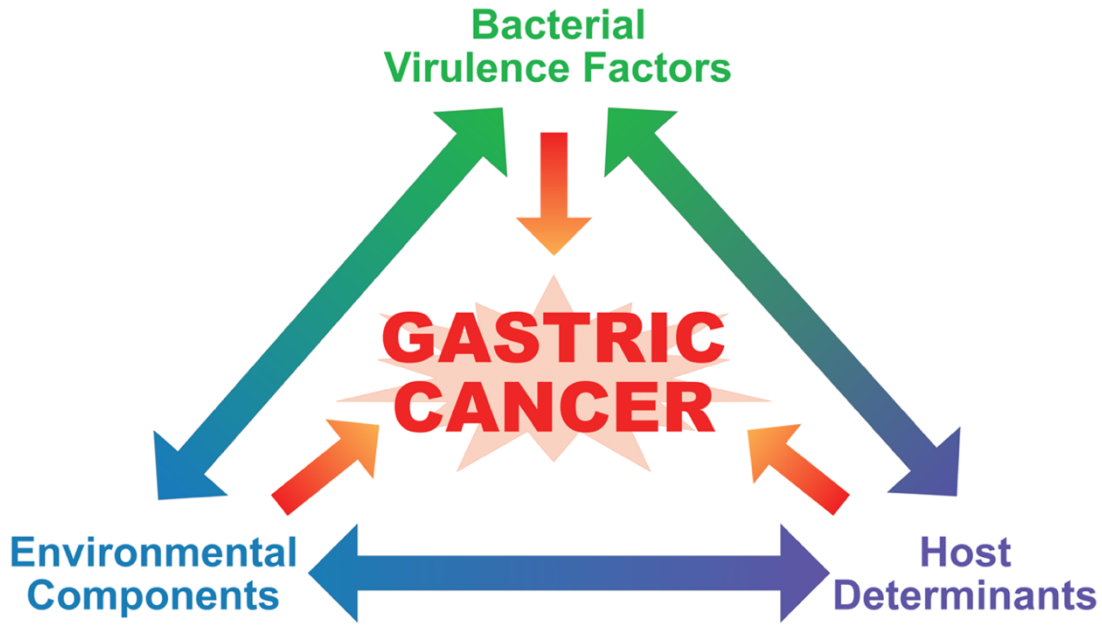

Figure 4. Host, bacterial, and environmental factors all contribute to the development of gastric cancer.

1.4. *H. pylori cag* Pathogenicity Island and T4SS

There are several well-known *H. pylori* virulence factors which are characterized by their allelic and phenotypic diversity and ability to modulate inflammation. Evolutionarily, inflammation is likely a necessary evil for microbes because it promotes nutrient acquisition but comes at the cost of reducing colonization and consequently decreasing the chance of transmission. Thus, a successful chronic infection by *H. pylori* is dependent on both inducing and precisely regulating host inflammatory responses. *H. pylori* strains exhibit a high level of genetic diversity; nearly every *H. pylori* isolate is unique at the DNA level as evidenced by whole genome sequencing [23, 78-84]. A key differentiator amongst *H. pylori* strains in determining virulence is the presence of a 40kb gene locus referred to as the *cag* pathogenicity island (*cag* PAI). The *cag* PAI is present in approximately 60-70% of all Western strains and as many as 90-100% of strains

from East Asia [85-89]. Although all *H. pylori* strains induce some level of gastritis, strains that harbor the *cag* PAI (*cag*$^{+}$) significantly augment the risk for severe gastritis, atrophy, dysplasia, and gastric adenocarcinoma compared to strains that lack the *cag* PAI (*cag*$^{-}$) [90-102]. Interestingly, the GC content of the *cag* PAI is lower the rest of chromosome, which is suggestive of acquisition via a horizontal gene transfer event [86].

Annotation of the *cag* PAI has demonstrated there are up to 31 encoded genes, some of which share homology to the prototypical DNA-translocating *virB/D4* encoded type IV secretion (T4SS) of *Agrobacterium tumefaciens* **(Figure 5A)** [103]. The *cag* PAI encodes for proteins required to assemble a T4SS and allows for the translocation of bacterial effector molecules into host gastric epithelial cells. To date, studies have shown that the *cag* T4SS is required for translocation of the effector protein CagA [104-108], peptidoglycan [109-113], a metabolic intermediary in the lipopolysaccharide (LPS) synthesis pathway, heptose-1,7-bisphosphate (HBP) [114-116], and of direct relevance to this thesis, DNA [117-119]. T4SSs are the most ubiquitous secretion systems amongst both Gram-positive and Gram-negative bacteria; however, they are also unique amongst bacterial secretion systems because they can translocate both protein and DNA. Studies have shown that *cag*$^{-}$ strains are predominantly localized in the mucous gel layer while *cag*$^{+}$ strains are found adjacent or adherent to the gastric epithelium which suggests that the *cag* PAI influences the topography of colonization and is involved in liberating nutrients from the host [120].

The primary *cag* T4SS-dependent phenotypes in infected epithelial cells, delivery of the effector CagA and induction of interleukin-8 (IL-8) via transcription factor NF-κB, require 21 of the approximately 30 genes that compose the *H. pylori cag* PAI [121, 122]. While some of these *cag* T4SS genes share some sequence similarity to other bacterial species, importantly to all 11

virB and *virD4* orthologs, nine genes are exclusive to *H. pylori* and display no homology to other bacterial proteins [123]. The *cag* core complex is 41nm in diameter and is composed of 5 *cag*-encoded proteins (Cag3, CagT, CagM, CagX, and CagY) (**Figure 5B)** [123], while the *A. tumefaciens* core complex has a diameter of only 20nm and is composed of 3 proteins, VirB7, VirB9 and VirB10 [124, 125]. Even with sequence and structural similarities to other T4SSs, the *H. pylori cag* T4SS remains highly unique as it is the only known T4SS that is currently capable of translocating a protein substrate (CagA), non-proteinaceous substrates (peptidoglycan, HBP), as well as DNA [118, 126].

The extracellular component of the *cag* T4SS comprises a pilus-like structure, which protrudes from the bacterial membrane and connects to the host cell surface **(Figure 5C).** Environmental and host conditions can regulate *cag* T4SS pili formation. Direct contact with host cells is required for pili formation, as plate-grown *H. pylori* exhibit no T4SS-pili [127, 128], and pili induction is enhanced under iron limitation conditions but dependent on the presence of zinc [129-131]. Electron microscopy has demonstrated the presence of both CagA [128] and CagL [128, 132] at the tips of the *cag* T4SS pili, suggesting that CagA may be transported through the pili for delivery into host cells. However, recent work using cyro-electron tomography has clouded the composition of the extracellular *cag* T4SS appendages, ironically while using higher resolution imaging techniques. These “sheathed tubes” appear structurally different than the aforementioned pili, have much larger diameters and correspond to extrusions of the outer membrane [133-136]. Either appendage appears to translocate CagA but which structure is more biologically relevant remains unclear. Another noteworthy *cag* T4SS protein is CagY, which is related to VirB10 of the T4SSs in other bacteria. CagY exhibits an additional large N-terminal domain containing two large repeat segments, providing surprising structural variability in CagY both by in-frame deletion or

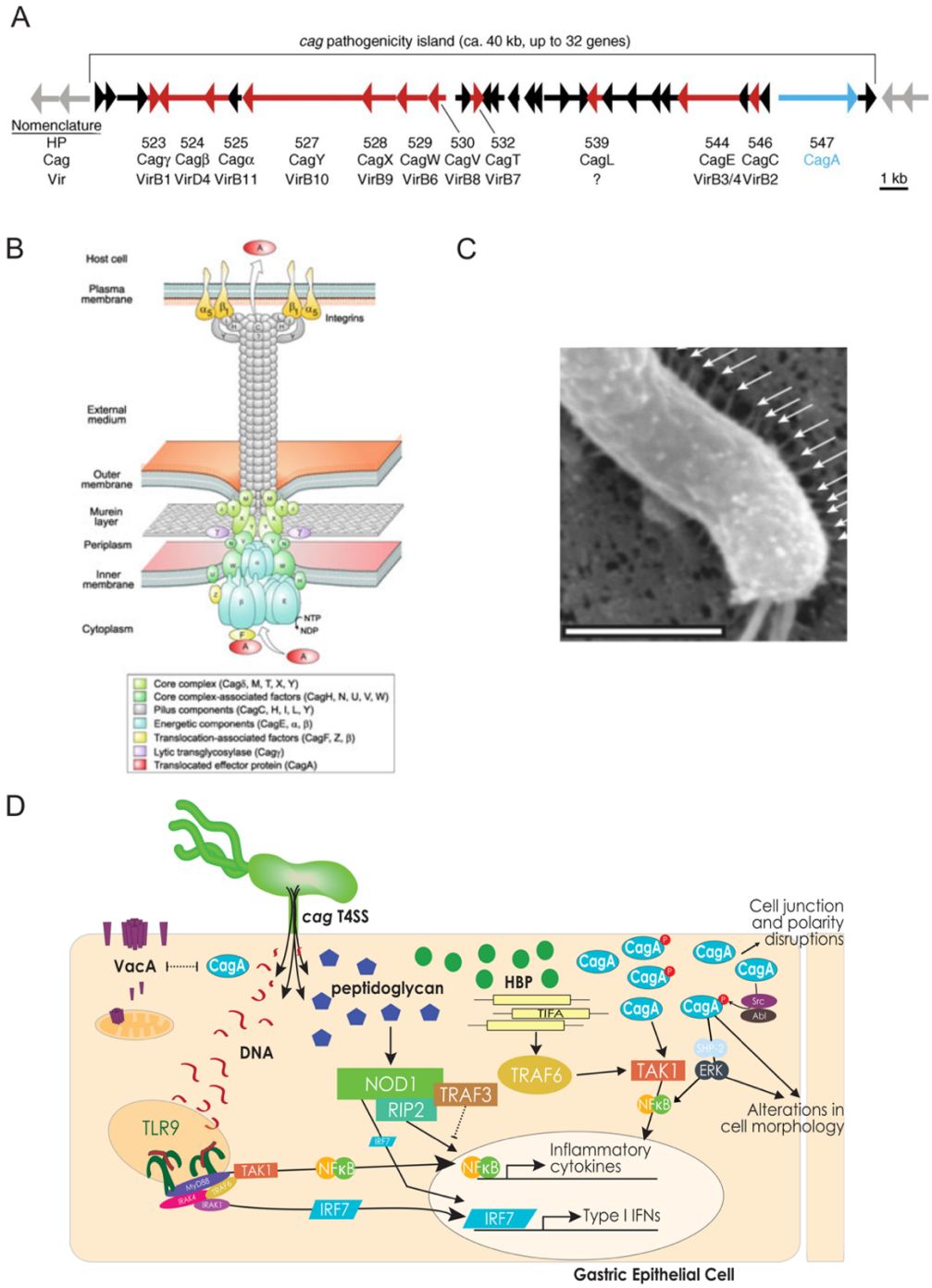

Figure 5. Structure and functions of the *H. pylori cag* T4SS. (A) The *cag* PAI is a 40kb gene locus that encodes 31 genes required for the assembly of the T4SS. Red arrows represent genes that share some homology to the *A. tumefaciens* archetypal T4SS. Blue arrow represents *cagA*, the primary effector molecule of the T4SS. Reprinted with permission from [132]. **(B)** Model of the *H. pylori cag* T4SS and localization of structural Cag proteins in complex with the host cell. Pilus components, core complex proteins, energetic components, and other factors are highlighted with different colors as indicated. The T4SS receptor integrin $\alpha_5\beta_1$, effector protein CagA, and the chaperone CagF are also shown. Reprinted with permission from [121]. **(C)** Electron micrograph of *H. pylori* T4SS pilli on an AGS gastric epithelial cell. Scale bar set to 1 micron. Reprinted with permission from [130]. **(D)** Schematic of *cag* T4SS translocated and associated substrates and selected host responses to them.

duplication events [137, 138]. Interestingly, these CagY rearrangements are sufficient to trigger loss or gain of *cag* T4SS functions, and are dictated by host immune responses [137, 139] or can be induced by the cancer chemopreventive agent α-difluoromethylornithine [140]. CagY has thus been proposed to be a *H. pylori* virulence factor that can distinctly function as a molecular switch to regulate host inflammatory responses in order to maintain persistence.

1.5. Effectors of the *cag* T4SS and Subsequent Cellular Interactions

The primary effector of the *cag* T4SS is CagA. *H. pylori* CagA is a bacterial oncoprotein that is injected into host cells upon bacterial attachment **(Figure 5D)**. CagA was linked to cancer long before the mechanism was understood, as *H. pylori* strains from cancer patients were typically $CagA^+$ while strains from patients with mild or no symptoms were $CagA^-$ [141]. Following translocation into host epithelial cells, CagA can be tyrosine phosphorylated by Src and Abl kinases or can remain unphosphorylated [142, 143]. Phosphorylation status dictates which of many host proteins CagA can interact with to disrupt host homeostasis [121]. Among these, phosphorylated CagA activates the phosphatase SHP-2 and ERK, which leads to cell elongation and scattering and appearance of the classic "hummingbird phenotype" [104, 142]. Unphosphorylated CagA has been shown to induce pro-inflammatory responses as well as weaken cell-cell junctions to induce a loss of cellular polarity that are important drivers of carcinogenesis [144, 145]. However, translocation of CagA, but not phosphorylation, can induce aberrant β-catenin activation that leads to disruption of apical-junctional complexes, loss of cellular polarity, and activation of genes involved in transformation [146-148]. Although phosphorylated and unphosphorylated CagA are sufficient to induce NF-κB activation, *H. pylori* NF-κB activation is predominantly T4SS-dependent while remaining CagA-independent [149, 150].

The immediate early response of the innate immune transcription factor NF-κB to *H. pylori* is required for expression of numerous pro-inflammatory chemokines, such as IL-6 and IL-8, which recruit neutrophils to the site of infection and promotes chronic inflammation. Central to the host response to infection, NF-κB activity affects cellular responses including inflammation and cell survival. The NF-κB family consists of RelA, RelB, c-Rel, p50, and p52 proteins. The transcription factors are present in the cytoplasm and repressed by inhibitors of NF-κB (IκBs) [151]. Canonical NF-κB induced by *H. pylori* is rapid, within 15 minutes of infection *in vitro*, and involves phosphorylation of the NF-κB inhibitors IκBα, IκBβ, and IκBε, and degradation of IκBα [150]. Transforming growth factor-activated kinase 1 (TAK1) signaling [152, 153] and tumor necrosis factor receptor-associated factor 6 (TRAF6) are also involved in NF-κB activation by *H. pylori* [153, 154]. The released NF-κB heterodimer, composed of RelA and p50, enters the nucleus where it regulates expression of pro-inflammatory target genes such as IL-8 [155]. Recent data provide evidence that translocated heptose-1,7-bisphosphate (HBP), a metabolite of LPS inner heptose core, contributes to *H. pylori* T4SS-dependent IL-8 secretion in human epithelial cells **(Figure 5D)** [114-116]. Translocated HBP and the adaptor protein TRAF-interacting protein with FHA domain (TIFA), which was described before to mediate HBP-dependent activity in other Gram-negative bacteria [156], were imperative for upstream NF-κB signaling including TAK1 activation [115, 116]. Additionally, and to be expanded on later in this dissertation, NF-κB activation by *H. pylori* can also be induced by *cag* T4SS translocated DNA via toll-like receptor 9 (TLR9) **(Figure 5D)** [117]. TLR9 is a multidimensional immune receptor based on its ability to mediate both a pro-inflammatory NF-κB-mediated and IRF7-mediated response [119, 157, 158].

In addition to the effectors CagA, HBP, and DNA the *cag* T4SS translocates peptidoglycan into host cells **(Figure 5D)**, though outer membrane vesicles can also deliver peptidoglycan

intracellularly [159]. Nucleotide binding oligomerization domain containing protein 1 (NOD1) is an innate immune receptor and cytoplasmic sensor of peptidoglycan components and is expressed by most gastrointestinal epithelial cells [160]. Activation of NOD1 by the muropeptide γ-D-glutamyl-meso-diaminopimelic acid (iE-DAP) leads to NF-κB-dependent cytokine production as well as induction of autophagy [161, 162]. In addition to epithelial cells, NOD1 is also expressed and activated within macrophages *in vivo* [163-165]. NOD1 sensing of *H. pylori* peptidoglycan induces NF-κB activation via RIP2 and expression of type I interferon (IFN) via IRF7, MIP-2, and β-defensin [109, 110, 161, 166]. In humans, genetic variation in *ATG16L1*, which encodes a key effector of NOD1-dependent autophagy and inflammation, alters susceptibility to *H. pylori* infection [167]. NOD1 activation is tightly regulated by a negative autocrine feedback system, in which NOD1-dependent effectors such as AP-1 and TRAF3 simultaneously suppress the downstream effects of NOD1 activation [166, 168, 169]. In addition to NOD1- and CagA-dependent induction, IL-8 induction can also be mediated by the *cag* T4SS via the mitogen-activated protein kinase (MAPK) family members JNK- and ERK1/2 [170].

However, not all *cag* T4SS-mediated responses result in adverse outcomes within the host cell. While seemingly counterintuitive, as a means of persistence, *H. pylori* has evolved the ability to regulate inflammatory responses from an additional virulence factor, vacuolating cytotoxin A (VacA), by actually translocating greater amounts of CagA. While all *H. pylori* strains contain the *vacA* gene, it is genetically diverse with specific alleles linked to increased virulence [171]. *H. pylori* secretes VacA, which in turn binds to the plasma membrane of host cells and forms an anion selective channel in endosomal membranes which subsequently leads to vacuolization due to swelling of the endosomal compartments [33]. The effects of this vacuolization include reductions in cellular trans-epithelial resistance, induction of apoptotic pathways via induction of

mitochondrial damage, and inhibition of antigen presentation to $CD4^+$ T-cells [172]. VacA can target mitochondria and induce apoptotic cell death; however CagA can inhibit apoptosis via the induction of the pro-survival proteins ERK-1/2 and the anti-apoptotic protein MCL-1 [173]. In addition, phosphorylated CagA can prevent pinocytosed VacA from reaching its intracellular targets. Direct CagA and VacA regulation of each other's cellular phenotypes are also observed in *in vitro* where CagA inhibits vacuolization and VacA can block the hummingbird phenotype induced by CagA in AGS gastric epithelial cells [174]. To further dampen the immune response, *H. pylori* can also modulate T-cell responses with its CagA and VacA proteins through nuclear factor of activated T-cells (NFAT) signaling, a transcription factor family that traditionally linked to cytokine induction [173]. VacA toxin can inhibit NFAT signaling in T-lymphocytes and has also been shown to counteract NFAT activation induced by CagA [173]. Collectively, these observations suggest yet another strategy for *H. pylori* to regulate host immune responses within the gastric niche and evade elimination from the detrimental effects induced by its own virulence factors.

1.6. *H. pylori* Outer Membrane Proteins

Independent of the *cag* PAI is another set of well-characterized *H. pylori* virulence factors that contribute to disease, a large family of outer membrane proteins (OMPs). *H. pylori* has a large number of OMPs compared to other bacteria with its genome containing over 50 OMPs, consisting of up to 4% of the coding potential [175]. These OMPs have been identified as porins, iron transporters, or adhesins [176]. *H. pylori* must initially attach to the gastric mucosal surface and maintain this attachment long-term to successfully colonize its host. The adhesin OMPs mediate attachment to the epithelial cell surface and structures present on the secreted mucus. The best

understood group of OMPs are the *Helicobacter* outer membrane protein (Hop) family of adhesins, specifically three of the 32: BabA (HopS), SabA (HopP), and HopQ **(Figure 6A)**. OMP expression can vary greatly across *H. pylori* strains, ranging from 40-80% or show allelic variation with distinct clinical phenotypes [175], suggesting that particular OMPs, or combinations of OMPs, may be key to disease outcomes, rather than simply maintaining persistence.

Fucosylated blood group antigens are expressed on gastric epithelial cells and the overlying mucus, and early on, *H. pylori* adhesion was correlated with the presence of these antigens [177]; subsequently, BabA (HopS) was the first adhesin discovered as a binding partner for these antigens [178]. Originally thought to only bind Lewis b antigen (Le^b), the binding specificity of BabA to blood group O antigens is restricted to certain *H. pylori* strains, named "specialist" strains, while BabA from the "generalist" strains can bind fucosylated blood group A antigens and globo H hexaglycosylceramide [179, 180]. Genetic analysis of *babA* revealed two loci (*babA1* and *babA2*) and a closely related paralogous *babB* locus [178]. BabA expression is regulated via phase variation and recombination events with the *babB* locus, as loss- and gain-of-function mutations *in vitro* and *in vivo* have been demonstrated [181-183]. In combination with other virulence factors, clinical *H. pylori* isolates containing $BabA^+$, $VacA^+$, and $CagA^+$ demonstrate greater colonization densities, elevated levels of gastric inflammation and a higher incidence of intestinal metaplasia in *H. pylori*-infected patients as compared to strains containing VacA and CagA only [184]. BabA-mediated adhesion of *H. pylori* to gastric epithelial cells has also been linked to enhanced CagA translocation and the induction of inflammation [185]. Epidemiologically, these "triple-positive" ($BabA^+$, $VacA^+$, $CagA^+$) strains are correlated with the greatest incidence of ulceration and gastric cancer compared to strains lacking BabA [186].

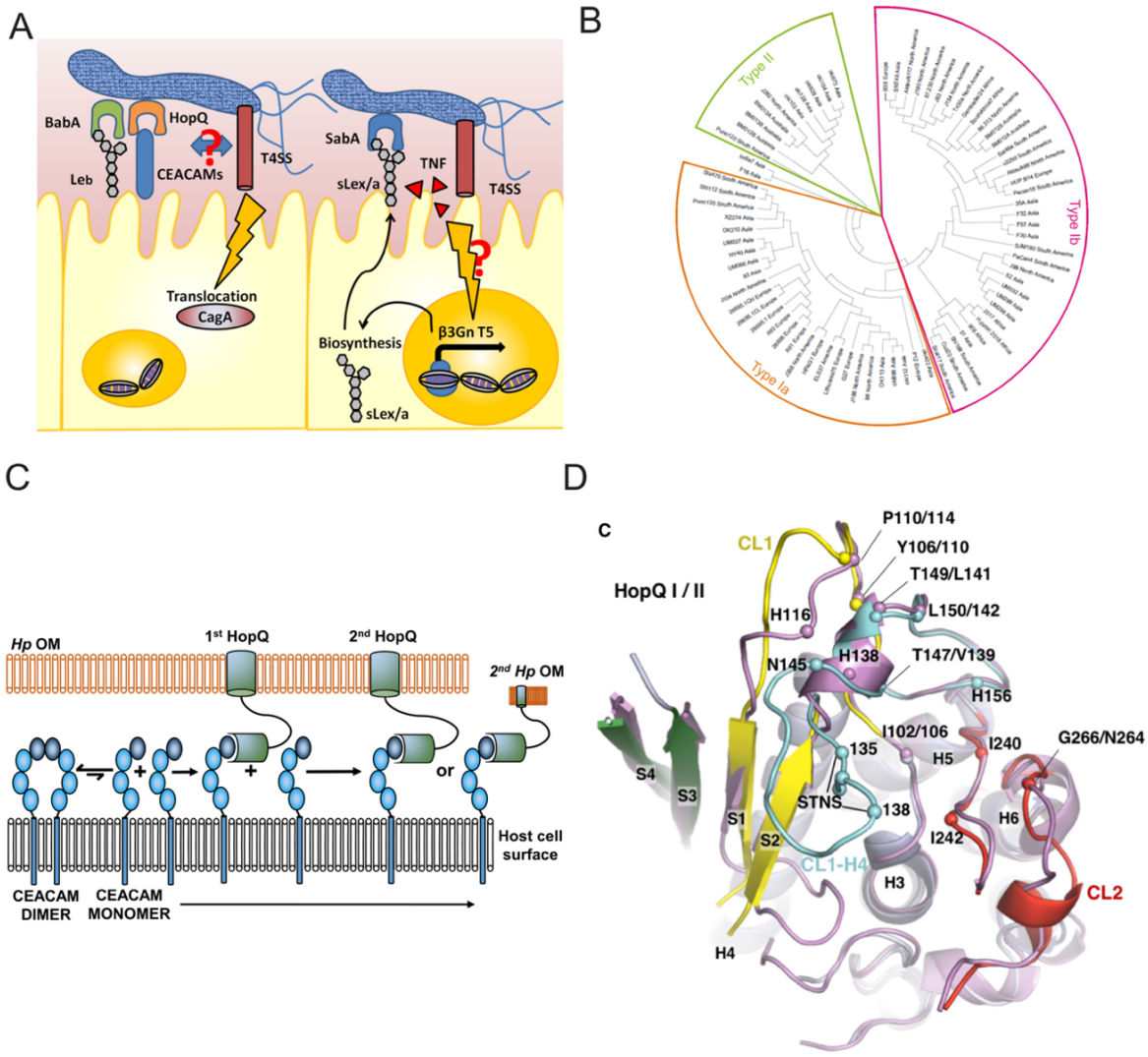

Figure 6. *H. pylori* outer membrane proteins including HopQ contribute to pathogenesis. (A) BabA interacts with Le[a] antigen and enhances CagA translocation). HopQ interacts with CEACAMs and is linked to *cag* T4SS phenotypes. Absence of sLe[x] antigen expression in the healthy stomach. *H. pylori* infection induces β3GnT5 expression in gastric epithelial cells and biosynthesis of the sLe[x] antigen; sLe[x] localizes to the membrane region of gastric epithelial cells. As a result, *H. pylori* can colonize by utilizing SabA, which interacts with the sLe[x] antigen. Although the detailed mechanism is unclear, TNF and the *cag* T4SS are suggested to induce β3GnT5 expression. Adapted from [187], under the terms of the Creative Commons Attribution 4.0 license. **(B)** The *hopQ* genes were collected from *H. pylori* isolates of all continents. The MEGA6 program was applied to infer DNA relatedness using the Neighbor-Joining method. The Maximum Composite Likelihood method was utilized to compute evolutionary distances. The *hopQ* genes grouped into two major allelic variants (type I and II). The type I alleles are more diverse and were further divided into the two subgroupings type Ia (orange shaded) and Ib (pink shaded), as indicated. The type II cluster is highlighted in green. Reprinted with permission from [188]. **(C)** Model of HopQ recruitment of CEACAM. CEACAM1 (blue) is predominately dimeric. HopQ (green) binding of CEACAM monomers causes redistribution of dimers to monomers which can bind further HopQ on the same bacterium or recruit other bacteria to the host cell. Reprinted with permission from [189]. **(D)** Top view of the overlay of HopQ type I adhesin domain (HopQAD-I) and HopQ type II adhesin domain (HopQAD-II). The CL1-H4 loop is missing in HopQAD-II, and minor additional structural rearrangements between HopQAD-I and HopQAD-II are observed in the CL2 and H3-S1 loop. Corresponding CEACAM-interacting residues of HopQAD-I and HopQAD-II are shown as a sphere and labeled; color scheme is: HopQAD-I (purple) and HopQAD-II (blue). HopQAD-II CL1 is colored in yellow, the CL2 in red, CL1-H4 in cyan, and β-strands of the insertion domain in green. Reprinted with permission from [190].

In addition to BabA-mediated adhesion, the *H. pylori* adhesin SabA binds to sialic acid-modified glycosphingolipids, namely sialyl-Lewis x/a (sLe^X and sLe^a) [191]. Notably, sLe^X is not present in healthy non-inflamed gastric mucosa [175], and therefore SabA-mediated adhesion only occurs after successful colonization and induction of inflammation in the stomach [191]. Further demonstrating how dynamic and regulated *H. pylori* adhesion is with just two of its adhesins, *H. pylori*-induced inflammation leads to elevated expression of the glycosyltransferase β3GnT5, which is vital for biosynthesis of the sLe^X antigen and thus helps maintain *H. pylori's* adhesion via SabA [192]. Further, the induction of β3GnT5 is dependent on tumor necrosis factor alpha (TNFα), but not IL-8, and cells expressing ectopic β3GnT5 exhibit higher adhesion rates for SabA-positive *H. pylori* strains [192] and acid-responsive signaling in *H. pylori* limits SabA transcription [193, 194]. Expression of *sabA* is subject to phase variation and gene conversion with its paralog *sabB,* and a majority of *H. pylori* strains lose *sabA in vitro,* suggesting selective pressures during human infection to maintain *sabA* and regulate adhesion [195].

While all *H. pylori* strains express *hopQ*, there is great genetic diversity across strains that can be categorized into two allelic families termed type I and type II **(Figure 6B)** [196]. These allelic types are correlated with geography and virulence [197]. The requirement of the HopQ adhesin for *cag*-mediated phenotypes is unclear and appears to be strain dependent. *H. pylori*-induced activation of NF-κB, translocation of CagA, and induction of IL-8 have been shown to require *hopQ* in strains G27 and P12 [149]. However, collaborations with the Cover group at Vanderbilt, which will be further explored in Chapter II, demonstrated that only certain *cag* T4SS functions are impacted by *hopQ* deletion. Loh et al. demonstrated that loss of *hopQ* in strain 26695 increased *H. pylori* adherence to AGS cells, leading to a hyper-adherent phenotype and subsequently increased CagA phosphorylation, while IL-8 induction was not affected [198].

Confirming these findings, I demonstrated that *cag*-mediated TLR9 induction in strains 26695 and 7.13 was significantly reduced in the absence of *hopQ,* but CagA translocation and IL-8 induction remained intact [199].

HopQ binds carcinoembryonic antigen-related cell adhesion molecules (CEACAMs), a large immunoglobulin superfamily with wide tissue distribution, specifically CEACAM1, CEACAM3, CEACAM5 or CEACAM6 **(Figure 6C)** [188, 200]. Variations in HopQ-CEACAM interactions are still being elucidated but HopQ binding can be species-specific. For example, HopQ binds human and rat CEACAM1, but not murine, bovine, or canine [188]. These binding interactions are also allelic-specific, as strains that carry type II HopQ can bind CEACAM5 but show only weak binding to CEACAM1 [190, 200]. Although *hopQ* has a similar genetic organization to *babA* and *sabA*, with an insertion domain that interacts with their host cell ligands, HopQ binding is fundamentally different as binding to CEACAMs is not mediated by *hopQ's* insertion domain [189]. Unlike the binding of BabA to Le^b, HopQ-CEACAM binding was demonstrated to be irreversible after being exposed to low pH, indicating it is less prone to disruption [189]. Structural work has shown that HopQ interacts with CEACAM monomers at their dimer interface and induces monomerization which abolishes CEACAM-dependent cell adhesion and signaling **(Figure 6C)**, and differences exist amongst type I and type II HopQ in CEACAM binding **(Figure 6D)** and NF-κB activation [189, 190].

The important role of HopQ-CEACAM interactions in *cag* T4SS phenotypes is starting to come into focus as direct binding of components of the *cag* T4SS to its host β1-integrin partners is not sufficient for CagA translocation, and these integrins, but not CEACAMs, are dispensable for CagA translocation in certain cell types [201]. However, in other cells, both integrin and CEACAMs are required [202]. Further, CEACAMs are expressed on the apical side of gastric

epithelial cells and serve as an attachment site for *H. pylori* whereas integrins are localized basolaterally [189]. Tegtmeyer et al. have also demonstrated that *cag* T4SS pilus formation and CagA delivery during infection of polarized cells occurs predominantly at basolateral membranes, and not at apical sites [203]. This would suggest that HopQ-CEACAM binding, and its subsequent cellular response, is important in early infection to establish *H. pylori* colonization, multiplication, and spread, whereas T4SS-integrin interactions following *H. pylori* cell migration occur later in infection and contribute greater to inflammation and metastasis [204]. Thus, further studies linking discrete cell signaling cascades to specific *hopQ* alleles and CEACAMs will be required to clarify this discordance and are addressed further in Chapter II. Collectively, these data suggest that *H. pylori* has likely evolved to harbor different alleles of *hopQ* that may confer selective binding and molecular signaling capacities.

1.7. Host Genetic Factors and Gastric Carcinogenic Risk

Bacterial virulence factors such as the *cag* PAI, VacA, and OMPs are not the only constituents that contribute to *H. pylori*-mediated inflammation and carcinogenesis. Host factors also play a fundamental role in a person's predisposition for adverse outcomes **(Figures 2 and 4)** and some of the most well-studied are host genetic polymorphisms of several cytokine genes and innate immune response genes. *IL-1β* and tumor necrosis factor α (*TNFα*) genes encode for pro-inflammatory cytokines with acid suppressive properties, and single nucleotide polymorphisms (SNPs) in these genes have been reported to increase the risk for atrophic gastritis and gastric adenocarcinoma [205-209]. These polymorphisms only affect the histologic outcome in *H. pylori* colonized patients, which highlights the significance of microbe-host interactions to impact disease outcome. As an example, a combined bacterial/host genotyping study demonstrated that patients

with high-expression *IL-1β* alleles colonized with *H. pylori cag*$^{+}$ strains showed a 25-fold increase in the risk for developing gastric adenocarcinoma compared to baseline [208]. Additionally, SNPs in a multitude of cytokines/chemokines including *IL-4, IL-6, IL-8, IL-10, IL-12, IL-17, IL-18,* and *IL-1R* have been linked to essential roles in promoting inflammation within the context of gastrointestinal cancers [210-217].

Although abnormal pro-inflammatory cytokines/chemokine expression is a critical promoter of gastric injury, functional defects of pattern recognition receptors (PRRs) that first encounter *H. pylori* and regulate downstream immune response, such as NOD-like receptors (NLRs) and TLRs are also strongly associated with gastric inflammation and carcinogenesis. The well-characterized NLRs, NOD1 and NOD2, are critical for producing pro-inflammatory cytokines/chemokines in response to *H. pylori* that are crucial for Th1 responses and lead to *H. pylori*-related gastric disorders [109, 159, 218]. However, investigations linking *NOD1/NOD2* gene polymorphisms to the severity of *H. pylori*-related disease are currently inconclusive. *NOD1* gene polymorphisms were not linked with susceptibility to *H. pylori* infection nor with gastric injury in Western populations [219, 220], whereas *NOD1* gene polymorphisms were associated with an elevated gastric cancer risk and gastric mucosal inflammation in Eastern populations [221, 222]. TLRs play a crucial role in the defense against infection and immune system regulation, and may be of greater importance within the context of tumor promotion [47], corroborated by widespread studies of TLR SNPs and their relationship with gastric carcinogenesis. SNPs within the TLR1, TLR2, TLR4, TLR5, and TLR9 have all demonstrated to increase the risk for the development of gastric cancer [223-230]. However, a more precise role and mechanism for PRRs in not only *H. pylori* recognition and infection, but gastric injury remains unsettled. This is a result

of *H. pylori* evolving mechanisms to evade the activation of those receptors central to its infection, which will be explored in the next section.

1.8. *H. pylori*-mediated Modulation of Pattern Recognition Receptors

Pattern recognition receptors (PRRs) orchestrate immune responses targeting pathogens and bridge innate and adaptive immunity via recognition of pathogen-associated molecular patterns (PAMPs) [47, 231]. PAMPs comprise a large variety of molecules including lipids, nucleic acids, and specific proteins that are derived from organisms of bacterial, viral, or fungal origin; they are highly conserved among groups of microorganisms that share different general 'patterns', or structures that are not found in their multicellular hosts (non-self) and thus allow the innate immune system to sense not only pathogens but also detect potential pathogen induced-disruptions generated in tissue homeostasis [232, 233]. These non-self sensing capacities of the innate immune response occur through germline-encoded PRRs. However, *H. pylori* harbors multiple PAMPs that function differently than the respective counterparts in other mucosal pathogens to evade detection by host PRRs **(Figure 7)**.

TLRs are expressed both on cell surfaces and within the cell. They can be localized to a wide array of cell types including macrophages and dendritic cells, as well as within non-immune cells including those of the gastric epithelium. Upon microbial ligand binding to its leucine rich repeat (LRR) ectodomain, TLRs dimerize and adaptor molecules such as MyD88 or TRIF complex with the intra-cytoplasmic Toll/IL-1 receptor (TIR) domain [234]. Activation of TLRs induces signaling cascades that eventually lead to the transcription of both pro- and anti-inflammatory cytokines, as well as type I IFN. Chronic activation of TLRs has been linked to the promotion of gastric carcinogenesis [235, 236] and this chronic activation typically results from a failure to clear

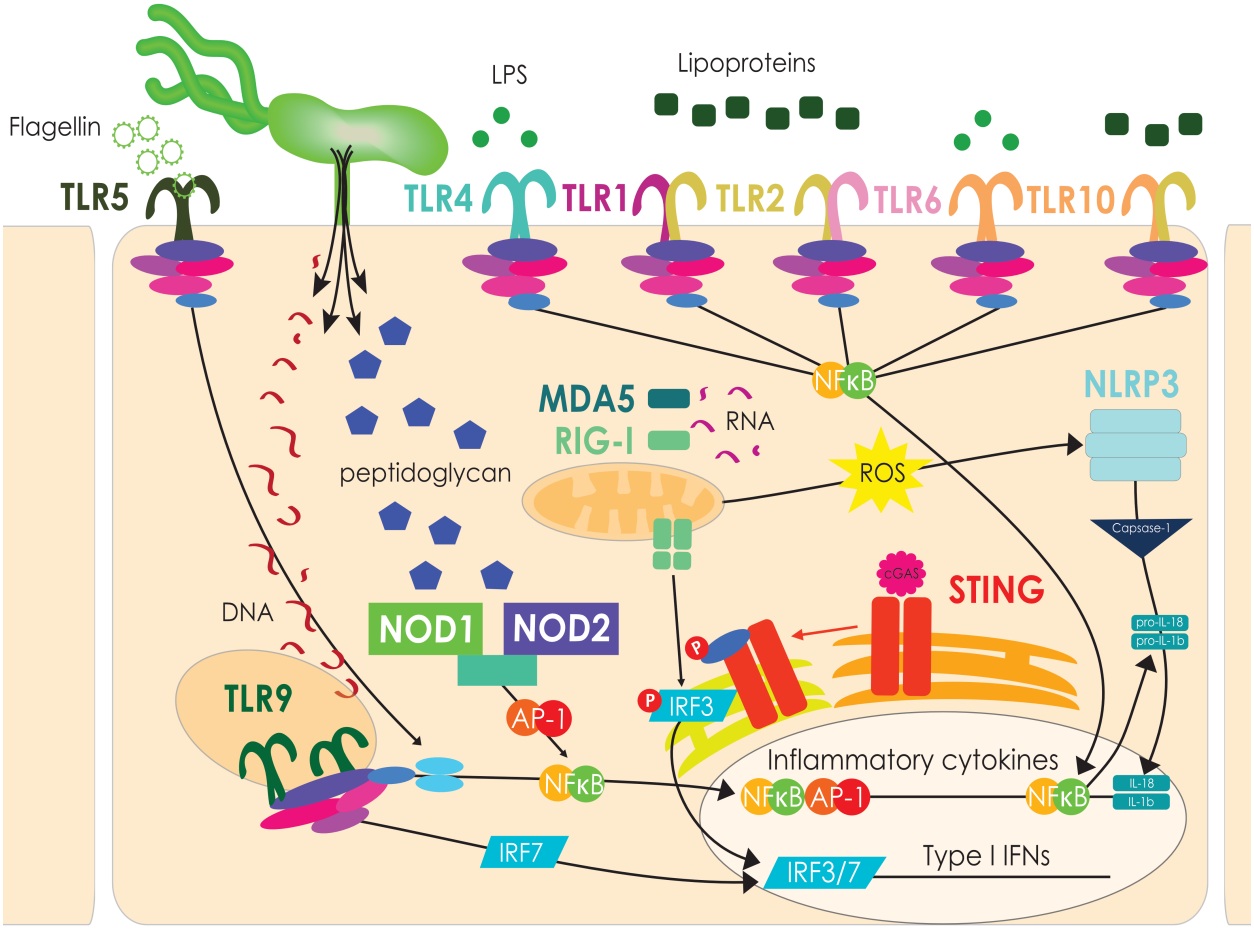

Figure 7. Pattern-recognition receptors associated with *Helicobacter pylori* infection. Toll-like receptors (TLRs) (TLR1, TLR2, TLR4, TLR5, TLR9, TLR10 and heterodimers TLR1/TLR2, TLR2/TLR6, TLR2/TLR10), NOD-like receptors (NLRs) (NOD1, NOD2, NLRP3), and RIG-I like receptors (RLRs) (RIG-I and MDA-5) have all been linked to *H. pylori* infection. Involvement of the cGAS/STING, a cytosolic DNA sensor/adaptor, is currently unclear. Only one generic cell type depicting the PRRs implicated in *H. pylori* infection is displayed for simplicity.

an invading pathogen such as *H. pylori.* There currently 10 identified human TLRs, however not all of them have been linked to *H. pylori* infection. TLR2 heterodimerizes with TLR1/6 (detects lipoteichoic acid and surface proteins NapA and Hsp60), TLR4 (detects LPS), TLR5 (detects flagellin subunits), TLR9 (detects DNA), and TLR10 (also heterodimerized with TLR2; hypothesized to detect lipopolysaccharides) have been shown to associate with *H. pylori* virulence factors [237-239].

During the initial phase of infection, extracellular TLRs (TLR2, TLR4, TLR5, TLR10) are among the first to be encountered by *H. pylori*. TLR4 is a PRR that detects bacterial LPS and induces a robust inflammatory response and early work on *H. pylori* innate immune responses primarily focused on TLR4 interactions. *H. pylori* LPS is a highly unique structure that is adapted to help maintain persistence within the gastric niche. This is primarily due to the expression of Lewis antigen decoration of the *H. pylori* LPS O-antigen, which is the outermost domain of the LPS molecule. These microbial Lewis antigens mimic the host Lewis antigens expressed on the apical surface epithelium and within the glands of both the antrum and corpus [240, 241]. Through this molecular mimicry, *H. pylori* can evade immune detection, but this occurs at the risk of eliciting autoimmune responses [242]. Additionally, *H. pylori* harbors unique modifications to the lipid A core domain [243-245]. The lipid A core is the inner most domain of LPS moieties, sometimes referred to as endotoxin, and is the ligand for the TLR4-MD2 immune complex. Compared to other bacterial LPS, *H. pylori* LPS has ~1,000 fold less endotoxicity [246-248]. This reduction has been attributed to three major modifications to *H. pylori*'s lipid A core: 1) a hypo-acylation pattern where *H. pylori* is tetra-acylated compared to hexa- or penta-acylated chains, 2) the hypo-acylated fatty acids have longer carbon chain lengths compared to the optimal chain lengths required for robust TLR4 activation, and 3) *H. pylori* LPS is hypo-phosphorylated, an adaption that also protects it from destruction by cationic antimicrobial peptides [243, 247].

The role of TLR4 in *H. pylori* immune activation is debated, but it appears that it has a diminishing role in immune activation to *H. pylori.* This is supported by studies demonstrating monoclonal anti-TLR4 antibodies in the presence of *H. pylori*-epithelial cell co-cultures failed to block IL-8 secretion [249] and that *H. pylori*-infected human embryonic kidney 293 (HEK293) cells transfected with TLR4 failed to induce NF-κB activation [40]. Additionally, immune

recognition of *H. pylori* by gastric epithelial cells occurred independent of TLR4 [250, 251] and there is evidence indicating *H. pylori* LPS may actually antagonize TLR4 [252]. While *H. pylori* doesn't robustly active TLR4, it can upregulate TLR4 expression in gastric epithelial cell lines [253]. Interestingly, Su et al. proposed *H. pylori* may upregulate TLR4 to use as a receptor for adherence to the epithelial cell surface [249]. Furthermore, while *H. pylori* LPS is a poor activator of TLR4, it can more strongly activate TLR2 as well as TLR10 during infection. TLR2 detection of LPS was dependent on TLR2/TLR1, TRL2/TLR6, or TLR2/TLR10 heterodimers however [239, 254]. During *H. pylori* infection, TLR2 has also demonstrated induction of the anti-inflammatory cytokine IL-10, while *Tlr2*-deficient mice more efficiently cleared infection than wild-type [255, 256]. Independent of LPS, the *H. pylori* proteins NapA, Hsp60, HpaA, and UreB have also been reported to activate TLR2 in cellular infection assays or animal models [257-260].

The natural ligand of TLR5 is flagellin, namely the highly conserved N-terminus of the D1 domain [261]. Since *H. pylori* is a flagellated bacterium and TLR5 is expressed in the gastric epithelium, it might be expected that *H. pylori* can induce TLR5-mediated pro-inflammatory signaling cascades. However, *H. pylori* flagellin is not recognized by TLR5 [262-264] due to a mutation in the conserved domain of the major *H. pylori* flagellin subunit FlaA [262]. This mutation, which occurs in the D0-D1 domain between amino acids 89-96, renders the flagella inert to TLR5 and when these amino acids are substituted into corresponding region of the *Salmonella enterica* serovar Typhimurium FliC subunit, it also loses the ability to activate TLR5 [262]. Taken together, these data suggest an important role in the *H. pylori* FlaA in maintaining persistence within the gastric niche by limiting the activation of TLR5.

In addition to extracellular TLRs, within the cytoplasm NLRs are able to recognize PAMPs in addition to damage-associated molecular patterns (DAMPs), which are endogenous ligands

produced after tissue injury or cell death [265]. The NLR family comprises three subfamilies: 1) the NOD family which includes NOD1-2, 2) the NLRPs including NLRP1–14 (also known as NALPs), and 3) the IPAF subfamily which consists of IPAF (NLRC4) and NAIP [265]. NOD1 and NOD2 primarily recognize fragments of bacterial peptidoglycan [161] while NLRPs are linked to the activation of the inflammasome, a crucial mechanism involved in many human diseases. The NLRP3 inflammasome, which is the most well studied member of the family, is a multimeric protein complex, made up of the NLRP3, the apoptosis-associated speck-like protein (ASC) and caspase-1 [266, 267]. This complex formation results in the activation of caspase-1, which in turn cleaves pro-IL-1 and pro-IL-18 to active cytokines [266-268]. NLRP3 has been reported to be a major activator of the inflammasome in innate immune cells in the context of *H. pylori* infection [260, 268, 269]. *H. pylori* induces IL-1β secretion in innate immune cells mainly through the activation of the NLRP3 inflammasome and requires the *cag* PAI [270, 271]. Additionally, NOD1 in gastric epithelial cells can sense fragments of peptidoglycans derived from *H. pylori*, which results from either internalization of *H. pylori*-derived outer-membrane vesicles, the corresponding digestion in autophagosomes [159] or translocation by the *cag* T4SS and results in NF-κB activation [109, 272]. However, *H. pylori* has evolved to evade host clearance via activation of a NOD1-dependent negative feedback loop through deacetylation of its peptidoglycan [160, 272-275]. RIG-I-like receptors (RLRs) are also localized in the cytoplasm, and typically recognize viral RNAs. Three members of this family have been identified at present: RIG-I; MDA5; and LGP2 [276, 277]. Knowledge of the role of these receptors in recognizing *H. pylori*-derived intracellular PAMPs is limited at the moment, but 5'-triphosphorylated RNA from *H. pylori* appears to be recognized by RIG-I and able to induce type I IFN [255]. Increased expression of MDA5 in antral mucosa from *H. pylori* infected patients has been demonstrated but the mechanism remains to be

elucidated [278]. The final known TLR implicated in *H. pylori* infection, TLR9, is of great interest to this dissertation and thus will be the focus of the following two dedicated sections.

1.9. TLR9 Regulation and Signaling

DNA is the fundamental molecule of nearly all living organisms and is normally sequestered within eukaryotic nuclear envelopes, bacterial cell walls, or viral capsids. However, during the course of infection aberrant DNA can arise from host degradation of an invading microbe, released by the microbe, or from damaged host cells. TLR9 is an endosome bound, transmembrane receptor that detects DNA and coordinates the appropriate immune response [279]. TLR9 expression is most abundant in DCs, B-cells, macrophages, and other APCs but is also expressed in epithelial cells. In DCs and B-cells, TLR9 activation classically leads to the release of pro-inflammatory cytokines and type I IFN, while epithelial responses are less well defined. TLR9 is a unique TLR because it does not fit the criteria of a classical PRR. Unlike most TLRs that recognize distinct molecular structures unique to pathogens, TLR9 cannot differentiate self- from non-self-DNAs. TLR9 was initially understood to discern pathogenic DNAs based upon the presence of hypomethylated CpG motifs (which are rare in eukaryotic genomes). However, accumulating evidence suggests that TLR9 can also recognize DNA in a sequence-independent manner via structural components such as the saccharide backbone [280-282]. Thus, likely in an attempt to prevent the recognition of self-DNA, evolutionary pressure has relegated TLR9 to endosomal sequestration [283]. The consequences of TLR9 surface expression were characterized in a study in which TLR9 transmembrane mutant mice were generated by swapping the localization signal of TLR9 with that of TLR4. The TLR9 transmembrane mutant mice died from systemic inflammation and anemia within four weeks [284].

Structurally, TLR9 is composed of three major segments: 1) a leucine-rich repeat (LRR) domain, 2) a transmembrane domain, 3) and a Toll/IL-1 receptor (TIR) domain **(Figure 8)** [281]. The LLR is involved in molecule recognition, and TIR interacts with downstream adaptor and signaling molecules. The TLR9 ectodomain forms a horseshoe-shaped solenoid assembled from 26 LRRs, with each LRR containing around 20–25 amino acids. The ends of the TLR9 ectodomain are capped by a cysteine-rich C-terminus (at the LRR end) and N-terminus (at the TIR end) [285]. In TLR9/ligand interactions, TLR9 is cleaved proteolytically at its ectodomain, resulting in TLR9 dimerization and activation [286]. DNA interacts with LRRs from both the N-terminal region and and C-terminal region but favors the C-terminal [281]. The dimerization of TLR9 is also mediated by cleavage of the Z-loop in the middle of the TLR9 ectodomain [287]. Sensing of DNA ligands by TLR9 is regulated by two mechanisms. The first involves the initial trafficking of TLR9 from the endoplasmic reticulum to endosomes and lysosomes with the presence of a multiple transmembrane protein, UNC93B1, and second, the cleavage of TLR9 in endolysosomes by endopeptidase [286]. DNA can bind uncleaved TLR9, but downstream signaling cannot occur until after the cleavage step [288]. DNA binding to mature, cleaved TLR9 within the endolysosome induces a conformational change that enables the interaction between the cytoplasmic TIR domains of the homodimer [77]. These dimerized TIR domains recruit the adaptor molecule MyD88 to form the myddosome and transmit downstream inflammatory signals [289].

Following localization to an endosome, the subsequent TLR9 trafficking dictates the type of downstream response **(Figure 8)** [290, 291]. For example, ligand binding within late endosomes can yield pro-inflammatory responses mediated by transcription factors such as NF-κB, AP-1, or CREB [289, 292, 293]. The myddosome complex is composed of activated MyD88, IL-1 receptor-associated kinase-1 (IRAK1), and IRAK4, and controls subsequent recruitment of TNF receptor-

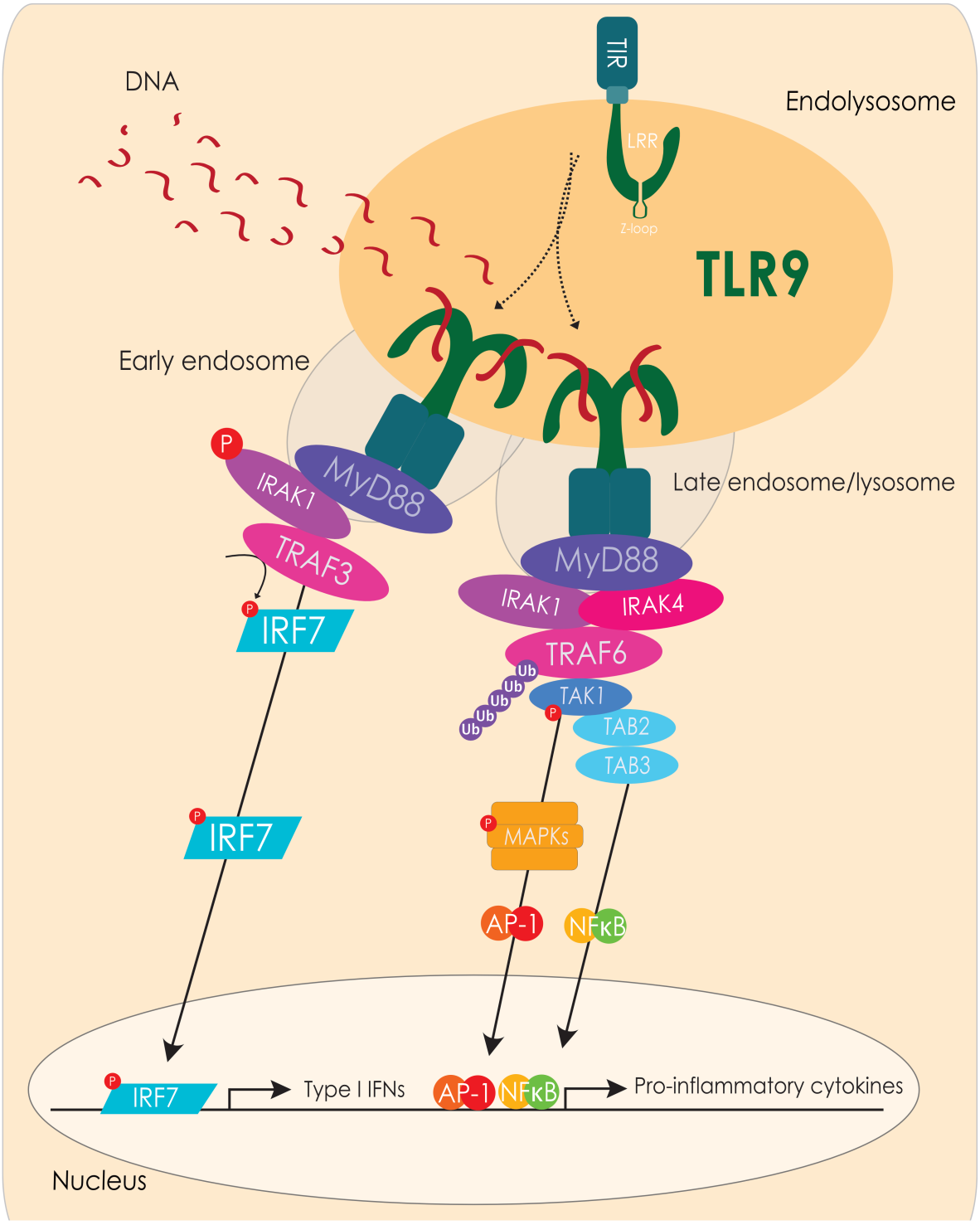

Figure 8. Overview of TLR9 signaling. Toll-like receptor 9 (TLR9) is cleaved inside the endolysosome, where the LRR domain is required for DNA binding, receptor oligomerization, and further signal transduction. The TIR domain of dimerized TLR9 recruits the adaptor protein MyD88 and forms the myddosome. Dependent on TLR9 trafficking to early or late endosomes, myddosome recruitment induces either 1) IRAK1/TRAF3 complex formation, to activate IRF7 and type I IFN expression, or 2) IRAK1/IRAK4/TRAF6 complex formation which can induce pro-inflammatory cytokine release via AP-1 or NF-κB.

associated factor-6 (TRAF6). TRAF6, in the presence of ubiquitin-conjugating enzymes UBC13 and UEV1A, activates K63-linked poly-ubiquitination of TRAF6 itself and the TAK1 complex associated with its TAB1, TAB2, and TAB3 subunits. Activation of TAK1 leads to activation of MAPK, AP-1, and NF-κB signaling pathways [289, 291]. NF-κB and AP-1 transcription factors then upregulate transcription of cytokine genes such as IL-6, IL-12, and TNFα and costimulatory molecules like CD80 and CD86 [294]. However, an IRF7-mediated, type I IFN response to CpG DNA is mediated by either 1) ligand binding within early endosomes, which recruit AP-3 to bind the myddosome, or 2) endosomal fusion with a lysosome related organelle facilitated with TRAF3 [295]. The dichotomous TLR9-mediated immune response **(Figure 8)** is not only dependent on cellular localization and ligand binding, but also the broader host-pathogen environment as described in the next section with regards to *H. pylori*.

1.10. *H. pylori*-mediated Modulation of TLR9

In the human gastric niche, TLR9 expression is upregulated in human gastric cancer specimens and primarily localized to the apical surface epithelium [296]. However, *H. pylori*-induced chronic active gastritis changes the expression pattern to the basolateral compartment only [297], suggesting TLR9 localization is key to inducing inflammation. TLR9 activation in the basolateral compartment of polarized intestinal epithelial cells preferentially mediates pro-inflammatory signaling [157, 236]. In downstream TLR9 signaling, cyclooxygenases (Cox) catalyze key steps that eventually lead to substrates for prostaglandin synthases. Prostaglandin synthases subsequently catalyze reactions that terminate in production of prostaglandins and eicosanoids. Importantly, prostaglandins regulate a diverse array of physiological responses including immune modulation and maintenance of vascular tone [298]. There are three isoforms

of Cox, Cox-1, -2, -3; each perform similar functions, but vary in their expression characteristics. Cox-1 and Cox-3 are constitutively expressed while Cox-2 can be upregulated by pro-inflammatory cytokines and growth factors [299]. The upregulation of Cox-2 is recognized as a tumor promotion event in colorectal cancer and has also been shown to be upregulated in *H. pylori*-induced premalignant and malignant gastric lesions [300-306]. Previous studies have shown that *H. pylori* can induce gastric epithelial cell expression of Cox2 in a TLR2/TLR9 dependent manner [305, 306]. Further, TLR2/TLR9 signaling in gastric epithelial cells was observed to induce MAPKs and subsequently allow transcription factor binding to both the CRE and AP-1 sites within the Cox2 promoter. As a result of Cox2 expression, prostaglandin E_2 is released which promotes gastric cancer cell invasion and angiogenesis [305]. The pro-carcinogenic potential of *H. pylori*-TLR9 interactions were extended by studies in which purified *H. pylori* DNA induced invasion of gastric epithelial cells *in vitro*, an effect that could be partially reduced with the endosomal inhibitor chloroquine [307]. Additionally, murine models of *H. pylori* infection have demonstrated TLR9 detects *H. pylori in vivo* and induces pro-inflammatory responses [255]. Finally, polymorphisms in the *TLR9* gene have also been shown to increase the risk for development of both premalignant and malignant gastric lesions [47, 64].

Despite the evolutionary homology of the *cag* T4SS to the archetypal *Agrobacterium tumefaciens* T4SS [308], DNA translocation by the *H. pylori cag* system had previously never been demonstrated. Consequently, considering the aforementioned evidence linking TLR9, gastric cancer, and *H. pylori* infection, Varga et al. set out to define *H. pylori*-TLR9 interactions to determine the mechanism by which *H. pylori* could engage this receptor [117]. To determine whether the *cag* T4SS is required for direct DNA delivery into host cells *H. pylori* DNA was labeled with BrdU and bacteria were subsequently co-cultured with AGS cells. Using this

technique, bacterial DNA could be easily distinguished from host DNA via incorporation of BrdU. Structured illumination microscopy demonstrated that wild-type *H. pylori* translocated BrdU-labeled DNA into host cells **(Figure 9A)** However, intracellular BrdU-labeled DNA was not observed in host cells infected with the *H. pylori cagE*$^{-}$ mutant **(Figure 9A)**. To confirm and quantify these results using an independent methodology, host intracellular levels of BrdU-labeled *H. pylori* DNA were assessed via flow cytometry. Levels of intracellular DNA were significantly increased in *H. pylori* wild type-infected compared to uninfected AGS cells. A significant reduction was observed in cells infected with the *cagE*$^{-}$ mutant compared to wild-type infected AGS cells **(Figure 9B)**.

Accordingly, these data demonstrated that *H. pylori* utilizes the *cag* T4SS to translocate microbial DNA into eukaryotic cells. Therefore, our laboratory investigated the role of the *cag* T4SS in mediating TLR9 activation. HEK293-TLR9 reporter cells, which are inherently devoid of most innate immune receptors except for transfected TLR9, were challenged with either wild-type strain J166, a *comB*$^{-}$ mutant (which attenuates DNA uptake in an additional *H. pylori* T4SS), a *pgdA*$^{-}$ mutant (which reduces peptidoglycan-mediated NOD1 activation [272]), an isogenic *cagA*$^{-}$ mutant (which lacks the effector protein CagA), or *cagE*$^{-}$ or *cagY*$^{-}$ mutants (which encode essential proteins for T4SS assembly). Loss of *comB, pgdA, or cagA* had no effect on TLR9 activation; however, *cagE*$^{-}$ or *cagY*$^{-}$ mutants were incapable of activating TLR9 **(Figure 9C)**.

These experiments indicated that a functional *H. pylori cag* T4SS is required for DNA translocation and subsequent TLR9 activation, but other known effector molecules translocated by this system (CagA and peptidoglycan) were dispensable for this phenotype. Additionally, human patient *H. pylori* strains were isolated from distinct high and low gastric cancer risk regions in Colombia and analyzed for their ability to activate TLR9 *in vitro*. The disparity in cancer risk but

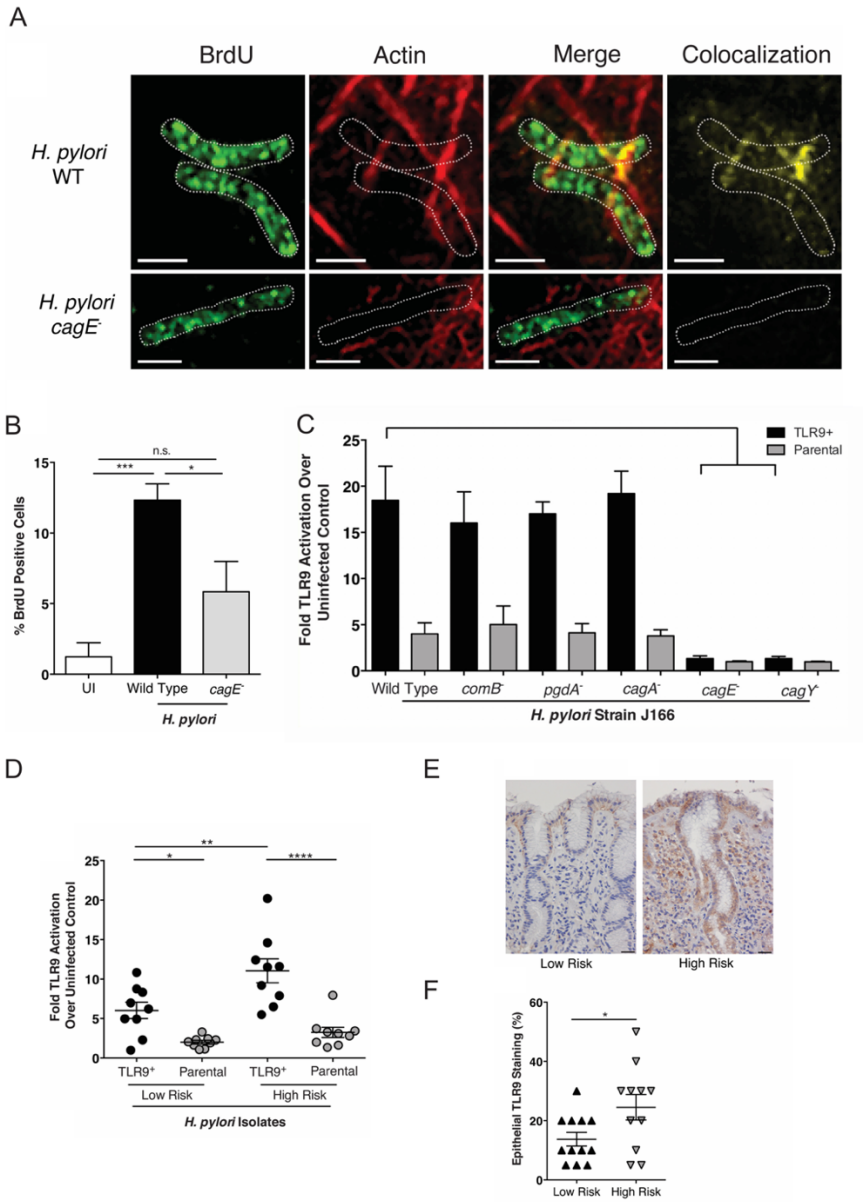

Figure 9. *H. pylori* strains translocate DNA and activate TLR9 via the *cag* T4SS. (A) *H. pylori* translocates DNA into host cells via the *cag* T4SS. *H. pylori*-mediated DNA translocation was assessed by structural illumination microscopy using AGS cells co-cultured with BrdU-labeled *H. pylori* strain J166. Images were probed for evidence of host intracellular BrdU staining (upper panels) and compared to the J166 cagE- (lower panels). Scale bar, 1µm. BrdU, green; actin, red; merge, yellow. *H. pylori* are outlined by dotted white lines. **(B)** BrdU-labeled *H. pylori* strain J166 or the *cagE*- mutant were co-cultured with AGS cells and then subjected to flow cytometry to assess levels of host intracellular BrdU. Each strain was tested at least 3 times. Mean±SEM are shown. *p<0.05, ***p<0.001. **(C)** *H. pylori* activation of TLR9 requires a functional *cag* T4SS. TLR9 activation induced by *H. pylori* strain J166 or its isogenic mutants (MOI 100), relative to uninfected control. Each strain was tested in duplicate in at least 3 independent experiments. Mean±SEM are shown. ****p<0.0001. **(D)** *H. pylori* activation of TLR9 in a human population. TLR9 activation by *H. pylori* isolates obtained from patients residing in a low or high gastric cancer risk regions of Colombia. Data are expressed as fold over uninfected control. n=9 isolates per group, each strain was tested in duplicate at least 3 times. Mean±SEM are shown. **(E)** Representative immunohistochemical staining for TLR9 in gastric biopsies. Magnification 40x; Scale bar, 50µm. Epithelial TLR9 staining of biopsies obtained from patients in the low (n=11) and high (n=12) gastric cancer risk regions of Colombia is quantified in (F). *p<0.05, **p<0.01, ****p<0.0001. **(A-F)** reprinted with permission from [117].

not *H. pylori* prevalence observed in these regions allowed our laboratory to further define links between both microbial and host determinants that play a role in carcinogenesis. *H. pylori* strains isolated from the high-risk region induced significantly higher levels of TLR9 activation compared to strains harvested from patients in the low-risk region **(Figure 9D)**. To determine whether the ability of high-risk *H. pylori* isolates to activate TLR9 *in vitro* translated into the more biologically relevant gastric niche, levels of epithelial TLR9 expression in gastric biopsies obtained from infected patients were quantified. Gastric epithelial TLR9 expression levels were significantly increased in high-risk region patients compared to the low-risk region **(Figure 9E,F)**, mirroring the *in vitro* data. Collectively, these results indicated that *H. pylori* strains linked to an increased risk for gastric cancer induce greater TLR9 activation *in vitro* and enhanced expression *in vivo.*

TLR9's auxiliary anti-inflammatory response has been demonstrated during the acute phase of *H. pylori* infection, which is mediated by type I IFNs [309], and purified *H. pylori* DNAs have been shown to alleviate DSS-induced colitis in mouse models [76, 77]. Our laboratory similarly demonstrated a protective effect for TLR9 *in vivo* in response to *H. pylori* infection **(Figure 10)** [119]. Varga et al. infected C57BL/6 wild type (WT) or *Tlr9*$^{-/-}$ mice with either the *cag*$^{+}$ *H. pylori* strain PMSS1, a PMSS1 *cagE*$^{-}$ isogenic mutant, or uninfected (Brucella Broth) control. Six weeks post infection, mice were sacrificed, and stomachs were harvested. A significant increase in the severity of inflammation was observed in *H. pylori*-infected *Tlr9*$^{-/-}$ mice versus infected wild-type mice **(Figure 10A,B)**. As expected, levels of inflammation were *cag*-dependent, as the *cagE*$^{-}$ mutant induced significantly less inflammation compared to the wild-type *H. pylori* strain, in both WT and *Tlr9*$^{-/-}$ mice **(Figure 10A,B)**.

Collectively, these data highlight the dual role of TLR9 during *H. pylori* infection. *H. pylori* may utilize TLR9 signaling to dampen the inflammatory response during the acute phase to

establish infection. However, in an inflammatory microenvironment in which cells have lost their polarity, TLR9 may execute pro-inflammatory cascades and further exacerbate the progression towards gastric cancer. Chapter II will explore TLR9 modulation by *H. pylori* further in which both pro- and anti-inflammatory responses are linked to a particular *cag*-associated bacterial adhesin, HopQ.

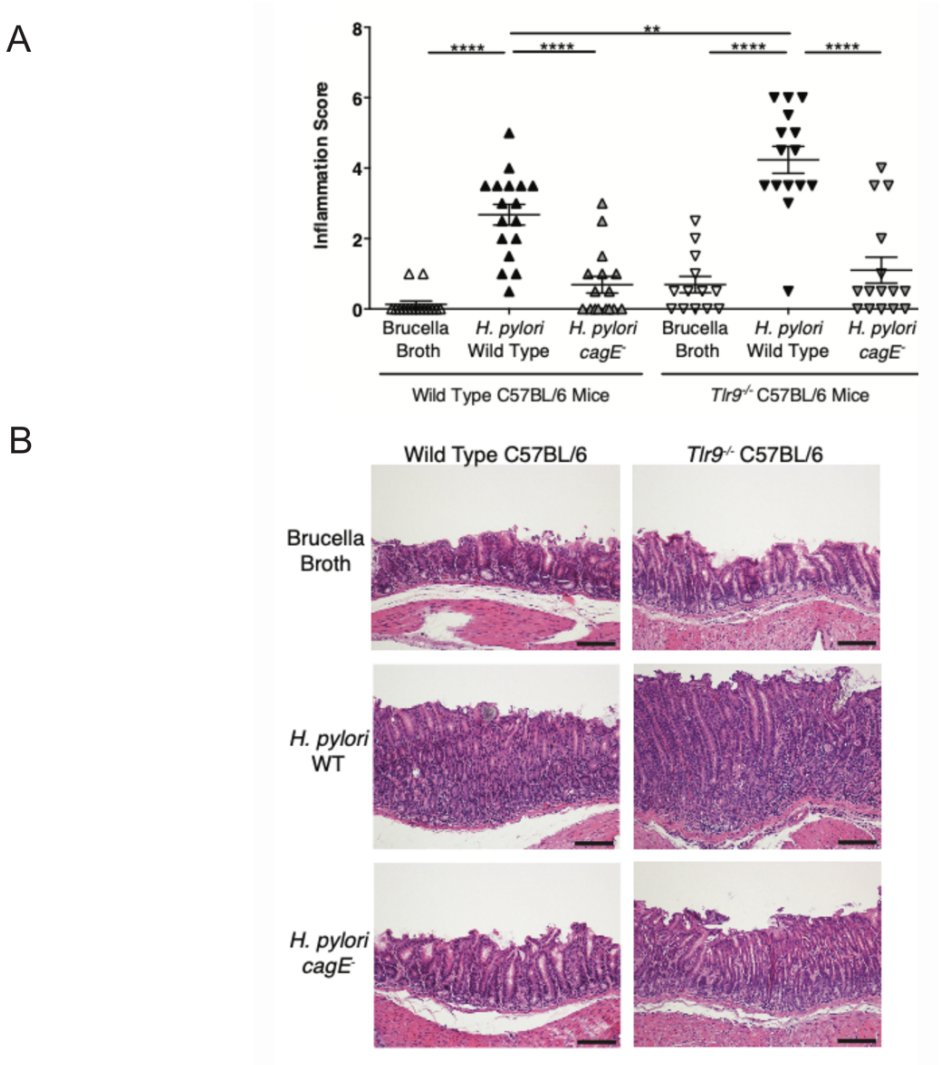

Figure 10. Loss of *Tlr9* exacerbates *H. pylori*-induced inflammation *in vivo*. C57Bl/6 wild type (WT) or *Tlr9*$^{-/-}$ mice were challenged with either uninfected (Brucella Broth) control, the mouse-adapted, *cag*$^{+}$ *H. pylori* strain PMSS1, or the PMSS1 isogenic *cagE*$^{-}$ mutant for 6 weeks. **(A)** Inflammation scores of WT or *Tlr9*$^{-/-}$ mice infected with or without *H. pylori*. Each data point represents the inflammation score of an individual animal. Two independent experiments were performed. n=13-17 mice per group, Mean±SEM are shown. **p<0.01,****p<0.0001. **(B)** Representative H&E images of infected or uninfected WT and *Tlr9*$^{-/-}$ mice at 20x magnification. Scale bar, 100 µm. **(A-B)** reprinted with permission from [119].

1.11. STING Regulation and Signaling

Aberrant nucleic acids in the cytosol are powerful activators of the innate immune system and can include non-self-DNA, derived from pathogens including viral and bacterial DNA and RNA, or self-DNA which includes damaged mitochondrial DNA (mtDNA), leaked/damaged nuclear DNA from chromosome instability, cytosolic DNA in micronuclei and from cell debris [310]. While DNA can be rapidly detected by endosomal TLR9, including translocated *H. pylori* DNA as discussed in the preceding section, another large family exists that detect cytoplasmic nucleic acids in virtually all types of host cells [311, 312]. These sensors include absent in melanoma 2 (AIM2) [313-315], interferon-inducible protein 16 (IFI16) [316], interferon-inducible protein X (IFIX) [317], and myeloid nuclear differentiation antigen (MNDA) [318]. Other sensors linked to cytosolic DNA detection include DNA-dependent activator of IRFs (DAI) [319], LRR binding FLII interacting protein 1 (LRRFIP1) [320], RNA polymerase III [321, 322], Ku70 and Ku80 [323, 324], DExD/H box helicases (DDX41) [325], meiotic recombinations 11 homolog A (MRE11) [326]. As previously mentioned, TLR9 can produce dual downstream responses which include production of type I IFNs and cytosolic nucleic acid sensors primarily lead to the production of type I IFNs/inflammatory cytokines as well. However, distinct from the sensors that stimulate IFN production, AIM2 activation in macrophages triggers the inflammasome, leading to caspase 1-dependent secretion of IL-1β [265].

While those PRRs are cell-type or DNA-sequence specific [327, 328], one additional cytosolic DNA sensor, cyclic GMP-AMP synthase (cGAS), is activated in response to double-stranded DNA in a sequence-independent manner [329-331]. Primarily thought to be a cytoplasmic protein, recent work has found that cGAS is more ubiquitous than previously understood. cGAS was reported to bind the plasma membrane to regulate its activity and prevent overactivation from

self-DNA [332] and other studies demonstrated that cGAS resides predominantly in the nucleus but is prevented from activation until translocation to the cytoplasm [333-335]. While either self- or non-self-DNA can cause cGAS activation following binding, the length of the DNA is important [310]. Short DNAs (~20bp) can bind to cGAS, but longer dsDNAs (~45bp) can form more stable ladder-like networks of cGAS dimers, leading to stronger enzymatic activity [334, 336].

Binding of DNA ligands to cGAS catalyzes the conversion of ATP and GTP into the dinucleotide 2',3'-cyclic GMP-AMP (cGAMP) which as a second messenger, directly activates stimulator of interferon genes (STING), a DNA sensor/adaptor protein localized to the endoplasmic reticulum (ER) **(Figure 11)** [311, 312, 337]. cGAS as well as DAI, RNA polymerase III, AIM2, and IFI16 primarily result in type I IFN production via convergence at STING [311]. In its resting state, STING is localized at the ER membrane but following cGAMP binding, the ligand-binding domain of STING closes, eliciting a conformational shift and its polymerization, and its translocation to the Golgi [338-341]. In the Golgi, STING is palmitoylated, which contributes to its activation [342]. The exact function of palmitoylation is still unclear, but it has been demonstrated that palmitoylation of STING also aids its polymerization, which is necessary for recruiting TANK-binding kinase 1 (TBK1) and scaffolding the interaction between TBK1 and IRF3 [343, 344]. In canonical STING signaling, this recruited TBK1, subsequently phosphorylates STING [345, 346]. Phosphorylated STING recruits the transcription factor interferon regulatory factor 3 (IRF3) for phosphorylation by TBK1, which is then mobilized to the nucleus to induce expression of type I IFNs (*e.g.*, IFNα, IFNß) **(Figure 11)** [347]. Ultimately, type I IFNs can induce IFN-stimulated genes (ISGs) expression through the janus kinases (JAKs)-signal transducer and activator of transcription (STAT) signaling pathways [348, 349]. In parallel, STING also activates IKK complexed with TAK1 to mediate the induction of NF-κB-driven inflammatory genes [330,

350]. In addition, recent work has demonstrated STING directly interacts with the autophagy initiator protein LC3 to induce non-canonical activation of autophagy to clear DNA from the cytosol [351].

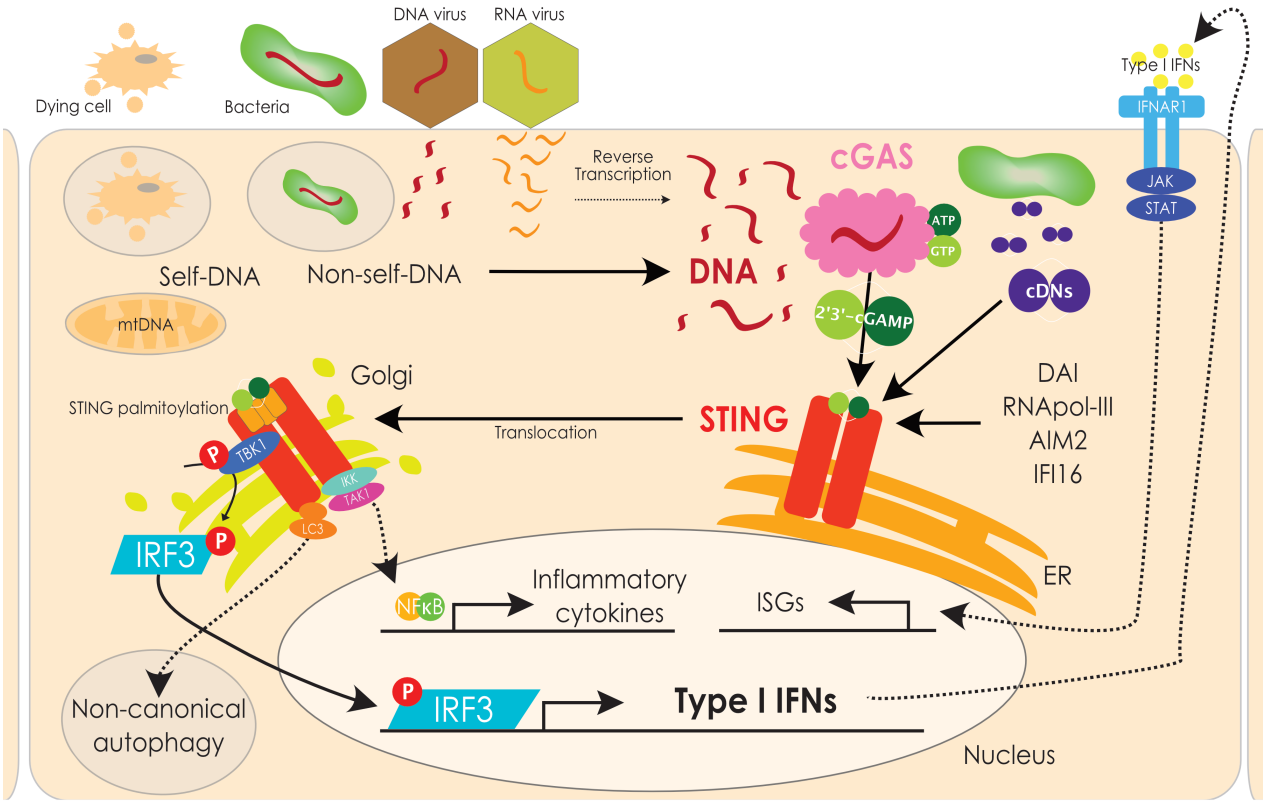

Figure 11. Overview of STING signaling. Cyclic GMP-AMP synthase (cGAS) is a cytosolic DNA sensor, which is activated in response to double-stranded DNA in a sequence-independent manner. Binding of DNA ligands to cGAS catalyzes the conversion of ATP and GTP into the dinucleotide 2',3'-cyclic GMP-AMP (cGAMP). cGAMP, as well as other cytosolic DNA sensors, can directly activate *st*imulator of *in*terferon *g*enes (STING), a DNA sensor/adaptor localized to the endoplasmic reticulum (ER). STING can also be directly activated in a cGAS-independent mechanism by cyclic dinucleotides secreted by bacteria. Sensing of cyclic dinucleotides induces a conformational change in STING that triggers trafficking of STING complexed with TANK-binding kinase 1 (TBK1) from the ER to endosomal/lysosomal compartments. Translocated TBK1 leads to phosphorylation and activation of the transcription factor interferon regulatory factor 3 (IRF3), which is then mobilized to the nucleus to induce expression of type 1 interferons (IFN) (*e.g.*, IFNα, IFNß). In parallel, STING also activates NF-κB and can induce non-canonical autophagy. Type I IFNs can activate JAK-STAT signaling and induce expression of interferon stimulated genes (ISG).

Of great interest to this dissertation, STING is expressed in gastric epithelial cells. Furthermore, STING expression in gastric cancer is significantly decreased in tumor versus non-tumor tissue, and low expression is associated with reduced survival [352]. There is precedent for direct STING activation by bacteria, occurring in a cGAS-independent mechanism by secreted cyclic dinucleotides [353-356]. Some of these pathogens have adapted to benefit from STING activation during infection. For example, the intracellular bacterium *Listeria monocytogenes* secretes cyclic di-AMP directly into the cytosol of a host cell, which binds and drives activation of STING, which resulted in suppressed development of T-cell mediated adaptive immunity to *L. monocytogenes* by an unknown mechanism [357]. STING's role in viral and bacterial infections is rapidly being explored but data from *L. monocytogenes* suggest other pathogens may deliberately manipulate STING for their own benefit as well, embracing and modulating signaling to promote persistence in the host.

1.12. Evasion of cGAS-STING Immunity by Chronic Pathogens

While some microbes activate cGAS-STING, certain chronic pathogens have developed strategies to evade cGAS-STING-mediated immune clearance, establish infection, and induce disease [311, 312, 358, 359]. Some pathogens target cGAS directly **(Figure 12A)**, such as herpes simplex virus 1 (HSV-1) and human cytomegalovirus (HCMV) which both encode proteins, VP22 and UL83 respectively, that bind cGAS and block downstream signaling [360, 361]. cGAS can also be targeted via post-translational modification, resulting in impaired 2′3′-cGAMP synthesis, a mechanism an additional HSV-1 protein, UL37 utilizes [362]. HCMV expresses two additional proteins which interfere with cGAS-DNA binding and resulting oligermization, UL31 and UL42 [363, 364]. Kaposi's sarcoma-associated herpesvirus (KSHV) also encodes a protein that inhibits

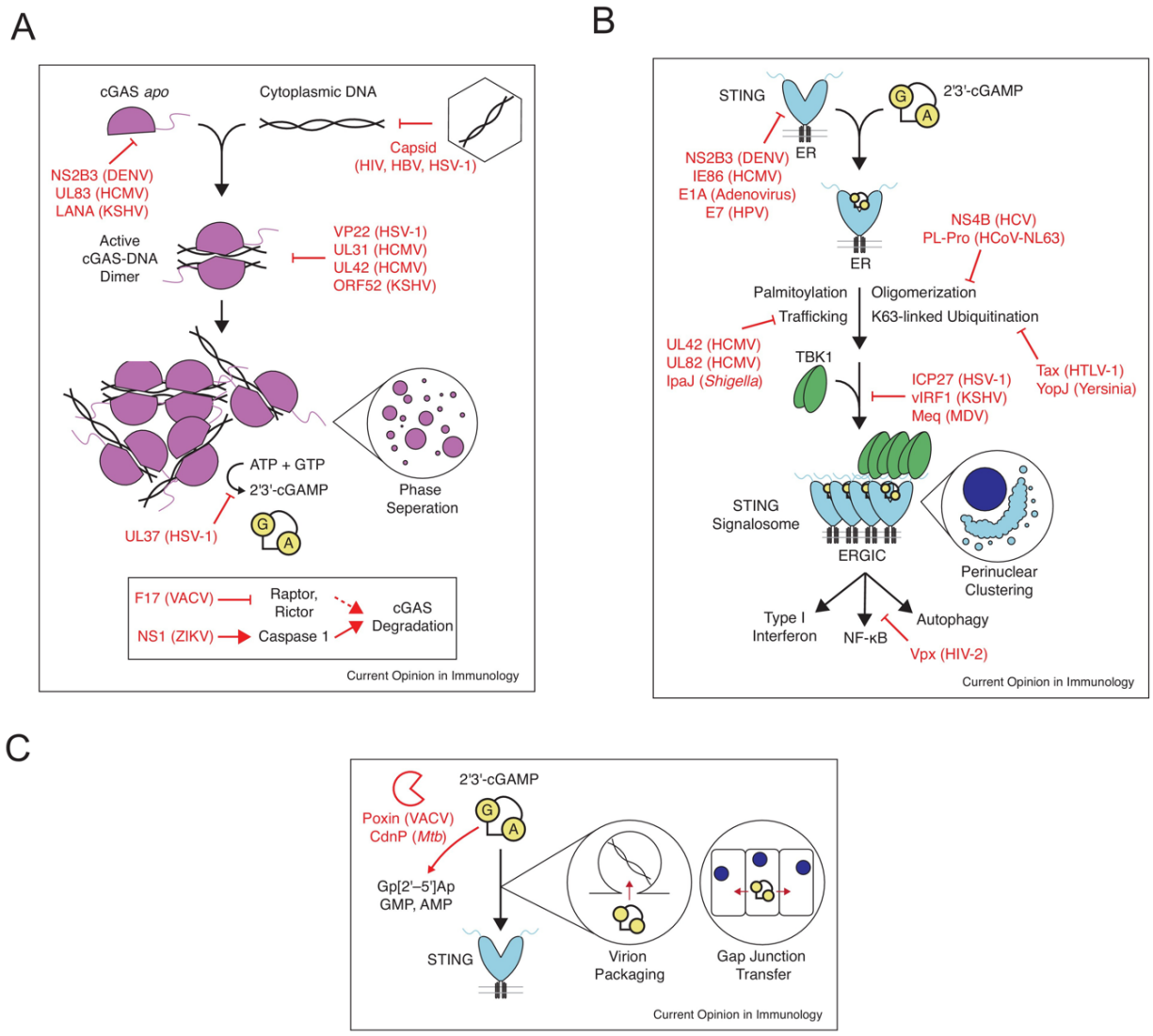

Figure 12. Mechanisms of cGAS-STING evasion by pathogens. (A) Pathogen factors block cGAS activation. Upon DNA binding, cGAS undergoes a conformational change activating 2′3′-cGAMP synthesis. Assembly into a minimal 2:2 complex is required for catalytic activity, but further assembly into long DNA ladder structures and larger oligomers bridged by interactions with the unstructured N-terminus results in formation of phase-separated liquid droplets. ATP and GTP are converted in a two-step process to 2′3′-cGAMP within the cGAS active site, which is released into the cytosol and diffuses throughout the cell. Red text and arrows indicate steps in this process at which different viral and bacterial factors prevent or interfere with signaling. The box at the bottom indicates indirect viral strategies which trigger cGAS degradation. **(B)** Pathogen strategies for restriction of STING signaling. STING binding to 2′3′-cGAMP triggers a conformational change which drives STING oligomerization and assembly into a signalosome complex through palmitoylation, oligomerization, ER to ERGIC trafficking, and ubiquitination. The downstream kinase TBK1 is recruited into the STING signalosome, driving trans-phosphorylation and activation of this kinase to promote downstream IRF3 binding and activation of type I interferon signaling. STING also stimulates NF-κB and autophagy signaling to restrict pathogen replication. Red text and arrows show steps at which pathogens intervene to prevent activation of downstream signaling by STING. **(C)** Viral and bacterial enzymes degrade 2′3′-cGAMP. The second messenger 2′3′-cGAMP is highly stable in the mammalian cytosol. 2′3′-cGAMP can be packaged within budding virions to activate STING in newly infected cells or spread cell-to-cell through gap junctions to activate bystander immunity in neighboring uninfected cells. Viral and bacterial enzymes degrade 2′3′-cGAMP in order to prevent binding to STING, and activation of downstream immune signaling. **(A-C)** reprinted from [359], under the terms of the Creative Commons Attribution 4.0 license.

cGAS, ORF52 [365]. ORF52 blocks cGAS activation through a mechanism which requires ORF52 to bind both cGAS and DNA. The KSHV LANA protein has also been shown to bind cGAS and block downstream signaling [366].

Disruption of the immune response occurs via inhibition of STING as well **(Figure 12B)**, including HCMV IE86 degradation of STING [367] and Hepatitis C virus NS4B interference with STING oligomerization [368, 369]. Another HCMV protein UL82, disrupts STING trafficking from the ER [370]. Likewise, HCMV UL42, along with its role in antagonizing cGAS oligomerization, is reported to block STING trafficking [364]. The KSHV vIRF1 protein blocks recruitment of TBK1 for activation by STING [371]. Mareck's disease virus is an avian oncogenic herpesvirus, and its oncoprotein Meq functions in a similar way, blocking recruitment of TBK1 to STING in chicken cells [372]. Additional carcinogenic DNA viruses human adenovirus 5 and human papillomavirus (HPV) 18 and their respective oncoproteins E1A and E7, have also been shown to bind and antagonize STING [358]. Further down the STING signaling cascade, HSV-1 ICP27 associates with the active STING/TBK1 complex and prevents IRF3 recruitment and phosphorylation to block the downstream type I IFN response [373].

Moreover, viral poxins abrogate STING signaling through degradation of cGAMP **(Figure 12C)**. VACV and similarly related poxviruses encode a nuclease called poxvirus immune nuclease (poxin) which degrades 2′3′-cGAMP to prevent activation of the cGAS–STING pathway [374]. The *Mycobacterium tuberculosis* CdnP enzyme can act on both host 2′3′-cGAMP and bacterial cyclic di-AMP, suggesting it may serve a dual function in infection to prevent host recognition of the bacterial cyclic di-AMP and degrade host 2′3′-cGAMP to limit the host response [375]. This wide repertoire of antagonists targeting the cGAS-STING pathway underscores the importance of

evolutionary pressures that select for pathogens that suppress innate immunity, evade detection, and possibly promote malignancy.

1.13. STING and Cellular Responses with Carcinogenic Potential

STING represents a critical role in the host defense against pathogens. Whereas the role of STING in human carcinogenesis is not yet fully understood, recent studies indicate that it exerts a crucial role in antitumor responses. STING activation has been shown to limit early neoplastic progression through recognition of self-DNA derived from damaged and dying cells [376, 377] and via its upregulation of a battery of inflammatory genes, namely type 1 IFNs, which stimulate tumor-specific T cells and natural killer (NK) cells [378, 379]. Also, independent of enhanced anti-cancer immunity, cGAS-STING pathway can directly activate senescence and apoptosis signaling pathways in cancer cells [380, 381]. As described in the previous section, chronic pathogens such as oncogenic DNA viruses utilize multiple mechanisms to abrogate STING signaling and, similarly, cancer cells also silence the cytosolic DNA sensing pathway to evade immune surveillance and drive pro-tumorigenic pathways. Decreased protein expression of cGAS and STING has been shown to be present in late-stage tumors, including gastric cancer [352, 382, 383]. Likewise, a pan-cancer analysis revealed that some tumors contain increased methylation in the promoters of cGAS and STING compared to matched normal tissues [384]. Suppression of STING in prostate and melanoma cancer cells leads to reduced immune infiltration and increased tumor growth [385, 386], and poor patient survival is associated with reduced cGAS and STING expression [352, 387].

In models of inflammation with premalignant potential such as chronic pancreatitis, inhibition of STING worsens disease via upregulation of IL-17A [388], which is a known promoter

of inflammation-induced malignancies including pancreatic cancer, colitis-associated carcinoma, and skin cancer [389-391]. Furthermore, during *H. pylori* infection, IL-17A is significantly upregulated **(Figure 13A)** and stimulates pro-inflammatory effects, such as neutrophil infiltration through IL-8 stimulation [392, 393]. Data from our own laboratory have demonstrated that in addition to IL-17A, the chemokines MIP-3α and IL1β, which can recruit and induce differentiation of Th17 cells respectively, are significantly upregulated following *H. pylori* infection **(Figure 13A)** and acute inflammation in *H. pylori* infected *Il-17a*$^{-/-}$ mice is significantly reduced **(Figure 13B)**. Further interrogation of infected mice, gerbil, and human tissues revealed increased expression of IL-17A and its associated cytokines **(Figure 13C,D,E)**. Of great interest to this dissertation, IL-17 production is exacerbated in the absence of TLR9 **(Figure 13F)** [119], possibly bridging nucleic acid sensors to this key driver in gastric carcinogenesis [394-397].

Direct links between STING and gastric cancer are limited at the present time. Song et al. observed STING expression in human patients is significantly decreased in tumor versus non-tumor tissue, and low expression is associated with reduced survival. Additionally, STING downregulation also promoted the carcinogenic responses of gastric cancer cells *in vitro* [352]. However, in another study utilizing macrophages *in vitro* instead of epithelial cells, Miao, Qi, Zhao, et al. demonstrated STING activation promoted a pro-inflammatory subtype and induced apoptosis [398]. Yang et al. have recently attempted to develop a cGAS-STING pathway-related genes prediction model to predict prognosis in gastric cancer patients via RNAseq. Their model however narrowly analyzes expression of the downstream targets *IFNB1*, *IFNA4*, *IL6*, *NFKB2*, and *TRIM25* in lieu of STING directly [399]. These data involving STING and gastric cancer are inconsistent, appear to be cell-specific, and almost exclusively do not account for *H. pylori* infection in assays. Further studies will be required to elucidate STING's current ambiguous role

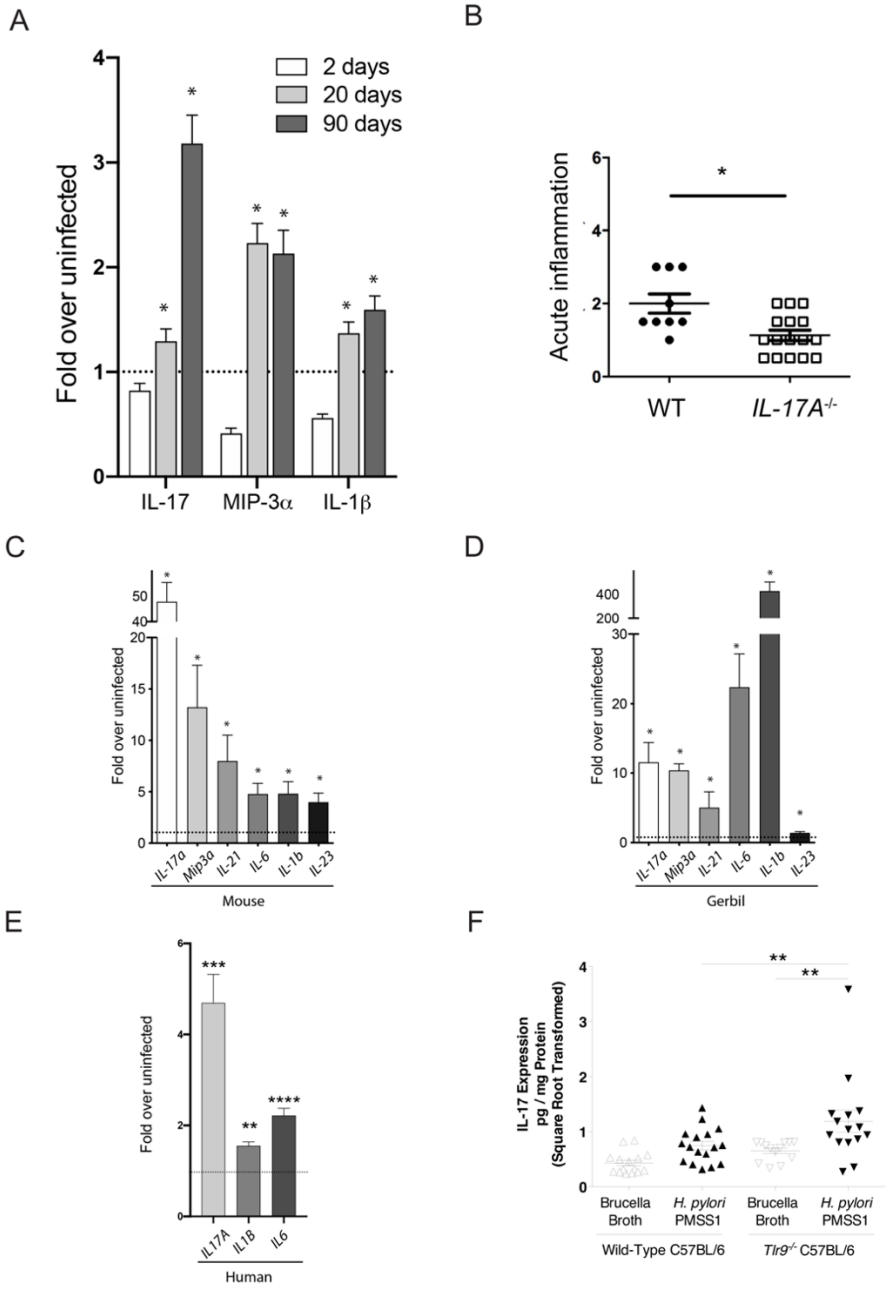

Figure 13. Th17 responses to *H. pylori* infection. (A) Gastric mucosal protein expression levels of cytokines in uninfected (n=12, 11, 7 at 2, 20 and 90 days, respectively) and *H. pylori*-infected (n=9, 11, 10 at 2, 20 and 90 days, respectively) WT C57BL/6 mice. Data are expressed as relative expression of infected to uninfected mice. Dotted line represents a baseline of 1. **(B)** WT C57Bl/6 or *Il-17A*$^{-/-}$ mice were infected with *H. pylori* PMSS1 and acute inflammation was scored 0-6 twelve weeks post-challenge. Each data point represents one individual animal. **(C,D)** Quantification of cytokine mRNA expression by real-time RT-PCR using RNA isolated from mouse **(C)** or gerbil **(D)** gastric tissue. Data are expressed as relative expression of *H. pylori* infected (n=18) to uninfected (n=6) mice or infected (n=10) to uninfected (n=10) gerbils. **(E)** Quantification of cytokine expression by real-time RT-PCR using RNA isolated from human gastric antral biopsies from *H. pylori*-infected Colombian patients with gastritis or uninfected persons. Data are expressed as relative expression of infected (n=23) to uninfected (n=11) samples. Dotted line represents a baseline of 1. **(F)** IL-17 expression in uninfected (n=15) and infected (n=17) WT C57BL/6 or *Tlr9*$^{-/-}$ murine gastric mucosa was determined by cytokine and chemokine array, and results are represented as picograms per milligram of protein (square root transformed). *, $p<0.05$; **, $p<0.01$; ***, $p<0.001$; ****, $p<0.0001$.

in gastric carcinogenesis.

Overall, these data have sparked the development of novel STING agonists that are being tested in clinical trials [312]. For example, in preclinical work utilizing murine gastric cancer cell lines, Hong et al. has recently suggested a potential therapeutic approach involving radiation therapy combined with immunotherapy to prime the immune system to eliminate cancer cells. They observed increased STING signaling following irradiation, increased immune cell invasion, and improved immunotherapy response [400]. Collectively, these data raise the exciting possibility that STING activation may not only improve cancer therapies but may also augment effectiveness of regimens targeting *H. pylori*.

1.14. Dissertation Summary and Goals

Chronic infection with the bacterial carcinogen *Helicobacter pylori* incurs the highest known risk for gastric cancer [53]. With an overwhelming majority of gastric cancer burden and 5.5% of all malignancies worldwide attributable to *H. pylori*-induced injury, gastric adenocarcinoma remains the fourth leading cause of cancer-related death worldwide [56]. In 2020 alone, gastric cancer was responsible for over one million new cases, and an estimated 769,000 deaths (equating to one in every 13 deaths globally) [37]. The prevalence of *H. pylori* infection is extraordinarily high, infecting greater than 50% of the world's population. However, less than 5% of infected hosts will develop cancer [22, 33]. Environmental factors, *H. pylori* strain differences, inflammatory responses governed by host genetic diversity, and/or specific interactions between host and microbial factors have been implicated in enhanced cancer risk. Delineating these distinct interactions which disrupt the delicate host-microbe homeostasis constitute the goals of this thesis and are imperative to identify mechanisms that influence oncogenesis.

Chapter II explores the capacity of bacterial constituents to promote gastric injury, specifically the virulence associated adhesin HopQ and its role in activating TLR9. Through the screening of a large cohort of *H. pylori* strains derived from human clinical specimens, I demonstrate that genetically distinct families of *hopQ* alleles were significantly associated with magnitude of gastric injury, *cag* T4SS function, and TLR9 activation. Additionally, I further define the role of HopQ in TLR9 activation by genetic deletion of *hopQ*, which significantly decreased *H. pylori*-induced TLR9 activation, implicating this adhesin in *H. pylori*-mediated disease. Chapter III further explores the hypothesis that *H. pylori* selectively activates nucleic acid PRRs, such as TLR9, to regulate the inflammatory response and evade immune clearance. Utilizing *in vitro* and *ex vivo* experiments, I identify a novel mechanism through which *H. pylori* actively suppresses STING and RIG-I-signaling via downregulation of IRF3. I reveal through a *Sting*-deficient mouse infection model that Th17 inflammatory responses to *H. pylori* are augmented within the context of *Sting*-deficiency in conjunction with induction of a known host immune regulator, TRIM30a. Finally, I uncover significant upregulation of TRIM30a homologs in samples harboring inflammation or cancer via examination of human gastric cancer samples. These novel mechanisms of innate immune suppression by *H. pylori* are likely a component of a finely tuned rheostat that *H. pylori* regulates to control the inflammatory response and maintain persistence in the host, and ultimately drive long-term carcinogenic pathways such as increased Th17 activation **(Figure 14)**.

The observations made in this dissertation demonstrate that *H. pylori* harbors a portfolio of mechanisms to manipulate the host immune response towards a tolerogenic phenotype to a chronic pathogen with oncogenic potential, which can manifest as activation of specific nucleic acid PRRs such as TLR9, active suppression of certain innate immune responses such as STING and RIG-I,

or induction of host immunomodulators, TRIM proteins. These data highlight the importance of identifying oncogenic constituents that regulate interactions of *H. pylori* with its host to promote carcinogenesis, provide mechanistic insights into other malignancies that arise within the context of inflammatory states (e.g. ulcerative colitis and colon cancer), and unveil novel strategies to prevent or treat pathologic outcomes induced by *H. pylori* infection.

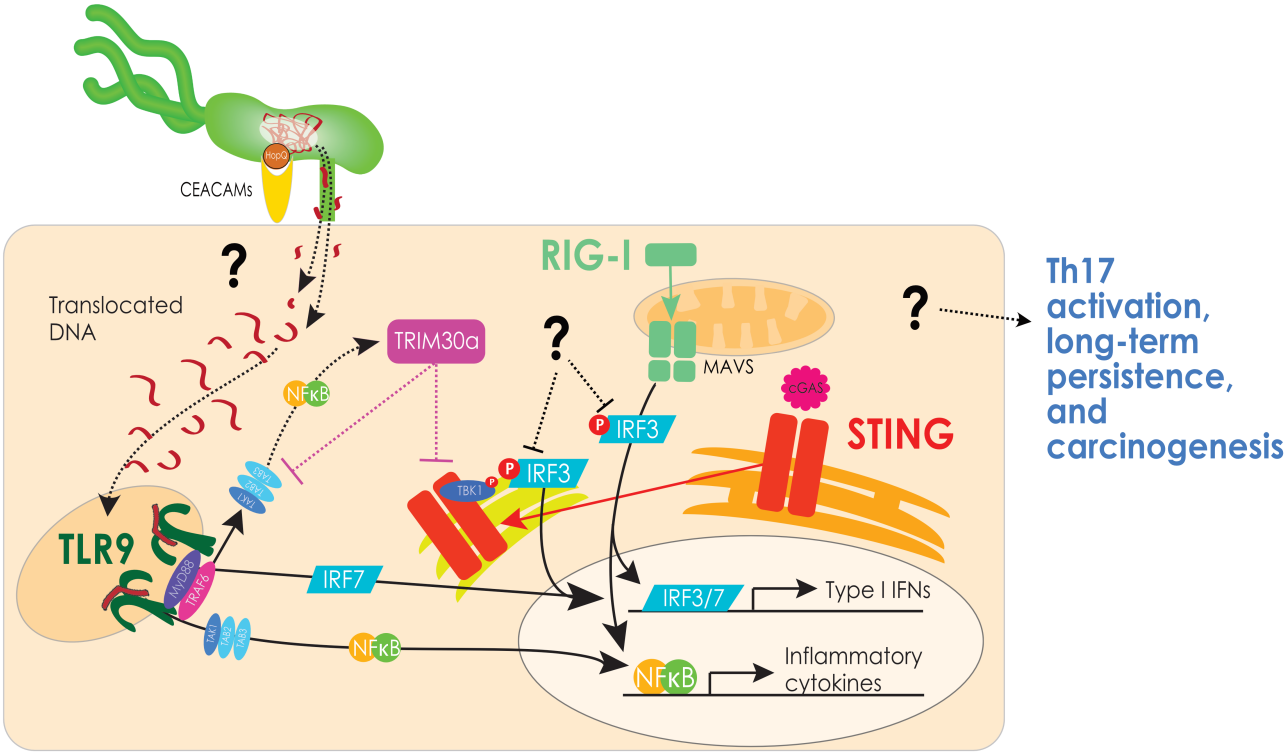

Figure 14. Dissertation overview. Proposed mechanism of *H. pylori* activation and suppression of innate immune signaling within gastric epithelial cells.

CHAPTER II

HELICOBACTER PYLORI-INDUCED TLR9 ACTIVATION AND INJURY ARE ASSOCIATED WITH THE VIRULENCE-ASSOCIATED ADHESIN HOPQ

This chapter is an adaptation of the following publication:
Dooyema SDR et al. (2021) "*Helicobacter pylori*-induced TLR9 Activation and Injury Associates with Allelic Status of the Virulence-Associated Adhesin HopQ" *The Journal of Infectious Diseases*. PMID: 33245103. [199]

2.1 Introduction

Helicobacter pylori incurs the highest known risk for developing gastric cancer [63], yet only 1–3% of infected individuals develop gastric adenocarcinoma [35]. One strain-specific *H. pylori* oncogenic determinant is the *cag* PAI which encodes a T4SS. The *cag* T4SS translocates effectors, such as CagA, peptidoglycan, HBP, and DNA into epithelial cells [117, 121]. Translocated DNA subsequently activates TLR9 and *H. pylori* strains that confer a higher risk for gastric cancer are more potent in their ability to activate TLR9 [117]. However, the precise molecular mechanisms regulating *H. pylori*-dependent TLR9 activation remain incompletely defined.

Most persons colonized with *cag* PAI$^+$ strains do not develop gastric cancer, raising the hypothesis that other *H. pylori* constituents may also affect disease risk. The outer membrane protein HopQ, which binds human CEACAM receptors, has been reported to facilitate CagA translocation [188, 201]. *H. pylori hopQ* exhibits a high level of diversity, and two genetically distinct families of *hopQ* alleles (type I and type II) have been previously described [196]. Type I alleles are present significantly more frequently in *cagA*$^+$ versus *cagA*$^-$ strains [196], suggesting

that HopQ may represent a microbial component that can regulate DNA translocation and TLR9 activation and play a role in disease.

2.2 Materials and Methods

Clinical Specimens

Gastric antral biopsies were collected for culture and immunohistochemistry [401]. Patients were prospectively enrolled after written informed consent and the study was approved by the institutional review boards of Vanderbilt University and the Nashville Department of Veterans Affairs. Histologic parameters were scored from 0-3 as outlined by the Sydney System [401].

Bacterial Strains

H. pylori cag PAI^{+} strain 26695 (which contains a single type I *hopQ* allele) [198], isogenic mutants, and clinical isolates were maintained on trypticase soy agar plates with 5% sheep blood (Hemostat Laboratories). Allele-specific PCRs were used to type *hopQ* [196] and stratify strains into *hopQ* allelic categories based on detection of type I alleles, type II alleles, or both. A kanamycin resistant 26695 *cagE*$^{-}$ mutant [117], which lacks functional *cag* T4SS activity, and a chloramphenicol (Cm) resistant 26695 *hopQ*$^{-}$ mutant (*hopQ*$^{-}$#1) were previously described [198]. An *H. pylori* 26695 *hopQ* complemented strain was generated by insertion of the *hopQ* gene into the *hp0177/0178* intergenic chromosomal region of *hopQ*$^{-}$#1. A second independent 26695 *hopQ*$^{-}$ mutant (*hopQ*$^{-}$#2) was constructed as previously described by insertional mutagenesis [117]. Additionally, a *hopQ* deletion mutant derivative of strain 7.13 was constructed by inserting Cm and kanamycin resistance cassettes into the two *hopQ* loci [402]. PCR-based typing of clinical isolates was performed for *hopQ* alleles and *cagA* status **(Table 1)** [196, 401]. TLR9 activation, adherence, CagA translocation, and IL-8 production assays were performed using the following

MOIs: 10:1, 25:1, 50:1, 100:1, and 200:1 **(Figure 15)**. Activation with minimal control activation by wild-type *H. pylori* for CagA translocation and IL-8 induction occurred at a MOI of 50:1 and for adherence and TLR9 activation at a MOI of 100:1.

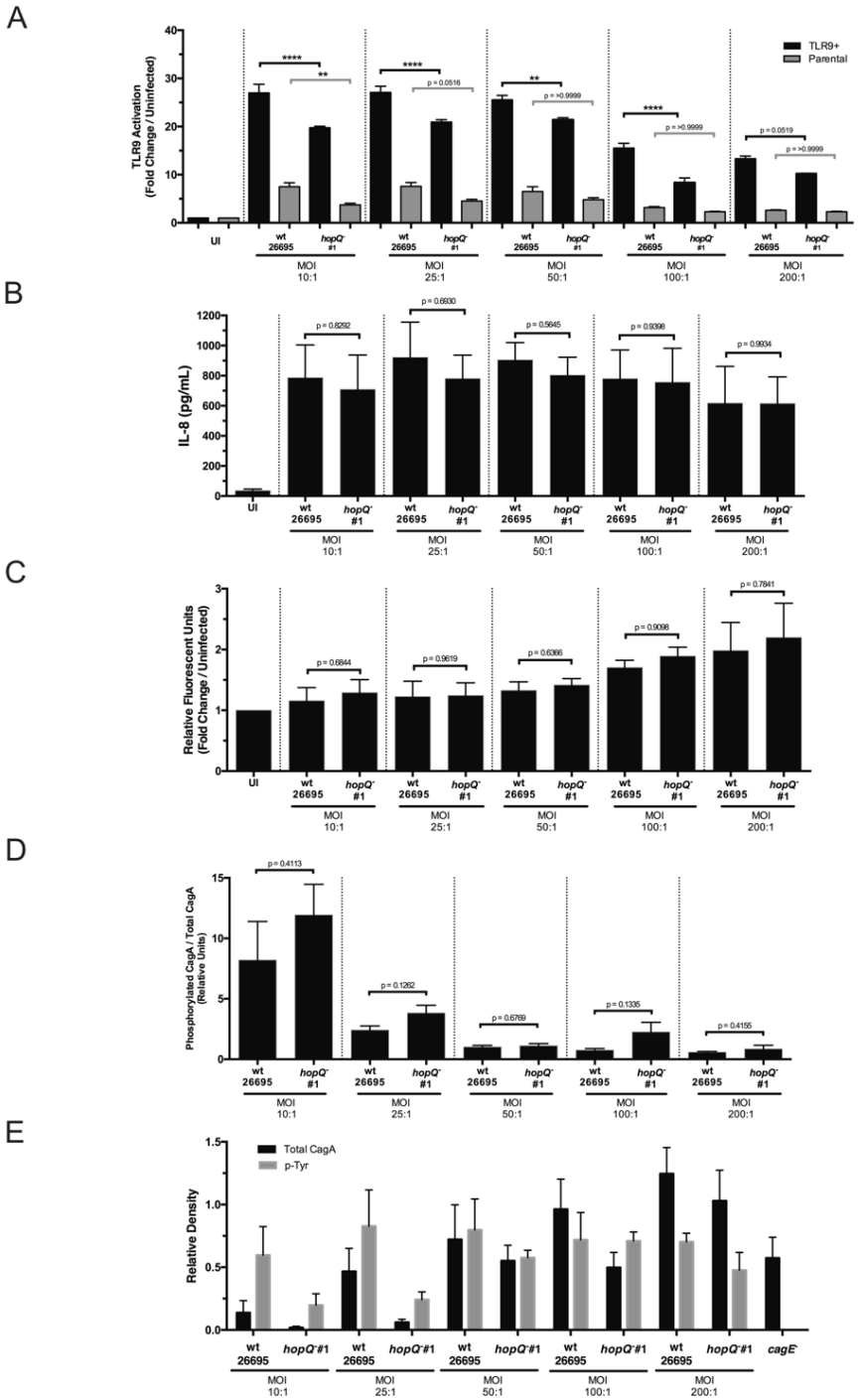

Figure 15. Multiplicity of infection (MOI) comparisons for co-culture assays at 10:1, 25:1, 50:1, 100:1, and 200:1. (A) TLR9-reporter or parental cells were challenged with *H. pylori* wild-type strain 26695 or a 26695 *hopQ*-

isogenic mutant. Strains were tested in duplicate at least 3 times and data are represented as fold change in infected over uninfected controls. **(B)** Levels of IL-8 were determined via ELISA in *H. pylori*:AGS cell supernatants following 4-hour of co-culture. Strains were tested at least 3 times and mean±SEM are shown. **(C)** Fluorescently-labeled *H. pylori* wild-type strain 26695 or a 26695 *hopQ*$^{-}$ isogenic mutant were co-cultured with AGS cells for 4 hours; cells were subsequently washed to remove non-adherent bacteria and analyzed for fluorescence. Strains were tested in duplicate and data are represented as fold change of infected over uninfected control. **(D,E)** CagA translocation was determined by quantifying levels of phospho-CagA in AGS cell lysates during 4-hour *H. pylori* co-culture by Western blotting. GAPDH served as a loading control. Data are shown as **(D)** normalized levels of phosphorylated CagA to total CagA/strain and **(E)** protein bands representing total CagA and phosphorylated CagA alone, quantitated by densitometry, relative to GAPDH loading control. Strains were tested at least 3 times and mean±SEM are shown. Student's t-tests were used to determine statistical significance between groups. **p<0.01, ****p<0.0001.

Real-Time PCR

RNA was extracted using the RNAeasy Mini Kit (Qiagen) from log-phase *H. pylori* cultures. cDNA was synthesized using High-Capacity cDNA Reverse Transcription Kit (ThermoFisher) and quantitative real-time PCR was performed using Power SYBR Green Master Mix (ThermoFisher) with gene-specific primers **(Table 1)**.

Table 1. List of primers used in Chapter II.

Primer Name	DNA sequence
***hopQ* allele primers**	
Type I *hopQ*-F	5′-CAACGATAATGGCACAAACT-3'
Type I *hopQ*-R	5′-GTCGTATCAATAACAGAAGTTG-3'
Type II *hopQ*-F	5′-TCCAATCCAGAAGCGATTAA-3'
Type II *hopQ*-R	5′-GTTTTAATGGTTACTTCCACC-3'
***cagA* status primers**	
cagA-F	5'-GATAACAGGCAAGCTTTTGAGG-3'
cagA-R	5'-CTGCAAAAGATTGTTTGGCAGA-3'
Real-time RT-PCR primers	
16S rRNA-F	5'-GGAGTACGGTCGCAAGATTAAA-3'
16S rRNA-R	5'-CTAGCGGATTCTCTCAATGTCAA-3'
Type I *hopQ*-F	5'-ATGGCACAAACTCAAAGACAAG-3'
Type I *hopQ*-R	5'-TAACACCGATCTCAACGCTAAA-3'
Type II *hopQ*-F	5'-CAACGCTCAACAAAGCGTATC-3'
Type II *hopQ*-R	5'-TGGTTACTTCCACCGTTGTT-3'

TLR9 and NOD1 Activation Assays

HEK293-Blue-hTLR9 cells (TLR9+), HEK293-Blue-hNOD1 cells (NOD1+), and HEK293-Blue-Null1 (Parental) cells were seeded in 96-well plates (Corning) in DMEM without antibiotics and challenged with agonist, *H. pylori,* or sterile PBS for 24 hours. Supernatants were added to QUANTI-Blue™ solution (Invivogen) and analyzed by spectrophotometer (Bitoek) at 650nm.

Cell Culture

AGS human gastric epithelial cells (ATCC CRL-1739) were grown in RPMI 1640 (ThermoFisher) with 10% FBS. HEK293-Blue hTLR9 (TLR9+), HEK293-Blue hNOD1, (NOD1+) and HEK293-Blue Null1 (Parental) cells (Invivogen) were grown in DMEM (ThermoFisher) supplemented with 10% FBS and 100µg/mL Zeocin (Invivogen). HEK293-Blue hTLR9 and HEK293-Blue hNOD1 cell media was supplemented with an additional selective antibiotic, Blasticidin (Invivogen) at 10µg/mL.

Complementation

The *H. pylori* 26695 *hopQ* complemented strain was generated by insertion of the 26695 *hopQ* gene into the *hp0177/0178* intergenic chromosomal region of *H. pylori hopQ*$^{-}$ mutant #1. Flanking sequences targeting *hp0177* and *hp0178* were cloned into the vector pGEMT-Easy (Promega), generating plasmid p177. A kanamycin resistance cassette, *ureA* promoter, and the *H. pylori* 26695 *hopQ* gene were then cloned into p177, yielding p177-*hopQ*. *H. pylori hopQ*$^{-}$#1 was then naturally transformed with p177-*hopQ* and colonies selected for chloramphenicol and kanamycin resistance were tested by RT-PCR to confirm re-expression of *hopQ* (data not shown).

Cytokine Assays

H. pylori were co-cultured with AGS cells for 4 hours; levels of IL-8, IFNα, and IFNβ in supernatants were quantified using Quantikine ELISA Kits (R&D Systems), per manufacturer's instructions.

CagA Translocation Assay

H. pylori cagA^{+} strains were co-cultured with AGS cells for 4 hours. Protein lysates were harvested in RIPA buffer, separated by SDS-PAGE, and transferred to PVDF membranes (ThermoFisher). Levels of total CagA (1:5000 anti-CagA antibody; Austral Biologicals) and phosphorylated (reflecting translocated protein) CagA (1:5000 anti-pY99 antibody; Santa Cruz) were determined via Western blotting. GAPDH (1:5000 anti-GAPDH, clone 6C5 antibody; Milipore Sigma) served as a loading control. Protein intensities were quantified using ImageJ software (NIH).

Adhesion Assays

H. pylori harvested from overnight cultures were diluted to an OD600 = 1.0. One µL of *Bac*Light™ Green Bacterial Stain (ThermoFisher) per 1mL of culture were mixed and incubated for 2 hours to label the bacteria. *H. pylori* were then washed with sterile PBS and co-cultured with AGS cells for 4 hours. Plates were washed and analyzed for fluorescence ($485_{Ex}/516_{Em}$).

Statistical Analysis

All experiments were repeated at least three times. The Mann-Whitney test or student's t-test was used for two group comparisons, while one-way ANOVA with Bonferroni correction was used for multiple group comparisons. Statistical significance was set at a p-value of <0.05.

2.3 Results

We first PCR-genotyped a cohort of clinical strains for *hopQ* allelic type and analyzed their ability to activate TLR9. Type I strains induced significantly higher levels of TLR9 activation compared to type I/II or type II strains **(Figure 16A, Figure 17)**. To determine whether gene expression may be associated with these differences, we analyzed expression of *hopQ* alleles in a subset of clinical strains by real-time RT-PCR. Expression of type I *hopQ* was significantly greater in type I strains compared to type I/II strains while expression of type II *hopQ* was significantly higher in type II strains compared to type I/II strains **(Figure 16B)**. To study potential downstream ramifications of these findings *in vivo*, severity of inflammation and premalignant lesions (e.g. intestinal metaplasia) in biopsies obtained from the source patients was stratified by *hopQ* genotypes of the infecting *H. pylori* isolates. Severity of chronic inflammation and intestinal metaplasia were significantly increased in patients infected with type I strains compared to patients infected with type II strains **(Figure 16C)**, while levels of acute inflammation were no different **(Figure 18)**. We also directly compared levels of *H. pylori*-induced TLR9 activation *in vitro* to the severity of gastric inflammation and injury induced by the same strains *in vivo*. Levels of TLR9 activation were significantly associated, albeit of weaker magnitude, with the intensity of chronic inflammation, intestinal metaplasia, as well as acute inflammation **(Figure 16C)**, suggesting that the capacity of *H. pylori* strains to induce higher levels of TLR9 activation *in vitro* is related in part to the extent of damage induced by these same strains *in vivo*. *H. pylori cagA*$^{+}$ type I *hopQ* strains also translocated significantly higher amounts of CagA per level of total CagA/strain compared to strains containing type I/II alleles or a type II allele; however, there were no significant associations between type I *hopQ* expression levels and pathologic outcomes or levels of CagA translocation **(Figure 16D, Figure 19, Figure 20)**.

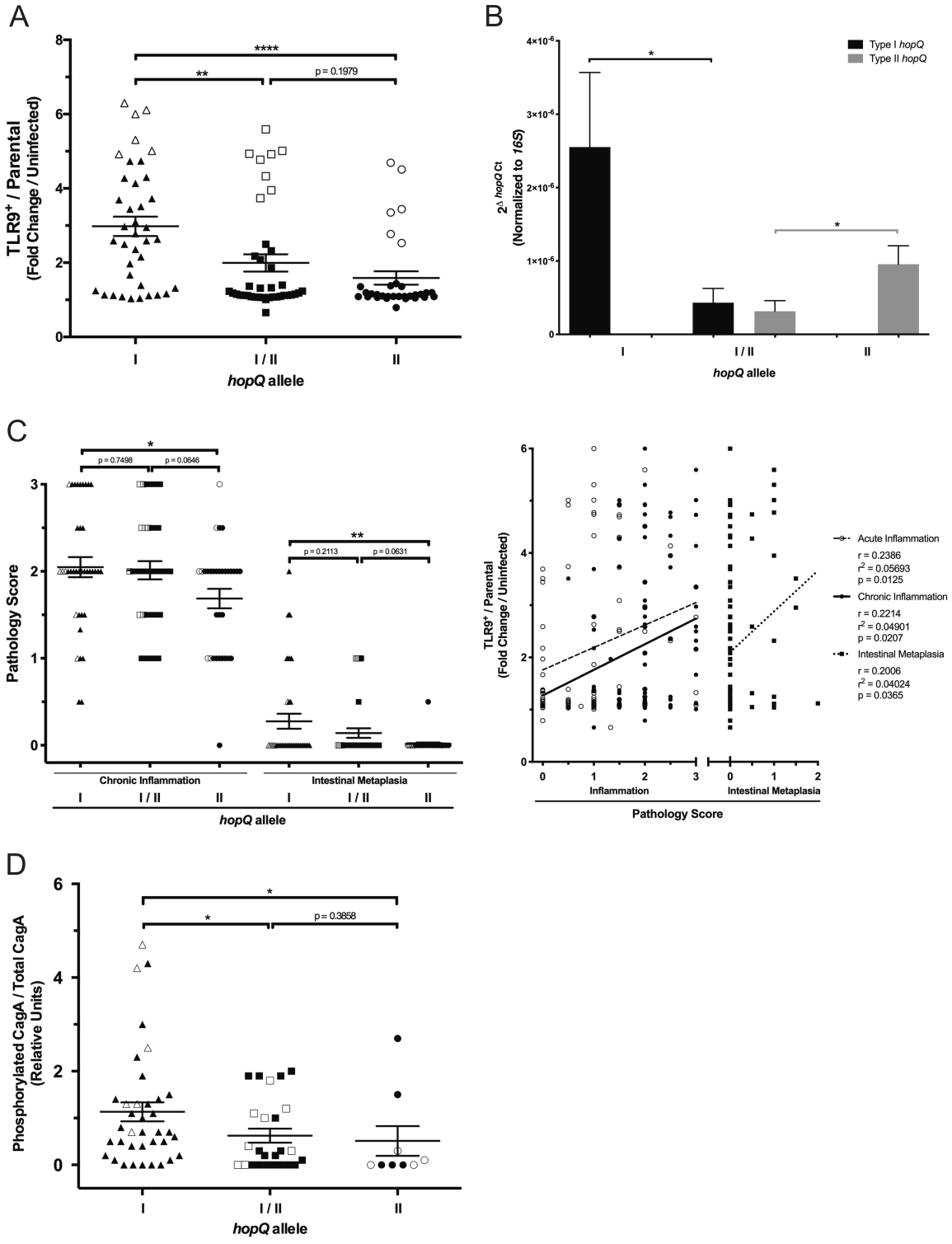

Figure 16. Clinical *H. pylori* type I *hopQ* strains enhance TLR9 activation and are more virulent than type I/II or type II strains. The highest *H. pylori* responder strains for each *hopQ* allelic category (type I, n=6; type I/II, n=8; type II, n=6) are designated as open symbols in Figure 16A; data points originating from gastric tissue harvested from patients infected with these same strains (Figure 16C) as well as data points depicting levels of CagA translocation by these same strains (Figure 16D) are also labelled as open symbols. **(A)** TLR9-reporter or parental cells were challenged

with clinical *H. pylori* strains. Data are represented as fold change in infected TLR9+ cells/parental cells over uninfected controls. Each strain was tested in duplicate at least 3 times (type I, n=38; type I/II, n=39; type II, n=32). **(B)** Expression of either type I *hopQ* or type II *hopQ* was assessed by RT-PCR on a random selection of clinical strains (type I, n=7; type I/II, n=8; type II, n=9). $2^{(\Delta hopQCt)}$ is the expression level of *hopQ* normalized to the reference gene *16S* rRNA. **(C)** Inflammation and intestinal metaplasia scores from patients infected with either *H. pylori* type I, type I/II, or type II *hopQ* strains. Each data point represents score from an individual patient (type I, n=38; type I/II, n=39; type II, n=32). TLR9 activation levels induced by the corresponding infecting *H. pylori* strains (n=109) are shown as fold change in infected TLR9+ cells/parental cells over uninfected controls. Spearman's correlation was performed to determine linear correlation. **(D)** AGS cells were co-cultured with *cagA*$^+$ clinical *H. pylori* strains (n=71) at MOI 50:1 for 4 hours. Levels of translocated CagA were quantified in cell lysates by Western blotting for phosphorylated CagA and total CagA. Data are represented as phosphorylated CagA over total CagA (type I, n=37; type I/II, n=25; type II n=9). Mean±SEM are shown for all groups. Mann-Whitney tests or student's t-test were used to determine statistical significance between groups *p<0.05, **p<0.01, ****p<0.0001.

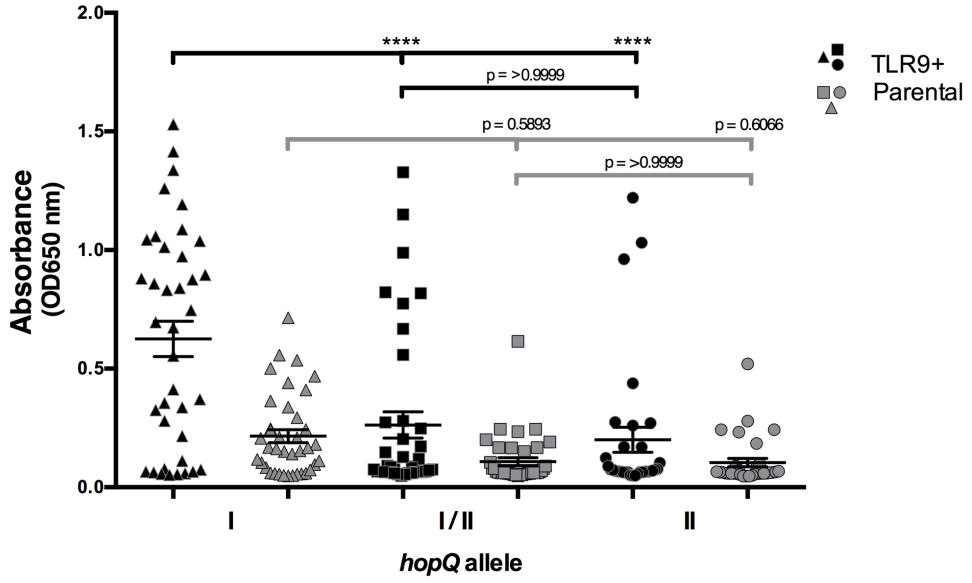

Figure 17. Clinical *H. pylori* type I *hopQ* strains enhance TLR9 activation. TLR9-reporter or parental cells were challenged with clinical *H. pylori* strains. Each strain was tested in duplicate at least 3 times from patients infected with either *H. pylori* type I, type I/II, or type II HopQ strains. Mean±SEM are shown for all groups and each data point represents the raw OD650 absorbance value from an individual strain (type I, n=38; type I/II, n=39; type II, n=32). ANOVA with Bonferroni correction was used to determine statistical significance between groups. ****p<0.0001.

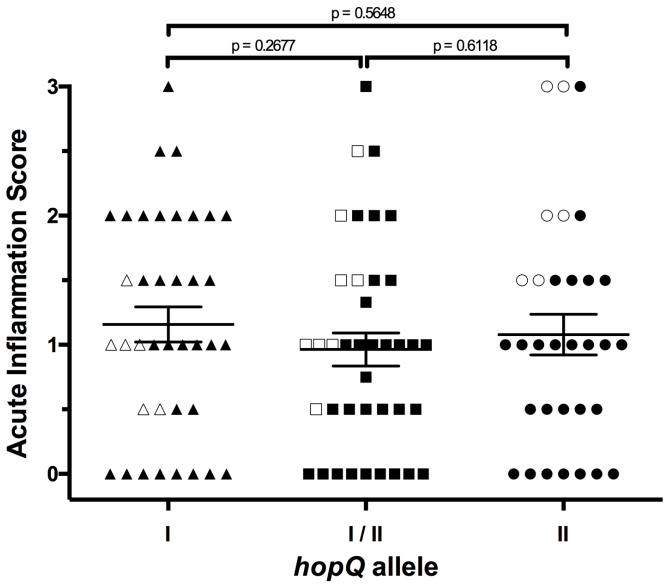

Figure 18. Acute inflammation scores segregated by *hopQ* genotype of infecting *H. pylori* strain. Acute inflammation scores from patients infected with either *H. pylori* type I, type I/II, or type II HopQ strains. Each data point represents the inflammation score from an individual patient (type I, n=38; type I/II, n=39; type II n=32). Data points originating from gastric tissue harvested from patients infected with the highest TLR9 activating *H. pylori* strains for each allelic category (Type I, n=6; Type I/II, n=8; Type II, n=6) are designated as open symbols. Mean±SEM are shown for all groups. Mann-Whitney tests were used to determine statistical significance between groups.

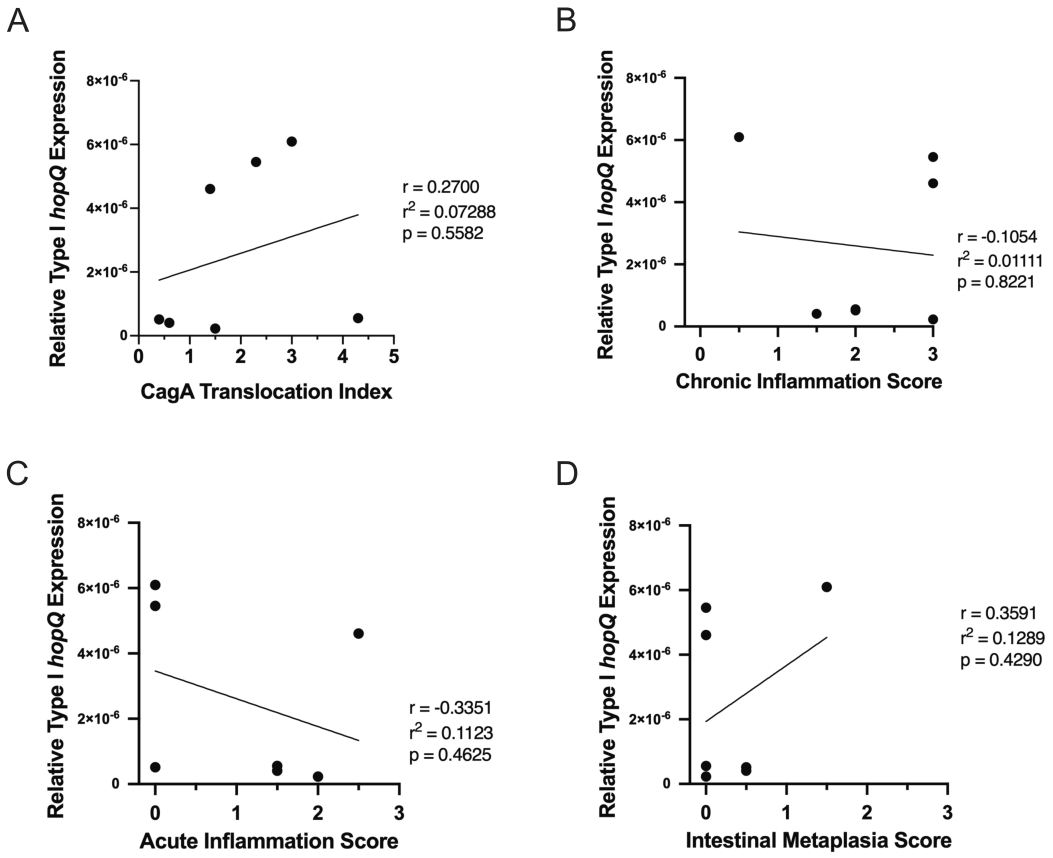

Figure 19. Type I *hopQ* expression levels by selected clinical *H. pylori* strains do not associate with CagA translocation or pathology scores. Data points represent **(A)** CagA translocation indices (phosphorylated CagA over total CagA) induced by individual *H. pylori* clinical strains, and **(B)** chronic inflammation scores, **(C)** acute inflammation scores, or **(D)** intestinal metaplasia scores from individual patient samples, each compared to relative type I *hopQ* expression levels of the corresponding infecting *H. pylori* strain (n=7). Pearson's correlation was performed to determine linear correlation.

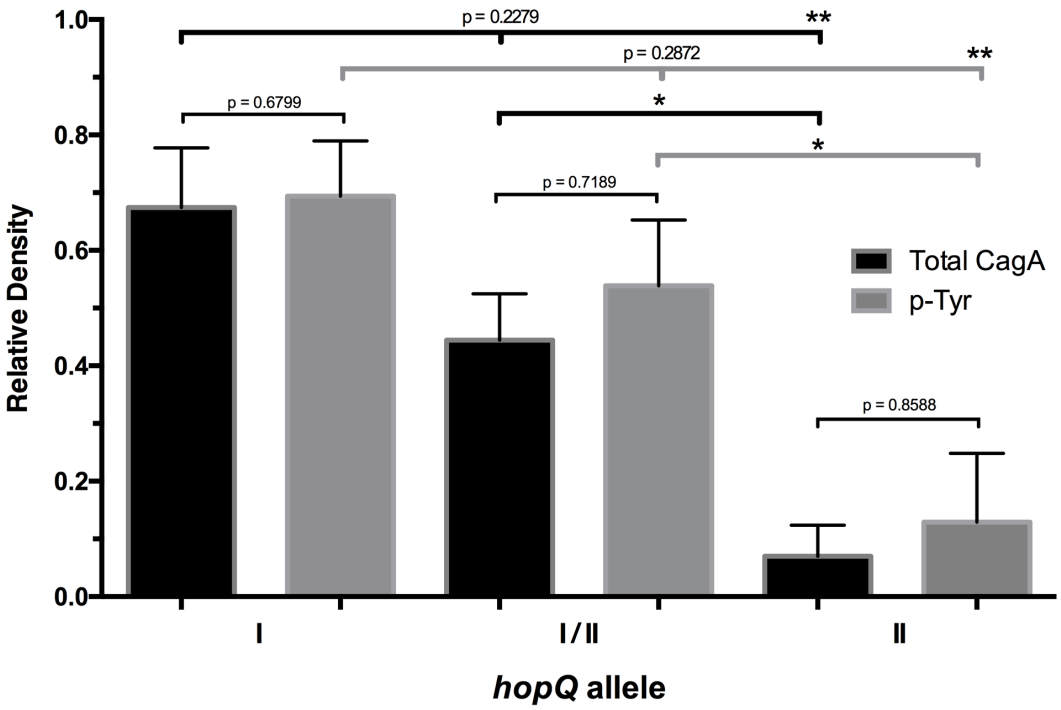

Figure 20. Clinical *H. pylori* strains containing type I *hopQ* alleles enhance CagA translocation. AGS cells were co-cultured with *cagA*$^{+}$ clinical *H. pylori* strains (n=71) at MOI 50:1 for 4 hours. Levels of translocated CagA were quantified in cell lysates by Western blotting for phosphorylated CagA and total CagA. Data shown are results from Western blots representing total CagA and phosphorylated CagA alone, quantitated by densitometry, relative to GAPDH loading control. Mean±SEM are shown for all groups (type I, n=37; type I/II, n=25; type II n=9). Mann-Whitney tests were used to determine statistical significance between groups. *p<0.05, **p<0.01.

Collectively, these results indicate that *H. pylori* type I strains induce more intense TLR9 activation *in vitro* and enhanced chronic inflammation and damage *in vivo*. This may reflect enhanced translocation of CagA, which has been shown to induce inflammation and promote the development of intestinal metaplasia [403]. We next more definitively defined the role of HopQ in TLR9 activation by genetically inactivating *hopQ*. *H. pylori* wild-type strain 26695 robustly induced TLR9 activation when compared to uninfected cells, while a *cagE*$^-$ mutant minimally activated TLR9. TLR9 activation was significantly diminished following co-culture with the *hopQ*$^-$ mutant compared to *H. pylori* wild-type 26695-infected cells, and complementation fully restored levels of TLR9 activation to levels induced by wild-type strain 26695 **(Figure 21A)**. To more strongly implicate *hopQ* allele status in TLR9 activation, we generated a second independent isogenic *hopQ*$^-$ mutant in the *H. pylori* 26695 strain background as well as a double *hopQ* mutant in *H. pylori* strain, 7.13, which contains 2 identical copies of type I *hopQ*. Levels of TLR9 activation induced by 26695 *hopQ*$^-$#2 and the 7.13 *hopQ*$^-$ mutant were significantly reduced compared to levels induced by the wild-type strains **(Figure 21A)**. Of note, levels of activation in parental cells infected by either of the wild-type strains were higher than in uninfected parental cells although this was not statistically significant, which may represent residual *cag* T4SS-dependent but HopQ-independent activation of NF-κB. Downstream signaling effectors activated by TLR9 include type I IFNs (IFNα, IFNβ). To investigate consequences of TLR9 activation, we co-cultured wild-type *H. pylori* strain 26695 and the 26695 isogenic *hopQ*$^-$ mutant with AGS cells and quantified IFNα and IFNβ production. Similar to TLR9, wild-type *H. pylori* strain 26695 induced significantly higher levels of type I interferons compared to the 26695 *hopQ*$^-$ mutant **(Figure 21B)**.

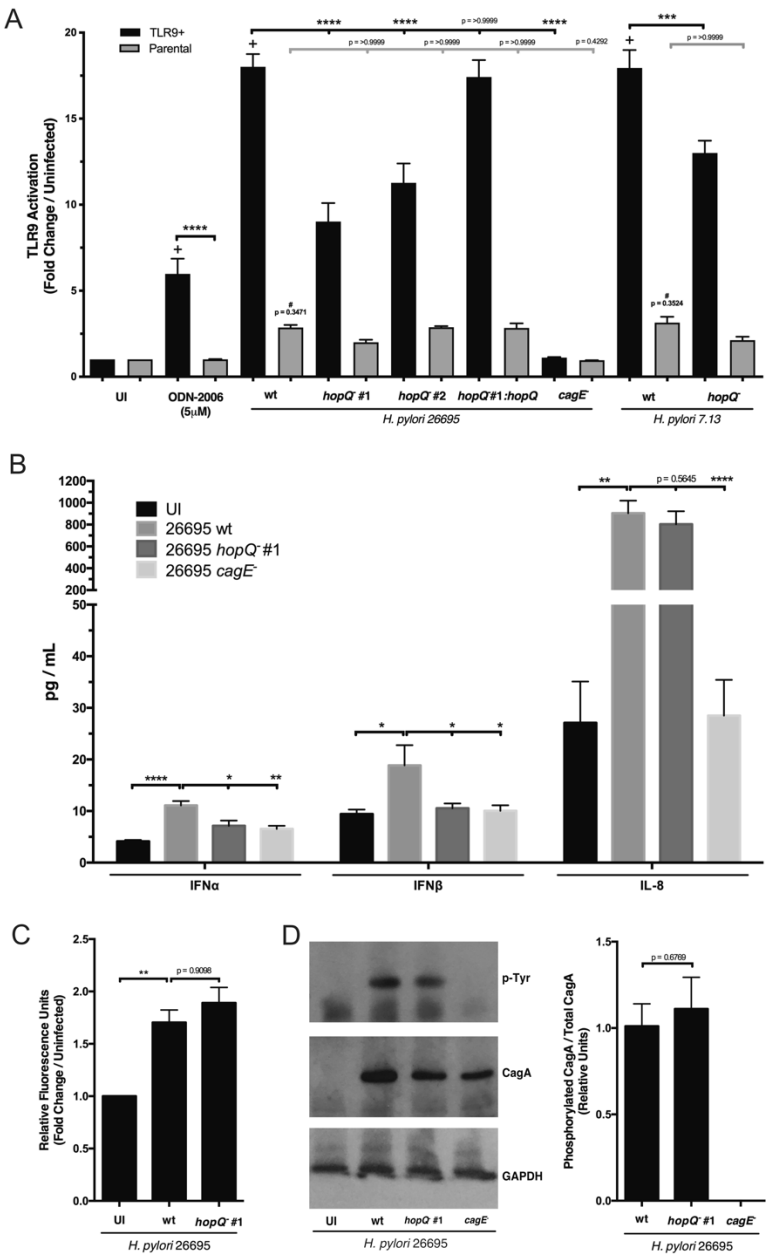

Figure 21. Deletion of *hopQ* significantly decreases TLR9 activation independent of cellular adhesion and *cag* T4SS function. (A) TLR9-reporter or parental cells were challenged with TLR9 agonist ODN-2006, *H. pylori* wild-type *cag* PAI$^+$ strain 26695, wild-type *cag* PAI$^+$ strain 7.13, respective *hopQ*$^-$ or *cagE*$^-$ isogenic mutant strains, or a complemented 26695 *hopQ* mutant. Samples were tested in duplicate at least 3 times and data are represented as fold change in infected over uninfected controls. **(B)** Levels of IFNα, IFNβ, and IL-8 were determined via ELISA in *H. pylori*:AGS cell supernatants. In each experiment, strains were tested at least 3 times and mean±SEM are shown. **(C)** Fluorescently-labeled *H. pylori* wild-type strain 26695 or a 26695 *hopQ*$^-$ isogenic mutant were co-cultured with AGS cells for 4 hours and analyzed for fluorescence. Strains were tested in duplicate and data are represented as fold change of infected over uninfected control. **(D)** CagA translocation was determined by quantifying levels of phospho-CagA in AGS cell lysates during *H. pylori* co-culture by Western blotting. Representative Western blots and densitometric analysis normalizing levels of phosphorylated CagA to total CagA from 3 replicates are shown. GAPDH served as a loading control. ANOVA with Bonferroni correction or student's t-test was used to determine statistical significance between groups. *p<0.05, **p<0.01, ***p<0.001, ****p<0.0001; + = p<0.00001 compared to uninfected TLR9+ cells; # = non-significant compared to uninfected parental cells.

Since HopQ is a bacterial adhesin, we determined whether reductions in TLR9 activation induced by the *hopQ*$^{-}$ mutant were dependent upon decreased adherence. No differences in binding to AGS cells were identified between the wild-type strain 26695 and the *hopQ*$^{-}$ isogenic mutant **(Figure 21C)**. Soft agar motility assays demonstrated that *H. pylori* parental strain 26695 exhibited similar motility to other *H. pylori* strains included in this study (data not shown). Type I *hopQ* alleles are in linkage disequilibrium with the *cag* T4SS [196] and specific HopQ-CEACAM interactions have been reported to be required for translocation of CagA into epithelial cells [188, 201]. Thus, to discern whether reductions in TLR9 activation were due to inactivation of *hopQ* per se and not due to concomitant loss of *cag* T4SS function, we analyzed *cag* T4SS-associated phenotypes in the *hopQ*$^{-}$ mutant. Both wild-type strains 26695 and 7.13 and their respective *hopQ*$^{-}$ or complemented *hopQ* mutants were similar in their ability to translocate CagA, as determined by levels of phosphorylated CagA per level of total CagA/strain, while, as expected, the *cagE*$^{-}$ mutant failed to translocate CagA **(Figure 21D, Figure 22)**. Further, no significant differences in levels of IL-8 production were observed between 26695 and 7.13 wild-type, *hopQ*$^{-}$ and *hopQ* complemented mutant-infected samples **(Figure 21B, Figure 22)**. There were also no differences between wild-type *H. pylori* strain 26695 and the *hopQ*$^{-}$ mutant in the ability to activate an independent *cag* T4SS-dependent effector, NOD1 **(Figure 23)**.

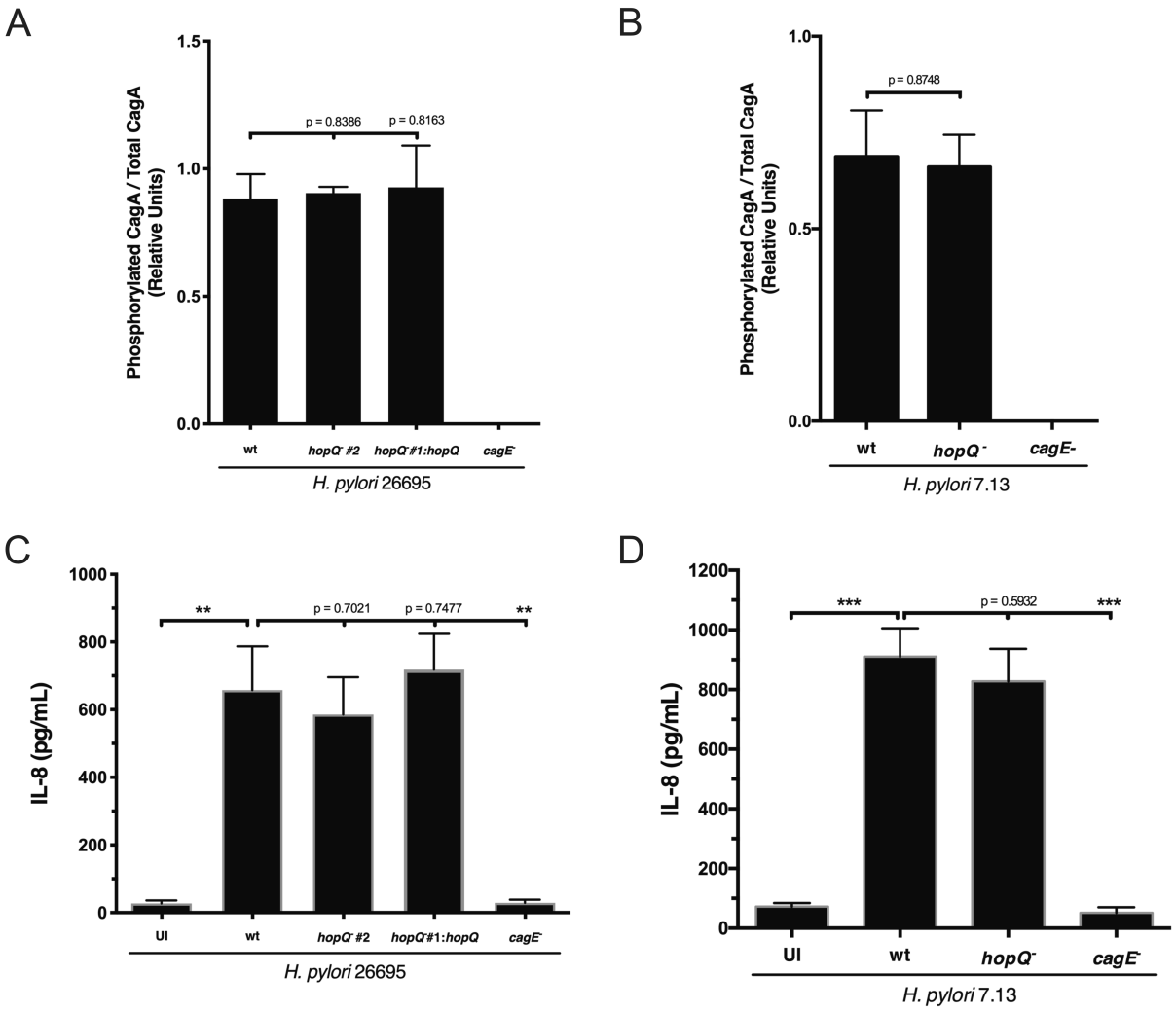

Figure 22. Deletion of *hopQ* does not alter *cag* T4SS function in *H. pylori* strains 26695 or 7.13. AGS cells were co-cultured with *H. pylori* wild-type *cag* PAI$^+$ strain 26695, wild-type *cag* PAI$^+$ strain 7.13, respective isogenic *hopQ*$^-$ or *cagE*$^-$ mutant strains, or a complemented *hopQ* 26695 strain at MOI 50:1 for 4 hours. **(A, B)** CagA translocation was determined by quantifying levels of phospho-CagA in AGS cell lysates during *H. pylori* co-culture by Western blotting. Densitometric analyses normalizing levels of phosphorylated CagA to total CagA from 3 replicates are shown. **(C, D)** Levels of IL-8 were determined via ELISA in *H. pylori*:AGS cell supernatants. In each experiment, strains were tested at least 3 times and mean±SEM are shown. Student's t-tests were used to determine statistical significance between groups. **p<0.01, ***p<0.001.

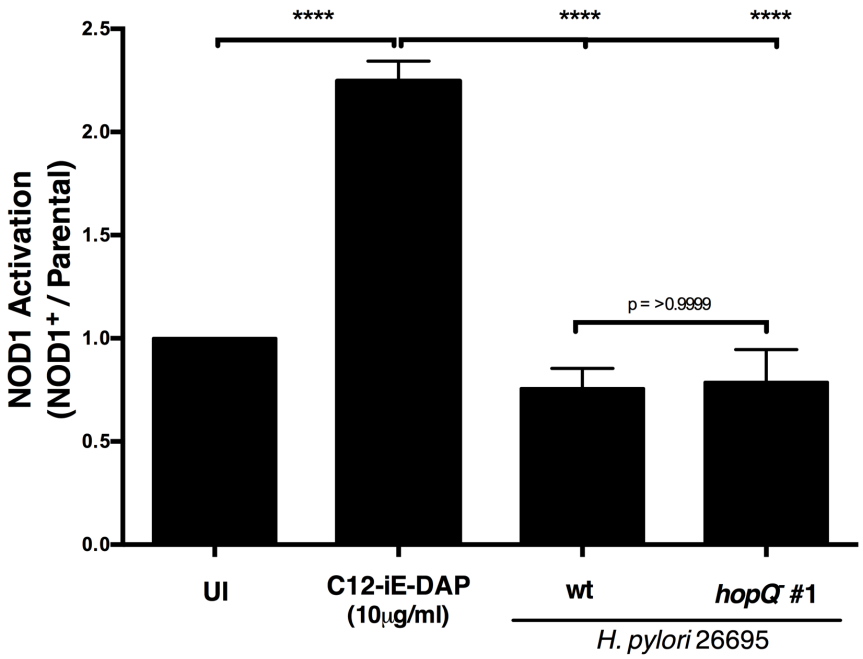

Figure 23. Deletion of *hopQ* does not alter NOD1 activation compared to wild-type *H. pylori*. NOD1-reporter or parental cells were challenged with NOD1 agonist C12-iE-DAP, *H. pylori* wild-type strain 26695, or a 26695 *hopQ*- isogenic mutant. Samples were tested in duplicate at least 3 times and data are represented as fold change of NOD1+/Parental cells in infected over uninfected controls. Mean±SEM are shown for all groups. ANOVA with Bonferroni correction was used to determine statistical significance between groups. ****p<0.0001.

2.4 Discussion

We identified a strain-variable *cag* PAI-independent *H. pylori* component, HopQ, that is associated with TLR9 activation and is linked to carcinogenic potential. There are several potential mechanisms that may underpin these observations. Structural analyses comparing type I HopQ to type II HopQ proteins have revealed a differential ability to bind specific CEACAMs [190]. Type I HopQ harbors a higher affinity for human CEACAM1 versus CEACAM6, raising the possibility that HopQ-CEACAM1 interactions are necessary for translocation of microbial DNA and TLR9 activation. Of interest, *H. pylori cagA*$^+$ strains induce higher levels of CEACAM expression than *cagA*$^-$ strains, and TLR9-regulated transcription factors such as NF-κB and AP-1 are linked to *H. pylori* infection and CEACAM regulation [188]. Although further studies linking discrete cell

signaling cascades to specific HopQ alleles and CEACAMs will be required, *H. pylori* has likely evolved to harbor different alleles of *hopQ* that may confer selective binding and molecular signaling capacities.

Our current results also indicate that *cag* T4SS function in *H. pylori* strains 26695 and 7.13 is not dependent on HopQ. Some, but not all, previous studies have demonstrated a more direct role for HopQ in *cag* PAI functions [188, 201]. However, these studies utilized independent *H. pylori* strains in different cell models under different conditions compared to our current study which may account for the varying results.

We recognize that not all of the *in vitro* and *in vivo* data are fully aligned and speculate that the lack of absolute concordance represents fundamental differences that exist between the reductionist *in vitro* TLR9 activation assay and the *in vivo* milieu colonized by *H. pylori*. For example, varying expression levels of CEACAM proteins may be present within different patient samples, which may alter HopQ function. Further, other microbial constituents and host signaling pathways, such as peptidoglycan and NOD1 as well as HBP and NF-κB, have been shown to affect inflammation *in vivo* [121]. The complexity of such interactions is heightened when comparing results from human tissue to rodent tissue. In humans, genetic polymorphisms within TLR9 have been linked to *H. pylori* persistence [404]. We previously demonstrated that *H. pylori* strains harvested from persons at increased risk for gastric cancer activated TLR9 more robustly than strains isolated from patients residing in a low-risk cancer region [117]. These data are consistent with the current results and with data from Qin et al. demonstrating that *H. pylori* and *H. pylori* DNA induces TLR9-dependent proliferation, migration, and invasion of human gastric epithelial cells [405] . However, our group also reported enhanced inflammation in *H. pylori*-infected *tlr9*$^{-/-}$ mice when compared to *H. pylori*-infected wild-type mice [406]. We speculate that this

discordance may be related to the duration of infection (years in humans, weeks in mice) as well as inherent differences in host responses to microbial pathogens across species, which, for TLR9 carries increased complexity since activation of TLR9 can lead to either pro- or anti-inflammatory responses *in vivo* depending on cellular context.

Collectively, the current results aid in delineating the route by which microbial DNA is delivered to host cells and may also reveal the impact that DNA translocation has on carcinogenesis *in vivo*.

CHAPTER III

HELICOBACTER PYLORI ACTIVELY SUPPRESS INNATE IMMUNE NUCLEIC ACID RECEPTORS

This chapter is an adaptation of the following submitted manuscript:
Dooyema SDR et al. "*Helicobacter pylori* Actively Suppress Innate Immune Nucleic Acid Receptors" *Gut Microbes.* In revision.

3.1 Introduction

Mucosal pathogens have evolved multiple strategies to manipulate the host immune response [263, 407]; consequently, microbes contribute to the development of greater than 2 million cases of cancer/year [53]. Gastric adenocarcinoma is the fourth leading cause of cancer-related death [37, 52, 63] and chronic infection with *Helicobacter pylori* confers the highest known risk for this disease [37, 53]. Initial components of the innate immune system encountered by *H. pylori* include epithelial cells, macrophages, and dendritic cells, and interactions between *H. pylori* and these constituents dysregulate signaling pathways that influence oncogenesis [43, 408]. Epithelial cells express effectors that can either eliminate bacteria or mobilize adaptive immune responses; these include pattern-recognition receptors (PRRs), which detect and respond to conserved microbial motifs [47, 231]. Functionally distinct PRR subclasses include NLRs, TLRs, and cytosolic DNA sensor/adaptor proteins (*e.g.*, STING), all of which are linked to gastric cancer [47, 352]. PRRs orchestrate immune responses targeting pathogens and bridge innate and adaptive immunity via recognition of pathogen-associated molecular patterns (PAMPs) [47, 231]. However, *H. pylori* harbors multiple PAMPs that function differently than the respective counterparts in other mucosal pathogens. Specifically, 1) *H. pylori* FlaA (the major flagellin

subunit) is a non-inflammatory molecule in terms of its ability to activate TLR5 [263], 2) *H. pylori* LPS induces an attenuated TLR4-mediated response [244, 248], 3) deacetylation of peptidoglycan allows *H. pylori* to evade host clearance via activation of a Nod1-dependent negative feedback loop [160, 272-274], and 4) TLR9 suppresses the injury response to this pathogen [119]. Thus, *H. pylori* has evolved an array of diverse phenotypes to subvert obstacles presented by the host, which promotes long-term colonization and carcinogenesis.

H. pylori strains exhibit a high level of genetic diversity [81, 409] and one strain-specific determinant that significantly augments cancer risk is the *cag* type IV secretion system (T4SS) [87, 89, 90, 410]. The *cag* T4SS translocates a pro-inflammatory and oncogenic protein, CagA, as well as peptidoglycan and a metabolic intermediary in the LPS synthesis pathway, heptose bis-phosphate, into epithelial cells [106, 109, 114-116, 411]. Our laboratory has demonstrated that the *cag* T4SS also translocates microbial DNA, which subsequently activates TLR9 [117, 119]. However, most persons colonized with $CagA^+$ strains do not develop cancer [32, 52, 63], suggesting that other *H. pylori* constituents also affect disease risk.

Microbial-specific nucleic acids are an important subclass of PAMPs, which are rapidly detected in the cytosol of host cells [311, 312]. Cyclic GMP-AMP synthase (cGAS) is a cytosolic DNA sensor, which is activated in response to double-stranded DNA in a sequence-independent manner. Binding of DNA ligands to cGAS catalyzes the conversion of ATP and GTP into the dinucleotide 2',3'-cyclic GMP-AMP (cGAMP). cGAMP can then directly activate stimulator of interferon genes (STING), a DNA sensor/adaptor localized to the ER [311, 312] and which is expressed in gastric epithelial cells [352]. Sensing of cyclic dinucleotides induces a conformational change in STING that triggers trafficking of STING complexed with TBK1 from the ER to endosomal/lysosomal compartments. Translocated TBK1 leads to phosphorylation and activation

of the transcription IRF3, which is then mobilized to the nucleus to induce expression of type 1 IFNs (*e.g.*, IFNα, IFNß) [311, 312]. STING activation can also trigger other downstream pathways such as NF-κB [350, 412], as well as autophagy, which clears DNA or pathogens from the cytosol [351].

However, certain chronic pathogens have developed strategies to evade STING-mediated immune clearance, establish infection, and induce disease [311, 312, 358]. Carcinogenic DNA viruses such as human papilloma virus (HPV) 18 and human adenovirus 5 encode the oncoproteins E7 and E1A, respectively, which antagonize STING. Kaposi's sarcoma-associated herpesvirus (KSHV) and hepatitis B express IRF1, tegument protein ORF52, and viral polymerases that potently disrupt the cGAS-STING pathway. Viral poxins abrogate STING signaling by degrading cGAMP [311, 312]. This wide repertoire of antagonists targeting cGAS-STING underscores the importance of evolutionary pressures that select for oncogenic pathogens that can both promote malignancy and suppress innate immunity.

The role of DNA sensing in human carcinogenesis is not fully understood but recent studies indicate that DNA sensors exert a crucial role in antitumor responses. Suppression of STING in prostate and melanoma cancer cells leads to increased tumor growth [385, 386], and poor patient survival is associated with reduced cGAS and STING expression [352, 387]. In gastric cancer, STING expression is significantly decreased in tumor versus non-tumor tissue, and low levels of expression are associated with reduced survival [352]. In models of inflammation with premalignant potential (*e.g.,* chronic pancreatitis), inhibition of STING worsens disease via upregulation of IL-17A [388], which promotes inflammation-induced malignancies including pancreatic cancer, colitis-associated carcinoma, and skin cancer [389-391].

We previously demonstrated that translocated *H. pylori* DNA can activate the microbial DNA sensor TLR9 *in vitro* and that TLR9 suppresses *H. pylori*-induced injury *in vivo*; however, the ability to suppress additional nucleic acid PRRs by *H. pylori* within the context of gastric carcinogenesis has not been fully investigated. Therefore, the goal of this study was to elucidate the effects of *H. pylori* constituents on STING signaling and, using a *Sting*-deficient mouse infection model, delineate the role of STING in the context of gastric injury and inflammation. Our findings identified a novel mechanism through which *H. pylori* actively suppresses STING-associated signaling in host cells via induction of an induced host effector, TRIM30a. These pathways may contribute to the ability of *H. pylori* to persist long-term in the stomach and ultimately promote gastric carcinogenesis.

3.2 Materials and Methods

Helicobacter pylori

The *H. pylori cag*$^{+}$ strains J166, PMSS1 [117, 119], G27 [413], B128 and 7.13 [414], were maintained on TSA blood agar plates (Remel). For *in vitro, ex vivo,* and *in vivo* experiments, *H. pylori* was cultured in Brucella broth (Becton Dickinson) supplemented with 10% heat-inactivated FBS with or without 2'3'-cGAMP (30μg/ml) (Invivogen) overnight at 37°C with 5% CO_2.

H. pylori strains were analyzed for growth as previously described [415]. Briefly, overnight cultures were sub-cultured in a 96 well flat-bottom plates and incubated in a microaerophilic chamber, as described above. Optical densities (OD) were recorded at 600 nm (BioTek) at 2, 4, 6, 8, 12, and 24 hours. The final OD value was normalized using uninfected media as a negative control.

Murine models of *Sting* deficiency

All animal studies were carried out in accordance with the recommendations in the *Guide for the Care and Use of Laboratory Animals* of the NIH. Vanderbilt University Institutional Animal Care and Use Committee approved all protocols. Male and female C57BL/6 wild-type (WT) and *Sting*$^{-/-}$ C57BL/6 mice were purchased from Jackson Laboratories and housed in the Vanderbilt University Animal Care Facilities. Mice were orogastrically challenged with Brucella broth (BB) alone, or with the wild-type *cag*$^{+}$ *H. pylori* strain PMSS1. Mice were euthanized at 8 weeks post challenge, and gastric tissue was harvested for quantitative culture, histology, immunohistochemistry, and RNA collection. For quantitative *H. pylori* culture, serial dilutions of homogenized tissue were plated on selective antibiotic TSA-blood agar plates [160].

Histopathology

A single pathologist (MBP) scored indices of inflammation and injury as described previously [146, 160]. Specifically, the following variables were graded on a 0 to 3 scale (0, none; 1, mild; 2, moderate; 3, severe) in the gastric antrum and body: acute inflammation (polymorphonuclear cell infiltration) and chronic inflammation (mononuclear cell infiltration independent of lymphoid follicles); thus, a maximum inflammation score of 12 was possible for each animal.

Immunohistochemistry

For immunohistochemistry, samples were stained with anti-TMEM173/STING ab #19851-1-AP (Proteintech; 1:100), anti-MPO ab #PP023AA (Biocare Medical; Ready-to-use), anti-CD68 ab #PM033AA (Biocare Medical; Ready-to-use), and anti-CD45 ab #10558 (Abcam; 1:4000). Anti-CD3 ab #Ab16669 (Abcam; 1:250) and anti-TRIM30 Ab #NBP2-41087 (Novus Biologicals; 10μg/ml) by the Vanderbilt University Medical Center Translational Pathology Shared Resource

(TPSR). A single pathologist (MBP) blindly evaluated all immunohistochemistry. TRIM30a, MPO, CD3, CD68 and CD45 were evaluated by quantifying positive cells in 5 HPFs (400x) with the highest counts in each mouse. STING staining was evaluated by assessing the percentage of positive epithelial cells and grading the intensity of staining in epithelial cells semi-quantitatively, as previously described [416].

Cell Culture

HEK293-Blue hSTING-R232 cells (STING+), HEK293-Blue Null (STING Parental) cells, HEK293-Lucia RIG-I cells (RIG-I+), and HEK293-Lucia Null cells (RIG-I Parental) (Invivogen) were grown in DMEM (ThermoFisher) supplemented with 10% FBS and 100µg/mL Zeocin (Invivogen). STING+ and RIG-I+ cell media was supplemented with an additional selective antibiotic, Blasticidin (Invivogen) at 10µg/mL. AGS human gastric epithelial cells (ATCC CRL-1739) were grown in RPMI 1640 (ThermoFisher) with 10% FBS. All cell lines were maintained at 37°C with 5% CO_2.

Human-derived gastric epithelial monolayers [417] and mouse primary gastric epithelial cell monolayers [160] were generated as previously reported [418]. Briefly, human fundus was collected during sleeve gastrectomies according to a University of Cincinnati Institutional Review Board-approved protocol (#2015-4869), after informed consent was obtained. For murine organoids, gastric glands were harvested from uninfected wild-type or *Sting*$^{-/-}$ mice at least 8 weeks of age. Gastric tissue was washed and digested, and isolated glands were incubated in Matrigel (Corning) [419]. Primary gastric organoids were then converted to 2D epithelial cell monolayers following Matrigel removal and 3D gastric organoids were plated on collagen-coated plates.

Bone marrow-derived dendritic cells (BMDC) were generated from bone marrow obtained from femurs of wild-type and *Sting*$^{-/-}$ mice. Briefly, marrows were treated with red blood cell lysis buffer (KD Medical) and washed with PBS and recovered white blood cells were plated in advanced DMEM media (Gibco) supplemented with 20% FBS and 40 ng/mL each of GM-CSF and IL-4 (Peprotech) for 6 days at 37°C and 5% CO_2 for differentiation.

Ex vivo and *in vitro* Infections

Primary 2D gastric monolayers were co-cultured with wild-type *H. pylori* strains J166 or PMSS1, with or without 2'3'-cGAMP (30μg/ml) at a multiplicity of infection (MOI) of 100:1 for 6 or 24 h. BMDCs and were co-cultured with wild-type *H. pylori* strain J166 at a multiplicity of infection (MOI) of 10:1 or ODN-1826 (6μg/ml) for 6, 12, or 24 hr. RNA and protein were then isolated from co-culture samples for RT-PCR and Western blot analysis respectively.

STING Reporter Assay

HEK293-Blue hSTING-R232 cells (STING+) and HEK293-Blue Null1 (Parental) cells were seeded in 96-well plates (Corning) at 50,000 cells per well in DMEM without antibiotics and challenged with either viable *H. pylori* (MOI 100:1), sterile PBS, and/or 2'3-cGAMP (30μg/ml) at 37 °C with 5% CO_2 for 24 hours. Supernatants were then added to QUANTI-Blue™ solution (Invivogen) and plates were analyzed by spectrophotometer (Bitoek) at 650nm. All experiments were performed in duplicate and repeated at least three times. Data are expressed as fold over uninfected control.

RIG-I Reporter Assay

HEK293-Lucia RIG-I cells (RIG-I+), and HEK293-Lucia Null cells (RIG-I Parental) cells were seeded in 96-well plates (Corning) at 50,000 cells per well in DMEM without antibiotics and challenged with either viable *H. pylori* (MOI 100:1), sterile PBS, and/or 3php-RNA (5000ng/ml)

at 37 °C with 5% CO_2 for 24 hours. Supernatants were then added to QUANTI-Luc™ solution (Invivogen) and plates were analyzed by luminometer (Bitoek). All experiments were performed in duplicate and repeated at least three times. Data are expressed as fold over uninfected control.

Cell Viability Assay

The effect of *H. pylori* and/or agonists on reporter cell viability was assessed in STING+, RIG-I+, and their respective parental cells using the CellTiter-Blue assay (Promega) according to the manufacturer's instructions. In brief, following co-culture, STING or RIG-I reporter cells were washed with PBS containing gentamycin (250μg/ml) and hygomycin (500μg/ml), followed by incubation with DMEM media containing gentamycin (250μg/ml) and hygomycin (500μg/ml). After a 30-minute incubation at 37°C to eliminate residual viable *H. pylori*, CellTiter-Blue reagent was added. Samples were incubated for 1 hour at 37°C and fluorescence was measured ($485_{Ex}/516_{Em}$) using a fluorescent imaging plate reader (Biotek).

CagA Translocation Assay

H. pylori cagA^{+} strain J166 grown in the presence or absence of 2'3'-cGAMP was co-cultured with AGS cells for 4 hours. Levels of total CagA and phosphorylated (reflecting translocated protein) CagA were determined via Western blotting. GAPDH served as a loading control. Protein intensities were quantified using ImageJ software (NIH).

Real-Time PCR

RNA was extracted using the RNAeasy Mini Kit (Qiagen) for all sample types per manufacturer's instructions. cDNA was synthesized using High-Capacity cDNA Reverse Transcription Kit (ThermoFisher) and quantitative real-time PCR was performed using Power SYBR Green Master Mix (ThermoFisher) for human samples and TaqMan™ Universal Master Mix II (ThermoFisher) for murine samples, with gene-specific primers **(Table 4)**.

Table 2. List of primers and assays used in Chapter III.

Human RT-PCR primers	
Primer Name	**DNA sequence**
CXCL10-F	5′-GCAGTTAGCAAGGAAAGGTCTAA-3’
CXCL10-R	5′-ATGTAGGGAAGTGATGGGAGAG-3’
GAPDH-F	5′-AGCCTCAAGATCATCAGCAATG-3’
GAPDH-R	5′-GGGTGCTAAGCAGTTGGTGG-3’
MX1-F	5′-GTGGCTGAGAACAACCTGTG-3’
MX1-R	5′-GGCATCTGGTCACGATCCC-3’
TRIM5-F	5′-GCTCTCCGAAACCACAGATAA-3’
TRIM5-R	5′-CCCAGGATGCCAGTACAATAA-3’
TRIM6-F	5′-GGAGGATGGGAAGGTCATTT-3’
TRIM6-R	5′-CCTGAAACTTCTCCTGGTACTC-3’
TRIM22-F	5′-TGGAAGATCGAGAGACAGAAGA-3’
TRIM22-R	5′-CCAGGTTATCCAGCACATTCA-3’
TRIM29-F	5′-GACCTGCATCTGCTACCTTT-3’
TRIM29-R	5′-ACAGCTCCGTCTCCTTCT-3’
Mouse Integrated DNA Technologies (IDT) PrimeTime™ qPCR probe assays	
Gene	**Assay ID**
Cxcl10	Mm.PT.58.43575827
Gapdh	Mm.PT.39a.1
Icos	Mm.PT.58.6938712
Ifng	Mm.PT.58.41769240
Il1b	Mm.PT.58.41616450
Il6	Mm.PT.58.10005566
Il12b	Mm.PT.58.12409997
Il17a	Mm.PT.58.6531092
Il17f	Mm.PT.58.9739903
Il23	Mm.PT.58.41340226
Irf4	Mm.PT.58.31041855
Mx1	Mm.PT.58.12101853
Trim30a	Mm.PT.56a.43098591

Western blot

AGS cells, human, and murine organoids co-cultured with *H. pylori* were lysed, centrifuged and proteins were separated using 6% (AGS cells) or 10% (organoids) SDS PAGE mini gels, transferred to PVDF membranes and membranes were blocked with BSA or milk as denoted. For detection of proteins, membranes were incubated overnight with anti-CagA rabbit Ab (Austral Biologicals; 1:5000, BSA), anti-pY99 antibody mouse mAb (Santa Cruz; 1:5000, BSA), anti-phospho-IRF-3 rabbit mAb #29047 (Cell Signaling Technology; 1:1000, BSA), anti-

IRF-3 rabbit mAb #11904 (Cell Signaling Technology; 1:1000, BSA), anti-phospho-TBK1/NAK rabbit mAb #5483 (Cell Signaling Technology; 1:1000, BSA), anti-TBK1/NAK rabbit mAb #38066 (Cell Signaling Technology; 1:1000, BSA), anti-LC3A/B rabbit Ab #4108 (Cell Signaling Technology; 1:1000, BSA), anti-TMEM173/STING rabbit Ab #19851-1-AP (Proteintech; 1:1000, milk), anti-GAPDH mouse mAb #MAB374 (Milipore Sigma; 1:5000, milk), or anti-TRIM30 rabbit Ab #NBP2-41087 (Novus Biologicals; 1:1000, milk). An anti-rabbit or anti-mouse HRP-conjugated secondary antibody (Promega; 1:10000) was then incubated with membranes for 1 hour.

TRIM30a immunofluorescence staining

Monolayers of primary gastric epithelial cells derived from C57BL/6 wild-type and *Sting*$^{-/-}$ mice were infected for 24 hours with *H. pylori* strains J166 or PMSS1. After infection, monolayers were subjected to immunofluorescence staining as previously described [160, 418]. Briefly, cells were fixed with 10% neutral-buffered formalin (Azer Scientific), permeabilized with Triton X-100 (Promega), and then blocked with Dako Protein Block Solution (Agilent) for 1 hour. Samples were incubated with anti-TRIM30 rabbit Ab #NBP2-41087 (Novus Biologicals; 1:50) overnight at 4°C before detection with Alexa-fluor secondary antibody (Invitrogen). Nuclei were detected using Hoescht (Invitrogen). Slides were mounted using ProLong Glass (Invitrogen), and images were acquired in an Olympus FV-1000 confocal microscope. Experiments were performed in part through the use of the Vanderbilt Cell Imaging Shared Resource (CISR).

RNA sequencing and analysis

Total RNA from C57BL/6 wild-type and *Sting*$^{-/-}$ mice was processed using a NEBNext® Ultra™ II RNA Library Prep sample prep kit following the manufacturer's instructions (New England Biosciences) and evaluated on a Qubit 3.0 fluorometer and an Agilent 2100 Bioanalyzer

to quantitate concentration and fragment size distribution prior to sequencing using the NovaSeq 6000 sequencer (Illumina). Sequencing was performed using a S4 flow cell with a PE 150 kit. Individually barcoded libraries were then pooled at an equal molar ratio and sequenced at 2×150 bp/read. Approximately 48 million paired-end sequence reads per sample (mean $\pm$ SD = 48.3856 $\pm$ 7.655 million; n = 34) were generated. Sample quality was assessed via FastQC software. The data were analyzed using the Dragen Software Version: 3.6.3 aligning the data to the mm10 reference genome. The Vanderbilt Technologies for Advanced Genomics (VANTAGE) core facility prepared the RNA library, assessed library quality, and performed sequencing. Differential expression analysis was performed using edgeR [420, 421] based on the following 2 major comparisons: C57BL/6 wild-type infected versus C57BL/6 wild-type Brucella broth control, and *Sting*$^{-/-}$ infected versus *Sting*$^{-/-}$ Brucella broth control. Filters used to identify differential expression were a q-value <0.1 and an absolute log2 fold change >1. Venn diagrams were created (Venny 2.1 software) using these two comparisons. Ingenuity Pathway Analysis software (Qiagen) was used to link DE genes in the dataset to particular biological functions and pathways.

Human Clinical Specimens

Snap frozen de-identified human gastric tissue samples were acquired from the Cooperative Human Tissue Network (CHTN). Normal gastric tissue, or gastric tissues harboring either gastritis alone or gastric adenocarcinoma were disrupted and homogenized using ZR BashingBead Lysis tubes (Zymo Research) prior to RNA extraction. The protocol was approved by the Vanderbilt University Medical Center Institutional Review Board (#210729).

Statistics

The student's t-test or Mann-Whitney test was used for two group comparisons, while one-way analysis of variance with Bonferroni correction was used for multiple group comparisons. Data were plotted and analyzed using Prism 6.0 (GraphPad). Statistical significance was set at a two-tailed p-value of <0.05. In all figures, means ± standard errors of the mean are shown.

3.3 Results

We first sought to directly assess the effects of *H. pylori* on STING signaling, by utilizing HEK293 cells transfected with a STING-specific reporter. While levels of STING activation increased 17-fold in cells co-cultured with 2'3'-cGAMP (a STING agonist), activation levels in cells co-cultured with the wild-type *cag*$^+$ *H. pylori* strain J166 were no different than uninfected controls **(Figure 24A)**. Because certain chronic pathogens have been shown to exert a suppressive effect on STING signaling and to facilitate long-term survival, we next simultaneously co-cultured or preincubated cells for 4 hours with *H. pylori* prior to the addition of 2'3'-cGAMP. *H. pylori* significantly reduced STING agonist-mediated activation by 50% in either condition **(Figure 24A)**. STING suppression by *H. pylori* was dose- **(Figure 24B)** and time-dependent **(Figure 24C)** with minimal effects on cell viability out to 16-24 hours **(Figure 25)**. Previous work defining the ability of *H. pylori* to activate the innate immune DNA sensor TLR9 utilized strain J166 [117]. Therefore, to determine if STING suppression was strain-specific, we repeated these studies using additional isolates and demonstrated that *H. pylori* strain G27, the mouse colonizing strains PMSS1 and 7.13, and clinical strain B128 all significantly reduced STING activation under either preincubation or co-culture conditions compared to agonist alone **(Figure 24D)**. To determine whether 2'3'-cGAMP altered bacterial growth or function *per se*, *H. pylori* was cultured with

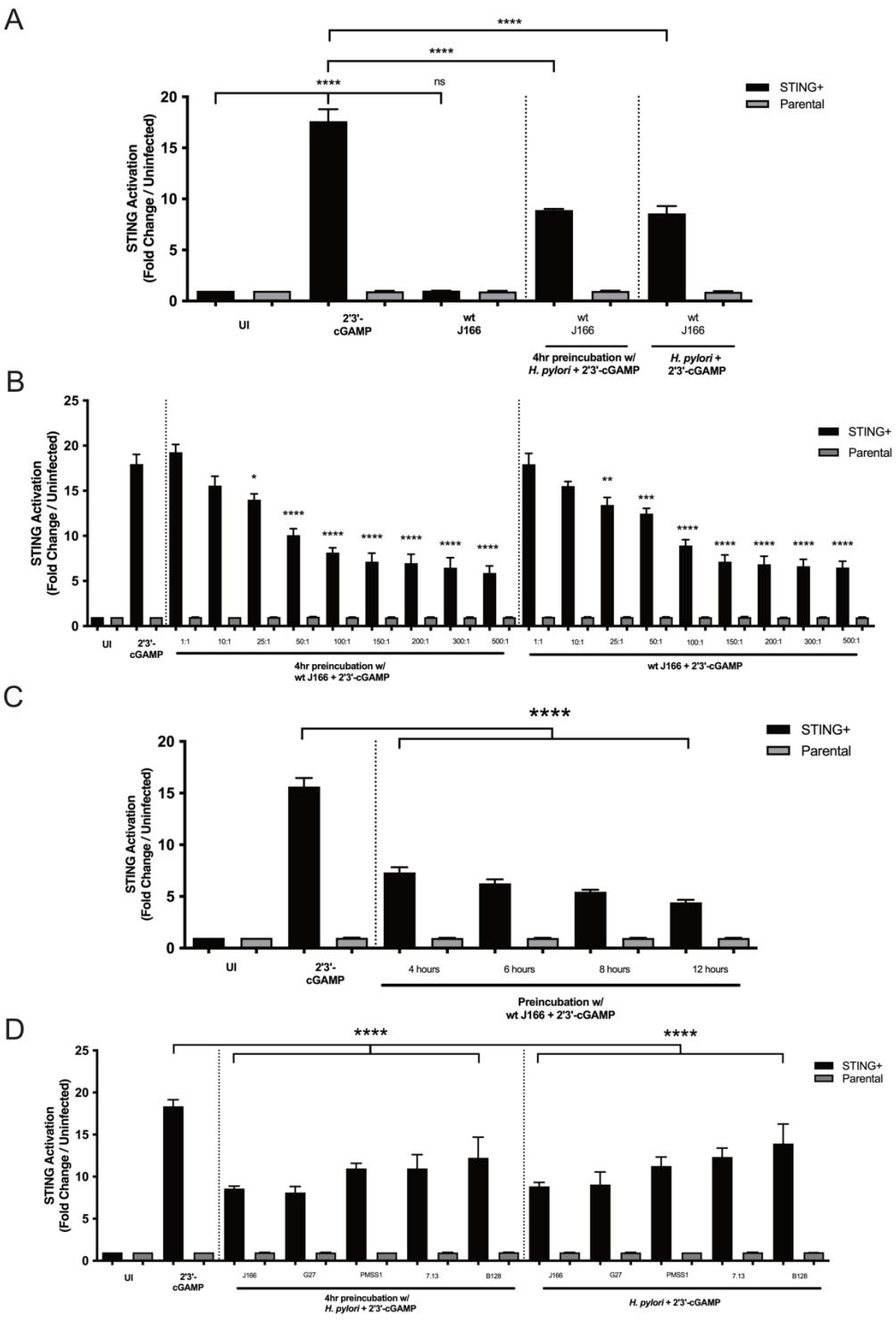

Figure 24. STING activation *in vitro* is attenuated by *H. pylori*. STING+ or parental cells were challenged with STING agonist 2'3'-cGAMP and/or viable *H. pylori* at multiplicity of infection (MOI) 100:1 for 24 hours. Data are shown as fold STING activation induced relative to uninfected control. Each condition was tested in duplicate at least 3 times. Cells were challenged with PBS alone (UI), 2'3'-cGAMP and/or **(A)** *H. pylori cag*$^{+}$ wild-type (wt) strain J166, **(B)** *H. pylori* strain J166 at varying MOIs, **(C)** increasing preincubation times, or **(D)** *H. pylori cag*$^{+}$ strains J166, G27, PMSS1, 7.13, or B128. ANOVA with Bonferroni correction was used to determine statistical significance between groups. ****p<0.0001, ns=not significant.

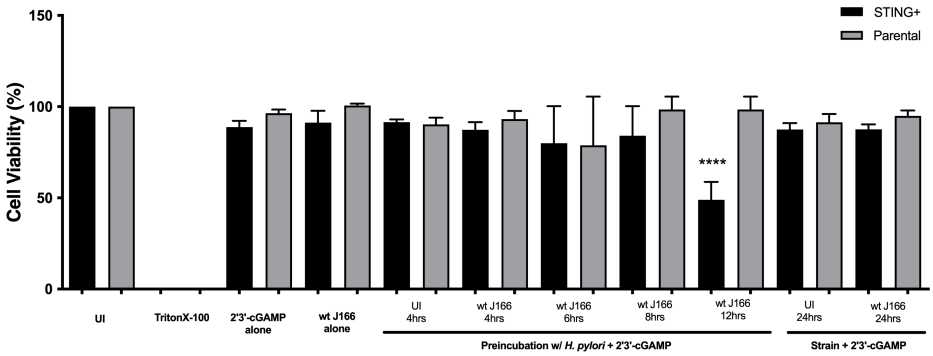

Figure 25. Cell viability of STING+ and parental cells. Following removal of supernatants for STING reporter assay, CellTiter-Blue® assay was performed to determine viability. Each condition was tested in duplicate at least 3 times. Data are shown as fold percent cell viability, relative to positive control uninfected cells and negative control TritonX-100 treated cells.

varying concentrations of 2'3'-cGAMP. No significant differences were observed in either growth or the ability to translocate CagA via the *cag* T4SS, between untreated versus 2'3'-cGAMP-treated bacteria **(Figure 26A,B)**.

Intracellular *Legionella* activates the host RNA sensor RIG-I via RNA polymerase-III, which recognizes the microbial DNA and generates an RNA intermediate [321, 322]. Therefore, the ability of *H. pylori* to suppress activation of RIG-I was also investigated. In HEK293 cells transfected with a RIG-I-specific reporter, RIG-I-associated activation increased 18-fold in cells co-cultured with 3pHp-RNA, a known RIG-I agonist, compared to untreated controls. Similar to results observed with STING activation, no RIG-I activity was observed in cells co-cultured with wild-type *H. pylori* alone **(Figure 27A)**. However, a suppression phenotype was observed during preincubation with *H. pylori* prior to addition of 3pHp-RNA or during co-culture of *H. pylori* and agonist together **(Figure 27A)**, and this occurred in a dose- **(Figure 27B)** and time-dependent manner **(Figure 27C)**. Cell viability of RIG-I reporter cells was not significantly affected by the presence of *H. pylori* and/or agonist **(Figure 28)**. Mirroring the STING results, multiple *H. pylori* strains were able to significantly attenuate RIG-I-associated signaling *in vitro* **(Figure 27D)**.

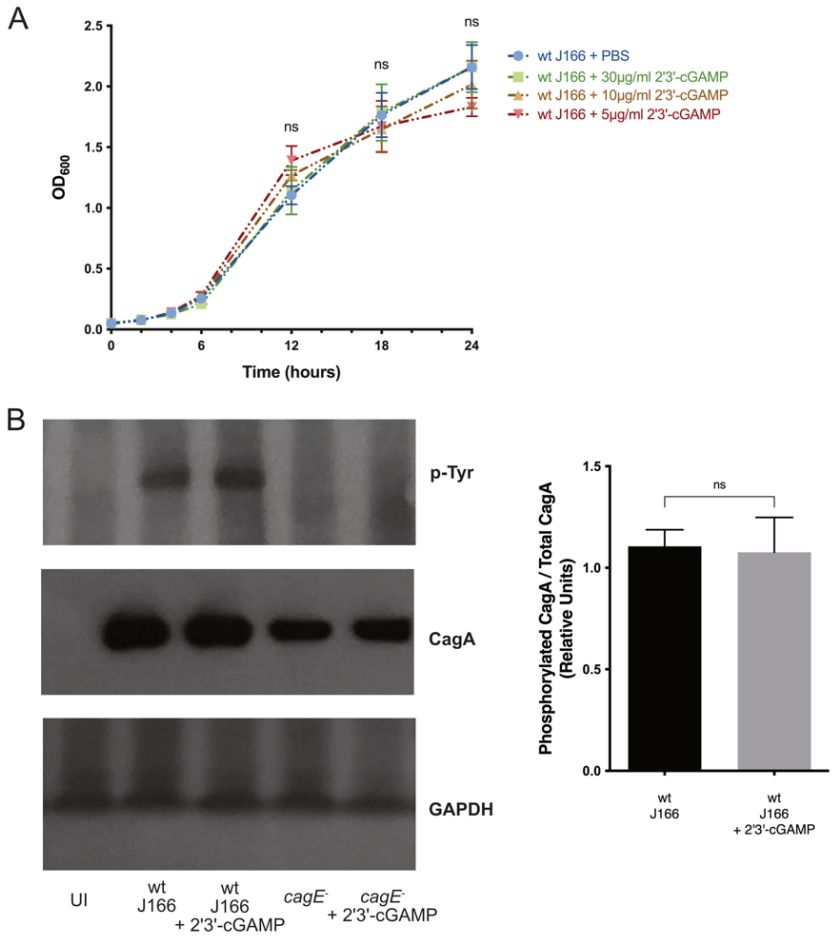

Figure 26. Positive STING agonist 2'3'-cGAMP does not alter *H. pylori* growth or *cag* T4SS function. (A) Growth of *H. pylori cag*$^{+}$ wild-type (wt) strain J166 cultured in Brucella broth supplemented with 10% fetal bovine serum (FBS) alone or supplemented with 5, 10, or 30µg/ml 2'3'-cGAMP was quantified at 2, 4, 6, 12, 18, and 24 hours by spectrophotometric reading at OD600. **(B)** *H. pylori* wild-type *cag* PAI+ strain J166 or isogenic *cagE*$^{-}$ mutant (negative control) strains were grown overnight in either the presence or absence of 2'3'-cGAMP. AGS cells were subsequently co-cultured at MOI 100:1 for 4 hours. CagA translocation was determined by quantifying levels of phospho-CagA in AGS cell lysates during *H. pylori* co-culture by Western blotting. Densitometric analysis normalizing levels of phosphorylated CagA to total CagA from 3 replicates are shown. ANOVA with Bonferroni correction or student's t-tests were used to determine statistical significance between groups. ns=not significant.

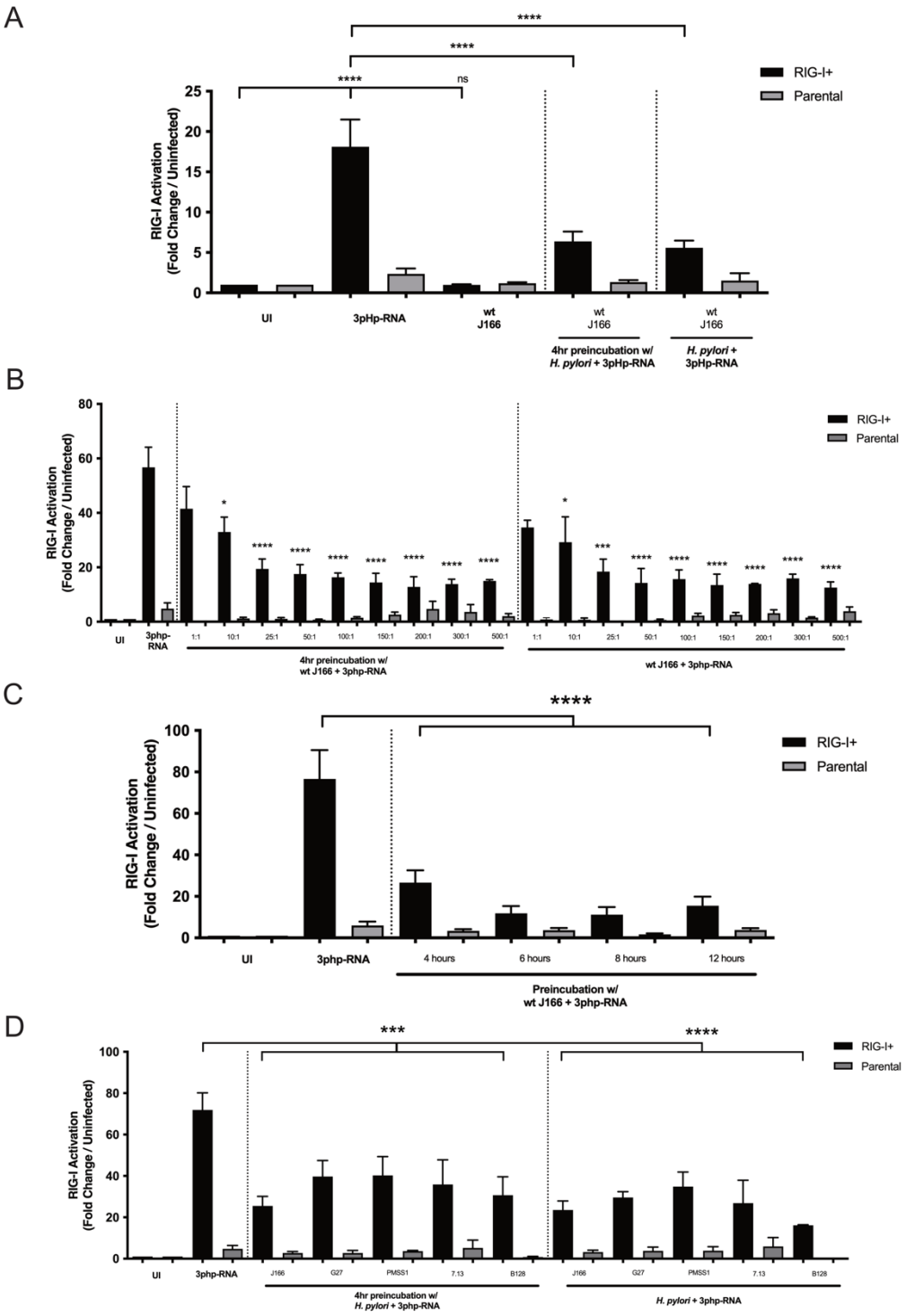

Figure 27. RIG-I activation *in vitro* is attenuated by *H. pylori*. RIG-I+ or parental cells were challenged with RIG-I agonist 3p-hpRNA and/or viable *H. pylori* at MOI 100:1 for 24 hours. Data are shown as fold RIG-I activation induced relative to uninfected control. Each condition was tested in duplicate at least 3 times. Cells were challenged with PBS alone (UI), 3p-hpRNA and/or **(A)** *H. pylori cag*$^{+}$ wild-type (wt) strain J166, **(B)** *H. pylori cag*$^{+}$ strain J166 at varying MOIs, **(C)** increasing preincubation times, or **(D)** *H. pylori* strains J166, G27, PMSS1, 7.13, or B128. ANOVA with Bonferroni correction was used to determine statistical significance between groups. ***p<0.001, ****p<0.0001, ns=not significant.

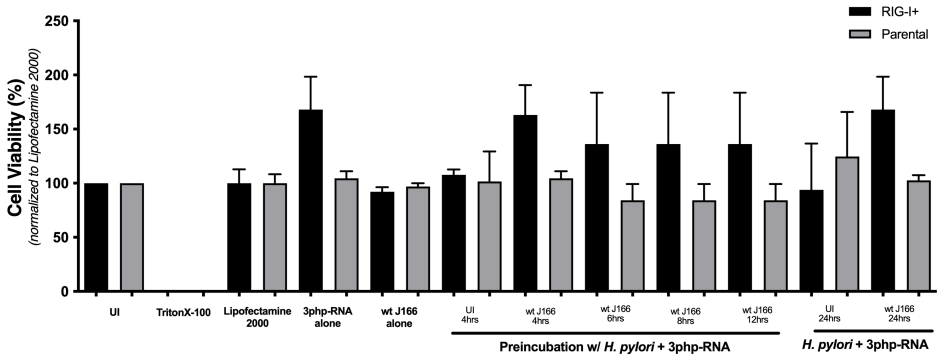

Figure 28. Cell viability of RIG-I+ and parental cells. Following removal of supernatants for RIG-I reporter assay, CellTiter-Blue® assay was performed to determine viability. Each condition was tested in duplicate at least 3 times. Data are shown as fold percent cell viability normalized to Lipofectamine 2000 control, relative to positive control uninfected cells and negative control TritonX-100 treated cells.

To determine whether the suppression phenotype for STING and RIG-I required an active interplay between *H. pylori* and host cells, we repeated the STING and RIG-I reporter assay experiments with wild-type *H. pylori* J166 that had been heat-inactivated for 1 hour at 56°C **(Figures 29A,B)**. Heat-inactivation abolished the suppressive phenotype for both STING and RIG-I. Further, *H. pylori* genomic DNA *per se* was unable to suppress STING- and RIG-I-associated signaling *in vitro* when compared to viable *H. pylori* **(Figure 29C,D)**. These results demonstrate that only viable *H. pylori* can suppress STING- and RIG-I- associated signaling *in vitro.*

The InvivoGen HEK293-Blue™ hSTING-R232 cells and HEK293-Lucia™ RIG-I cells used for these assays are predominantly dependent on activation of IRF3 which, when phosphorylated, induces type I interferon (IFN) gene expression. The IFN-stimulated response elements (ISRE) luciferase reporter in RIG-I reporter cells, however, can also be activated by type I IFN activation which is induced by JAK/STAT signaling through ISG54. Therefore, to determine whether the observed RIG-I phenotype was IRF3- versus JAK/STAT-dependent, we utilized the inhibitor Ruxonitlib, which inhibits downstream type I IFN signaling via the JAK-STAT pathway,

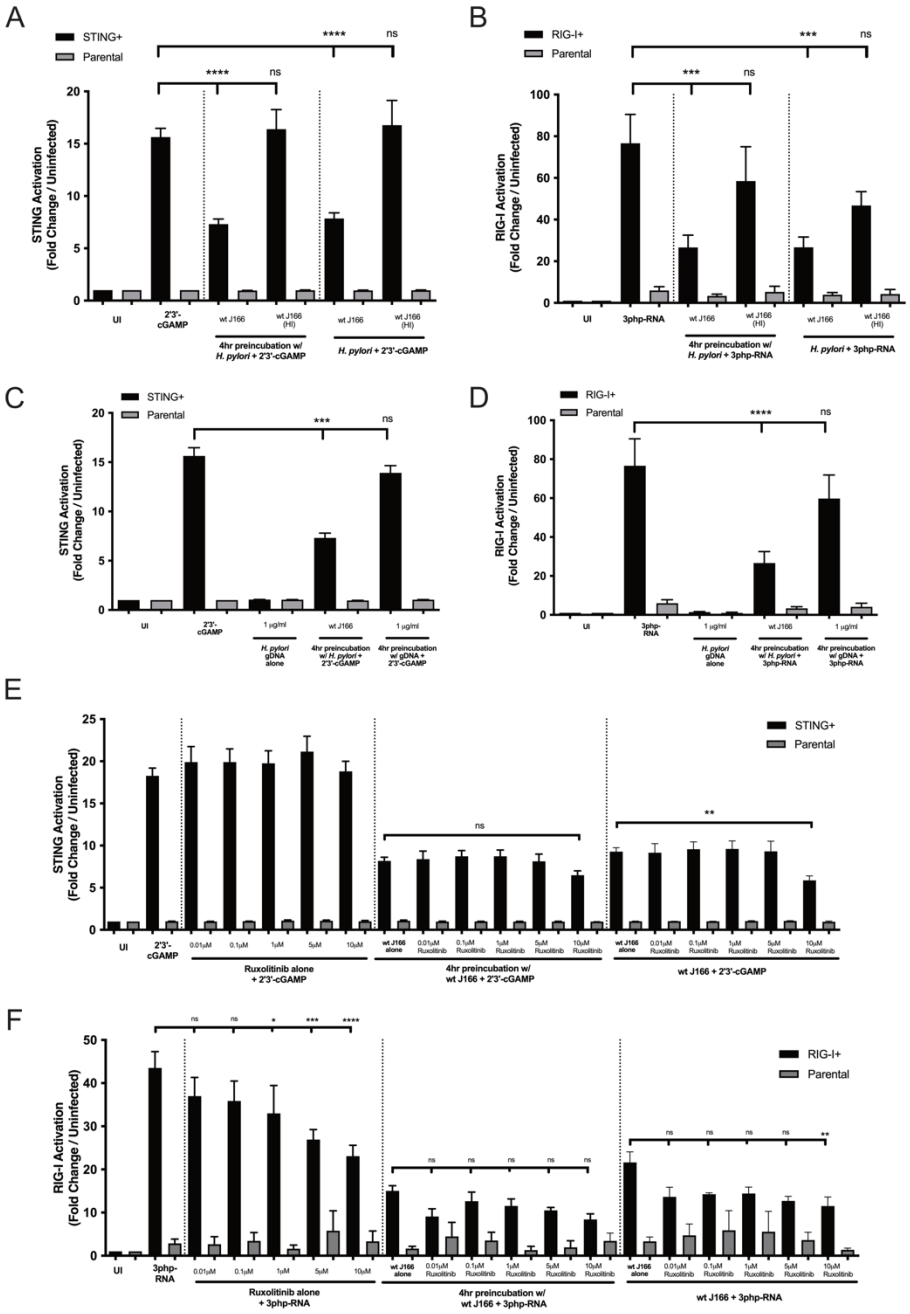

Figure 29. *H. pylori* actively suppress STING and RIG-I activation *in vitro*. STING+, RIG-I+, and respective parental cells were challenged with positive agonists and/or *H. pylori* at MOI 100:1 or *H. pylori* gDNA for 24 hours. Data are shown as fold activation induced relative to uninfected control. Each condition was tested in duplicate at least 3 times. **(A)** STING+ or parental cells were challenged with PBS alone (UI), 2'3'-cGAMP and/or viable or heat inactivated (HI) *H. pylori* wild-type (wt) strain J166. **(B)** RIG-I+ or parental cells were challenged with 3p-hpRNA and/or viable or heat inactivated *H. pylori* strain J166. **(C)** STING+ or parental cells were challenged with 2'3'-cGAMP, and/or *H. pylori* strain J166 or *H. pylori* gDNA. **(D)** RIG-I+ or parental cells were challenged with 3p-hpRNA and/or *H. pylori* strain J166 or *H. pylori* gDNA. **(E)** STING+ or parental cells were challenged with 2'3'-cGAMP, and/or *H. pylori* strain J166 in the presence of increasing concentrations of Ruxonitilib. **(F)** RIG-I+ or parental cells were challenged with 3p-hpRNA and/or *H. pylori* strain J166 in the presence of increasing concentrations of Ruxonitilib. ANOVA with Bonferroni correction was used to determine statistical significance between groups. *p<0.05, **p<0.01, ***p<0.001, ****p<0.0001, ns=not significant.

leaving IRF3-dependent signaling unaffected. Ruxonitlib in the presence of *H. pylori* and positive agonists failed to alter suppression when compared to *H. pylori* and agonist alone **(Figure 29E,F)**. However, when Ruxonitlib and agonist alone were co-cultured without *H. pylori*, RIG-I-associated signaling but not STING-associated signaling was significantly reduced compared to the agonist alone **(Figure 29E,F)**. These data suggest that *H. pylori* likely exerts inhibitory effects at the level of IRF in these signaling pathways.

Gastroids are polarized, replenishable epithelial culture systems that can be readily generated from non-transformed gastric epithelium [422, 423]. We previously developed and optimized gastroid models of *H. pylori* infection originating from both human and murine gastric tissues [160, 418]; therefore, we capitalized on this manipulatable *ex vivo* system as a biologically relevant model that more faithfully recapitulates the gastric niche to extend our *in vitro* results using reporter systems. Primary gastric organoids generated from human patients were co-cultured for 6 or 24 hours with wild-type *H. pylori* strain J166, with or without the positive STING agonist, and lysates were subsequently probed for downstream effectors of STING activation via Western blotting. *H. pylori*-infected human organoids harbored significantly lower levels of phosphorylated IRF3, an effector activated by STING, compared to uninfected controls at both 6 and 24 hours **(Figure 30A)**. The positive control 2'3'-cGAMP alone induced significantly higher levels of pIRF3 at 6 hours compared to controls but this did not occur during co-culture with *H. pylori* **(Figure 30A)**. Concordantly, expression levels of the IRF3-dependent type I interferon stimulated genes *MX1* and *IP-10* were significantly upregulated in human gastric organoids following co-culture with 2'3'-cGAMP **(Figure 30B)**, but expression was significantly reduced in samples co-infected with *H. pylori* and 2'3'-cGAMP **(Figure 30B)**. These results indicate that *H. pylori* infection of organoids recapitulated the suppressive phenotype observed in reporter cell assays.

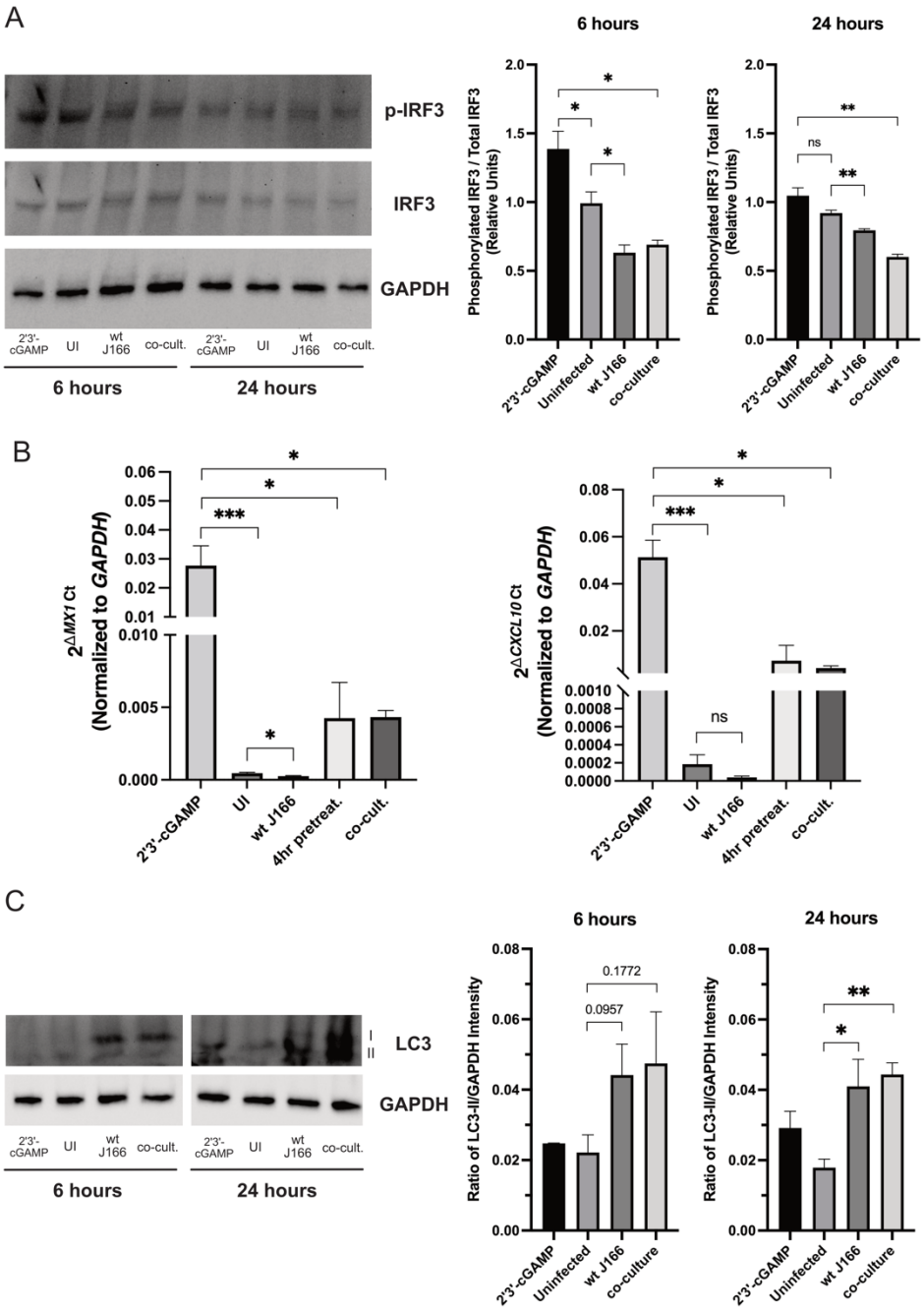

Figure 30. *H. pylori* infection of human gastric organoids downregulates phosphorylation of IRF3 but induces autophagy. Human gastric organoid monolayers were challenged with PBS alone (UI), *H. pylori* wild-type (wt) strain J166, and/or STING agonist 2'3'-cGAMP at MOI 100:1 for 6 hours or 24 hours. **(A)** IRF3 phosphorylation was determined by quantifying levels of phospho-IRF3 in co-cultured organoid lysates by Western blotting. Representative images and densitometric analysis normalizing levels of phosphorylated IRF3 to total IRF3 from 3 replicates are shown at each time point. **(B)** RT-PCR analysis of *MX1* and *CXCL10* transcript levels in co-cultured organoid lysates. Data are represented as relative gene expression levels normalized to levels of *GAPDH* gene expression. **(C)** Induction of autophagy was determined by quantifying levels of LC3-II in co-cultured organoid lysates by Western blotting. Representative images and densitometric analysis normalizing levels of LC3-II to GAPDH from 3 replicates are shown at each time point. In each experiment, conditions were tested at least 3 times and student's t-tests were used to determine statistical significance between groups. *p<0.05, **p<0.01, ***p<0.001.

STING complexes can recruit effectors which drive autophagy-like responses, that are independent of IRF3-mediated *Ifnb* transcription [424]. *H. pylori* can also induce autophagy. Therefore, we analyzed autophagy under these conditions. All *H. pylori*-infected samples demonstrated a significant increase in levels of autophagy compared to uninfected samples by 24 hours when utilizing increases in the autophagosome marker LC3-II as a proxy for autophagy **(Figure 30C)**. Collectively, these results suggest that *H. pylori* can suppress STING signaling via IRF3 and that *H. pylori*-induced autophagy is independent of STING [425, 426].

We next extended these findings by defining the role of STING in *H. pylori*-induced injury *in vivo*. C57BL/6 wild-type and *Sting*-deficient mice (*Sting*$^{-/-}$) were infected with the *H. pylori in vivo*-adapted *cag*$^{+}$ strain PMSS1, which harbors the ability to suppress STING-associated signaling *in vitro* **(Figure 24D)**. No significant differences in levels of *H. pylori* colonization were present between wild-type and *Sting*$^{-/-}$ mice following 8 weeks of infection **(Figure 31A)**.

As expected, wild-type mice infected with wild-type *H. pylori* developed significantly increased levels of acute and chronic inflammation compared to uninfected controls **(Figure 31B)**. However, genetic deficiency of *Sting* augmented acute, but not chronic inflammation, compared to infected wild-type mice **(Figure 31B)**. Further immunophenotyping by immunohistochemistry staining revealed significantly higher levels of neutrophils in infected *Sting*$^{-/-}$ mice compared to infected wild-type mice **(Figure 31C)**, while the number of macrophages, T cells, and B cells remained unchanged in the presence *H. pylori* regardless of *Sting* status **(Figure 32)**, suggesting that STING alters acute inflammatory events during *H. pylori* infection.

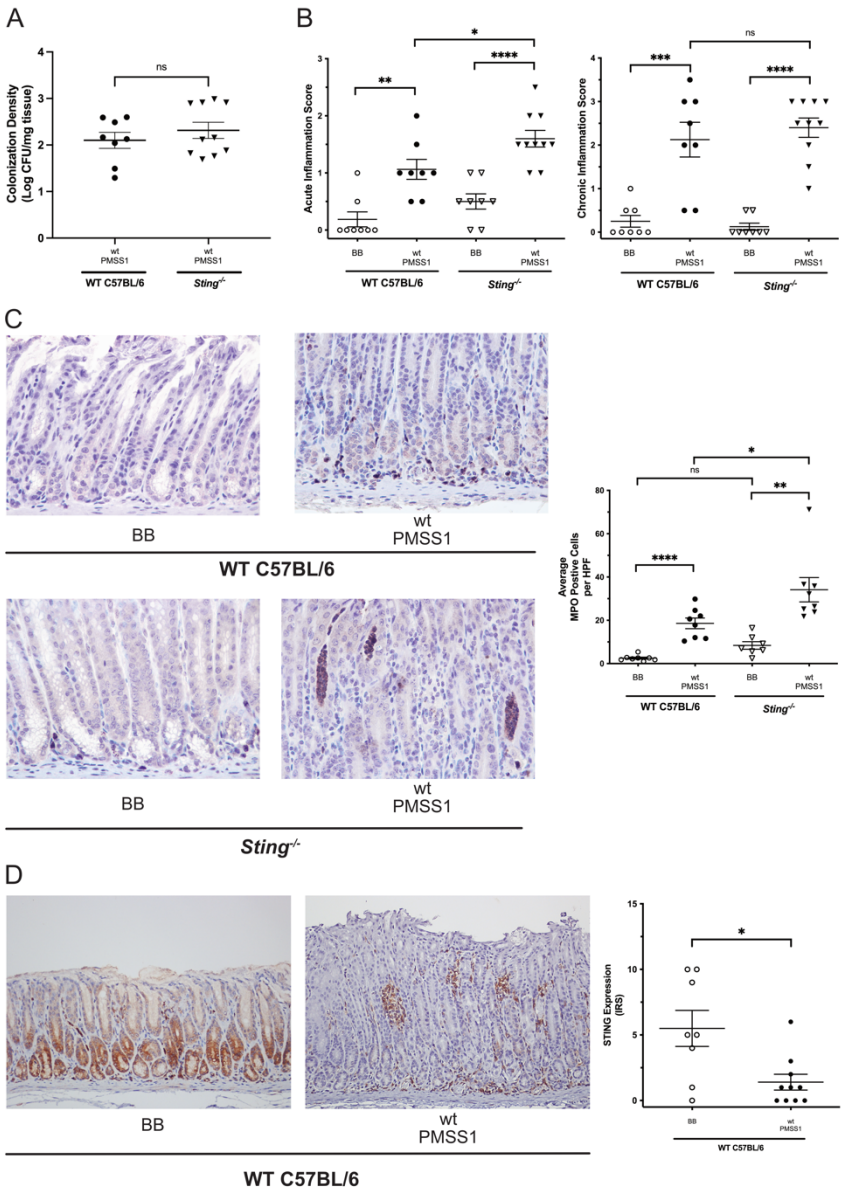

Figure 31. *H. pylori* infection significantly augments acute immune responses in *Sting*-deficient mice and decreases STING expression in wild-type mice. C57BL/6 wild-type (WT) and *Sting*$^{-/-}$ mice were challenged with Brucella broth (BB) or *H. pylori* wild-type (wt) strain PMSS1 for 8 weeks. **(A)** Stomach sections were homogenized and serially diluted on blood-agar plates to quantify *H. pylori* colonization levels in infected mice after 8 weeks of infection. **(B)** Acute or chronic inflammation scores of C57BL/6 wild-type or *Sting*$^{-/-}$ mice infected with or without *H. pylori* as determined by a pathologist blinded to treatment groups. Histologic parameters were scored from 0-3 as outlined by the Sydney System [427]. **(C)** Levels of MPO in wild-type or *Sting*$^{-/-}$ mice infected with or without *H. pylori*. Representative images are shown at 400x magnification of immunohistochemistry staining for MPO. MPO^{+} cells were enumerated in 5 high-powered fields (HPF) from each animal and averaged. **(D)** Levels of STING in *H. pylori*-infected versus uninfected C57BL/6 tissue. Representative images are shown at 200x magnification of immunohistochemistry staining (brown) for STING in uninfected or *H. pylori*-infected wild-type mice. Immunoreactive score (IRS) gives a range of 0–12 as a product of multiplication between positive cells proportion score (0–4) and staining intensity score (0–3) across 5 HPFs from each animal. Each data point represents an individual animal (WT BB, n=8; WT PMSS1, n=8; *Sting*$^{-/-}$ BB, n=8; *Sting*$^{-/-}$ PMSS1, n=10). Student's t-tests were used to determine statistical significance between groups. *p<0.05, **p<0.01, ***p<0.001, ****p<0.0001, ns=not significant.

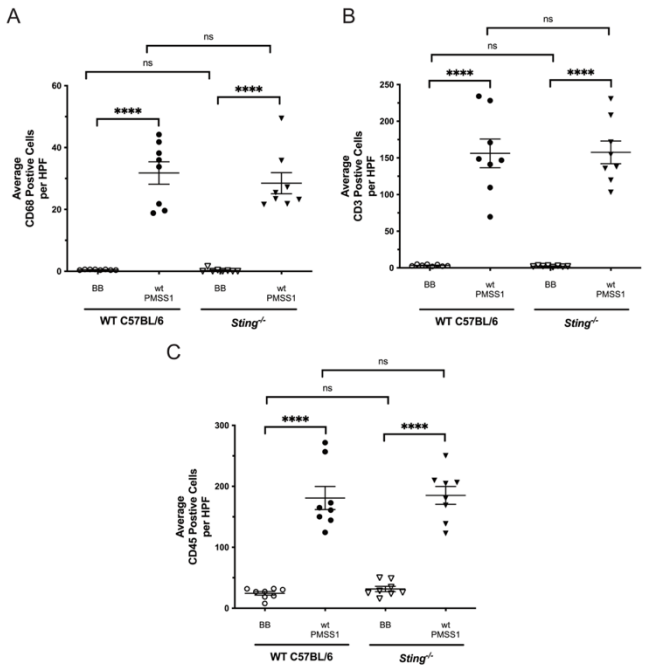

Figure 32. Levels of macrophages, T-cells, and B-cells *in vivo* remained unchanged in the presence of *H. pylori* regardless of host *Sting* status. Levels of **(A)** CD68 **(B)** CD3 and **(C)** CD45 positive cells in wild-type or *Sting*$^{-/-}$ mice infected with or without *H. pylori*. Each data point represents an individual animal (WT BB, n=8; WT PMSS1, n=8; *Sting*$^{-/-}$ BB, n=8; *Sting*$^{-/-}$ PMSS1, n=10). Positive cells were enumerated in 5 high-powered fields from each animal and averaged. Student's t-tests were used to determine statistical significance between groups. ****p<0.0001, ns=not significant.

Decreased STING expression has been shown to be an independent and adverse predictor of overall survival in human gastric cancer patients [352]. Examination of wild-type murine samples by immunohistochemistry revealed that levels of STING expression in *H. pylori*-infected gastric tissue were significantly reduced compared to uninfected samples **(Figure 31D)** and as expected, undetectable in *Sting*$^{-/-}$ mice (data not shown). These data indicate that *H. pylori* can not only suppress STING signaling but can also reduce levels of STING expression.

To identify specific effectors mediating suppression of STING signaling by *H. pylori in vivo*, we next performed a discovery-based RNA-seq analysis utilizing RNA isolated from whole gastric mucosa from wild-type and *Sting*$^{-/-}$ mice. Two different comparisons were performed to

identify *Sting*-dependent responses following *H. pylori* challenge. First, to identify genes differentially expressed following *H. pylori* infection, datasets from the wild-type uninfected and infected mice were termed Comparison 1, while differentially expressed genes between *Sting*$^{-/-}$ uninfected and infected mice were termed Comparison 2 **(Figure 33A)**. Comparison 1 revealed 213 upregulated and 19 downregulated genes following *H. pylori* infection **(Appendix A, Table 1)** while Comparison 2 identified 840 genes differentially expressed in *Sting*$^{-/-}$ mice following *H. pylori* infection, with 382 upregulated genes and 458 downregulated genes **(Appendix A, Table 2)**. Ingenuity Pathway Analysis software was then used to harmonize the datasets to identify predicted biological functions and pathways to reveal possible mechanisms that may underpin the suppressive phenotypes **(Table 2)**.

Pathway analysis revealed that predicted functions related to IL-17 signaling had significant activation scores ($\geq$2) in both wild-type and *Sting*$^{-/-}$ mice **(Figure 33B)**, consistent with prior data demonstrating the ability of *H. pylori* to induce IL-17 production and Th17 responses [119, 160, 392, 428, 429] in conjunction with observations that inhibition of STING activation is associated with increased Th17 cell infiltration, increased production of IL-17A, and worsening inflammation in conditions such as chronic pancreatitis [391]. Therefore, to independently validate potential differences in IL-17 signaling due to *Sting* deficiency within the context of *H. pylori* infection, we examined Th17 differentiation and stabilization factors via RT-PCR of RNA isolated from gastric tissue. Differentiation and formation of Th17 cells can be driven by transcription factors such as IRF4 and cytokines such as IL-23. Transcript levels of *Irf4* and *Il23* in *H. pylori*-infected *Sting*$^{-/-}$ mice were significantly increased compared to infected wild-type mice while no significant differences were observed in levels of *Il1b* and *Il6,* suggesting that in the absence of *Sting*, Th17 differentiation is primarily driven by IL-23 **(Figure 33C)**. Transcript levels of *Il17a*

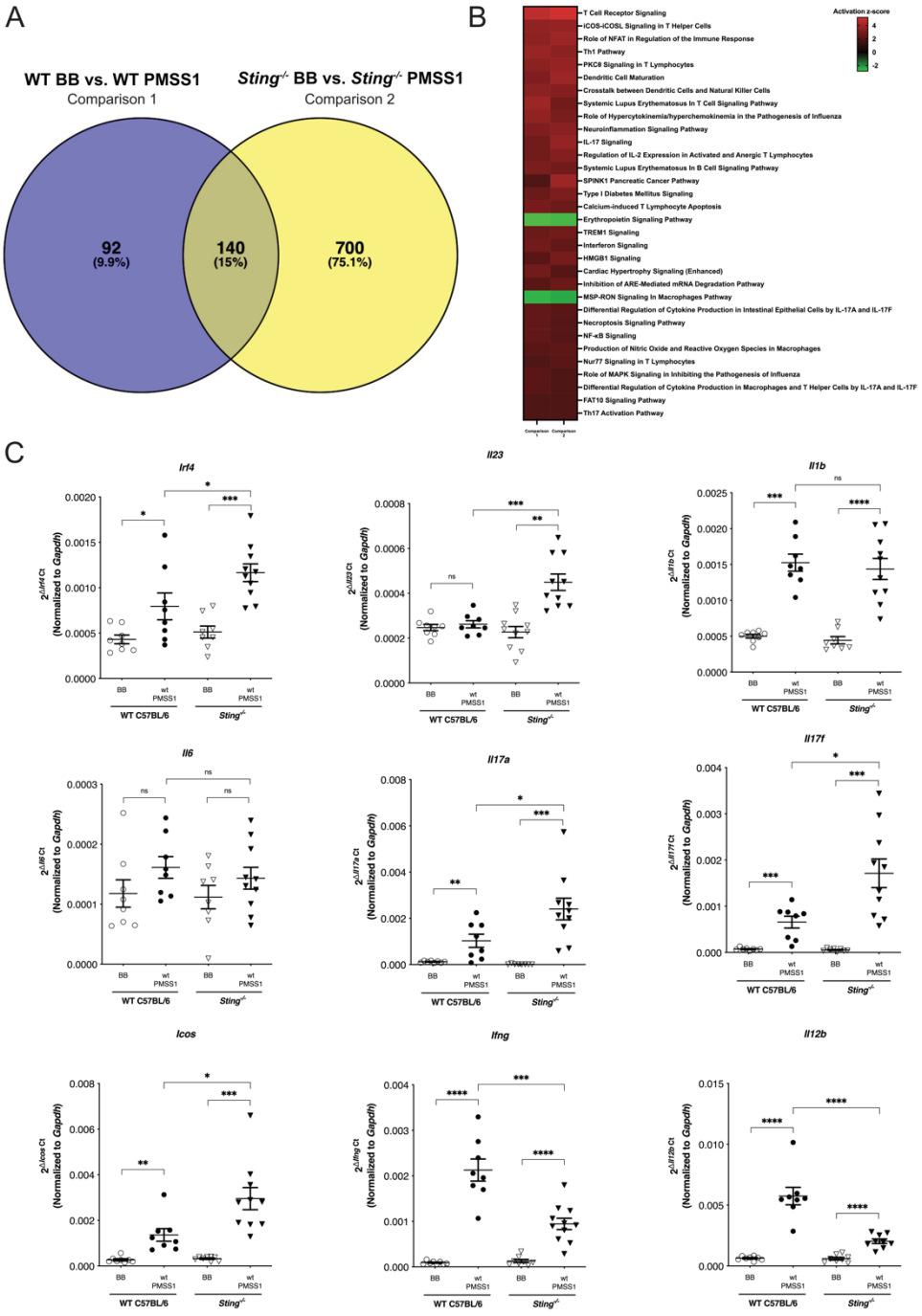

Figure 33. Differential expression analysis on RNA-seq dataset between C57BL/6 wild-type and *Sting*$^{-/-}$ infected and uninfected control mice. (A) Venn diagram representing differentially expressed genes in the RNA-seq dataset of C57BL/6 wild-type (WT) and *Sting*$^{-/-}$ mice. **(B)** Top significantly affected ($2.0 < Z\ score < -2.0$) canonical pathways based on Ingenuity Pathway Analysis (IPA). The horizontal bars denote the different pathways based on the Z-scores. Red indicates activation, while green indicates suppression. **(C)** mRNA expression of Th17-related genes in uninfected and *H. pylori*-infected wild-type mice, and uninfected and *H. pylori*-infected *Sting*$^{-/-}$ mice. Data are represented as relative gene expression levels normalized to levels of *Gapdh* gene expression. Each data point represents an individual animal (WT BB, n=8; WT PMSS1, n=8; *Sting*$^{-/-}$ BB, n=8; *Sting*$^{-/-}$ PMSS1, n=10). Student's t-tests were used to determine statistical significance between groups. *p<0.05, **p<0.01, ***p<0.001, ****p<0.0001, ns=not significant.

Table 3. Top significantly affected (2.0 < Z score < −2.0) canonical pathways based on Ingenuity Pathway Analysis between comparison 1 and comparison 2**.**

Pathway	Comparison 1	Comparison 2
T Cell Receptor Signaling	4.747	5.209
iCOS-iCOSL Signaling in T Helper Cells	3.606	3.742
Role of NFAT in Regulation of the Immune Response	3.464	3.873
Th1 Pathway	3.771	3.5
PKCθ Signaling in T Lymphocytes	3.464	3.742
Dendritic Cell Maturation	3.207	3.873
Crosstalk between Dendritic Cells and Natural Killer Cells	3.464	3.317
Systemic Lupus Erythematosus in T Cell Signaling Pathway	3.873	2.828
Role of Hypercytokinemia/hyperchemokinemia in the Pathogenesis of Influenza	3.606	3.051
Neuroinflammation Signaling Pathway	3.207	3.441
IL-17 Signaling	2.828	3.742
Regulation of IL-2 Expression in Activated and Anergic T Lymphocytes	2.828	3.317
Systemic Lupus Erythematosus in B Cell Signaling Pathway	3.051	2.84
SPINK1 Pancreatic Cancer Pathway	2	3.873
Type I Diabetes Mellitus Signaling	2.646	3.162
Calcium-induced T Lymphocyte Apoptosis	3	2.714
Erythropoietin Signaling Pathway	-2.828	-2.714
TREM1 Signaling	2.646	2.828
Interferon Signaling	2.828	2.449
HMGB1 Signaling	2.236	3
Cardiac Hypertrophy Signaling (Enhanced)	2.828	2.183
Inhibition of ARE-Mediated mRNA Degradation Pathway	2.236	2.646
MSP-RON Signaling in Macrophages Pathway	-2.53	-2.309
Differential Regulation of Cytokine Production in Intestinal Epithelial Cells by IL-17A and IL-17F	2.449	2.236
Necroptosis Signaling Pathway	2.449	2.121
NF-κB Signaling	2.449	2.121
Production of Nitric Oxide and Reactive Oxygen Species in Macrophages	2.236	2.333
Nur77 Signaling in T Lymphocytes	2	2.236
Role of MAPK Signaling in Inhibiting the Pathogenesis of Influenza	2.236	2
Differential Regulation of Cytokine Production in Macrophages and T Helper Cells by IL-17A and IL-17F	2.236	2
FAT10 Signaling Pathway	2	2
Th17 Activation Pathway	2	2

and *Il17f* were also significantly increased in *H. pylori*-infected *Sting*$^{-/-}$ mice compared to infected wild-type mice **(Figure 33C)**. Inducible Costimulator (ICOS) has been shown to be critical for the development of Th17 cells; accordingly, significantly higher levels of *Icos* were observed in infected *Sting*$^{-/-}$ mice compared to infected wild-type mice, and conversely, significantly lower levels of the Th17 inhibitors *Ifng*, and *Il12b* were present in infected *Sting*-deficient mice **(Figure 33C)**.

We next sought to recapitulate our human *ex vivo* findings **(Figure 30)** demonstrating that *H. pylori* infection can selectively downregulate phospho-IRF3-dependent pathways in gastric epithelial cells and further delineate the role of *H. pylori* in regulating phenotypes linked to *Sting* deficiency within our murine model systems. Gastroid monolayers isolated from mice were infected *ex vivo* with *H. pylori* strains J166 or PMSS1 for 24 hours and were used to analyze STING downstream pathways via RT-PCR. IRF3-dependent type I interferon stimulated genes *Mx1* and *Cxcl10* were significantly upregulated in wild-type murine gastric organoids following co-culture with 2'3'-cGAMP, but expression was significantly reduced in samples co-infected with *H. pylori* and 2'3'-cGAMP, and no changes were observed in *Sting*$^{-/-}$ monolayers **(Figure 34A,B)**.

We next sought to further refine the identification of mediators of STING suppression in response to *H. pylori* by filtering the overall differentially expressed gene lists to identify *Sting*-dependent genes. Using the Comparison 1 list **(Appendix A, Table 1)**, any differentially expressed gene that was also found in Comparison 2 was removed **(Appendix A, Table 2)**, leaving only genes whose differential expression depended on the presence of *Sting* during *H. pylori* infection **(Figure 35A; Table 3)**. The resulting heatmap **(Figure 35B)** identified a target that has previously been shown to directly suppress STING in mice, tripartite motif-containing 30A (*Trim30a)*. TRIM

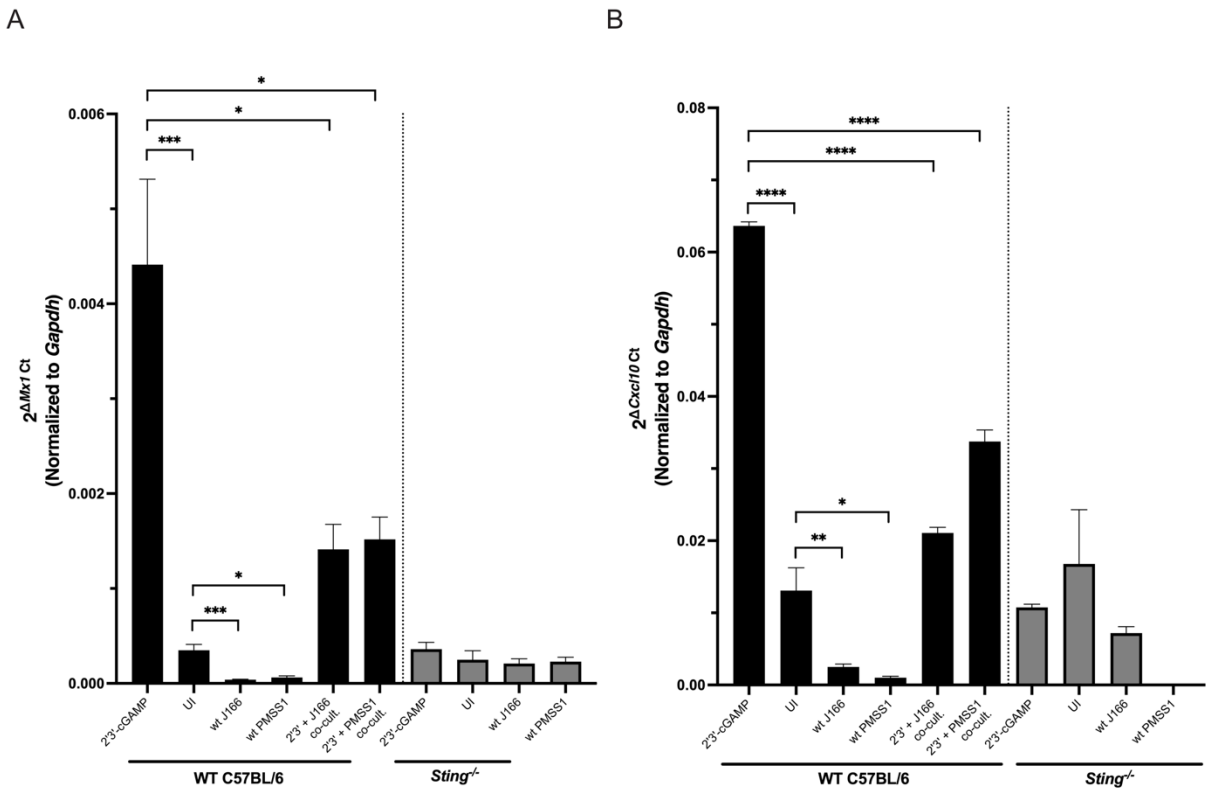

Figure 34. *H. pylori* infection of murine gastric organoids downregulates IRF3-dependent type I interferon stimulated genes. Murine gastric organoid monolayers were challenged with PBS alone (UI), *H. pylori* wild-type (wt) strain J166 or PMSS1 at MOI 100:1, and/or STING agonist 2'3'-cGAMP for 6 hours or 24 hours. RT-PCR analysis of **(A)** *Mx1* and **(B)** *Cxcl10* transcript levels was assessed in co-cultured organoid lysates. Data are represented as relative gene expression levels normalized to levels of *Gapdh* gene expression. In each experiment, conditions were tested at least 3 times and student's t-tests were used to determine statistical significance between groups. *p<0.05, **p<0.01, ***p<0.001, ****p<0.0001.

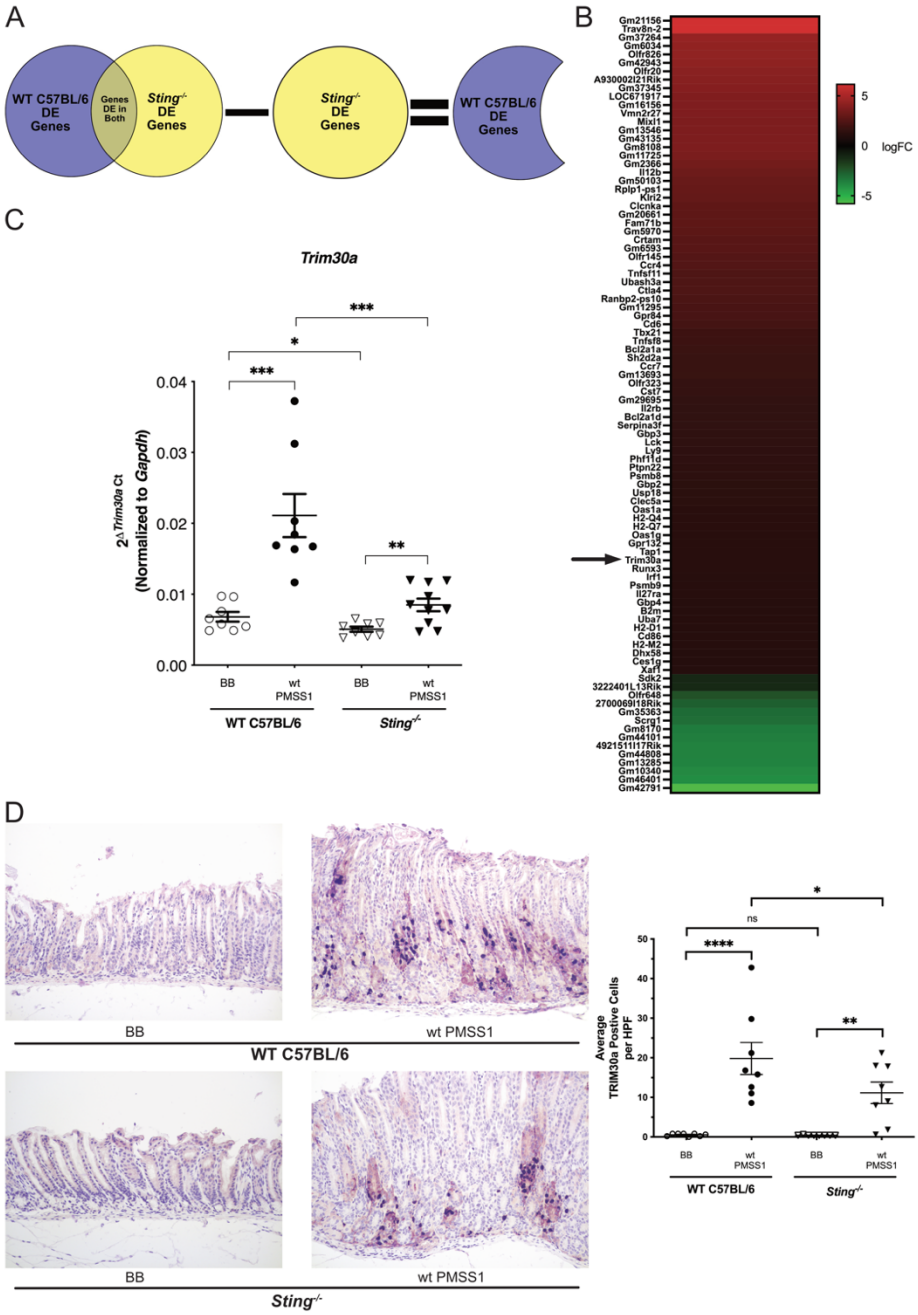

Figure 35. *Trim30a*, a known STING suppressor, is upregulated by *H. pylori in vivo* in a *Sting*-dependent manner. (A) Venn diagram representing differentially expressed genes in the RNA-seq dataset of C57BL/6 wild-type (WT) and *Sting*$^{-/-}$ mice and schematic of how STING-dependent genes were determined. **(B)** Genes that were determined to be dependent on *Sting* are shown by heatmap. Heatmap is displayed as logFC and red indicates upregulation, while green indicates downregulation. *Trim30a* is denoted by →. **(C)** RT-PCR analysis of *Trim30a* mRNA levels in uninfected and *H. pylori* infected wild-type mice, and uninfected and *H. pylori* infected *Sting*$^{-/-}$ mice. Data are represented as relative gene expression levels normalized to levels of *Gapdh* gene expression. **(D)** Levels of TRIM30a in wild-type or *Sting*$^{-/-}$ mice infected with or without *H. pylori*. Representative images are shown at 400x magnification for TRIM30a. TRIM30a staining was evaluated by quantifying positive cells (very strong staining compared to the surrounding tissue) and enumerated in 5 high-powered fields (HPF) from each animal and averaged. Each data point represents an individual animal (WT BB, n=8; WT PMSS1, n=8; *Sting*$^{-/-}$ BB, n=8; *Sting*$^{-/-}$ PMSS1, n=10). Student's t-tests were used to determine statistical significance between groups. *p<0.05, **p<0.01, ***p<0.001, ****p<0.0001, ns=not significant.

Table 4. STING-dependent differentially expressed genes as identified by RNA-seq in *H. pylori* infected C57BL/6 wild-type mice. Up- and downregulated genes in C57Bl/6 wild-type (WT) *H. pylori* infected mice versus C57Bl/6 WT uninfected mice that did not appear in *Sting*$^{-/-}$ *H. pylori* infected mice versus *Sting*$^{-/-}$ uninfected mice. Differential expression analysis was performed on RNAseq reads. Threshold: log2 fold change ≥ | 2 | and FDR ≤ 0.05.

Gene	log2 FC
Gm21156	6.147387588
Trav8n-2	6.140669365
Gm37264	4.402125897
Gm6034	4.267729045
Olfr826	4.254651177
Gm42943	4.181455358
Olfr20	4.07809106
A930002I21Rik	3.998040963
Gm37345	3.927665286
LOC671917	3.799049006
Gm16156	3.761233687
Vmn2r27	3.754814719
Mixl1	3.710721859
Gm13546	3.703781216
Gm43135	3.701501962
Gm8108	3.69986602
Gm11725	3.601786512
Gm2366	3.397587749
Il12b	3.230298547
Gm50103	3.086897256
Rplp1-ps1	3.022573925
Klri2	2.957754572
Clcnka	2.79099282
Gm20661	2.774499802
Fam71b	2.772439568
Gm5970	2.712423179
Crtam	2.6003228
Gm6593	2.595129532
Olfr145	2.492549029
Ccr4	2.459354918
Tnfsf11	2.365471002
Ubash3a	2.363320208
Ctla4	2.324780781
Ranbp2-ps10	2.246190307
Gm11295	2.192886019
Gpr84	2.159302175
Cd6	2.065275293
Tbx21	1.838599839
Tnfsf8	1.815705912
Bcl2a1a	1.758799003
Sh2d2a	1.731369243
Ccr7	1.729753456
Gm13693	1.69660395
Olfr323	1.586216282
Cst7	1.559881949
Gm29695	1.485116653
Il2rb	1.469236752
Bcl2a1d	1.462793664
Serpina3f	1.446857109

Gbp3	1.386324632
Lck	1.382141983
Ly9	1.36219576
Phf11d	1.355360699
Ptpn22	1.338582203
Psmb8	1.321643755
Gbp2	1.284264829
Usp18	1.281815099
Clec5a	1.259740759
Oas1a	1.225680027
H2-Q4	1.20655141
H2-Q7	1.200389341
Oas1g	1.197482227
Gpr132	1.165118966
Tap1	1.160037974
Trim30a	1.148855488
Runx3	1.146764074
Irf1	1.136309609
Psmb9	1.125740501
Il27ra	1.123910469
Gbp4	1.0690801
B2m	1.063555331
Uba7	1.060774202
H2-D1	1.060208913
Cd86	1.057121669
H2-M2	1.051679464
Dhx58	1.047740405
Ces1g	1.026262495
Xaf1	1.023047517
Sdk2	-1.054259617
3222401L13Rik	-1.142080967
Olfr648	-2.29420284
2700069I18Rik	-2.658640189
Gm35363	-3.017991589
Scrg1	-3.092599714
Gm8170	-3.460204743
Gm44101	-3.542672499
4921511I17Rik	-3.649908962
Gm44808	-3.650198377
Gm13285	-3.718217905
Gm10340	-3.845960272
Gm46401	-3.969586309
Gm42791	-5.794915899

family proteins regulate critical cellular processes such as innate immunity, transcription, and autophagy [430-432] and can serve as effectors of innate immunity in response to signaling by cytokines such as IFN and TNFα and via pattern recognition receptors (PRRs) such as Toll-like receptor (TLR), RIG-I, and STING [432-435]. Altered levels of *Trim30a* expression were subsequently validated by RT-PCR and significantly higher levels of *Trim30a* were observed in infected wild-type mice compared to *Sting*$^{-/-}$ mice **(Figure 35C)**. To more precisely define the topography of TRIM30a protein expression and clarify localization of the TRIM30a in the gastric niche, immunohistochemistry was performed on the murine gastric tissue. Positive staining was observed in immune cells such as polymorphonuclear leukocytes (PMNs) and mononuclear leukocytes as well as epithelial cells **(Figure 35D)**. When images were quantitated, *H. pylori* infection significantly induced higher levels of Trim30a expression compared to uninfected controls in both wild-type and *Sting*$^{-/-}$ mice but similar to RNA-seq and RT-PCR data, significantly lower levels of TRIM30a were demonstrated in infected *Sting*$^{-/-}$ mice compared to infected wild-type mice **(Figure 35D)**.

In TLR- and STING-mediated signaling, TRIM30a serves as an important negative feedback regulator that controls excessive inflammatory responses via suppression of type I IFNs production and is expressed in a variety of cell types [435-437]. Therefore, we next sought to further investigate *ex vivo* and *in vitro* TRIM30a activation by *H. pylori* in a cell-specific manner. To examine TRIM30a protein expression within gastric epithelial cells, Western blot analysis was performed on co-culture lysates from murine gastroid monolayers infected *ex vivo* with *H. pylori* strains J166 and PMSS1 for 24 hours. Significantly increased levels of TRIM30a expression was present in both *H. pylori*-infected wild-type and *Sting*$^{-/-}$ organoids compared to uninfected cells where no expression was observed **(Figure 36A)**. Comparable TRIM30a expression patterns were

also demonstrated when examined by immunofluorescence in wild-type and *Sting*$^{-/-}$ organoids following a 24-hour co-culture with *H. pylori* **(Figure 37)**.

Bone marrow derived dendritic cells (BMDC) are also an important source of TRIM30a [435, 436]; therefore, we next treated BMDCs isolated from wild-type or *Sting*$^{-/-}$ mice with wild-type *H. pylori*. Total mRNA isolated from wild-type BMDCs was subjected to RT-PCR to quantify expression levels of *Trim30a* which demonstrated significant increases in *Trim30a* expression in *H. pylori* treated samples over a 24-hour time course while *Sting*$^{-/-}$ BMDCs demonstrated significantly lower levels of *Trim30a* **(Figure 36B)**. Western blots on BMDC protein lysates co-cultured with *H. pylori* revealed similar findings, with lower protein levels observed in infected *Sting*$^{-/-}$ BMDC compared to wild-type BMDCs **(Figure 36C)**.

The mouse specific TRIM30a shares greatest homology with specific human TRIMs including TRIM5, TRIM6, and TRIM22 **(Figure 38A)**. To extend our findings into human patients, we utilized tissues from a gastric cancer patient cohort to probe for *Trim30a* human ortholog expression by RT-PCR. Expression of *TRIM6* and *TRIM22* but not *TRIM5* was significantly increased in patient samples that harbored inflammation or cancer **(Figure 38B,C; Figure 39)**. Another human TRIM homolog, *TRIM29,* has been directly implicated in STING modulation as well as gastric cancer outcomes [438-440]; thus, we also analyzed expression levels of *TRIM29* within the patient cohort and demonstrated significantly higher levels of expression in patient samples that harbored inflammation or cancer **(Figure 38D)**. These results raise the possibility that TRIMs represent targets induced by *H. pylori* infection, that can suppress STING activation and promote pro-inflammatory and pro-tumorigenic responses *in vivo*.

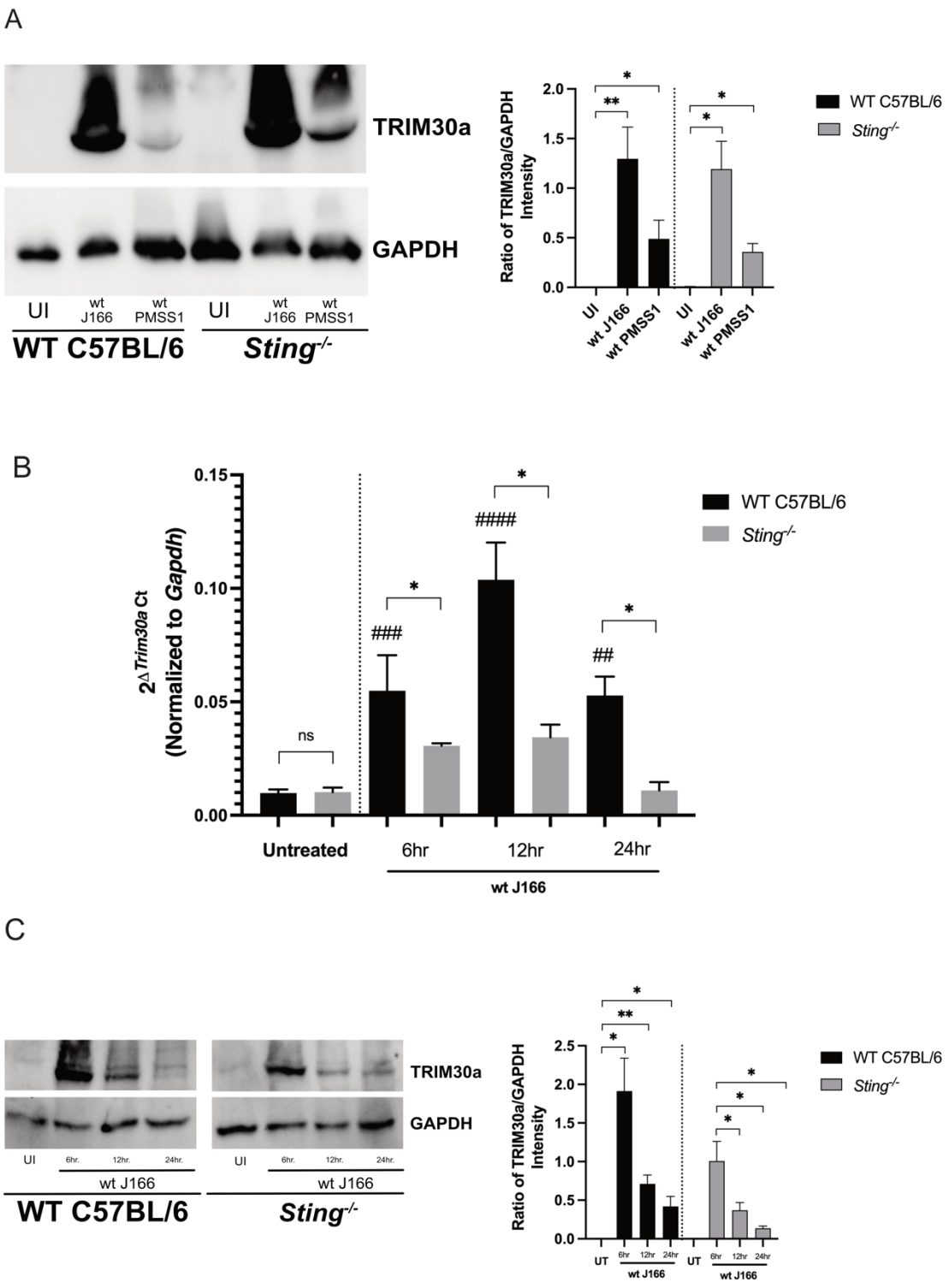

Figure 36. TRIM30a is upregulated by *H. pylori* in a STING-dependent manner. Gastric organoid monolayers or bone marrow derived dendritic cells (BMDC) derived from C57BL/6 wild-type (WT) or *Sting*$^{-/-}$ mice were challenged with PBS alone (UI), *H. pylori* wild-type (wt) strain J166 or PMSS1 at MOI 100:1 for 24 hours. **(A)** Induction of TRIM30a was determined by quantifying levels of protein in co-cultured organoid lysates by Western blotting. Representative images and densitometric analysis normalizing levels of TRIM30a to GAPDH from 3 replicates are shown. **(B)** RT-PCR analysis of *Trim30a* mRNA levels in uninfected and *H. pylori* infected wild-type and *Sting*$^{-/-}$

BMDCs. Data are represented as relative gene expression levels normalized to levels of *Gapdh* gene expression. **(C)** Induction of TRIM30a was determined by quantifying levels of protein in co-cultured BMDC lysates by Western blotting. Representative images and densitometric analysis normalizing levels of TRIM30a to GAPDH from 3 replicates are shown. In each experiment, conditions were tested at least 3 times and student's t-tests were used to determine statistical significance between groups. $^{\#\#}p<0.05$, $^{\#\#\#}p<0.01$, $^{\#\#\#\#}p<0.001$ compared to uninfected TLR9+ cells; $*p<0.05$, $**p<0.01$, $***p<0.001$, ns=not significant.

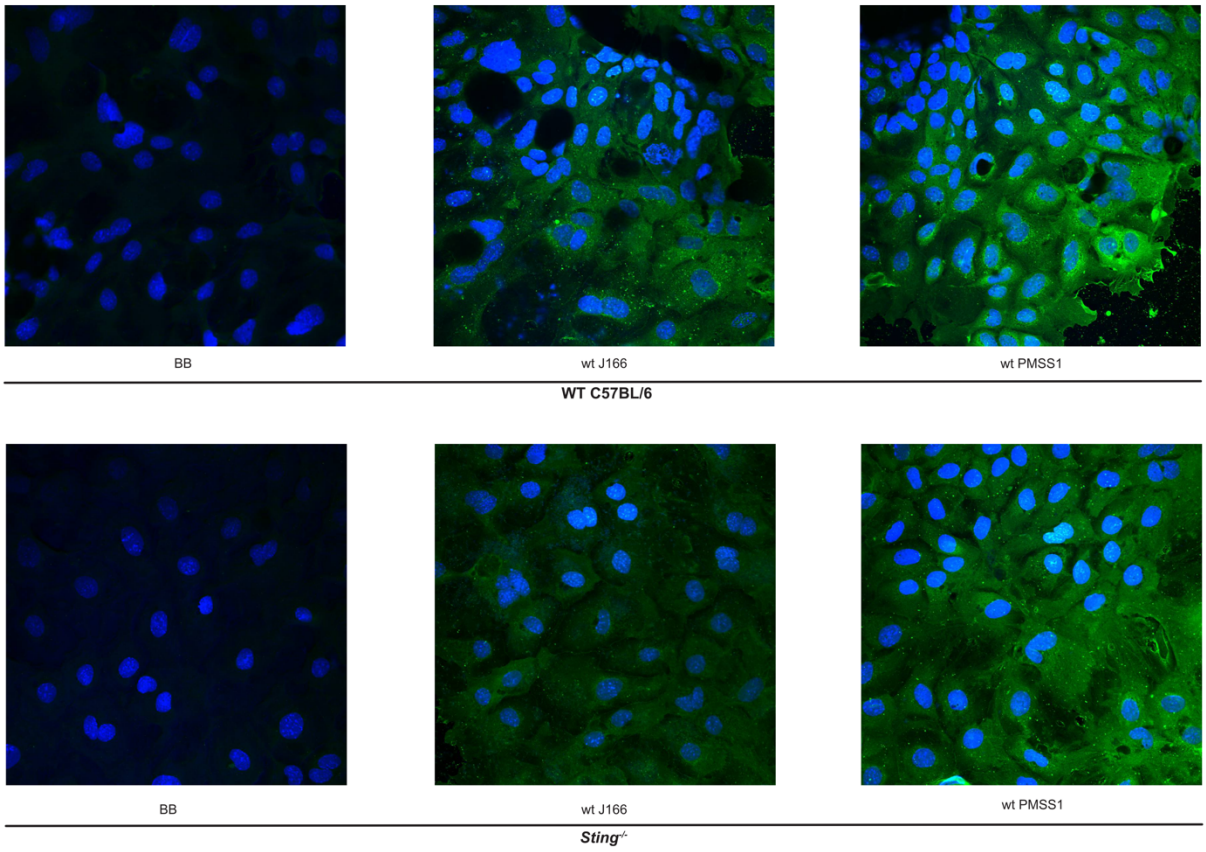

Figure 37. Immunofluorescence for TRIM30a. Organoid monolayers derived from wild-type or *Sting*$^{-/-}$ mice were challenged with PBS alone (UI), *H. pylori* wild-type strain J166 or PMSS1 at MOI 100:1 for 24 hours. Green: TRIM30a; blue: DAPI. 40X magnification.

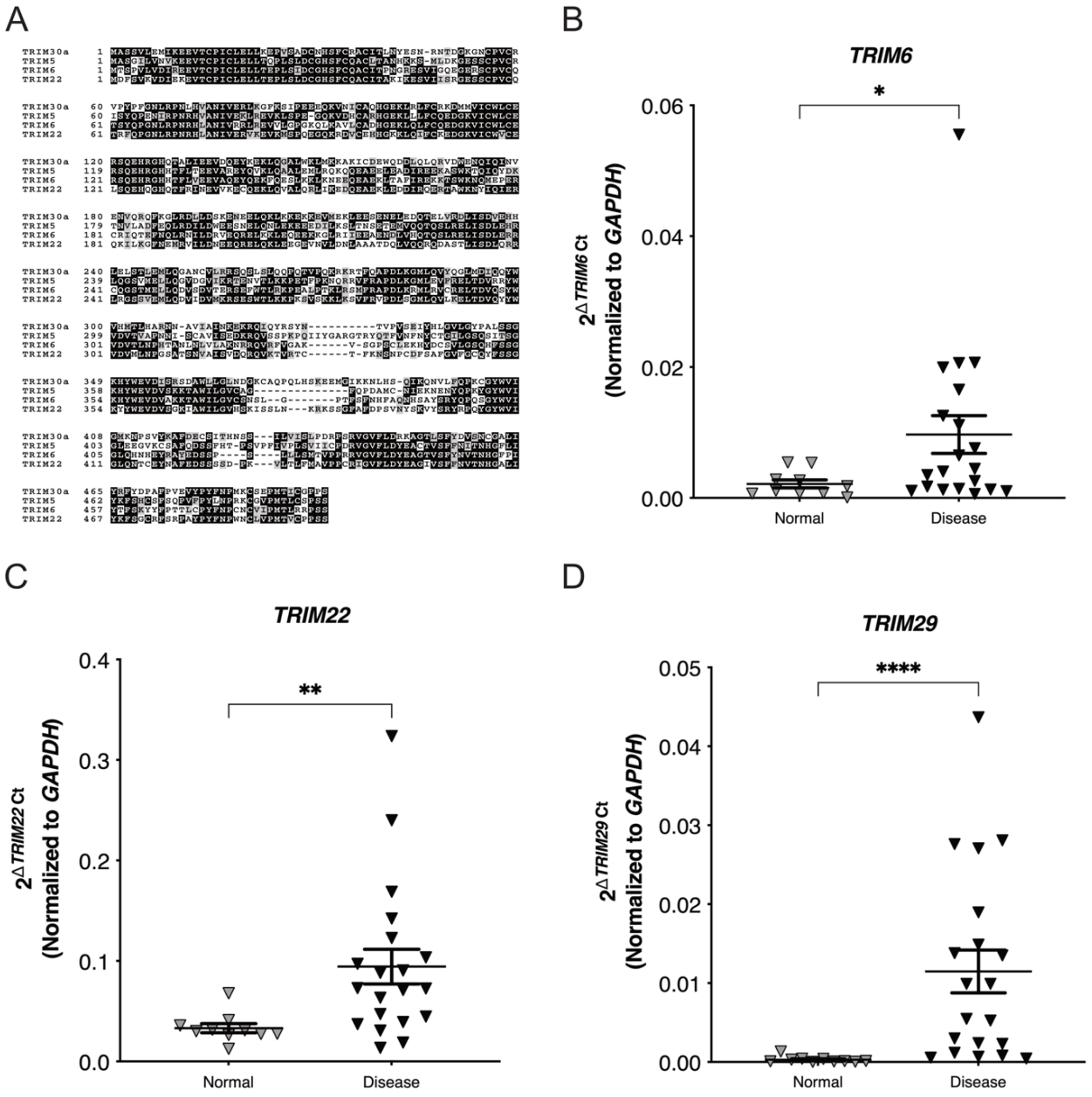

Figure 38. *TRIM6*, *TRIM22*, and *TRIM29* are upregulated in inflamed or cancerous human clinical gastric specimens. (A) Multiple sequence alignment of human TRIM30a orthologs to the murine TRIM30a protein sequence. The sequence alignment was performed using the T-Coffee program. RT-PCR analysis of **(B)** *TRIM6,* **(C)** *TRIM22,* and **(D)** *TRIM29* expression in patient samples of normal gastric tissue or samples that harbored inflammation or cancer. Data are represented as relative gene expression levels normalized to levels of *GAPDH* gene expression. Each data point represents an individual patient sample (normal, n=10; diseased, n=20). Mann-Whitney t tests were used to determine statistical significance between groups. *p<0.05, **p<0.01, ****p<0.0001.

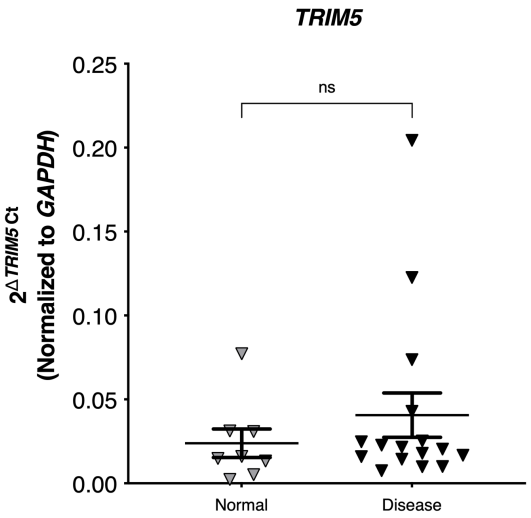

Figure 39. *TRIM5* expression in human clinical stomach specimens. RT-PCR analysis of *TRIM5* expression in patient samples with normal gastric tissue or samples that harbored inflammation or cancer. Data are represented as relative gene expression levels normalized to levels of *GAPDH* gene expression. Each data point represents an individual patient sample (normal, n=10; diseased, n=20). Mann-Whitney t test were used to determine statistical significance between groups. ns=not significant

3.4 Discussion

Our laboratory has previously demonstrated that *H. pylori* can translocate DNA into host cells activating TLR9 [117, 119] but the role of other innate immune nucleic acid sensors during *H. pylori* infection has remained undefined. We now demonstrate using *in vivo, ex vivo* and *in vitro* data that both STING and RIG-I-associated signaling was suppressed in the presence of viable *H. pylori*. One possible host mechanism for this phenomenon uncovered in our RNA-seq analysis is upregulation of TRIM proteins, which are known innate immune modulators. One such TRIM that was only upregulated in the presence of *Sting* and *H. pylori* was *Trim30a*, a known STING suppressor [435]. TRIM30a inhibits NF-κB activation induced by TLR signaling, including TLR9, via a K48-linked ubiquitination mechanism that degrades TAB2 and TAB3. However, NF-κB activation is required for initial upregulation of TRIM30a expression [436]. This suggests that

TRIM30a may be initially induced by *H. pylori* infection through activation of TLR9 which can then act as a negative regulator of both TLR9 and STING to dampen the subsequent immune response to *H. pylori*.

Other *Trim* genes revealed to be upregulated by *H. pylori* **(Appendix A)** that can modulate innate immune suppression include *Trim40*, which targets the downstream RIG-I regulator MAVS for K48-linked ubiquitination [434] and *Trim10*, which can suppresses IFN/JAK/STAT signaling pathway through blocking the interaction between IFNAR1 and TYK2 to negatively regulate type I IFN signal transduction [441]. Our *in vitro* and *ex vivo* work also demonstrated that *H. pylori* could directly mediate innate immune signaling via direct suppression of IRF3.

This complex system of both host and bacterial innate immune suppression and activation builds on our previous work focused on the duality of TLR9 signaling during *H. pylori* infection and suggests that DNA translocation, induction of TRIM proteins, and inhibition of IRF3 may be yet another component of a finely tuned rheostat that *H. pylori* utilizes to regulate the inflammatory response and maintain persistence in the host, and ultimately drive long-term carcinogenic pathways such as those promoted by increased Th17 activation.

In conclusion, this study demonstrates that *H. pylori* actively suppress innate nucleic acid sensors STING and RIG-I via downregulation of IRF3 and induction of TRIM proteins. Additionally, loss of STING augments acute inflammatory responses to *H. pylori* within the context of gastric carcinogenesis. This work lays the foundation for further exploration into the role of *H. pylori*-induced TRIMs in human hosts and suggest that manipulation of TRIMs may represent a novel strategy to prevent or treat pathologic outcomes induced by *H. pylori* infection.

CHAPTER IV

SUMMARY AND FUTURE DIRECTIONS

4.1 Thesis Summary

Chronic mucosal pathogens have evolved multiple strategies to manipulate the host immune response; consequently, microbes contribute to the development of >2 million cases of cancer/year. To persist for the entirety of its human host's lifetime, *Helicobacter pylori* has acquired a wide variety of tools to survive the unique environment of the stomach and evade detection by the immune system. Armed with a multitude of virulence factors that disrupt host cellular signaling, *H. pylori* has successfully colonized over half the world's population and remains a deadly threat as the greatest risk factor for development of gastric cancer. Progress has been made in the 30 years since *H. pylori's* discovery. The global gastric cancer burden has decreased by nearly 60% as a result of diminishing prevalence of risk factors such as *H. pylori* infection and smoking, in combination with broader *H. pylori* screening and eradication programs [442]. Nonetheless, this most feared outcome of *H. pylori* infection is still responsible for nearly one in every 13 deaths worldwide, yet the vast majority of *H. pylori* infected persons remain asymptomatic.

H. pylori infection is highly treatable with antibiotic therapy, although this has been more difficult in recent years due to the rise in antibiotic resistant strains [443]. However, with *H. pylori* infection inversely linked to esophageal cancers or acid reflux incidence, widespread test and treat approaches may be counter intuitive, possibly eliminating benefits to *H. pylori* colonization. Also, while gastric cancer incidence rates are high enough in the developing world to warrant such an

approach, it is a difficult economic ask in impoverished nations with a multitude of health issues. This contrast of commensal or carcinogen is an outstanding question in the field. How can a pathogen promote such severe gastric injury in some, but be completely benign by others? Consequently, *H. pylori's* relationship with its human host remains anything but simple. It has been well established, that no one particular risk factor, microbial, host, or environmental is an absolute requirement for adverse clinical outcomes. *H. pylori's* complicated relationship with humans is constantly being investigated to tease out the microbial and host mechanisms that drive responses to infection. Therefore, defining mechanisms of pathogenesis and identifying *H. pylori* strains and patients at greatest cancer risk will permit physicians to effectively implement and legislate personalized programs of targeted eradication therapy and cancer prevention.

The greatest microbial risk factor for gastric cancer development remains the presence of the *H. pylori* strain-specific virulence locus, the *cag* PAI, which encodes a T4SS. This *cag* T4SS translocates the pro-inflammatory and oncogenic protein CagA, peptidoglycan, and heptose bis-phosphate into epithelial cells. Additionally, our laboratory previously demonstrated that the *cag* T4SS can also translocate DNA into gastric epithelial cells and activate the microbial DNA sensor TLR9 *in vitro* and further that TLR9 suppresses *H. pylori*-induced injury *in vivo*. These data raised the hypothesis underpinning this thesis; namely that *H. pylori* selectively activates nucleic acid PRRs to regulate the inflammatory response and evade immune clearance. The work described in Chapter II further defined *H. pylori's* interactions with the innate immune receptor TLR9. Exogenous to the *cag* T4SS, the microbial mediators regulating *H. pylori* DNA translocation and TLR9 activation remain undefined. The outer membrane protein HopQ facilitates adherence of *H. pylori* to gastric epithelial cells and CagA translocation. Additionally, specific *hopQ* alleles have been identified which are linked to strain virulence. To address the possibility that HopQ represents

a microbial component that can regulate DNA translocation and TLR9 activation and, therefore, play a role in disease, the relationship between *hopQ* genotypes and the capacity to activate TLR9 was interrogated using a well-defined cohort of clinical *H. pylori* strains. These results were complemented using a focused mutagenesis approach to determine more definitively the role of HopQ and TLR9 activation by *H. pylori*.

As the first line of defense against *H. pylori* infection, gastric epithelial cells express effectors that can either eliminate bacteria or mobilize adaptive immune responses. These host effectors include pattern-recognition receptors, which detect conserved microbial motifs and TLRs (including the aforementioned TLR9), NLRs, and cytosolic DNA sensor/adaptor proteins (e.g. STING). The data in Chapter III demonstrated that *H. pylori* harbors a portfolio of mechanisms to manipulate the host immune response which can manifest as activation of specific nucleic acid PRRs such as TLR9, or active suppression of cytosolic STING- and RIG-I-signaling via downregulation of IRF3. Additionally, *in vivo* evidence revealed that *H. pylori* infection in the absence of STING drives pro-carcinogenic Th17 pathways and induces a known host immune modulator TRIM30a. Moreover, and of direct clinical relevance, observations that *H. pylori*-induced TRIM proteins are upregulated in a gastric cancer patient cohort raise the tantalizing possibility that these host immune modulators may represent biomarkers for disease outcomes.

Taken together, this complex system of both host and bacterial innate immune suppression and activation builds on prior work focused on the duality of TLR9 signaling during *H. pylori* infection and suggests that HopQ-mediated TLR9 activation, induction of TRIM proteins, and inhibition of IRF3 and STING may be yet another component of a finely tuned rheostat that *H. pylori* utilizes to regulate the inflammatory response and maintain persistence in the host, and ultimately drive long-term carcinogenic pathways. These studies have laid a foundation for

identifying oncogenic constituents that regulate interactions of *H. pylori* with its host to promote carcinogenesis and unveiled novel targets to prevent or treat pathologic outcomes induced by *H. pylori* infection. However, many questions remain unsettled, and prompt further investigations **(Figure 40)**. The remainder of this chapter highlights experiments that are ongoing, in addition to future directions.

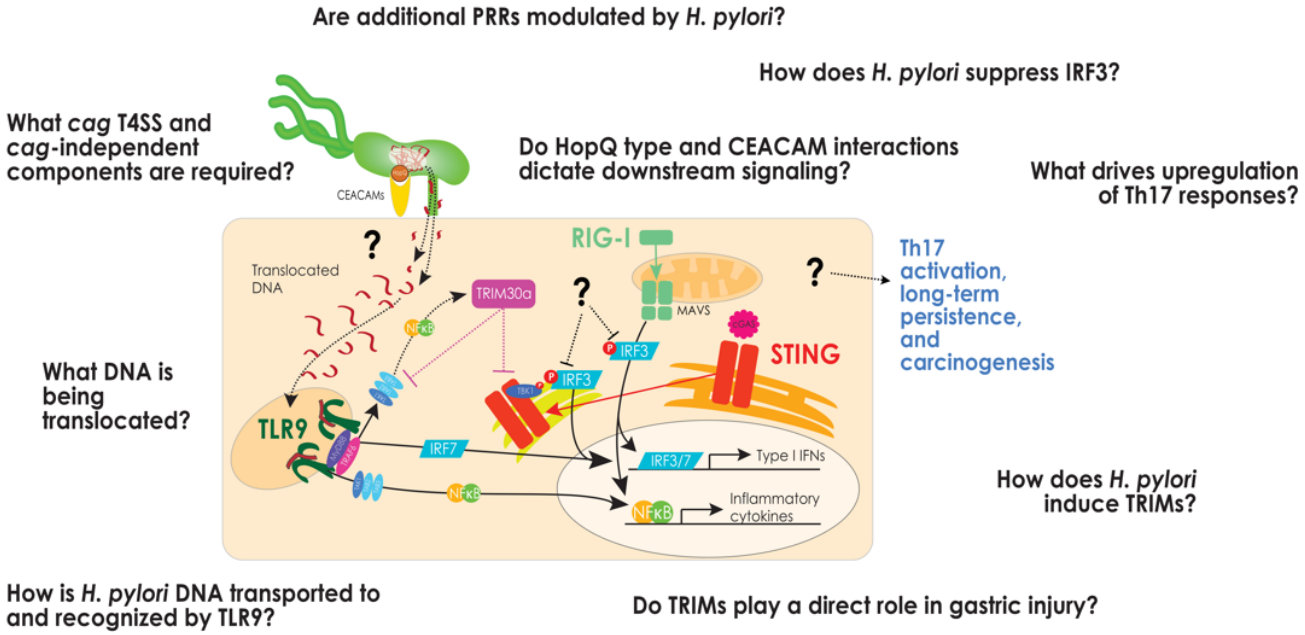

Figure 40. Thesis summary and outstanding questions. *H. pylori* translocates DNA into gastric epithelial cells activating TLR9. This phenotype is mediated by the bacterial adhesin HopQ's interactions with host CEACAMs. Subsequent NF-κB induction drives upregulation of TRIM30a which can in turn negatively regulate TLR-signaling and suppress STING. In addition, *H. pylori* can suppress IRF3 to dampen the immune response. *H. pylori* infection also upregulates additional TRIM proteins that can modulate other innate immune responses like RIG-I and JAK-STAT. This tight regulation of inflammatory responses by both active *H. pylori* and host mechanisms in response to infection maintain this pathogen's persistence and the host and ultimately drive long-term carcinogenic pathways like Th17. Questions remain regarding 1) how the specific mechanisms of DNA translocation and STING suppression are dictated by *H. pylori* and 2) the upregulation and direct role of TRIM proteins in promoting gastric injury?

4.2 Microbial Mechanisms of *H. pylori* DNA Translocation and TLR9 Activation

HopQ-CEACAM Interactions

The work outlined in Chapter II identified a strain-variable *cag* PAI-independent *H. pylori* component, HopQ, that is associated with TLR9 activation and is linked to carcinogenic potential. The two genetically distinct families of *hopQ* alleles (type I and type II) displayed significantly different *cag* T4SS phenotypes and pathological outcomes within a clinical cohort. This would initially appear to be linked to increased pro-inflammatory responses to TLR9 induction and translocated CagA, in parallel with increased levels of HopQ expression. However, no significant associations were observed between type I *hopQ* expression levels and pathologic outcomes or levels of CagA translocation **(Figure 19)**, suggesting more specific interactions than increased *cag* phenotpyes accompany increased HopQ. While a strong association between type I *hopQ* alleles and carcinogenic phenotypes was uncovered, the mechanism by which HopQ modulates downstream TLR9 signaling remains undefined and will be of great interest in future work. The biological advantage for harboring two different *hopQ* alleles in a single genome remains to be determined, but all currently sequenced *H. pylori* genomes contain *hopQ* [196], suggesting that it is advantageous for *H. pylori* to retain this adhesin throughout its evolution with human hosts. Notably, *H. pylori cagA*$^{+}$ strains induce higher expression levels of HopQ's human binding partner, CEACAM, than *cagA*$^{-}$ strains [6], and TLR9-regulated transcription factors such as NF-κB and AP-1 are linked to *H. pylori* infection and CEACAM regulation [7]. This suggests that *H. pylori* has likely evolved to harbor different alleles of *hopQ* that may confer selective binding and molecular signaling capacities.

Structural analyses comparing type I HopQ to type II HopQ proteins have revealed a differential ability to bind specific CEACAMs [190]. Type I HopQ harbors a higher affinity for

human CEACAM1 versus CEACAM6, raising the possibility that HopQ-CEACAM1 interactions are critical for translocation of microbial DNA and robust TLR9 activation. Although further studies linking discrete cell signaling cascades to specific *hopQ* alleles and CEACAMs will be required, preliminary work has implicated distinct downstream TLR9 signaling differences linked to HopQ. In Chapter II, IFNα and IFNβ levels in AGS cells following co-culture with the *H. pylori hopQ* deletion mutant were significantly reduced compared to levels induced by the wild-type strain **(Figure 21B)**. Alternatively, TLR9-mediated pro-inflammatory responses can be induced following activation of the transcription factor, NF-κB. AGS cells stably expressing a NF-κB-dependent luciferase reporter have been generated in our lab [272]. The transfected vector contains five copies of an NF-κB response element (NF-κB-RE) that drives transcription of the luciferase reporter gene. NF-κB induced by *H. pylori* infection of AGS cells can bind the NF-κB-RE, producing the luciferase protein. Co-culture of the same strains from Chapter II with the NF-κB-dependent luciferase reporter AGS cells demonstrated that *H. pylori* NF-κB activation *in vitro* does not require HopQ **(Figure 41)**, unlike type I IFN induction. This is important because while unable to differentiate between upstream activators like TLR9 or NOD1, AGS cells do contain CEACAMS 1, 5 , and 6 [202], which are absent in HEK293 cells [188, 190, 200]. These results suggest that specific HopQ-CEACAM interactions are required for TLR9 activation within the gastric niche, and HopQ is required for a type I IFN-mediated TLR9 response. Currently unclear, defining how *H. pylori* DNA is trafficked to and recognized by TLR9 will be key in clarifying these HopQ-mediated differences in the *H. pylori* TLR9 response, as cellular TLR9 localization and binding of its DNA ligand dictates the downstream response [290, 291].

It has been well demonstrated that gastric epithelial cells express different levels of CEACAMs that are altered upon *H. pylori* infection [188, 200, 201, 444]. Genetic manipulation

of individual CEACAMs to knockdown or knockout their expression in cultured cell lines and organoids, followed by co-culture with *H. pylori* could be utilized to investigate whether TLR9-specific responses are pro- or anti-inflammatory or achievable at all in the absence of CEACAM. Additionally, co-culture with *hopQ* mutants, both type I and type II strains to differentiate amongst allelic differences, would be important to systematically determine which specific HopQ-CEACAM interactions are essential to TLR9 signaling. These observations may aid in delineating the route by which microbial DNA is delivered to host cells via cellular attachment, and selective TLR9 activation mediated through HopQ would indicate the impact that DNA translocation has on carcinogenesis *in vivo*, independent of other known *H. pylori* effectors.

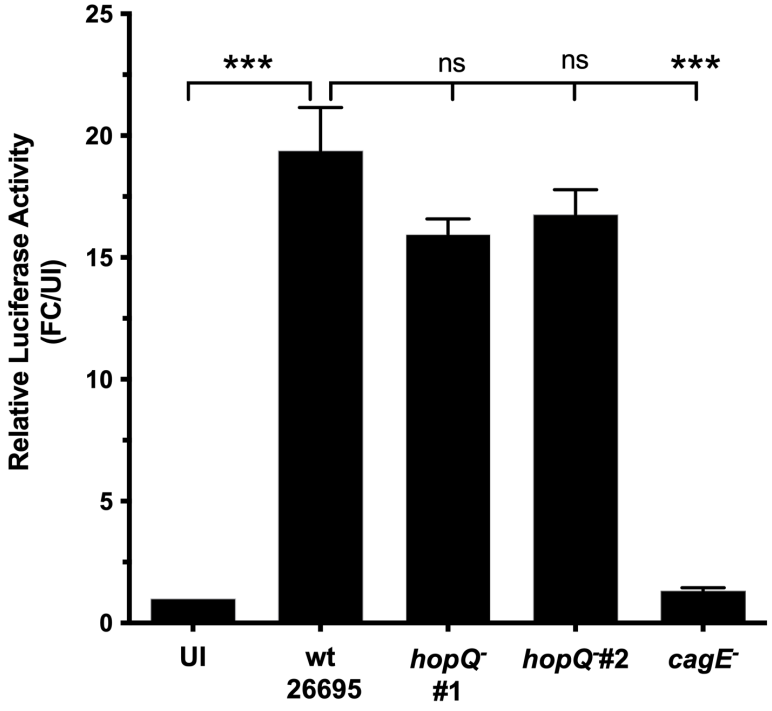

Figure 41. Genetic deletion of *hopQ* does not significantly alter NF-κB activation *in vitro*. Wild-type (wt) *cag*$^{+}$ strain 26695, respective *hopQ*$^{-}$ or *cagE*$^{-}$ isogenic mutant strains were co-cultured with AGS-NF-κB reporter cells at multiplicity of infection (MOI) of 10:1 for 4 hours to determine NF-κB induction. The data represent results of three independent experiments. Values represent means ± standard error of the mean (SEM). Statistical significance among groups was determined by student's t-test. ***p<0.001, ns=not significant.

Delineating *cag* T4SS Requirements for TLR9 Signaling

This section is adapted from the following publication:
Lin AS, **Dooyema SDR** et al. (2020) "Bacterial energetic requirements for *Helicobacter pylori* Cag Type IV secretion system-dependent alterations in gastric epithelial cells" *Infection and Immunity*. PMID: 31712269. [445]

Work in Chapter II focused on identifying *cag* T4SS-independent microbial mediators of DNA translocation and TLR9 activation. However, the mechanisms of how *H. pylori* DNA is translocated via the *cag* T4SS remains relatively undefined. The prior work done by Varga et al. on *cag* T4SS-dependent TLR9 signaling demonstrated that a functional and intact secretion system was required for TLR9 activation by *H. pylori* **(Figure 42, Table 5)**. In collaboration the Cover group at Vanderbilt, we set out to further delineate *cag* T4SS requirements for TLR9 signaling.

Approximately 17 of the 31 genes in the *cag* PAI are essential for CagA translocation into gastric epithelial cells, and approximately 14 are essential for *H. pylori*-induced IL-8 production by host cells [446]. Five proteins encoded by genes in the *cag* PAI (CagY, CagX, CagT, CagM, and Cag3) assemble into a large core complex that spans the inner and outer membranes [123, 133, 134, 136], and other *cag* PAI-encoded proteins assemble into an inner membrane complex [136]. Three of the proteins localized to the *cag* T4SS inner membrane complex are putative ATPases known as Cagα, Cagβ, and CagE [136, 446, 447]. These correspond to VirB11, VirD4, and VirB4, respectively, in prototypical VirB/VirD4 T4SSs (*E. coli* conjugation systems and the *Agrobacterium tumefaciens* VirB/VirD4 system) [308].

H. pylori CagA, HBP, peptidoglycan, and DNA all enter host cells through *cag* T4SS-dependent processes, but these bacterial components are recruited and delivered into host cells likely through disparate mechanisms. In support of this, Fischer et al. showed that translocation of CagA into gastric epithelial cells requires several *cag* PAI-encoded proteins that are not required

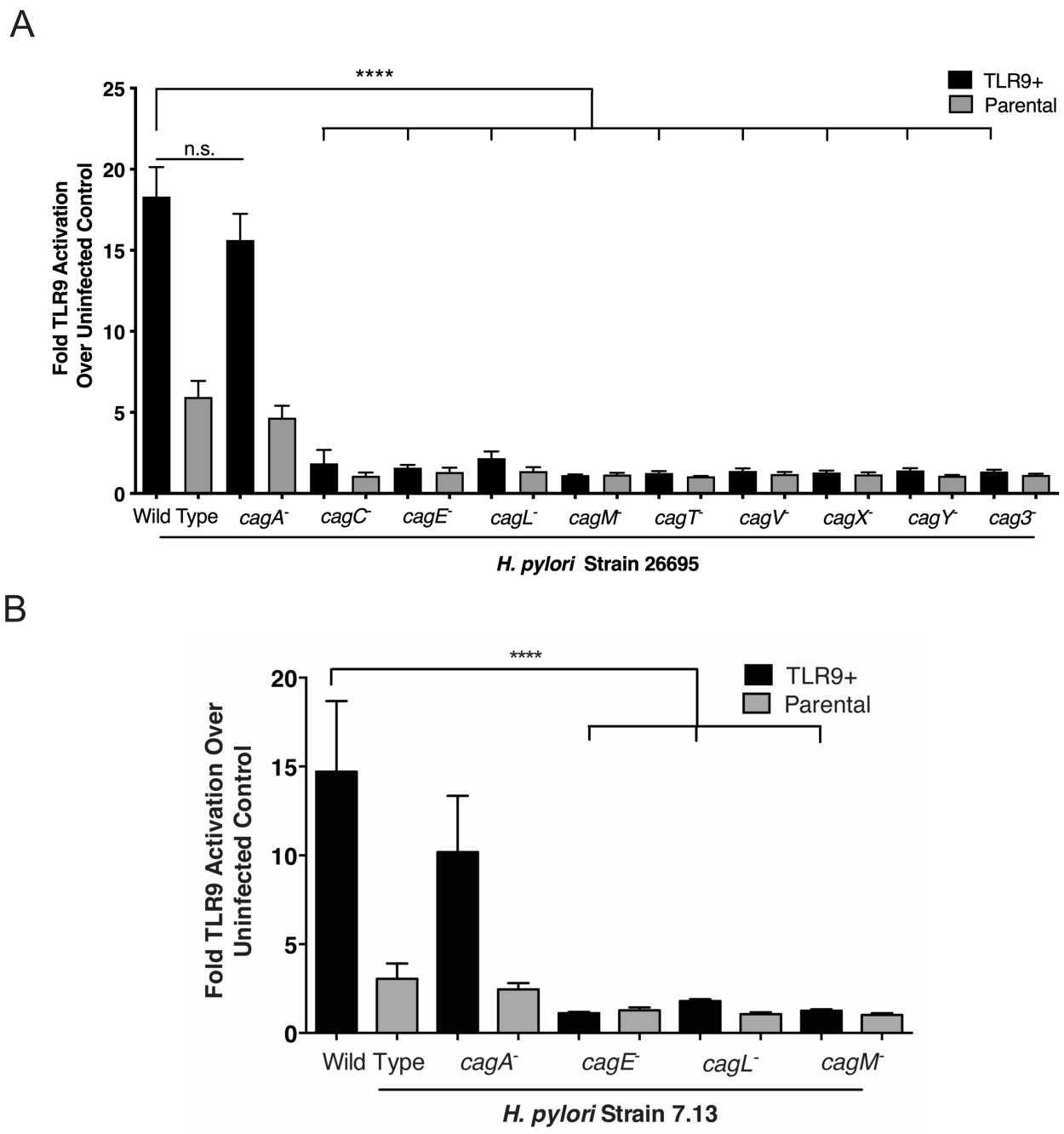

Figure 42. *H. pylori* activation of TLR9 requires a functional *cag* T4SS. *H. pylori cag*$^{+}$ strains **(A)** 26695 or **(B)** 7.13 or its isogenic mutants were used to challenge TLR9-reporter or parental cells at an MOI of 100 for 24 hours. Data displayed as TLR9 activation induced by *H. pylori*, relative to uninfected control. Each strain was tested in duplicate in at least 3 independent experiments. Mean±SEM are shown. Statistical significance among groups was determined by ANOVA with Bonferroni correction. ****p<0.0001. **(A-B)** reprinted with permission from [117].

Table 5: Nomenclature, localization, and functional importance of T4SS proteins encoded by the *Helicobacter pylori cag* PAI**.**

J166 Gene Annotation	Protein Name	Size (aa)	Sub-cellular Localization	Classification and Proposed Function	Required for...		
					CagA Translocation ?	IL-8 Induction ?	TLR9 Activation ?
EG65_04385	**Cagζ/Cag1**	116	IM	Nonessential factor	No	No	-
EG65_04390	**Cagε/Cag2**	80	C	Nonessential factor	No	No	-
EG65_04395	**Cagδ/Cag3**	481	OM	Core complex factor	Yes	Yes	Yes
EG65_04400	**Cagγ/Cag4**	169	PP	PG hydrolase	Yes	Yes	-
EG65_04415	**Cagβ/Cag5**	748	IM	Coupling protein, NTPase	Yes	No	No
EG65_04420	**Cagα**	330	C, IM	NTPase	Yes	Yes	Yes
EG65_04425	**CagZ**	199	C, IM	Cagβ stabilization	Yes	Yes	Yes
EG65_04430	**CagY**	1927	IM, OM, S	Core complex factor, integrin binding	Yes	Yes	Yes
EG65_04435	**CagX**	522	IM, OM, S	Core complex factor	Yes	Yes	Yes
EG65_04440	**CagW**	535	IM	Core complex-associated factor	Yes	Yes	-
EG65_04445	**CagV**	252	IM	Core complex-associated factor	Yes	Yes	Yes
EG65_04450	**CagU**	218	IM	Core complex-associated factor	Yes	Yes	Yes
EG65_04455	**CagT**	280	OM, S	Core complex factor, OM lipoprotein	Yes	Yes	Yes
EG65_04460	**CagS**	196	C	Nonessential factor	No	No	-
EG65_04465	**CagQ**	126	IM	Nonessential factor	No	No	-
EG65_04470	**CagP**	114	IM	Nonessential factor	No	No	-
EG65_04475	**CagM**	376	OM	Core complex factor	Yes	Yes	Yes
EG65_04480	**CagN**	306	PP, IM	Core complex-associated factor	No	No	-
EG65_04485	**CagL**	237	PP, S	Pilus biogenesis, integrin targeting	Yes	Yes	Yes
EG65_04490	**CagI**	381	PP, S	Pilus biogenesis, integrin targeting	Yes	No	Yes
EG65_04495	**CagH**	370	IM	Pilus biogenesis, core complex-associated factor	Yes	Yes	Yes
EG65_04500	**CagG**	142	PP	Accessory factor	Yes	No	-
EG65_04505	**CagF**	268	C, IM	Chaperone for CagA	Yes	No	No
EG65_04510	**CagE**	983	IM	NTPase	Yes	Yes	Yes
EG65_04515	**CagD**	207	IM, PP, S	Accessory factor	Maybe	No	-
EG65_04520	**CagC**	115	IM, OM, S	Pilus subunit	Yes	Yes	No
EG65_04525	**CagB**	75	C	Unknown	-	-	-
EG65_04300	**CagA**	1186	C, S	Translocated effector protein	Yes	No	No

for *H. pylori*-induced IL-8 production [446]. One of the proteins required for CagA translocation but not required for IL-8 production is Cagβ (a VirD4 homolog) [446, 448]. In *Escherichia coli* conjugation systems and the *A. tumefaciens* VirB/VirD4 system, VirD4 acts as a coupling protein that recruits DNA and the relaxosome from the cytoplasm to the T4SS [449-451]. The role of Cagβ in *H. pylori*-induced TLR9 activation, attributed to entry of bacterial DNA into host cells [117], has remained undefined. VirD4 acts as a coupling protein required for recruitment and translocation of DNA in conjugative T4SSs and the *A. tumefaciens* T4SS [450, 452, 453], suggesting that Cagβ might be essential for recruitment and delivery of *H. pylori* DNA into host cells.

Therefore, we sought to further investigate the bacterial energetic requirements for T4SS-dependent, *H. pylori*-induced alterations in host cells, including TLR9 activation. Deletion mutants were generated in the *cag*$^{+}$ *H. pylori* strain 26695 for *cagα*, *cagβ*, and *cagE* in addition to genetically manipulated control strains containing the corresponding restored intact genes. Mutants were then tested in cell culture assays to assess CagA translocation and CagA-independent cellular alterations (IL-8 production, NF-κB activation, and TLR9 activation). To assess if the individual Cag ATPases are required for CagA translocation into host cells, co-cultured *H. pylori* strains with AGS cells were analyzed for phosphorylation of CagA; reflecting translocated CagA. The ATPase deletion mutant strains (*Δcag*α, *Δcag*β, and *Δcag*E) along with genetically manipulated control strains containing restored wild-type *cag*α, *cag*β, and *cag*E sequences (named ASL12.1 [restored WT *cagα*], ASL14.1 [restored WT *cagβ*], and ASL16.1 [restored WT *cagE*]) were analyzed in all assays [445].

Tyrosine-phosphorylated CagA was detected when the wild-type strain and control strains were co-cultured with AGS cells but was not detected when any of the individual ATPase mutants

were co-cultured with AGS cells **(Figure 43A)**. These results indicated that all three ATPases are required for CagA translocation into AGS cells. When co-cultured with gastric epithelial cells, *H. pylori* strains containing an intact *cag* T4SS stimulate activation of NF-κB and production of pro-inflammatory cytokines such as IL-8. Multiple genes encoding components of the *cag* T4SS are required for these phenotypes [123, 446, 454, 455]. To investigate whether the individual ATPases are required for these phenotypes, wild-type and mutant *H. pylori* strains were co-cultured with AGS cells or AGS-NF-κB reporter cells and quantified IL-8 induction and NF-κB activation. The *Δcag*α and *Δcag*E mutants were defective in both IL-8 induction and NF-κB activation, whereas the *Δcag*β mutant stimulated IL-8 induction and NF-κB activation similar to the wild-type strain **(Figure 43B,C)**. The IL-8 induction and NF-κB phenotypes were intact in each of the control strains containing wild-type ATPase sequences **(Figure 43B,C)**. These data indicated that Cagα and CagE are each required for IL-8 secretion and NF-κB activation in gastric epithelial cells, but Cagβ is not required.

As shown in **(Figure 42)**, when co-cultured with HEK293-TLR9 reporter cells, *H. pylori* strains containing an intact *cag* PAI activate TLR9 through a process that requires multiple genes encoding components of the *cag* T4SS. To determine if the individual ATPases are required for TLR9 activation, the wild-type strain, mutant strains, and genetically manipulated control strains were co-cultured with TLR9 reporter cells. The *Δcag*α and *Δcag*E mutants were defective in activating TLR9, whereas the *Δcag*β mutant retained the TLR9 activation phenotype **(Figure 43D)**. The genetically manipulated control strains containing restored wild-type ATPase sequences (ASL12.1, ASL14.1, and ASL16.1) exhibited an intact TLR9 activation phenotype **(Figure 43D)**. These data indicated that Cagα and CagE are required for *H. pylori*-induced TLR9 activation, but Cagβ is not required.

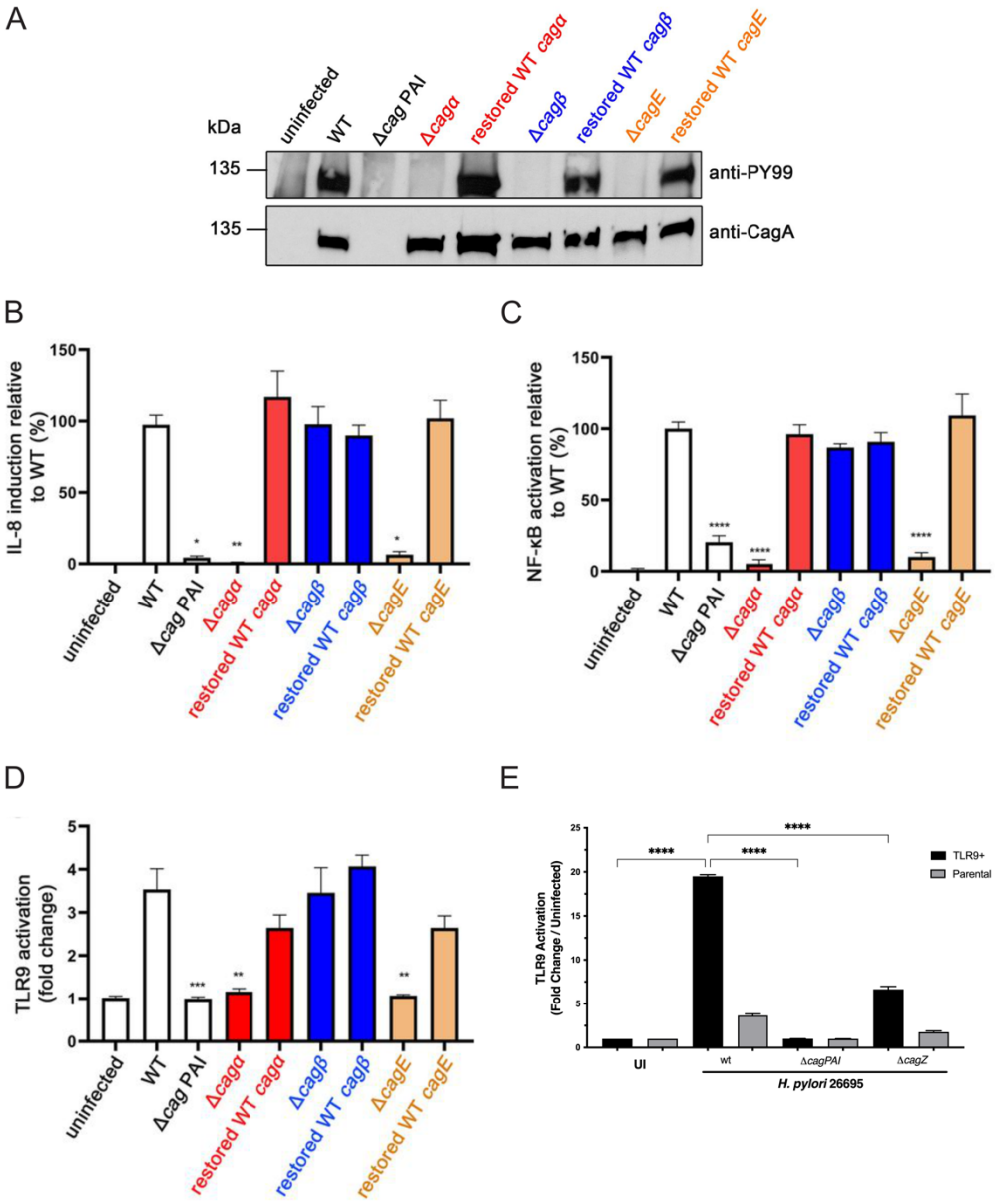

Figure 43. Requirement of Cagα, Cagβ, CagE, and CagZ for *cag* T4SS-dependent functions in host cells. (A) Wild-type (WT) strain 26695, a Δ*cag* PAI mutant strain, and the deletion mutant strains (Δ*cagα*, Δ*cagβ*, and Δ*cagE*) were co-cultured with AGS cells at multiplicity of infection (MOI) of 100:1 for 6 hours. Genetically manipulated strains containing restored wild-type ATPase sequences (named ASL12.1 [restored WT *cagα*], ASL14.1 [restored WT *cagβ*], and ASL16.1 [restored WT *cagE*]) were tested as controls. Extracts from *H. pylori*-gastric epithelial cell co-cultures were immunoblotted with an anti-CagA antibody to detect CagA and an anti-phosphotyrosine antibody (anti-PY99) to detect phosphorylated CagA. WT strain 26695 and respective mutants were co-cultured with AGS cells to determine **(B)** IL-8 induction, AGS-NF-κB reporter cells to determine **(C)** NF-κB induction, or TLR9-reporter or parental cells to determine **(D)** TLR9 activation at MOI of 100:1 for 6, 2.5, and 24 hours respectively. The data represent results of three independent experiments with multiple technical replicates. Values represent means ± standard error of the mean (SEM). Statistical significance among groups was determined by Kruskal-Wallis test with Dunnett's multiple comparison test. *p<0.05; **p<0.01; *** p<0.001; **** p<0.0001. (E) TLR9-reporter or parental cells were challenged with WT strain 26695, respective Δ*cag* PAI or Δ*cagZ* isogenic mutant strains. Samples were tested in duplicate at least 3 times and data are represented as fold change in infected over uninfected controls. ANOVA with Bonferroni correction was used to determine statistical significance between groups. ****p<0.0001. **A-D** reprinted from [445], under the terms of the Creative Commons Attribution 4.0 license.

These results demonstrated that the energetic requirements for *H. pylori*-induced TLR9 activation are identical to requirements for IL-8 production and NF-κB activation (i.e., requiring CagE and Cagα but not Cagβ) **(Figure 43)**. While Varga et al. reported that CagE was required for *H. pylori*-induced TLR9 activation [117], additional *cag*-mediated energetic requirements for this phenotype had not been previously studied in detail. These *cag* T4SS data differ from the requirement of a Cagβ homolog (VirD4) for delivery of DNA into recipient cells by *E. coli* conjugative T4SSs or the *A. tumefaciens* VirB/VirD4 T4SS [450, 452]. Additionally, *H. pylori* mutant strains harboring point mutations in sites predicted to be required for ATPase enzymatic activity were also defective for *in vitro* TLR9 activation, similar to the deletion mutant strains [445], suggesting that enzymatic activities of the three ATPases are required for TLR9 activation.

The observation that a Cagβ mutant is defective in CagA translocation but still capable of stimulating IL-8 production, NF-κB activation, and TLR9 activation provides important insights into the mechanisms by which these processes occur. Specifically, these results suggest that the *H. pylori* substrates mediating IL-8 induction, NF-κB activation, or TLR9 activation are recruited or delivered to host cells through one or more *cag* T4SS-dependent pathways that differ from those used for recruitment and delivery of CagA. One currently proposed model is that CagA is recruited from the cytoplasm to the inner membrane complex of the T4SS through interactions with Cagβ, a VirD4 homolog [448]. Similarly, in *E. coli* conjugative T4SSs and the *A. tumefaciens* T4SS, VirD4 acts as a coupling protein, responsible for recruiting DNA and protein substrates [450, 452]. Since *H. pylori*-induced IL-8 secretion, NF-κB activation, and TLR9 activation do not require Cagβ, HBP, peptidoglycan, or DNA might diffuse from the cytoplasm or periplasm into the T4SS apparatus through a nonspecific process that does not require recruitment by a coupling protein.

Alternatively, HBP, peptidoglycan, or DNA might transit the bacterial cell envelope through one or more mechanisms that are different from those used for secretion of CagA. For example, these nonprotein *H. pylori* constituents could potentially be released into the extracellular environment through bacterial autolysis, as components of outer membrane vesicles, or through other processes, and the *cag* T4SS may then facilitate the entry of these PAMPs into host cells. Consistent with the latter hypothesis, treatment of *H. pylori*-host cell co-cultures with DNase I partially reduced the level of TLR9 activation [117].

In addition to the *cag* T4SS, the *H. pylori* 2665 strain utilized in these studies harbors a second T4SS (ComB system), which is required for natural transformation and conjugative transfer of DNA [456]. Cross talk among *H. pylori* T4SSs could potentially occur (for example, an ATPase from the ComB system contributing to the function of the Cag T4SS), but there is no experimental evidence at present to support this possibility [117]. In future studies, it will be important to determine whether *H. pylori* DNA, HBP, and peptidoglycan enter cells independently or if proteins analogous to the relaxosome utilized in conjugation systems and the *A. tumefaciens* VirB/VirD4 system are required.

These studies demonstrated individual Cag ATPases are essential for translocation of CagA into host cells, indicating that the three Cag ATPases have nonredundant functions required for CagA translocation. Cagα and CagE, but not Cagβ, are required for *H. pylori*-induced NF-κB activation, IL-8 induction and TLR9 activation in host cells (three Cag T4SS-dependent phenotypes linked to cellular uptake of nonprotein bacterial components). The nonessentiality of Cagβ (a VirD4 homolog) for TLR9 activation contrasts with the requirement of VirD4 for DNA transfer by conjugation systems and *A. tumefaciens*. Further, preliminary screening of the Cagβ-stabilization factor CagZ in the TLR9 assay indicate CagZ is important for TLR9 activation, as it

is for CagA translocation [448]. TLR9 activation was significantly diminished following co-culture with the Δ*cagZ* mutant compared to *H. pylori* wild-type 26695-infected cells, albeit not to the levels of the non-functional Δ*cagPAI* mutant **(Figure 43E).** Binding of the CagZ-Cagβ complex to the *cag* T4SS apparatus has been suggested to recruit CagA to the translocation channel [448], but relatively little else is known about this understudied *cag* PAI protein. A potential role for CagZ as a chaperone has been suggested based on its similarity to T3SS chaperone proteins [448, 457]. Considering CagZ's association with the inner membrane and requirement for translocation of CagA, these data suggest CagZ may also be critical for *H. pylori* DNA translocation and TLR9 activation, potentially as a chaperone protein to recruit an unknown DNA binding protein to deliver DNA to the cag T4SS apparatus. Determining which *cag* factors are required for T4SS functions is akin to assembling a puzzle together piece by piece **(Table 5)** but provide a framework for establishing how DNA is translocated in a *cag*-dependent manner. Collectively, these data suggest that *cag* T4SS-dependent delivery of the nonprotein bacterial constituents into host cells occurs through mechanisms different from the mechanism used for the recruitment and delivery of CagA into host cells, and that CagZ may represent a unique target for *cag*-mediated DNA delivery.

Identification of Novel *H. pylori* Genes Impacting DNA Translocation and TLR9 activation

TLR9 activation by *H. pylori* has been shown to occur in a *cag* T4SS-dependent manner [117], and work in Chapter II demonstrated that HopQ is involved with TLR9 activation and inducing gastric injury. Though not part of the *cag* PAI, HopQ has been previously implicated with additional *cag* T4SS functions such as CagA translocation, though these data remain unsettled as previously discussed. As a result, I set out to identify novel genes regulating TLR9 activation

through the screening of a random insertion mutagenesis library in *H. pylori* strain J166 [458]. Isogenic mutants were created as previously described [199] of library clones that failed to activate TLR9, which revealed disruption of genes *EG65_06635* and *EG65_04365* significantly decreased levels of TLR9 activation compared to wild-type *H. pylori* **(Figure 44A)**. *EG65_06635* encodes a 153aa hypothetical protein of unknown function and *EG65_04365* encodes a 687aa predicted transport protein with nuclease domains. Characterization of isogenic mutants of these two candidate genes show no differences in growth and viability compared to wild-type as seen in growth curve analysis of the strains **(Figure 44B)**. Importantly, comparison of CagA translocation and IL-8 induction levels after co-culture with AGS cells indicate that *cag* T4SS function is unimpaired in both isogenic mutants **(Figure 44C,D)**, implying *cag*-independent mechanisms may also regulate TLR9 activation.

While the impact of these candidate genes on TLR9 activation will still need to be validated through genetic complementation to establish that TLR9 phenotypes are solely due to the disruption these genes, identification of genes exogenous to the *cag* PAI that impact TLR9 activation are important for a few reasons. 1) Disruption of the *cag* T4SS eliminates the translocation of not only DNA but other known substrates with carcinogenic potential such as CagA, HBP, and peptidoglycan. Identification of *cag*-independent components is of great importance then, not only to delineate the route by which microbial DNA is delivered to host cells, but to determine a direct role of DNA translocation and TLR9 activation has on carcinogenesis *in vivo*, independent of other known *H. pylori* effectors. 2) Apart from the requirement of the *cag* T4SS the mechanisms of *H. pylori*-mediated DNA translocation remain obscure. The strains previously tested for TLR9 activation do not possess native plasmids [86, 117, 459], indicating a significant difference from other bacteria which are capable of interkingdom DNA translocation.

Candidate gene *EG65_04365* being a predicted transport protein containing nuclease domains is exciting as it could lend evidence to the DNA being translocated into host cells through targeted identification of the nuclease cut sites. Further interrogation of these candidate genes and/or identification of others through additional discovery-based methods will be necessitated, but the potential of identifying the source of *H. pylori* DNA translocation cannot be ignored.

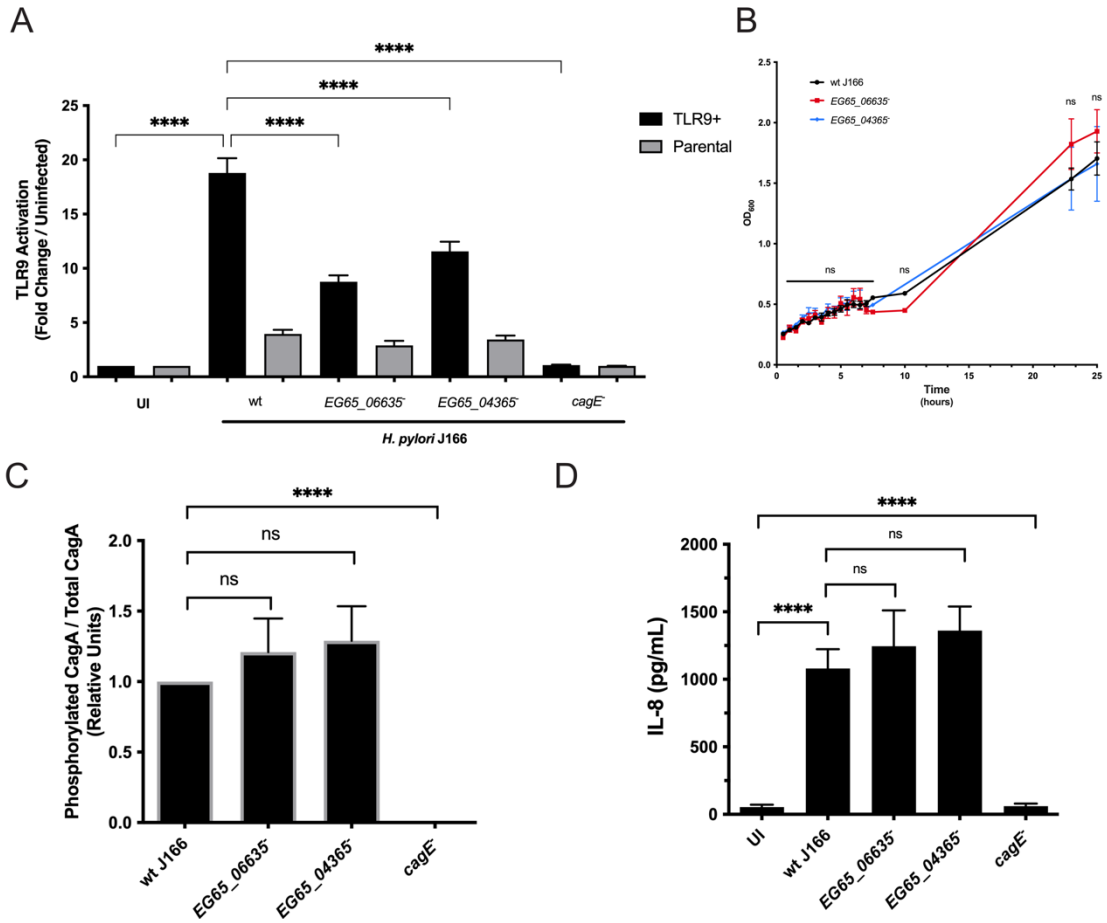

Figure 44. Genetic deletion of genes *EG65_06635* and *EG65_04365* in *H. pylori* strain J166 significantly decreases TLR9 activation but does not alter *H. pylori* growth or *cag* T4SS function. (A) *H. pylori* wild-type (wt) *cag* PAI^{+} strain J166 or isogenic mutant strains *EG65_06635*$^{-}$ and *EG65_04365*$^{-}$ were used to challenge TLR9-reporter or parental cells at an MOI of 100 for 24 hours. Data displayed as TLR9 activation induced by *H. pylori*, relative to uninfected control. Each strain was tested in duplicate in at least 3 independent experiments. Mean±SEM are shown. **(B)** Growth of *H. pylori* wt strain J166 or isogenic mutant strains was quantified at 0.5, 1, 1.5, 2, 2.5, 3, 3.5, 4, 4.5, 5, 5.5 6, 6.5, 7, 7.5, 10, 23, and 24 hours by spectrophotometric reading at OD600. *H. pylori* wt *cag* strain J166 or isogenic mutants were grown overnight and AGS cells were subsequently co-cultured at MOI 100:1 for 4 hours. **(C)** CagA translocation was determined by quantifying levels of phospho-CagA in AGS cell lysates during *H. pylori* co-culture by Western blotting and **(D)** levels of IL-8 in the resulting cell supernatants were quantified as an additional functional measure of the *cag* T4SS. ANOVA with Bonferroni correction or student's t-tests were used to determine statistical significance between groups. ****p<0.000, ns=not significant.

4.3 Microbial Mechanisms Mediating Active Suppression of STING by *H. pylori*

While data in Chapter III demonstrated suppression of IRF3 by *H. pylori*, the mechanism regulating this phenotype remain unclear. To investigate possible molecular mechanisms regulating STING suppression by *H. pylori*, targeted isogenic mutants were created as described previously [199] and screened in the HEK293-STING reporter assay. Strains with mutations in genes involved with STING suppression would be expected to have robust STING activation levels more similar to 2'3'-cGAMP agonist alone, unable to suppress STING *in vitro* compared to wild-type *H. pylori*. DNA translocation and TLR9 activation are dependent on the *cag* T4SS, so strain lacking a functional T4SS (*cagE*$^{-}$*)* was first assessed in the STING reporter assay. However, STING suppression occurred independently of the *cag* T4SS **(Figure 45A)**. Belogolova, Bauer, Pompaiah, Asakura, et al. uncovered *hopQ*'s association with the *cag* T4SS through a transposon screen of the *H. pylori* genome [149]. They demonstrated that transposons mutants mapping to *hopQ* and two other *cag*-independent loci were shown to disrupt NF-κB activation *in vitro*. Therefore, with STING suppression occurring without the need for a functional *cag* T4SS, I took interest in the two additional *cag*-independent transposon mutants' loci from Belogolova, Bauer, Pompaiah, Asakura, et al.'s screen and created isogenic mutants of these loci in *H. pylori* J166 to investigate the mutants' ability to suppress STING *in vitro.*

One of the insertions mapped to a region of overlap in two hypothetical proteins, WP_026938020 and WP_000780227. Subsequently, an isogenic mutant lacking both genes was created, mirroring the paper's finding. This double mutant, named *EG65_02145..50*$^{-}$ after the genetic loci nomenclature, showed recovery of the STING activation in both 4-hour preincubation and co-culture conditions similar to agonist alone **(Figure 45B)**. To next reveal if one gene or both *EG65_02145*$^{-}$ and *EG65_02150*$^{-}$ were required for STING suppression, isogenic mutants were

created of each individual gene in *H. pylori* J166. The STING suppression phenotype compared to wild-type J166 was still seen in the *EG65_02150*$^{-}$ mutant **(Figure 45B)** but preincubation or co-culture with *EG65_02145*$^{-}$ alone demonstrated no significant change in STING activation compared to the 2'3'-cGAMP agonist alone **(Figure 45C)** revealing a possible molecular mechanism of STING suppression by *H. pylori* mediated by *EG65_02145* (noted *HP1029* in strain 26695, which will be used hereafter). HP1029 belongs to the DUF386 conserved protein domain family and a single study has characterized its structure and proposed possible functions [460]. Vallese et al. suggest a possible role for HP1029 in the metabolism of bacterial surface saccharides, due to the genomic context of *HP1029* in *Helicobacter spp.* and related organisms. While this doesn't define a direct role for HP1029 in innate immune suppression at present, the DUF386 family consists of bacterial proteins that can influence biofilm formation by toxin-antitoxin systems [460]. Another member of this family, YhcH, encodes a possible sugar isomerase of sialic acid catabolism [461]. A STRING analysis of HP1029 I performed revealed co-occurrence associated with LolA, a *H. pylori* lipoprotein packaging protein, and HP0605, an outer membrane efflux protein (data not shown). *H. pylori* lipoproteins are believed to have important functions in bacterial adhesion and colonization of the stomach, altering cell migration and signaling, and stimulating interferons [462]. Thus, HP1029 is possibly involved with a *H. pylori* lipoprotein that can modulate host immune cell signaling, but further work will need to be done to first verify these targets through genetic complementation, followed by identification of HP1029's hypothetical lipoprotein partner.

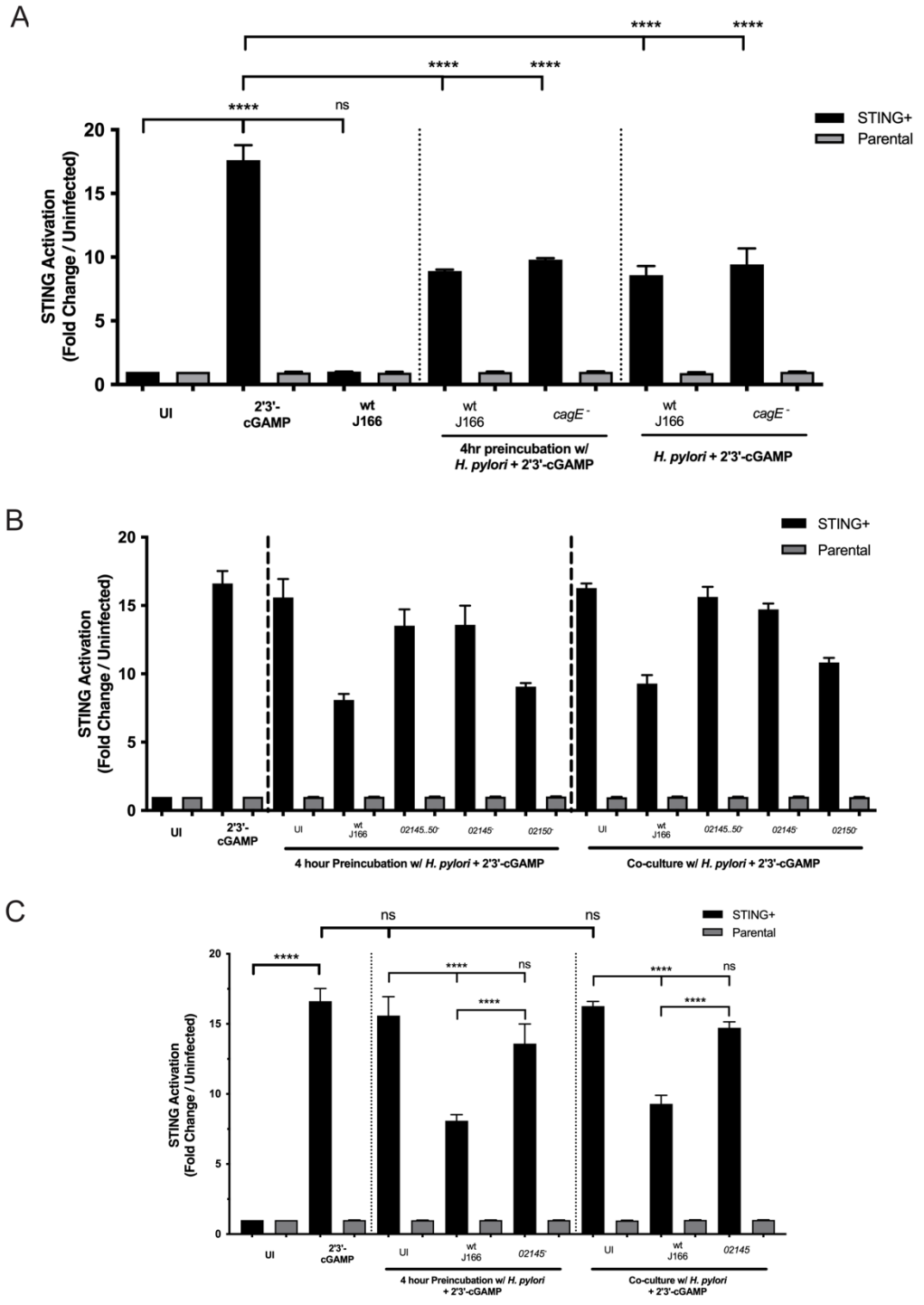

Figure 45. STING suppression by *in vitro* by *H. pylori* is *cag*-independent and deletion of *EG65_02145* alone prevents STING suppression. HEK293-STING reporter cells were co-cultured with viable *H. pylori* strains and/or a positive STING agonist 2'3'-cGAMP for 24 hours. STING-reporter or parental cells were challenged with STING agonist 2'3'-cGAMP, *H. pylori* wild-type strain J166, **(A)** a *cagE*$^{-}$ or **(B)** respective *EG65_02145..50, EG65_02145, or EG65_02150* isogenic mutant strains. **(C)** Statistical analysis of *EG65_02145*$^{-}$ alone. ANOVA with Bonferroni correction was used to determine statistical significance between groups. In each experiment, samples were tested in duplicate at least 3 times and data are represented as fold change in infected over uninfected controls strains were tested at least 3 times and mean±SEM are shown. ****p<0.0001, ns=not significant

4.4 *H. pylori* Infection Induces TRIM Proteins

Our laboratory has previously demonstrated that *H. pylori* can translocate DNA into host cells activating TLR9 [117, 119], and data in Chapter III demonstrated that additional nucleic acid sensors, STING and RIG-I, were suppressed in the presence of viable *H. pylori*. A possible host mechanism for this phenomenon was uncovered in the RNA-seq analysis, upregulation of a known family of innate immune modulators, TRIM proteins, specifically TRIM30a. Immunohistochemistry (IHC) provided initial observations on localization of TRIM30a in the gastric environment **(Figure 35D)**, which was corroborated by Western blots in both murine organoid monolayers and BMDCs **(Figure 36 A,C)**. A complimentary technique to IHC, fluorescence *in situ* hybridization (FISH), could be utilized to further detail TRIM30a expression in both epithelial and immune cells. These data and prior TRIM30a observations suggest *H. pylori* induced TRIM30a is negatively regulating TLR9 and STING, but further genetic manipulation of *Trim30a* will be required to fully encompass the mechanisms of this immune system regulator. It is unknown if *H. pylori* actively engages TRIM30a, similar to viral particles that engage with TRIM proteins, such as TRIM5 or TRIM21 [463]. Conversely, TRIM30a induction may be mediated indirectly via type I IFNs such as other TRIM proteins [432, 464]. Creation of a *Trim30a* genetic knockout mouse and the resulting infection model would directly implicate TRIM30a in *H. pylori* pathogenesis. The demonstrated roles of TRIM30a as an immunomodulator suggest a loss of *Trim30a* would result in adverse gastric outcomes and greater levels of *H. pylori* conization. However, loss of *H. pylori*'s host immunosuppressor could provide improved levels of microbial clearance. Thus, deletion of *Trim30a in vitro* and *in vivo* will ascertain its role in response to *H. pylori* infection, and how this relatively obscure host protein can be manipulated to fine-tune the gastric environment for long-term *H. pylori* survival.

Additionally, to recapitulate our findings in human patient samples, expression of *Trim30a* human orthologs and other STING-related TRIMs were analyzed by RT-PCR and significantly higher levels of expression of *TRIM6*, *TRIM22*, and *TRIM29* in patient samples that harbored inflammation or cancer were observed **(Figure 38)**. These results raise the possibility that TRIMs represent targets induced by *H. pylori* infection, that can suppress STING activation and promote pro-inflammatory and pro-tumorigenic responses *in vivo*. Due to the wide variation in expression levels within the human biopsies, these exploratory results will require further RT-PCR validation with additional housekeeping genes and begin analysis within *ex vivo* and *in vitro* infection models. In our laboratory, preliminary *in vitro* investigation on TRIM29 is underway by Jennifer Noto. She observed significant upregulation of *TRIM29* following 4- and 8-hour co-culture with *H. pylori* strains 7.13 and 60190 in AGS cells **(Figure 46)**. Further evidence of *H. pylori*-mediated TRIM29 may be linked to another oncogenic pathogen, Epstein-Barr virus (EBV), which has been found in co-infection with *H. pylori* in both malignant and non-malignant gastric outcomes [465-467]. Crosstalk of both pathogens may be critical in their carcinogenesis processes. In fact, EBV demonstrates suppression of local immunity to promote persistence via upregulation TRIM29, which in turn induces ubiquitination and subsequent degradation of STING [468]. These observations suggest TRIM30a could similarly benefit *H. pylori* and the suppressive effects of TRIM29 and TRIM30a would mutually benefit both pathogens. In addition to TRIM29, TRIM21, TRIM32, and TRIM56 have been associated with STING to regulate its signaling and would be of great interest in the future to determine if their expression is *H. pylori*-dependent. TRIM21 functions as a negative feedback modulator by promoting ubiquitination and proteasomal degradation of IRF3 and IRF7 following viral TLR stimulation [469-471], and STING signaling activity can be regulated by TRIM32 and TRIM56 mediated ubiquitination [472, 473].

While *Trim30a* was the only *Trim* gene in the Chapter III RNA-seq analysis whose expression was STING-dependent, further probing of the differentially expressed genes **(Appendix A)** also revealed *Trim10, Trim58, Trim15, Trim40, Trim12a,* and *Trim 54* to be upregulated following *H. pylori* infection **(Table 6)**. Many of these TRIMs can also modulate innate immune responses like TRIM30a. Notably, TRIM40 targets the downstream RIG-I regulator MAVS for K48-linked ubiquitination [434] and TRIM10 can suppress IFN/JAK/STAT

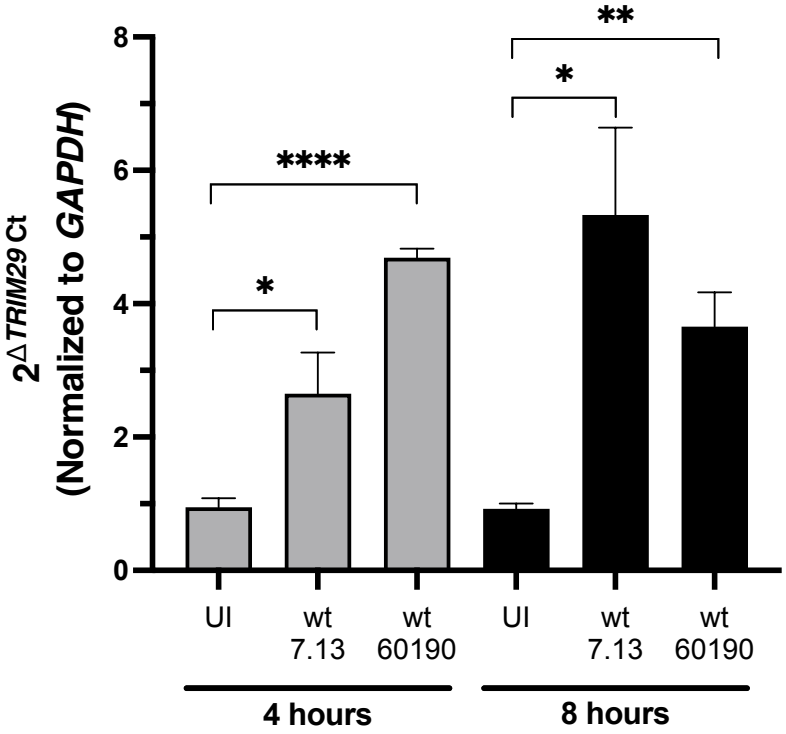

Figure 46. *H. pylori* induces *TRIM29 in vitro*. AGS cells were challenged with PBS alone (UI), *H. pylori* wild-type (wt) strain 7.13 or 60190 at MOI 100:1 for 4 hours or 8 hours. RT-PCR analysis of *TRIM29* transcript levels in co-cultured AGS lysates. Data are represented as relative gene expression levels normalized to levels of *GAPDH* gene expression. In each experiment, conditions were tested at least 2 times and student's t-tests were used to determine statistical significance between groups. *p<0.05, **p<0.01, ****p<0.0001.

Table 6. Murine TRIMs differentially expressed in the Chapter III RNAseq assay.

Grouping	Gene Name	Observed Phenotype and/or Mechanism(s)	
C57BL/6 WT Only	***Trim30a***	↑	TRIM30a promoted the degradation of STING via K48-linked ubiquitination at Lys275 through a proteasome-dependent pathway[435]; Negatively regulates NLRP3 inflammasome activation by modulating reactive oxygen species production [474]. TRIM30a is induced by TLR ligands and functions as a negative regulator of NF-κB activation; TRIM30a is a negative regulator of the TLR-mediated NF-κB signaling pathway by targeting TAB2 through a feedback mechanism [436].
WT and *Sting*$^{-/-}$	***Trim10***	↑	TRIM10 suppresses IFN/JAK/STAT signaling pathway through blocking the interaction between IFNAR1 and TYK2. TRIM10 binds to IFN-α/β receptor 1 to negatively regulate type I IFN signal transduction [441].
	Trim58	↑	TRIM58 suppresses the tumor growth in gastric cancer by inactivation of β-catenin signaling via ubiquitination; TRIM58 restrains intestinal mucosal inflammation by negatively regulating TLR2 in myeloid cells [475]; Overexpression of TRIM58, but only in presence of the RING domain, promoted proteasome-dependent degradation of TLR2, inhibiting its signaling activity [476].
***Sting*$^{-/-}$ Only**	***Trim15***	↑	TRIM15 exerts anti-tumor effects through suppressing cancer cell invasion in gastric adenocarcinoma [477]; High Expression of TRIM15 is associated with tumor invasion and predicts poor prognosis in patients with gastric cancer [478]; TRIM15 blocked the growth and metastasis of ESCC in part through inhibiting the Wnt/β-catenin signaling pathway [479].
	Trim40	↑	Riok3 recruits and interacts with the E3 ubiquitin ligase TRIM40, leading to the degradation of RIG-I and melanoma differentiation-associated gene-5 (MDA5) via K48- and K27-linked ubiquitination [434].
	Trim12a	↑	Mouse only TRIM5 ortholog; Among the seven mouse TRIM5 homologues tested, TRIM12a, -b, and -c all activated innate immune signaling, and the TRIM30 proteins did not; Another interesting finding made in this work is that TRIM12a encodes a truncated protein that is identical to TRIM12c in the N-terminal domains but lacking the C-terminal SPRY domain [480]. Intriguingly, whereas TRIM12a and TRIM12c are encoded by separate genes in the mouse, a similar truncated TRIM5 occurs in primates, presumably due to RNA or protein processing, which acts as a silencer of TRIM5. This raises the possibility that TRIM12a also induced by IFNs and TLR signaling may act as a negative regulator of TRIM12c [481].
	Trim54	↓	TRIM54 is essential for maintenance of ventricular integrity and function after myocardial infarction; Recently, several E3 ligases such as TRIM54 and CHIP have been implicated in the development of acute myocardial infarction [482].

signaling pathway through blocking the interaction between IFNAR1 and TYK2 to negatively regulate type I IFN signal transduction [441]. TRIM58 restrains intestinal mucosal inflammation by negatively regulating TLR2, as overexpression of TRIM58 promoted proteasome-dependent degradation of TLR2, inhibiting its signaling activity [476]. In the RNA-seq analysis, *Trim10* and *Trim58* were both differentially expressed regardless of *Sting* deficiency **(Appendix A)**. Altered levels of expression were subsequently validated by RT-PCR and significantly higher levels of *Trim10* and *Trim58* expression were observed in infected mice compared to uninfected mice in both genetic backgrounds **(Figure 47A,B)**. Interestingly, significantly higher levels of *Trim58* expression were observed in infected *Sting*$^{-/-}$ mice compared to infected wild-type mice but *Trim10* expression was comparable in both the wild-type and *Sting*$^{-/-}$ mice **(Figure 47B)**.

While these data are preliminary, this could suggest that TRIM58 is regulated by STING, and in the absence of STING, TRIM58 expression is unimpeded. Recent work has implicated TRIM58 in regulating the tumor growth of gastric cancer. TRIM58 expression was significantly reduced in tumor tissues of gastric cancer patients and gastric cancer cell lines, which Liu et al. attributed to inactivation of β-catenin signaling via ubiquitination to suppresses tumor growth [475]. Paradoxically, this would suggest that suppression of STING enhances expression of tumor-suppressing TRIM58, which would in turn inhibit proliferation by preventing cell-cycle progression and promoting cell apoptosis *in vitro* [475]. However, upregulation of TRIM58 would also dampen other responses like TLR-immunity which could reinforce microbe persistence, albeit at the expense of decreasing pro-neoplastic events.

Regardless, TRIM58 and other TRIMs provide novel targets for better understanding *H. pylori*-mediated host responses and promotion of gastric injury. Also, of direct clinical relevance, the demonstration that *H. pylori*-induced TRIM proteins are upregulated in a gastric cancer patient

cohort raises the intriguing possibility that these host immune modulators may represent biomarkers for disease outcomes. The gastric cancer field is beginning to investigate this very possibility with a large increase of publications in recent years attempting to associate individual TRIMs to overall survival and clinical outcomes. It must be noted that many of these studies are merely genetic associations with human patient samples, and mechanistic work is still mostly undefined. The additional TRIMs presently known to associate with gastric cancer have been summarized as a framework for further exploring the role of *H. pylori*-induced TRIMs in human hosts **(Table 7)**. Thus, manipulation of TRIMs may represent a novel strategy to prevent or treat pathologic outcomes induced by *H. pylori* infection.

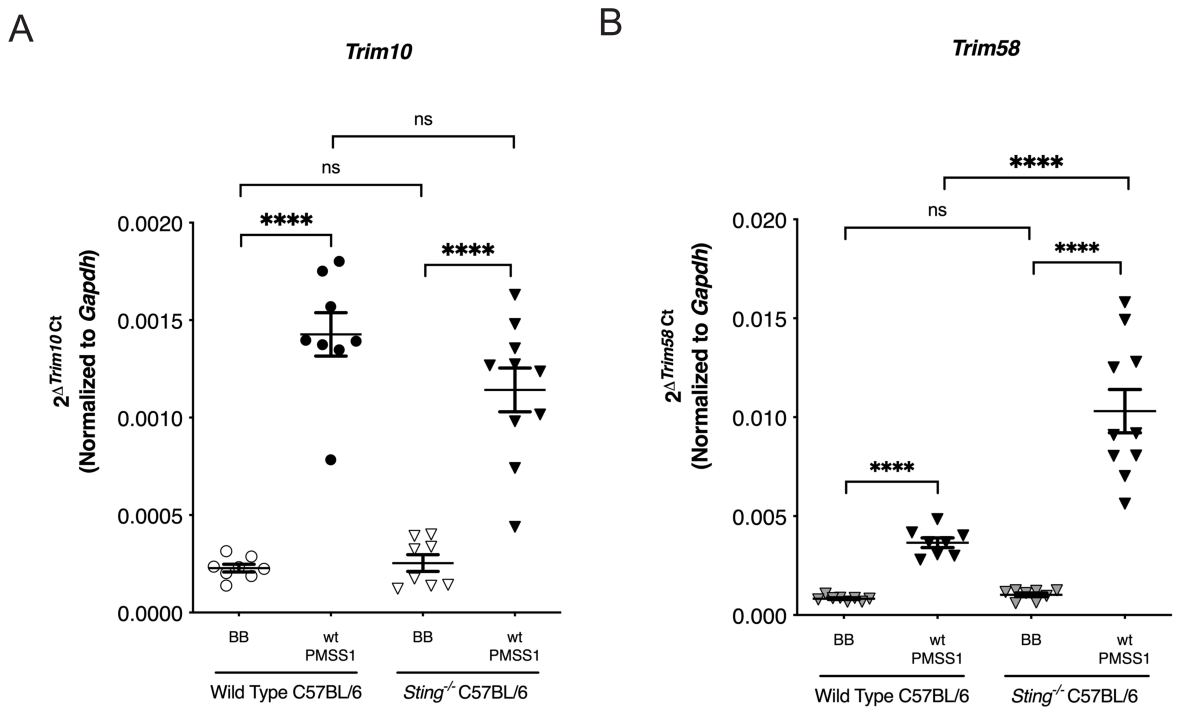

Figure 47. *Trim10* and *Trim58* are upregulated by *H. pylori in vivo*, and *Trim58* expression is suppressed in the presence of *Sting*. mRNA expression of **(A)** *Trim10* and **(B)** *Trim58* in uninfected and *H. pylori*-infected wild-type mice, and uninfected and *H. pylori*-infected *Sting*$^{-/-}$ mice. Data are represented as relative gene expression levels normalized to levels of *Gapdh* gene expression. Each data point represents an individual animal (WT BB, n=8; WT PMSS1, n=8; *Sting*$^{-/-}$ BB, n=8; *Sting*$^{-/-}$ PMSS1, n=10). Student's t-tests were used to determine statistical significance between groups. ****p<0.0001, ns=not significant.

Table 7. Human TRIM proteins associated with gastric cancer.

Protein Name	Observed Phenotype and/or Mechanism(s)	
TRIM3	↓	Decreased expression of exosomal TRIM3 protein and TRIM3 mRNA predicts a poor prognosis in gastric cancer [483, 484].
TRIM11	↑	TRIM11 promotes proliferation, migration, invasion and epithelial–mesenchymal transition of gastric cancer by activating β-catenin signaling [485].
TRIM14	↑	TRIM14 promotes the migration and invasion of gastric cancer by regulating epithelial-mesenchymal transition via activation of AKT signaling regulated by miR1955p [486]; TRIM14 promotes autophagy and chemotherapy resistance of gastric cancer cells by regulating AMPK/mTOR pathway [487].
TRIM15	↓↑	TRIM15 exerts anti-tumor effects through suppressing cancer cell invasion in gastric adenocarcinoma [477]; High Expression of TRIM15 is associated with tumor invasion and predicts poor prognosis in patients with gastric cancer [478];TRIM15 blocked the growth and metastasis of ESCC in part through inhibiting the Wnt/β-catenin signaling pathway [479].
TRIM23	↑	Elevated *TRIM23* expression predicts poor prognosis in a Chinese gastric cancer patient cohort [488].
TRIM24	↑	TRIM24 promotes the aggression of gastric cancer via the Wnt/β-catenin signaling pathway [489].
TRIM25	↑	TRIM25 significantly promoted the migration and invasion. Further experiments with TGF-β inhibitor suggested that TRIM25 may exert its function through TGF-β pathway [490]; TRIM25 RING-finger E3 ubiquitin ligase is essential for RIG-I-mediated antiviral activity [491].
TRIM29	↑	Patients with a high *TRIM29* expression showed a worse survival rate than those with a low *TRIM29* expression [440]; Expression levels of β-catenin, cyclin D1 and c-Myc were all downregulated in *TRIM29* knockdown cells, indicating that TRIM29 is involved in regulating the activity of Wnt/β-catenin signaling pathway [439].
TRIM31	↑	TRIM31 is overexpressed in gastric cancer and regulated by the ubiquitin-proteasome system [492, 493].
TRIM32	↑	TRIM32 promotes cell proliferation and invasion by activating β-catenin signaling in gastric cancer [494].
TRIM36	↑	High expression of TRIM36 is associated with radiosensitivity in gastric cancer [495].
TRIM37	↑	TRIM37 promotes cell invasion and metastasis by regulating SIP1-mediated epithelial-mesenchymal transition in gastric cancer [496]; Knockdown of TRIM37 promotes apoptosis and suppresses tumor growth in gastric cancer by inactivation of the ERK1/2 pathway [497].
TRIM44	↑	Overexpression of TRIM44 contributes to malignant outcome in gastric carcinoma [498].
TRIM47	↑	*Trim47* mRNA expression in gastric cancer tissues was significantly higher than adjacent normal tissues, as was TRIM47 protein expression [499].
TRIM58	↓	TRIM58 suppresses the tumor growth in gastric cancer by inactivation of β-catenin signaling via ubiquitination; TRIM58 restrains intestinal mucosal inflammation by negatively regulating TLR2 in myeloid cells [475]; Overexpression of TRIM58, but only in presence of the RING domain, promoted proteasome-dependent degradation of TLR2, inhibiting its signaling activity [476].
TRIM59	↑	TRIM59 is upregulated in gastric tumors, promoting ubiquitination and degradation of p53 [500].

4.5 Final Remarks

Aristotle once remarked, “All men by nature desire to know.” In science, we have a particular desire to know how the natural world around us works, and the goal of any scientist is to observe, explain, and make known the unknown. Thus, this work has provided several novel insights to advance the field of microbe-host interactions and further dissect *Helicobacter pylori*’s seemingly never-ending game of cat and mouse with its human hosts. First, these results demonstrate that *H. pylori* harbors a portfolio of mechanisms to manipulate the host immune response which can manifest as activation of specific nucleic acid PRRs such as TLR9 or active suppression of certain innate immune responses such as STING and RIG-I. Second, *H. pylori* utilizes specific virulence factors such as HopQ and inhibition of IRF3 to mediate these mechanisms via a delicate balance of both pathogen and host. Third, *in vivo* evidence revealed that *H. pylori* infection in the absence of STING drives pro-carcinogenic Th17 pathways and induces a known immune modulator TRIM30a. Finally, and of direct clinical relevance, the observations that *H. pylori*-induced TRIM proteins are upregulated in a gastric cancer patient cohort raise the possibility that these host immune modulators may represent biomarkers for gastric disease outcomes. In closing, by defining the molecular pathways induced by pathogenic *H. pylori* that drive innate immune responses with carcinogenic potential, this thesis contributes a small, but hopefully critical, understanding to the global progress to reduce *H. pylori*-induced malignancies.

APPENDIX

A. RNA SEQUENCING DATASETS

Table 1. Comparison 1: Differentially expressed genes in C57BL/6 wild-type (WT) *H. pylori*-infected mice versus C57BL/6 WT uninfected mice.
Differential expression (DE) analysis was performed on RNAseq reads. Threshold: log2 fold change ≥ | 2 | and FDR ≤ 0.05.

Gene Symbol	Description	Fold Change	DE Genes
Gm46328	predicted gene, 46328	150.6232105	232
Gm8714	predicted gene 8714	108.664799	
Gm21156	predicted gene, 21156	70.8839742	**Upregulated**
Trav8n-2	T cell receptor alpha variable 8n-2	70.55465496	213
CT010467.1		66.35566281	
Trbv29	T cell receptor beta, variable 29	65.12213167	**Downregulated**
Igdcc3	immunoglobulin superfamily, DCC subclass, member 3	39.39636958	19
Gm47398	predicted gene, 47398	37.54239757	
Khdc1c	KH domain containing 1C	35.15501682	
Ubd	ubiquitin D	33.15050302	
Gm30363	predicted gene, 30363	31.48196279	
Trbv13-3	T cell receptor beta, variable 13-3	28.70710956	
Ighv7-3	immunoglobulin heavy variable 7-3	27.41222606	
Cd8b1	CD8 antigen, beta chain 1	24.94058207	
Fam221b	family with sequence similarity 221, member B	23.95016934	
Clca3a2	chloride channel accessory 3A2	23.86053564	
Gm37264	predicted gene, 37264	21.14325948	
Igkv17-121	immunoglobulin kappa variable 17-121	20.86047086	
Gm15444	predicted gene 15444	20.7704637	
Gm6034	predicted gene 6034	19.26258002	
9930120I10Rik	RIKEN cDNA 9930120I10 gene	19.16182902	
Olfr826	olfactory receptor 826	19.08875594	
Nphs1	nephrosis 1, nephrin	18.95489884	
Il17a	interleukin 17A	18.58327617	
Gm42943	predicted gene 42943	18.14443663	
Gm4841	predicted gene 4841	17.89738016	

Gm16216	predicted gene 16216	17.22357535	
Olfr20	olfactory receptor 20	16.8899255	
Gm12250	predicted gene 12250	16.67933166	
A930002I21Rik	RIKEN cDNA A930002I21 gene	15.97828833	
Chil1	chitinase-like 1	15.43268169	
Gm37345	predicted gene, 37345	15.21756145	
Ifit1bl1	interferon induced protein with tetratricpeptide repeats 1B like 1	14.58780152	
Olfr56	olfactory receptor 56	14.04714256	
AC168977.2	component of Sp100-rs-like	13.91963046	
Gm16156	predicted gene 16156	13.55951514	
Vmn2r27	vomeronasal 2, receptor27	13.49931895	
Mixl1	Mix1 homeobox-like 1 (Xenopus laevis)	13.09298243	
Gm5431	predicted gene 5431	13.05235702	
Gm13546	predicted gene 13546	13.03014484	
Gm43135	predicted gene 43135	13.00957531	
Gm8108	predicted gene 8108	12.99483149	
Zbp1	Z-DNA binding protein 1	12.92272564	
Gm11725	predicted gene 11725	12.14075732	
Igtp	interferon gamma induced GTPase	11.84118105	
Acod1	aconitate decarboxylase 1	10.98200718	
Slfn4	schlafen 4	10.96384774	
Tgtp1	T cell specific GTPase 1	10.93437647	
Gm17344	predicted gene, 17344	10.72001624	
Gm2366	predicted gene 2366	10.53842782	
Gm20234	predicted gene, 20234	10.49533207	
Khdc1a	KH domain containing 1A	9.888736939	
Gm16685	predicted gene, 16685	9.517429118	
Cxcl9	chemokine (C-X-C motif) ligand 9	9.460036181	
Il12b	interleukin 12b	9.38462142	
Gm26550	predicted gene, 26550	9.313705956	
Ifi47	interferon gamma inducible protein 47	9.1214811	
Ifng	interferon gamma	8.951692134	
Trat1	TCR associated transmembrane adaptor 1	8.867793084	
Gm45418	predicted gene 45418	8.827519759	
Gm50103	predicted gene, 50103	8.496668364	
F830016B08Rik	RIKEN cDNA F830016B08 gene	8.334190488	
Rplp1-ps1	ribosomal protein, large, P1, pseudogene 1	8.12616087	
Klri2	killer cell lectin-like receptor family I member 2	7.769138183	

Gm12185	predicted gene 12185	7.10015754	
Clcnka	chloride channel, voltage-sensitive Ka	6.921059079	
Gm20661	predicted gene 20661	6.842387466	
Fam71b	family with sequence similarity 71, member B	6.832623198	
Cxcl10	chemokine (C-X-C motif) ligand 10	6.815801776	
Irgm1	immunity-related GTPase family M member 1	6.814624377	
Olfr60	olfactory receptor 60	6.655413654	
Gm5970	predicted gene 5970	6.554215821	
Mmel1	membrane metallo-endopeptidase-like 1	6.523220356	
Tgtp2	T cell specific GTPase 2	6.518806472	
Trim10	tripartite motif-containing 10	6.465786526	
Mcpt1	mast cell protease 1	6.144670507	
Cd8a	CD8 antigen, alpha chain	6.128078197	
Crtam	cytotoxic and regulatory T cell molecule	6.064222971	
Cxcr6	chemokine (C-X-C motif) receptor 6	6.044319215	
Gm6593	predicted gene 6593	6.042432837	
Apol9b	apolipoprotein L 9b	6.035048109	
Tnip3	TNFAIP3 interacting protein 3	6.024949066	
Lat	linker for activation of T cells	5.699729837	
Iigp1	interferon inducible GTPase 1	5.696572164	
Olfr145	olfactory receptor 145	5.627714062	
Nlrc5	NLR family, CARD domain containing 5	5.624043946	
AW112010	expressed sequence AW112010	5.611400252	
Gm4951	predicted gene 4951	5.534170159	
BC023105	cDNA sequence BC023105	5.506881544	
Ccr4	chemokine (C-C motif) receptor 4	5.4997076	
9330175E14Rik	RIKEN cDNA 9330175E14 gene	5.458627116	
Cd177	CD177 antigen	5.329645435	
Irgm2	immunity-related GTPase family M member 2	5.185359259	
Serpina3g	serine (or cysteine) peptidase inhibitor, clade A, member 3G	5.172958437	
Tnfsf11	tumor necrosis factor (ligand) superfamily, member 11	5.153208631	
Ubash3a	ubiquitin associated and SH3 domain containing, A	5.145531865	
H2-Q6	histocompatibility 2, Q region locus 6	5.063623411	
Ctla4	cytotoxic T-lymphocyte-associated protein 4	5.009896438	
Icos	inducible T cell co-stimulator	4.953912782	
Duoxa2	dual oxidase maturation factor 2	4.881344952	
Cd226	CD226 antigen	4.789364538	
Ranbp2-ps10	RAN binding protein 2, pseudogene 10	4.744283779	

Oasl2	2'-5' oligoadenylate synthetase-like 2	4.707249185	
Tnf	tumor necrosis factor	4.648506201	
Gm11295	predicted gene 11295	4.5721921	
Oas2	2'-5' oligoadenylate synthetase 2	4.544022137	
Batf2	basic leucine zipper transcription factor, ATF-like 2	4.535941601	
Gpr84	G protein-coupled receptor 84	4.466987368	
Ccl8	chemokine (C-C motif) ligand 8	4.455344806	
Nkg7	natural killer cell group 7 sequence	4.439002304	
Sftpd	surfactant associated protein D	4.396523971	
Cd160	CD160 antigen	4.373086151	
H2-DMb1	histocompatibility 2, class II, locus Mb1	4.367344549	
Pdcd1	programmed cell death 1	4.319030517	
Ccl4	chemokine (C-C motif) ligand 4	4.281999879	
Itk	IL2 inducible T cell kinase	4.273006577	
Cyp2d34	cytochrome P450, family 2, subfamily d, polypeptide 34	4.258818962	
Ms4a4b	membrane-spanning 4-domains, subfamily A, member 4B	4.2207576	
Tcrg-C2	T cell receptor gamma, constant 2	4.202381731	
Cd6	CD6 antigen	4.185138286	
Slfn2	schlafen 2	4.137299089	
Apol7b	apolipoprotein L 7b	4.131647081	
Gbp6	guanylate binding protein 6	4.078284693	
Cd200r4	CD200 receptor 4	3.826266951	
Ido1	indoleamine 2,3-dioxygenase 1	3.79972197	
Grap2	GRB2-related adaptor protein 2	3.768794593	
Xcl1	chemokine (C motif) ligand 1	3.766630217	
Sit1	suppression inducing transmembrane adaptor 1	3.765587248	
Trac	T cell receptor alpha constant	3.745120422	
Cd3d	CD3 antigen, delta polypeptide	3.652635263	
BE692007	expressed sequence BE692007	3.615458915	
Scimp	SLP adaptor and CSK interacting membrane protein	3.602292918	
Cd3g	CD3 antigen, gamma polypeptide	3.594705028	
Trim58	tripartite motif-containing 58	3.592638502	
Tbx21	T-box 21	3.576627419	
Tnfsf8	tumor necrosis factor (ligand) superfamily, member 8	3.520318379	
Cd74	CD74 antigen	3.484675908	
H2-DMa	histocompatibility 2, class II, locus DMa	3.479529986	
Ifit3b	interferon-induced protein with tetratricopeptide repeats 3B	3.446610703	
Cxcl5	chemokine (C-X-C motif) ligand 5	3.39683165	

Bcl2a1a	B cell leukemia/lymphoma 2 related protein A1a	3.38416287	
Sh2d2a	SH2 domain containing 2A	3.320428064	
Ccr7	chemokine (C-C motif) receptor 7	3.316711337	
Cd69	CD69 antigen	3.298301383	
Ciita	class II transactivator	3.268351478	
Gm13693	predicted gene 13693	3.241370534	
Cd274	CD274 antigen	3.197576485	
Duox2	dual oxidase 2	3.18985155	
Ctsw	cathepsin W	3.167426343	
Slc2a6	solute carrier family 2 (facilitated glucose transporter), member 6	3.152138101	
Mmp25	matrix metallopeptidase 25	3.151836769	
Cd3e	CD3 antigen, epsilon polypeptide	3.112386626	
Olfr323	olfactory receptor 323	3.002608298	
Spn	sialophorin	2.987772352	
Rtp4	receptor transporter protein 4	2.983642554	
H2-Ab1	histocompatibility 2, class II antigen A, beta 1	2.976386761	
Slamf8	SLAM family member 8	2.962447576	
Cst7	cystatin F (leukocystatin)	2.948297175	
Il18bp	interleukin 18 binding protein	2.891670244	
Tnfsf14	tumor necrosis factor (ligand) superfamily, member 14	2.887198711	
Gm29695	predicted gene, 29695	2.799398076	
Il2rb	interleukin 2 receptor, beta chain	2.768753758	
Itgae	integrin alpha E, epithelial-associated	2.768399514	
Bcl2a1d	B cell leukemia/lymphoma 2 related protein A1d	2.756416051	
Cd2	CD2 antigen	2.752408198	
Serpina3f	serine (or cysteine) peptidase inhibitor, clade A, member 3F	2.726135192	
Ikzf3	IKAROS family zinc finger 3	2.705293172	
Rdh16	retinol dehydrogenase 16	2.651697874	
Irf7	interferon regulatory factor 7	2.636598748	
Gbp3	guanylate binding protein 3	2.614118664	
Lck	lymphocyte protein tyrosine kinase	2.606550809	
H2-Eb1	histocompatibility 2, class II antigen E beta	2.584351966	
Ly9	lymphocyte antigen 9	2.57076148	
Ccr5	chemokine (C-C motif) receptor 5	2.565993512	
Phf11d	PHD finger protein 11D	2.558610779	
Ptpn22	protein tyrosine phosphatase, non-receptor type 22 (lymphoid)	2.529026586	
Psmb8	proteasome (prosome, macropain) subunit, beta type 8	2.499507326	

Rasal3	RAS protein activator like 3	2.483660177	
Vnn1	vanin 1	2.45896296	
Rnf213	ring finger protein 213	2.444695175	
Il1b	interleukin 1 beta	2.442777593	
Gbp2	guanylate binding protein 2	2.435579084	
Usp18	ubiquitin specific peptidase 18	2.431446923	
Itgal	integrin alpha L	2.427978027	
H2-K1	histocompatibility 2, K1, K region	2.416248635	
Clec5a	C-type lectin domain family 5, member a	2.394527093	
Apol7e	apolipoprotein L 7e	2.383732383	
Samhd1	SAM domain and HD domain, 1	2.354538488	
Oas1a	2'-5' oligoadenylate synthetase 1A	2.338656584	
H2-Q4	histocompatibility 2, Q region locus 4	2.307853122	
H2-Q7	histocompatibility 2, Q region locus 7	2.298016794	
Oas1g	2'-5' oligoadenylate synthetase 1G	2.293390819	
Itgax	integrin alpha X	2.279696145	
Parp14	poly (ADP-ribose) polymerase family, member 14	2.256657829	
Gpr132	G protein-coupled receptor 132	2.242517069	
Tap1	transporter 1, ATP-binding cassette, sub-family B (MDR/TAP)	2.234633095	
Zc3h12a	zinc finger CCCH type containing 12A	2.220055302	
Trim30a	tripartite motif-containing 30A	2.217379165	
Runx3	runt related transcription factor 3	2.214167053	
Irf1	interferon regulatory factor 1	2.198180124	
Psmb9	proteasome (prosome, macropain) subunit, beta type 9	2.182135216	
Il27ra	interleukin 27 receptor, alpha	2.179368973	
Psmb10	proteasome (prosome, macropain) subunit, beta type 10	2.120041548	
Muc4		2.10294752	
Gbp4	guanylate binding protein 4	2.09809514	
B2m	beta-2 microglobulin	2.090075895	
Uba7	ubiquitin-like modifier activating enzyme 7	2.08605067	
H2-D1	histocompatibility 2, D region locus 1	2.085233457	
Cd86	CD86 antigen	2.080776007	
H2-M2	histocompatibility 2, M region locus 2	2.072941587	
Dhx58	DEXH (Asp-Glu-X-His) box polypeptide 58	2.067289455	
Ces1g	carboxylesterase 1G	2.036740946	
Xaf1	XIAP associated factor 1	2.032207219	
Sdk2	sidekick cell adhesion molecule 2	-2.076652207	
3222401L13Rik	RIKEN cDNA 3222401L13 gene	-2.206991338	

Olfr648	olfactory receptor 648	-4.904829	
2700069I18Rik	RIKEN cDNA 2700069I18 gene	-6.31437608	
Gm35363	predicted gene, 35363	-8.100391236	
Scrg1	scrapie responsive gene 1	-8.53031912	
Gm8170	predicted gene 8170	-11.00589636	
Gm44101	predicted gene, 44101	-11.65334723	
4921511I17Rik	RIKEN cDNA 4921511I17 gene	-12.55255344	
Gm44808	predicted gene 44808	-12.55507183	
Gm13285	predicted gene 13285	-13.16118882	
Gm10340	predicted gene 10340	-14.37968604	
Gm46401	predicted gene, 46401	-15.66623184	
Ctrl	chymotrypsin-like	-22.36308455	
Cela2a	chymotrypsin-like elastase family, 2A	-35.22070563	
Pnlip	pancreatic lipase	-46.82340937	
Ctrb1	chymotrypsinogen B1	-47.17242437	
Prss2	protease, serine 2	-53.2540948	
Gm42791	predicted gene 42791	-55.51923943	

Table 2. Comparison 2: Differentially expressed genes in C57BL/6 *Sting*$^{-/-}$ *H. pylori*-infected mice versus C57BL/6 *Sting*$^{-/-}$ uninfected mice.
Differential expression (DE) analysis was performed on RNAseq reads. Threshold: log2 fold change ≥ | 2 | and FDR ≤ 0.05.

Gene Symbol	Description	Fold Change	DE Genes
Igkv17-127	immunoglobulin kappa variable 17-127	426.5954912	840
AY036118		263.8400054	**Upregulated**
Gm8714	predicted gene 8714	119.4199717	382
Gcat	glycine C-acetyltransferase (2-amino-3-ketobutyrate-coenzyme A ligase)	116.7527036	**Downregulated**
Igkv4-61	immunoglobulin kappa chain variable 4-61	100.4725857	458
Ighv2-6	immunoglobulin heavy variable 2-6	87.98541518	
Trbv13-3	T cell receptor beta, variable 13-3	75.91725438	
Ighv1-42	immunoglobulin heavy variable V1-42	75.01314982	
Igkv12-98	immunoglobulin kappa variable 12-98	72.91474528	
Igkv1-133	immunoglobulin kappa variable 1-133	66.24707604	
Olfr60	olfactory receptor 60	63.8534325	
Ighv13-2	immunoglobulin heavy variable 13-2	60.26932819	
Igkv4-50	immunoglobulin kappa variable 4-50	59.19520247	
Ubd	ubiquitin D	54.97564202	
Hacl1	predicted gene, 49387	54.07867094	
Igkv8-28	immunoglobulin kappa variable 8-28	51.22495713	
Ighv1-77	immunoglobulin heavy variable 1-77	48.93566379	
Igkv4-90	immunoglobulin kappa chain variable 4-90	48.2503575	
Ighv5-9	immunoglobulin heavy variable 5-9	48.10136617	
Ighv1-85	immunoglobulin heavy variable 1-85	45.64386737	
Khdc1a	KH domain containing 1A	44.60733982	
Clca3a2	chloride channel accessory 3A2	39.2901445	
A1bg	alpha-1-B glycoprotein	38.17460901	
Ighv1-71	immunoglobulin heavy variable 1-71	36.45116066	
Igkv4-58	immunoglobulin kappa variable 4-58	33.91909661	
Ighv1-19	immunoglobulin heavy variable V1-19	32.71814739	
Ighv7-3	immunoglobulin heavy variable 7-3	32.50697776	
Trbv29	T cell receptor beta, variable 29	31.21087409	
Ighv5-17	immunoglobulin heavy variable 5-17	31.13053737	
Ighv1-62-2	immunoglobulin heavy variable 1-62-2	29.45313539	
Gm12250	predicted gene 12250	29.41186549	
Il17a	interleukin 17A	28.09866548	

Igkv9-124	immunoglobulin kappa chain variable 9-124	27.18209216	
Ighv5-9-1	immunoglobulin heavy variable 5-9-1	26.4661335	
Ighv1-34	immunoglobulin heavy variable 1-34	26.31424824	
Gm45418	predicted gene 45418	25.86325975	
Khdc1c	KH domain containing 1C	24.74231097	
Ifit1bl1	interferon induced protein with tetratricpeptide repeats 1B like 1	24.45438137	
Gm29247	predicted gene 29247	23.72914646	
Igkv17-121	immunoglobulin kappa variable 17-121	23.41940409	
Ighv1-20	immunoglobulin heavy variable V1-20	20.93716928	
Cd8b1	CD8 antigen, beta chain 1	20.65787277	
Ighv1-12	immunoglobulin heavy variable V1-12	20.5901955	
Ighv1-18	immunoglobulin heavy variable V1-18	19.95827403	
Ighv1-78	immunoglobulin heavy variable 1-78	19.75906964	
Ighj4	immunoglobulin heavy joining 4	19.21626605	
Zbp1	Z-DNA binding protein 1	18.72830277	
Chil1	chitinase-like 1	18.7252924	
Igtp	interferon gamma induced GTPase	18.68775009	
Igkv3-2	immunoglobulin kappa variable 3-2	18.41821482	
Igkv6-32	immunoglobulin kappa variable 6-32	17.41407981	
Iglv3	immunoglobulin lambda variable 3	17.23993223	
Igkv15-103	immunoglobulin kappa chain variable 15-103	16.9949304	
Cd8a	CD8 antigen, alpha chain	16.73204143	
Slfn1	schlafen 1	16.5406752	
Gm43802	predicted gene 43802	16.08496097	
Igkv14-111	immunoglobulin kappa variable 14-111	15.7732449	
Igkv8-30	immunoglobulin kappa chain variable 8-30	15.50179933	
Igkv1-88	immunoglobulin kappa chain variable 1-88	15.31332041	
Gm12185	predicted gene 12185	15.10518879	
Igkv8-27	immunoglobulin kappa chain variable 8-27	14.9116427	
Ifng	interferon gamma	14.88569962	
Ifi47	interferon gamma inducible protein 47	14.78193657	
Slfn4	schlafen 4	14.62090238	
Gm20234	predicted gene, 20234	14.06194037	
Ighv1-61	immunoglobulin heavy variable 1-61	13.90082272	
Klrb1c	killer cell lectin-like receptor subfamily B member 1C	13.84202189	
Tgtp1	T cell specific GTPase 1	13.46052542	
Gm5431	predicted gene 5431	13.38203674	
Ighv1-80	immunoglobulin heavy variable 1-80	13.17219492	

Gm4841	predicted gene 4841	12.8146939	
Ighv1-54	immunoglobulin heavy variable V1-54	12.56693974	
Igkv3-7	immunoglobulin kappa variable 3-7	12.43849208	
Trat1	T cell receptor associated transmembrane adaptor 1	12.31365631	
Trim15	tripartite motif-containing 15	12.26413848	
Trim40	tripartite motif-containing 40	11.87500907	
Cxcl9	chemokine (C-X-C motif) ligand 9	11.57118922	
Ighv2-9-1	immunoglobulin heavy variable 2-9-1	11.56637273	
Sftpd	surfactant associated protein D	11.52609397	
Tcrg-C2	T cell receptor gamma, constant 2	11.29078261	
Ighv1-74	immunoglobulin heavy variable V1-74	11.01714483	
Ighv8-8	immunoglobulin heavy variable 8-8	10.98685908	
Igkv4-57	immunoglobulin kappa variable 4-57	10.8125531	
Gm16685	predicted gene, 16685	10.72839227	
Prl2c2	prolactin family 2, subfamily c, member 2	10.52037394	
Sit1	suppression inducing transmembrane adaptor 1	10.41793183	
Ighv9-3	immunoglobulin heavy variable V9-3	10.29335072	
Igkv4-59	immunoglobulin kappa variable 4-59	10.19705813	
Prg2	proteoglycan 2, bone marrow	10.08037016	
Ighv2-5	immunoglobulin heavy variable 2-5	9.815549383	
Ighv5-12	immunoglobulin heavy variable 5-12	9.812064749	
Igkv10-94	immunoglobulin kappa variable 10-94	9.655448684	
Ly6i	lymphocyte antigen 6 complex, locus I	9.626818887	
Ighv4-1	immunoglobulin heavy variable 4-1	9.198466738	
Reg3g	regenerating islet-derived 3 gamma	9.076267246	
Ighv1-4	immunoglobulin heavy variable 1-4	9.063651139	
Ccr8	chemokine (C-C motif) receptor 8	8.835204579	
Igkv3-12	immunoglobulin kappa variable 3-12	8.767536593	
Mmp25	matrix metallopeptidase 25	8.703240096	
Irgm1	immunity-related GTPase family M member 1	8.656307107	
Ighv1-52	immunoglobulin heavy variable 1-52	8.595193325	
Cd177	CD177 antigen	8.493743043	
Csprs	component of Sp100-rs	8.248444962	
Ighv1-75	immunoglobulin heavy variable 1-75	8.178842041	
Cd160	CD160 antigen	8.174759932	
Apol9b	apolipoprotein L 9b	8.144275883	
Slamf1	signaling lymphocytic activation molecule family member 1	8.085018729	
BC023105	cDNA sequence BC023105	8.027423421	

Tnip3	TNFAIP3 interacting protein 3	8.000907826	
Trim10	tripartite motif-containing 10	7.961021302	
Cd200r4	CD200 receptor 4	7.91556211	
Cd226	CD226 antigen	7.888244252	
Tigit	T cell immunoreceptor with Ig and ITIM domains	7.790745005	
Acod1	aconitate decarboxylase 1	7.647388745	
Fasl	Fas ligand (TNF superfamily, member 6)	7.631140133	
Igha	immunoglobulin heavy constant alpha	7.613124602	
H2-DMb1	histocompatibility 2, class II, locus Mb1	7.5996393	
Trgv2	T cell receptor gamma variable 2	7.596916824	
Serpina3g	serine (or cysteine) peptidase inhibitor, clade A, member 3G	7.583268852	
Tgtp2	T cell specific GTPase 2	7.559131237	
Ighv5-6	immunoglobulin heavy variable 5-6	7.415647173	
Ighg2b	immunoglobulin heavy constant gamma 2B	7.408870671	
Igkv3-4	immunoglobulin kappa variable 3-4	7.358114916	
Irgm2	immunity-related GTPase family M member 2	7.060007246	
Igkc	immunoglobulin kappa constant	7.014841999	
Igkv12-41	immunoglobulin kappa chain variable 12-41	7.001475878	
Ighv10-3	immunoglobulin heavy variable V10-3	6.968100894	
Trac	T cell receptor alpha constant	6.859115476	
Iigp1	interferon inducible GTPase 1	6.826929135	
Cxcr6	chemokine (C-X-C motif) receptor 6	6.587975592	
Lat	linker for activation of T cells	6.579340656	
Il18rap	interleukin 18 receptor accessory protein	6.569281692	
Cd7	CD7 antigen	6.554486669	
Mcpt1	mast cell protease 1	6.545575006	
Olfr56	olfactory receptor 56	6.543039491	
Ighv1-72	immunoglobulin heavy variable 1-72	6.509565162	
Igkv6-23	immunoglobulin kappa variable 6-23	6.490855236	
Cd3e	CD3 antigen, epsilon polypeptide	6.453185947	
Apol9a	apolipoprotein L 9a	6.423224023	
Gpr31c	G protein-coupled receptor 31, D17Leh66c region	6.30861453	
Ms4a4b	membrane-spanning 4-domains, subfamily A, member 4B	6.296512085	
Cd3g	CD3 antigen, gamma polypeptide	6.294322243	
Cxcl10	chemokine (C-X-C motif) ligand 10	6.265318119	
Gimap7	GTPase, IMAP family member 7	6.255129952	
Sprr2f	small proline-rich protein 2F	6.238988861	
Nkg7	natural killer cell group 7 sequence	6.206125547	

Igkv12-46	immunoglobulin kappa variable 12-46	6.059014559	
Batf2	basic leucine zipper transcription factor, ATF-like 2	6.049464154	
AW112010	expressed sequence AW112010	6.035572536	
Igkv4-55	immunoglobulin kappa variable 4-55	5.999531748	
Igkv8-21	immunoglobulin kappa variable 8-21	5.963501149	
Igkv13-85	immunoglobulin kappa chain variable 13-85	5.944093568	
Gm35028	predicted gene, 35028	5.929301845	
Igkv4-68	immunoglobulin kappa variable 4-68	5.86783053	
Klra2	killer cell lectin-like receptor, subfamily A, member 2	5.755946084	
Jchain	immunoglobulin joining chain	5.747486059	
Nox1	NADPH oxidase 1	5.694162242	
Pth2r	parathyroid hormone 2 receptor	5.682091297	
Cd74	CD74 antigen (invariant polypeptide of major histocompatibility complex, class II antigen-associated)	5.664558399	
Grap2	GRB2-related adaptor protein 2	5.654573757	
Ighv1-64	immunoglobulin heavy variable 1-64	5.643368738	
Nlrc5	NLR family, CARD domain containing 5	5.607997887	
Cyp3a16	cytochrome P450, family 3, subfamily a, polypeptide 16	5.582244332	
Ighg2c	immunoglobulin heavy constant gamma 2C	5.580508819	
Ighv1-55	immunoglobulin heavy variable 1-55	5.568810694	
Mzb1	marginal zone B and B1 cell-specific protein 1	5.545870689	
Ighv1-11	immunoglobulin heavy variable V1-11	5.530312452	
Iglv1	immunoglobulin lambda variable 1	5.513877076	
F830016B08Rik	RIKEN cDNA F830016B08 gene	5.460747178	
Cyp3a41a	cytochrome P450, family 3, subfamily a, polypeptide 41A	5.448191926	
Gpr171	G protein-coupled receptor 171	5.432314746	
Ighv1-7	immunoglobulin heavy variable V1-7	5.393365179	
Ighv6-6	immunoglobulin heavy variable 6-6	5.367207722	
Cd28	CD28 antigen	5.334024261	
BE692007	expressed sequence BE692007	5.314494099	
Icos	inducible T cell co-stimulator	5.291281295	
Cyp3a41b	cytochrome P450, family 3, subfamily a, polypeptide 41B	5.289378141	
Sult2a1	sulfotransferase family 2A, dehydroepiandrosterone (DHEA)-preferring, member 1	5.244336651	
Ighv1-9	immunoglobulin heavy variable V1-9	5.199833311	
Igkv9-120	immunoglobulin kappa chain variable 9-120	5.198739937	
Spn	sialophorin	5.192974934	
Cd3d	CD3 antigen, delta polypeptide	5.182511092	
Lta	lymphotoxin A	5.133405569	
9330175E14Rik	RIKEN cDNA 9330175E14 gene	5.112962499	

Slfn2	schlafen 2	5.111260095	
Iglc1	immunoglobulin lambda constant 1	5.108307231	
Itk	IL2 inducible T cell kinase	5.091362187	
Ccl28	chemokine (C-C motif) ligand 28	5.071157628	
Ighv1-15	immunoglobulin heavy variable 1-15	4.980401597	
Zfp831	zinc finger protein 831	4.953396965	
Xcl1	chemokine (C motif) ligand 1	4.943944581	
Ighv1-22	immunoglobulin heavy variable 1-22	4.939242739	
Trbc2	T cell receptor beta, constant 2	4.887934111	
Dmbt1	deleted in malignant brain tumors 1	4.858618816	
Cd101	CD101 antigen	4.857009644	
Igkv4-86	immunoglobulin kappa variable 4-86	4.846658793	
Ighv1-62-3	immunoglobulin heavy variable 1-62-3	4.82738618	
Pdcd1	programmed cell death 1	4.801288506	
H2-DMa	histocompatibility 2, class II, locus DMa	4.796376074	
BC100530	cystatin domain containing 5	4.737466125	
Zap70	zeta-chain (TCR) associated protein kinase	4.708316956	
Bst2	bone marrow stromal cell antigen 2	4.706990841	
Igkv13-84	immunoglobulin kappa chain variable 13-84	4.693210819	
Fcgbp	Fc fragment of IgG binding protein	4.690764628	
Il1b	interleukin 1 beta	4.644981336	
A530030E21Rik	RIKEN cDNA A530030E21 gene	4.623185132	
Oasl2	2'-5' oligoadenylate synthetase-like 2	4.576277098	
Lypd8	LY6/PLAUR domain containing 8	4.573999426	
Tnfsf13os	tumor necrosis factor (ligand) superfamily, member 13, opposite strand	4.534989509	
Ikzf3	IKAROS family zinc finger 3	4.530790656	
H2-Aa	histocompatibility 2, class II antigen A, alpha	4.522268901	
Ccl17	chemokine (C-C motif) ligand 17	4.520811285	
Fcgr4	Fc receptor, IgG, low affinity IV	4.50404597	
Cyp3a44	cytochrome P450, family 3, subfamily a, polypeptide 44	4.487408021	
Osm	oncostatin M	4.486670175	
Cd96	CD96 antigen	4.454421572	
Igkv2-109	immunoglobulin kappa variable 2-109	4.401718621	
Cxcr3	chemokine (C-X-C motif) receptor 3	4.392247549	
Ccl8	chemokine (C-C motif) ligand 8	4.381009092	
Tnfrsf17	tumor necrosis factor receptor superfamily, member 17	4.375489023	
Cd163l1	scavenger receptor family member expressed on T cells 1	4.368466606	
Tnf	tumor necrosis factor	4.366862641	

Gm36161	predicted gene, 36161	4.340813234	
Igkv3-5	immunoglobulin kappa chain variable 3-5	4.326335144	
Igkv6-13	immunoglobulin kappa variable 6-13	4.321482459	
H2-Ab1	histocompatibility 2, class II antigen A, beta 1	4.310412152	
Gbp6	guanylate binding protein 6	4.304804354	
Ccl22	chemokine (C-C motif) ligand 22	4.300881022	
Sirpb1c	signal-regulatory protein beta 1C	4.279564357	
Duoxa2	dual oxidase maturation factor 2	4.266362915	
Gsdmc4	gasdermin C4	4.256874278	
Adgrg5	adhesion G protein-coupled receptor G5	4.243698553	
P2ry10	purinergic receptor P2Y, G-protein coupled 10	4.230867393	
Ighv1-76	immunoglobulin heavy variable 1-76	4.212405719	
Trbc1	T cell receptor beta, constant region 1	4.189342985	
Tnfsf14	tumor necrosis factor (ligand) superfamily, member 14	4.15979012	
Gpr141	G protein-coupled receptor 141	4.154289974	
Igkv2-137	immunoglobulin kappa chain variable 2-137	4.149257823	
Gm43302	predicted gene 43302	4.094535604	
Bpifa5	BPI fold containing family A, member 5	4.078677504	
Slamf7	SLAM family member 7	4.076287917	
Slamf6	SLAM family member 6	4.061306799	
Ighv1-53	immunoglobulin heavy variable 1-53	4.033372229	
Gm4951	predicted gene 4951	4.030028276	
Mefv	Mediterranean fever	3.97653923	
Ctsw	cathepsin W	3.970775353	
Iglv2	immunoglobulin lambda variable 2	3.949503705	
Igkv14-100	immunoglobulin kappa chain variable 14-100	3.940234113	
Ifit3b	interferon-induced protein with tetratricopeptide repeats 3B	3.926151843	
Phf11a	PHD finger protein 11A	3.901072474	
Ciita	class II transactivator	3.899905203	
C130026I21Rik	RIKEN cDNA C130026I21 gene	3.887191804	
H2-Q6	histocompatibility 2, Q region locus 6	3.885936853	
Slamf8	SLAM family member 8	3.844996013	
Igkv4-70	immunoglobulin kappa chain variable 4-70	3.824746214	
Igkv4-91	immunoglobulin kappa chain variable 4-91	3.801242588	
Igkv8-19	immunoglobulin kappa variable 8-19	3.776550182	
Gm8221	predicted gene 8221	3.763713165	
Cd244	CD244 molecule A	3.752238111	
Gsdmc2	gasdermin C2	3.752187098	

AC174678.2	predicted gene, 49378	3.75165208	
Slc2a6	solute carrier family 2 (facilitated glucose transporter), member 6	3.739963355	
Oas2	2'-5' oligoadenylate synthetase 2	3.733095581	
Ighv1-81	immunoglobulin heavy variable 1-81	3.72086263	
Apol7b	apolipoprotein L 7b	3.711819801	
Itgax	integrin alpha X	3.704478141	
Ighg3	Immunoglobulin heavy constant gamma 3	3.691270665	
Gzmb	granzyme B	3.682952773	
Sult2a2	sulfotransferase family 2A, dehydroepiandrosterone (DHEA)-preferring, member 2	3.662328174	
Cd274	CD274 antigen	3.621836867	
Rasal3	RAS protein activator like 3	3.621275151	
Cyp2d34	cytochrome P450, family 2, subfamily d, polypeptide 34	3.590886961	
Tnfrsf9	tumor necrosis factor receptor superfamily, member 9	3.587572072	
Dmp1	dentin matrix protein 1	3.570381179	
Klrb1b	killer cell lectin-like receptor subfamily B member 1B	3.536456846	
Scimp	SLP adaptor and CSK interacting membrane protein	3.517300469	
Tbc1d10c	TBC1 domain family, member 10c	3.515560265	
Ighv1-26	immunoglobulin heavy variable 1-26	3.513130318	
Igkv3-10	immunoglobulin kappa variable 3-10	3.483506624	
Ltb	lymphotoxin B	3.483193822	
Igkv12-44	immunoglobulin kappa variable 12-44	3.460283381	
Sp110	Sp110 nuclear body protein	3.458958861	
Gpr174	G protein-coupled receptor 174	3.45558599	
Iglc2	immunoglobulin lambda constant 2	3.454896085	
Ccr10	chemokine (C-C motif) receptor 10	3.445817878	
Il1rl1	interleukin 1 receptor-like 1	3.438490406	
Selplg	selectin, platelet (p-selectin) ligand	3.413981676	
Gsdmc3	gasdermin C3	3.369137649	
Trim58	tripartite motif-containing 58	3.36856766	
Atp6v0d2	ATPase, H+ transporting, lysosomal V0 subunit D2	3.368198377	
Apol7e	apolipoprotein L 7e	3.35272473	
Gimap3	GTPase, IMAP family member 3	3.344677856	
Gm10916	predicted gene 10916	3.337595754	
Rdh16	retinol dehydrogenase 16	3.300209861	
Igkv4-57-1	immunoglobulin kappa variable 4-57-1	3.283784187	
Cass4	Cas scaffolding protein family member 4	3.277346021	
Ccr5	chemokine (C-C motif) receptor 5	3.262784572	
Ccl4	chemokine (C-C motif) ligand 4	3.239362299	

Itgal	integrin alpha L	3.230789031	
Sp100	nuclear antigen Sp100	3.218368322	
Plaur	plasminogen activator, urokinase receptor	3.178142706	
H2-Eb1	histocompatibility 2, class II antigen E beta	3.151037866	
Gfi1	growth factor independent 1 transcription repressor	3.150290332	
Cxcl5	chemokine (C-X-C motif) ligand 5	3.143538769	
Il18bp	interleukin 18 binding protein	3.117773431	
Vnn1	vanin 1	3.095950048	
Casp1	caspase 1	3.095949716	
Btla	B and T lymphocyte associated	3.094965003	
Ighv5-16	immunoglobulin heavy variable 5-16	3.089255352	
Cxcl1	chemokine (C-X-C motif) ligand 1	3.080999885	
Mcpt2	mast cell protease 2	3.065154591	
Itgae	integrin alpha E, epithelial-associated	3.050259379	
Gm47015	predicted gene, 47015	3.040421069	
Muc13	mucin 13, epithelial transmembrane	3.039552584	
Ugt1a5	UDP glucuronosyltransferase 1 family, polypeptide A5	3.037957852	
Cd52	CD52 antigen	3.037406116	
Skap1	src family associated phosphoprotein 1	3.009635878	
Mpeg1	macrophage expressed gene 1	2.976030343	
Cd2	CD2 antigen	2.971847203	
Slc22a26	solute carrier family 22 (organic cation transporter), member 26	2.969630815	
Ptprc	protein tyrosine phosphatase, receptor type, C	2.932414194	
AC160962.1	predicted gene, 49391	2.910051611	
Duox2	dual oxidase 2	2.87616064	
Dnase1l3	deoxyribonuclease 1-like 3	2.866868381	
Clec9a	C-type lectin domain family 9, member a	2.838171048	
Zc3h12a	zinc finger CCCH type containing 12A	2.794508658	
Pigr	polymeric immunoglobulin receptor	2.788525004	
Smpdl3b	sphingomyelin phosphodiesterase, acid-like 3B	2.782783421	
Irf8	interferon regulatory factor 8	2.756060411	
Cyp17a1	cytochrome P450, family 17, subfamily a, polypeptide 1	2.754064392	
Il12rb1	interleukin 12 receptor, beta 1	2.749072331	
Il2ra	interleukin 2 receptor, alpha chain	2.692282313	
Cd69	CD69 antigen	2.685143161	
Plac8	placenta-specific 8	2.57890591	
Muc4		2.561440156	
Nckap1l	NCK associated protein 1 like	2.527082554	

Rtp4	receptor transporter protein 4	2.517007931	
Btnl4	butyrophilin-like 4	2.493395093	
Ido1	indoleamine 2,3-dioxygenase 1	2.47113352	
Cd14	CD14 antigen	2.450655167	
Hsd17b6	hydroxysteroid (17-beta) dehydrogenase 6	2.440550115	
Npc1l1	NPC1 like intracellular cholesterol transporter 1	2.439598064	
Lipg	lipase, endothelial	2.415623499	
Mlkl	mixed lineage kinase domain-like	2.408310505	
Coro1a	coronin, actin binding protein 1A	2.405913244	
Reg3b	regenerating islet-derived 3 beta	2.400249199	
Cybb	cytochrome b-245, beta polypeptide	2.394449517	
Prss32	protease, serine 32	2.372198678	
H2-K1	histocompatibility 2, K1, K region	2.369203049	
Omp	olfactory marker protein	2.36334415	
Tm4sf5	transmembrane 4 superfamily member 5	2.343076444	
Plet1	placenta expressed transcript 1	2.311019035	
Itgb2	integrin beta 2	2.308776207	
Chil4	chitinase-like 4	2.295173946	
9930111J21Rik2	RIKEN cDNA 9930111J21 gene 2	2.293205615	
Naip5	NLR family, apoptosis inhibitory protein 5	2.272958351	
AU020206	expressed sequence AU020206	2.268595661	
Lrg1	leucine-rich alpha-2-glycoprotein 1	2.252121621	
Rnf213	ring finger protein 213	2.250859919	
Parp14	poly (ADP-ribose) polymerase family, member 14	2.22009783	
Sis	sucrase isomaltase (alpha-glucosidase)	2.217909385	
2310057J18Rik	RIKEN cDNA 2310057J18 gene	2.202035088	
Irf7	interferon regulatory factor 7	2.196993355	
Laptm5	lysosomal-associated protein transmembrane 5	2.182800054	
Nfkbiz	nuclear factor of kappa light polypeptide gene enhancer in B cells inhibitor, zeta	2.175502821	
Dock11	dedicator of cytokinesis 11	2.171041736	
Vil1	villin 1	2.160960714	
Psmb10	proteasome (prosome, macropain) subunit, beta type 10	2.142900222	
Ptprr	protein tyrosine phosphatase, receptor type, R	2.142075765	
Cxcl16	chemokine (C-X-C motif) ligand 16	2.133838591	
Apobec1	apolipoprotein B mRNA editing enzyme, catalytic polypeptide 1	2.11843506	
Samhd1	SAM domain and HD domain, 1	2.104877008	
Gvin1	GTPase, very large interferon inducible 1	2.093473469	
Btnl5-ps	butyrophilin-like 5, pseudogene	2.086354288	

Gsdmd	gasdermin D	2.083358871	
Dtx3l	deltex 3-like, E3 ubiquitin ligase	2.079888626	
Tapbp	TAP binding protein	2.073373387	
Trim12a	tripartite motif-containing 12A	2.07188339	
Misp	mitotic spindle positioning	2.065853815	
Ly6d	lymphocyte antigen 6 complex, locus D	2.040739274	
Tapbpl	TAP binding protein-like	2.02235154	
H2-T22	histocompatibility 2, T region locus 22	2.009469568	
Actn2	actinin alpha 2	-2.010832662	
Eno3	enolase 3, beta muscle	-2.016060579	
AC034099.1	predicted gene, 49369	-2.025358795	
Actc1	actin, alpha, cardiac muscle 1	-2.123324086	
Eef1a2	eukaryotic translation elongation factor 1 alpha 2	-2.150261968	
Sln	sarcolipin	-2.167137245	
Pygm	muscle glycogen phosphorylase	-2.167710901	
Srl	sarcalumenin	-2.179634487	
Mybpc1	myosin binding protein C, slow-type	-2.196032022	
Csrp3	cysteine and glycine-rich protein 3	-2.201008957	
Mup11	major urinary protein 11	-2.205548875	
Myo18b	myosin XVIIIb	-2.229903005	
Mup9	major urinary protein 9	-2.233764348	
Cacna1s	calcium channel, voltage-dependent, L type, alpha 1S subunit	-2.247011228	
Klhl41	kelch-like 41	-2.253140403	
Ryr1	ryanodine receptor 1, skeletal muscle	-2.28566357	
Obscn	obscurin, cytoskeletal calmodulin and titin-interacting RhoGEF	-2.287784022	
Xirp2	xin actin-binding repeat containing 2	-2.290476912	
Ankrd23	ankyrin repeat domain 23	-2.32425525	
Col6a5	collagen, type VI, alpha 5	-2.346301436	
Nrap	nebulin-related anchoring protein	-2.374690335	
Myl1	myosin, light polypeptide 1	-2.390680859	
Txlnb	taxilin beta	-2.39115485	
Hrc	histidine rich calcium binding protein	-2.451501326	
Mup2	major urinary protein 2	-2.465266042	
Neb	nebulin	-2.487351049	
Casq1	calsequestrin 1	-2.509225387	
Ckm	creatine kinase, muscle	-2.513675725	
Myh8	myosin, heavy polypeptide 8, skeletal muscle, perinatal	-2.527513616	
Gm28523	predicted gene 28523	-2.536280736	

Mylpf	myosin light chain, phosphorylatable, fast skeletal muscle	-2.546834432	
Ttn	titin	-2.552959938	
Sim2	single-minded family bHLH transcription factor 2	-2.563747744	
Nkx2-4	NK2 homeobox 4	-2.56957186	
Acta1	actin, alpha 1, skeletal muscle	-2.56977896	
Myl3	myosin, light polypeptide 3	-2.584022153	
B230303O12Rik	RIKEN cDNA B230303O12 gene	-2.614184254	
2310008N11Rik	RIKEN cDNA 2310008N11 gene	-2.629437824	
Gm5771	predicted gene 5771	-2.635377477	
Pgam2	phosphoglycerate mutase 2	-2.650964414	
Actn3	actinin alpha 3	-2.651383974	
Gm29773	predicted gene, 29773	-2.654207597	
Lmod3	leiomodin 3 (fetal)	-2.654619005	
Mb	myoglobin	-2.654751604	
Smtnl1	smoothelin-like 1	-2.657441844	
Myot	myotilin	-2.660945277	
Hfe2	hemojuvelin BMP co-receptor	-2.664717599	
Myoz1	myozenin 1	-2.679485672	
Gm29340	predicted gene 29340	-2.685880733	
Gm38287	predicted gene, 38287	-2.691041437	
Lmod2	leiomodin 2 (cardiac)	-2.691337821	
Tnnt3	troponin T3, skeletal, fast	-2.717445065	
Klhl31	kelch-like 31	-2.719204808	
Myom2	myomesin 2	-2.721346744	
Cox6a2	cytochrome c oxidase subunit 6A2	-2.723545935	
Vmn1r223	vomeronasal 1 receptor 223	-2.72783057	
4731419I09Rik	RIKEN cDNA 4731419I09 gene	-2.747889937	
Asb14	ankyrin repeat and SOCS box-containing 14	-2.755047146	
2310002F09Rik	RIKEN cDNA 2310002F09 gene	-2.761890979	
Gm17344	predicted gene, 17344	-2.767027982	
Calcoco2	calcium binding and coiled-coil domain 2	-2.771891459	
Gm50169	predicted gene, 50169	-2.784876027	
Tnnc2	troponin C2, fast	-2.816127351	
Igkv5-45	immunoglobulin kappa chain variable 5-45	-2.846274124	
Gm15983	predicted gene 15983	-2.858122156	
Trdn	triadin	-2.864028285	
Tcap	titin-cap	-2.869404512	
Gm18313	predicted gene, 18313	-2.882050014	

AI427809	macrophage expressed LXRa(NR1H3)-dependent amplifier of Abca1 transcription lncRNA	-2.888219763	
Mup17	major urinary protein 17	-2.907964887	
Gm29966	predicted gene, 29966	-2.94166751	
Gm43627	predicted gene 43627	-2.94817882	
Atp2a1	ATPase, Ca++ transporting, cardiac muscle, fast twitch 1	-2.967187573	
Mstn	myostatin	-2.987769482	
Mylk3	myosin light chain kinase 3	-2.997978133	
Mylk2	myosin, light polypeptide kinase 2, skeletal muscle	-2.998598844	
Pcdhb10	protocadherin beta 10	-3.00068002	
Nctc1	non-coding transcript 1	-3.015814375	
Rsc1a1	regulatory solute carrier protein, family 1, member 1	-3.085701376	
Trim54	tripartite motif-containing 54	-3.09077939	
Ckmt2	creatine kinase, mitochondrial 2	-3.094976329	
Fmr1nb	Fmr1 neighbor	-3.107040208	
Atp1b4	ATPase, (Na+)/K+ transporting, beta 4 polypeptide	-3.13261041	
Igkv5-39	immunoglobulin kappa variable 5-39	-3.147690306	
Gcnt7	glucosaminyl (N-acetyl) transferase family member 7	-3.150190589	
Asb10	ankyrin repeat and SOCS box-containing 10	-3.156387938	
Gm44527	predicted gene 6600	-3.189879214	
Myh1	myosin, heavy polypeptide 1, skeletal muscle, adult	-3.200274059	
Mmel1	membrane metallo-endopeptidase-like 1	-3.228256786	
Gm13620	predicted gene 13620	-3.234864978	
Dhrs7c	dehydrogenase/reductase (SDR family) member 7C	-3.268382739	
Chrna1	cholinergic receptor, nicotinic, alpha polypeptide 1 (muscle)	-3.28346523	
Gm10501	predicted gene 10501	-3.285805815	
Chrnd	cholinergic receptor, nicotinic, delta polypeptide	-3.298770627	
Gm20388	polypeptide N-acetylgalactosaminyltransferase 2-like	-3.302566222	
Gm8918	predicted gene 8918	-3.310484075	
Fbxo40	F-box protein 40	-3.354132321	
Gm49727	predicted gene, 49727	-3.371000968	
Gm10143	predicted gene 10143	-3.388114072	
Art1	ADP-ribosyltransferase 1	-3.412515415	
Gm44643	predicted gene 44643	-3.423558463	
2310039L15Rik	RIKEN cDNA 2310039L15 gene	-3.427587661	
5430431A17Rik	RIKEN cDNA 5430431A17 gene	-3.427672123	
Prr33	proline rich 33	-3.431823647	
Trpm1	transient receptor potential cation channel, subfamily M, member 1	-3.444100036	

Diras1	DIRAS family, GTP-binding RAS-like 1	-3.482186111	
Nmrk2	nicotinamide riboside kinase 2	-3.494465735	
Rps27a-ps1	ribosomal protein S27A, pseudogene 1	-3.499754999	
Gm4221	predicted gene 4221	-3.530141593	
Gm14493	predicted gene 14493	-3.547154015	
Gm8790	predicted gene 8790	-3.548544793	
Serpinb1c	serine (or cysteine) peptidase inhibitor, clade B, member 1c	-3.581875601	
Pgpep1l	pyroglutamyl-peptidase I-like	-3.737573738	
Olfr77	olfactory receptor 77	-3.755285786	
Olfr1152	olfactory receptor 1152	-3.808546725	
Tmem233	transmembrane protein 233	-3.811345492	
Gm37348	predicted gene, 37348	-3.820363217	
Raver1	predicted gene, 38431	-3.838597852	
Lrrc74b	leucine rich repeat containing 74B	-3.882357848	
Prss3	protease, serine 3	-3.925250703	
Gm15536	predicted gene 15536	-3.932067817	
Mylf-ps	myosin light chain, alkali, fast skeletal muscle, pseudogene	-3.958807392	
Mup15	major urinary protein 15	-3.971908959	
Pnliprp1	pancreatic lipase related protein 1	-3.9940563	
Rnase1	ribonuclease, RNase A family, 1 (pancreatic)	-4.004803345	
Mybpc2	myosin binding protein C, fast-type	-4.016731312	
2310065F04Rik	RIKEN cDNA 2310065F04 gene	-4.026607925	
BC037039	cDNA sequence BC037039	-4.035026567	
Asb18	ankyrin repeat and SOCS box-containing 18	-4.092820284	
Hspb3	heat shock protein 3	-4.116810484	
Galnt6os	polypeptide N-acetylgalactosaminyltransferase 6, opposite strand	-4.134444842	
Gm20422	predicted gene 20422	-4.14128259	
Gm44729	predicted gene 44729	-4.175028749	
Rnu3b2		-4.178386732	
Gm831	predicted gene 831	-4.197688198	
Gm48061	predicted gene, 48061	-4.219511714	
Aqp2	aquaporin 2	-4.225325653	
2310002L09Rik	RIKEN cDNA 2310002L09 gene	-4.231271285	
Slco1a1	solute carrier organic anion transporter family, member 1a1	-4.307468515	
Olfr24	olfactory receptor 24	-4.311253493	
Try4	trypsin 4	-4.377494781	
Rundc3a	RUN domain containing 3A	-4.399637175	

Gm9662	predicted gene 9662	-4.631308126	
Gm11175	predicted gene 11175	-4.646497001	
Gm26619	ribosomal protein S18, pseudogene 4	-4.662909051	
Serpini2	serine (or cysteine) peptidase inhibitor, clade I, member 2	-4.718013916	
Gm39321	predicted gene, 39321	-4.82577269	
AL592187.6	apolipoprotein L 10C, pseudogene	-4.849621368	
Gm45524	predicted gene 45524	-4.87322747	
AC126028.1	predicted gene, 49188	-4.879126112	
1700040D17Rik	RIKEN cDNA 1700040D17 gene	-5.015577884	
Gm26596	predicted gene, 26596	-5.04832484	
Rnase9	ribonuclease, RNase A family, 9 (non-active)	-5.086871798	
Gm29684	predicted gene, 29684	-5.089640679	
Gm45713	predicted gene 45713	-5.224039878	
Neu4	sialidase 4	-5.242192664	
Olfr455	olfactory receptor 455	-5.261180085	
Myh4	myosin, heavy polypeptide 4, skeletal muscle	-5.312823642	
Npcd	neuronal pentraxin chromo domain	-5.339276149	
Gm34280	predicted gene, 34280	-5.468442832	
Gm48342	predicted gene, 48342	-5.480419682	
Cela1	chymotrypsin-like elastase family, member 1	-5.498554712	
Gm42890	predicted gene 42890	-5.503432935	
Mup1	major urinary protein 1	-5.546249536	
Gm2238	predicted gene 2238	-5.572099348	
Gm10165	predicted gene 10165	-5.640222668	
Gm26592	predicted gene, 26592	-5.643727893	
Gm21045	predicted gene, 21045	-5.663799789	
Gm11707	predicted gene 11707	-5.692658313	
Gm10874	predicted gene 10874	-5.751526054	
Gm20721	predicted gene, 20721	-5.781950933	
Gm15283	predicted gene 15283	-5.875276615	
Mup14	major urinary protein 14	-5.939409786	
AC163664.1	RIKEN cDNA 1810028F09 gene	-5.98303036	
Mamdc4	MAM domain containing 4	-6.07266058	
Gm27232	predicted gene 27232	-6.084184009	
Gabrb1	gamma-aminobutyric acid (GABA) A receptor, subunit beta 1	-6.120551192	
Serpina1e	serine (or cysteine) peptidase inhibitor, clade A, member 1E	-6.153085079	
Mup21	major urinary protein 21	-6.19886786	
Mobp	myelin-associated oligodendrocytic basic protein	-6.227436172	

Rnu3b3		-6.290772852	
Gm38374	predicted gene, 38374	-6.360796295	
Gm17035	predicted gene 17035	-6.405965885	
Cyp2d9	cytochrome P450, family 2, subfamily d, polypeptide 9	-6.440557042	
Gm28592	predicted gene 28592	-6.471799087	
Gm43533	predicted gene 43533	-6.502126498	
Tldc2	TBC/LysM associated domain containing 2	-6.647589047	
Mup12	major urinary protein 12	-6.665164245	
Prss54	protease, serine 54	-6.685517059	
Olfr1389	olfactory receptor 1389	-6.696686256	
AC167229.1	predicted gene, 35533	-6.729151326	
Gm49643	predicted gene, 49643	-6.792496616	
Cyp4a12a	cytochrome P450, family 4, subfamily a, polypeptide 12a	-6.87433603	
Lsmem1	leucine-rich single-pass membrane protein 1	-6.939303195	
Gm47512	predicted gene, 47512	-6.999765762	
Olfr373	olfactory receptor 373	-7.036735332	
AC131029.2	predicted gene, 49164	-7.052226447	
Bpifb3	BPI fold containing family B, member 3	-7.074196127	
Olfr354	olfactory receptor 354	-7.081409233	
4732463B04Rik	RIKEN cDNA 4732463B04 gene	-7.177971343	
Gm10434	predicted gene 10434	-7.40130227	
Gm11408	predicted gene 11408	-7.576939664	
Ins2	insulin II	-7.582244364	
Gm20521	predicted gene 20521	-7.590979306	
Gm42759	predicted gene 42759	-7.804637477	
Gm20708	predicted gene 20708	-7.92018594	
B130046B21Rik	RIKEN cDNA B130046B21 gene	-8.155931742	
Gm45193	predicted gene 45193	-8.256681832	
A630072L19Rik	RIKEN cDNA A630072L19 gene	-8.384837111	
Gm10564	predicted gene 10564	-8.42175273	
Klk1b5	kallikrein 1-related peptidase b5	-8.546788754	
Gm35842	predicted gene, 35842	-8.557020955	
Hoxa13	homeobox A13	-8.577887323	
BC106175	cDNA sequence BC106175	-8.61996464	
Sycn	syncollin	-8.766885836	
Gm44510	predicted gene 44510	-8.868806256	
B430218F22Rik	RIKEN cDNA B430218F22 gene	-8.883774015	
Kdm4d	lysine (K)-specific demethylase 4D	-9.004693187	
A530083I20Rik	RIKEN cDNA A530083I20 gene	-9.029392161	

Gm48710	predicted gene, 48710	-9.046552577	
4921539H07Rik	RIKEN cDNA 4921539H07 gene	-9.12801365	
Gucy2d	guanylate cyclase 2d	-9.155398599	
4930444P10Rik	RIKEN cDNA 4930444P10 gene	-9.161146222	
Gm26631	predicted gene, 26631	-9.20127383	
Gm47503	predicted gene, 47503	-9.323894558	
Gm17641	predicted gene, 17641	-9.56018945	
Olfr290	olfactory receptor 290	-9.599562274	
Gm39318	predicted gene, 39318	-9.738305199	
Gm13480	predicted gene 13480	-9.783984767	
1810012K08Rik	RIKEN cDNA 1810012K08 gene	-9.845742462	
Gm22516	predicted gene, 22516	-9.869009019	
Gm37857	predicted gene, 37857	-9.927163368	
Gm43937	predicted gene, 43937	-9.966782853	
Serpina4-ps1	serine (or cysteine) peptidase inhibitor, clade A, member 4, pseudogene 1	-9.988393857	
4933428G20Rik	RIKEN cDNA 4933428G20 gene	-10.09018603	
Gm48284	predicted gene, 48284	-10.26718994	
Olfr790	olfactory receptor 790	-10.29364482	
Gm26796	predicted gene, 26796	-10.45526607	
Gm14524	predicted gene 14524	-10.48149851	
Olfr12	olfactory receptor 12	-10.6854035	
Gm47072	predicted gene, 47072	-10.9970362	
Gm47388	predicted gene, 47388	-11.26438426	
Olfr1446	olfactory receptor 1446	-11.31758426	
Gm27194	predicted gene 27194	-11.36274125	
Gm45222	predicted gene 45222	-11.40962443	
AC118475.1	predicted gene, 49496	-11.42126069	
Gm16185	predicted gene 16185	-11.49141842	
4930500M09Rik	RIKEN cDNA 4930500M09 gene	-11.81775684	
Gm43910	predicted gene, 43910	-12.07109631	
Cel	carboxyl ester lipase	-12.07639951	
Gm17494	predicted gene, 17494	-12.09874696	
Dspp	dentin sialophosphoprotein	-12.29546528	
Gm37868	predicted gene, 37868	-12.3881671	
Gm14372	predicted gene 14372	-12.42499917	
Boll	boule homolog, RNA binding protein	-12.47938103	
Gm39214	predicted gene, 39214	-12.52523075	
Gm47544	predicted gene, 47544	-12.55756113	

Mup20	major urinary protein 20	-12.68423393	
Gm13554	predicted gene 13554	-12.77734442	
Gm47959	predicted gene, 47959	-12.94538011	
Gm48678	predicted gene, 48678	-12.94958846	
1700022I11Rik	RIKEN cDNA 1700022I11 gene	-12.96236299	
A230020J21Rik	RIKEN cDNA A230020J21 gene	-13.05477765	
Gm29200	predicted gene 29200	-13.32922395	
Gm29609	predicted gene 29609	-13.37822498	
Gm44749	predicted gene 44749	-13.46261024	
Amy2b	amylase 2b	-13.46946064	
Gm6409	predicted gene 6409	-13.50721632	
Gm37562	predicted gene, 37562	-13.93221267	
Gm34397	predicted gene, 34397	-13.99882359	
1810008B01Rik	RIKEN cDNA 1810008B01 gene	-14.21404494	
Olfr1280	olfactory receptor 1280	-14.24369399	
Gm20687	predicted gene 20687	-14.57590829	
4931406B18Rik	RIKEN cDNA 4931406B18 gene	-14.65222979	
Vmn2r110	vomeronasal 2, receptor 110	-14.72417464	
Gm38000	predicted gene, 38000	-14.77819513	
Igkv14-130	immunoglobulin kappa variable 14-130	-14.97691467	
Tssk3	testis-specific serine kinase 3	-15.00817653	
Gadl1	glutamate decarboxylase-like 1	-15.18345337	
Hsd3b5	hydroxy-delta-5-steroid dehydrogenase, 3 beta- and steroid delta-isomerase 5	-15.26443611	
Ighv1-31	immunoglobulin heavy variable 1-31	-15.4540012	
A230059L01Rik	RIKEN cDNA A230059L01 gene	-15.47497279	
Gm14912	predicted gene 14912	-15.5285455	
Gm14812	predicted gene 14812	-15.53020675	
Gm37284	predicted gene, 37284	-15.55427259	
Gm47027	predicted gene, 47027	-15.55427259	
Gm45352	predicted gene 45352	-15.56461435	
Gm24388		-15.57466962	
Gm42837	predicted gene 42837	-15.60658982	
Gm17080	predicted gene 17080	-15.6329507	
Prokr2	prokineticin receptor 2	-15.74602258	
Gm20756	predicted gene, 20756	-15.80976506	
Gm28956	predicted gene 28956	-15.82744304	
Gm44937	predicted gene 44937	-16.04443218	
9930120I10Rik	RIKEN cDNA 9930120I10 gene	-16.08635337	

Olfr64	olfactory receptor 64	-16.14204985	
Gm50205	predicted gene, 50205	-16.3076891	
AC129537.1	predicted gene, 32764	-16.61744323	
B430305J03Rik	RIKEN cDNA B430305J03 gene	-16.62880911	
Gm44123	predicted gene, 44123	-16.659394	
Gm28539	predicted gene 28539	-16.68351115	
Vmn2r63	vomeronasal 2, receptor 63	-16.81616093	
Olfr1066	olfactory receptor 1066	-16.86694867	
Gm32736	predicted gene, 32736	-16.86849719	
Gm44369	predicted gene, 44369	-16.87164877	
Serpina16	serine (or cysteine) peptidase inhibitor, clade A (alpha-1 antiproteinase, antitrypsin), member 16	-16.88122739	
Olfr283	olfactory receptor 283	-16.9234606	
Gm26550	predicted gene, 26550	-17.0537976	
Gm44103	predicted gene, 44103	-17.11712948	
Elovl3	elongation of very long chain fatty acids (FEN1/Elo2, SUR4/Elo3, yeast)-like 3	-17.46273479	
Olfr1258	olfactory receptor 1258	-17.56067576	
Gm28449	predicted gene 28449	-17.67229496	
Gm42416	predicted gene, 37013	-17.85376131	
Gm50443	predicted gene, 50443	-17.91946161	
Gm16216	predicted gene 16216	-17.94726716	
Mup7	major urinary protein 7	-17.99159254	
Maats1os	MYCBP-associated, testis expressed 1, opposite strand	-18.06231771	
Defa21	defensin, alpha, 21	-18.1847859	
Gm27178	predicted gene 27178	-18.18814021	
Kiss1	KiSS-1 metastasis-suppressor	-18.20725239	
Gm17163	predicted gene 17163	-18.41672072	
Gucy2e	guanylate cyclase 2e	-18.70451006	
Gm14233	predicted gene 14233	-18.90690675	
Gp2	glycoprotein 2 (zymogen granule membrane)	-19.39325009	
Slc22a2	solute carrier family 22 (organic cation transporter), member 2	-19.74970214	
Gm20671	predicted gene 20671	-20.243264	
Gm37939	predicted gene, 37939	-20.25796949	
Gm12147	predicted gene 12147	-20.46515146	
Gm37443	predicted gene, 37443	-20.65152131	
Gm16130	predicted gene 16130	-20.73130817	
4930555B11Rik	RIKEN cDNA 4930555B11 gene	-20.81236465	
Gm43164	predicted gene 43164	-20.87084606	

1700095J03Rik	RIKEN cDNA 1700095J03 gene	-21.13705328	
Krtap20-2	keratin associated protein 20-2	-22.19984947	
Gm27427		-22.20178007	
Cyp4a12b	cytochrome P450, family 4, subfamily a, polypeptide 12B	-22.35637405	
Gm13999	predicted gene 13999	-22.38731224	
Amy2a1	amylase 2a1	-22.72145531	
4930555F03Rik	RIKEN cDNA 4930555F03 gene	-23.02868729	
AC134869.1	predicted gene, 49354	-23.14387055	
Mrgpra18-ps	MAS-related GPR, member A18, pseudogene	-23.48039132	
Olfr1284	olfactory receptor 1284	-23.75801431	
Zic4	zinc finger protein of the cerebellum 4	-23.82641515	
Gm44924	predicted gene 44924	-23.84018363	
Tmed11	transmembrane p24 trafficking protein 11	-24.32530024	
Erp27	endoplasmic reticulum protein 27	-24.35366484	
Gm7271	predicted gene 7271	-24.42027261	
Gm25473		-24.78177213	
Psg19	pregnancy specific glycoprotein 19	-24.86760389	
Gm44356		-25.11528012	
Calhm1	calcium homeostasis modulator 1	-25.19411663	
Gm35040	predicted gene, 35040	-25.25539218	
Gm15444	predicted gene 15444	-25.54498692	
AC107792.1		-26.01498056	
Olfr988	olfactory receptor 988	-26.10928838	
4921514A10Rik	RIKEN cDNA 4921514A10 gene	-26.48466082	
Gm30191	predicted gene, 30191	-26.67069782	
Gm14164	predicted gene 14164	-26.86040348	
A230009B12Rik	RIKEN cDNA A230009B12 gene	-27.2942082	
1700102F20Rik	RIKEN cDNA 1700102F20 gene	-27.97820263	
Hoxd13	homeobox D13	-28.11225518	
Atp5o	ATP synthase, H+ transporting, mitochondrial F1 complex, O subunit	-28.39746151	
Gm30363	predicted gene, 30363	-28.5076816	
Gm8176	predicted gene 8176	-28.73497623	
BC055402	cDNA sequence BC055402	-28.82572255	
Gm48901	predicted gene, 48901	-29.27217364	
Gm26473	predicted gene, 26473	-29.81756785	
Gm37419	predicted gene, 37419	-30.2343539	
Nphs1	nephrosis 1, nephrin	-30.57234876	
Gm37067	predicted gene, 37067	-31.2795416	

Gm45579	predicted gene 45579	-32.0039578	
Igdcc3	immunoglobulin superfamily, DCC subclass, member 3	-32.07638341	
Amy2a4	amylase 2a4	-33.14309825	
Reg2	regenerating islet-derived 2	-33.4267966	
Vmn2r70	vomeronasal 2, receptor 70	-33.63288664	
Gm48707	predicted gene, 48707	-33.9146692	
AC152453.1	predicted gene, 49358	-34.08998358	
Il24	interleukin 24	-34.14707982	
Mup-ps19	major urinary protein, pseudogene 19	-34.71617036	
Amy2a3	amylase 2a3	-34.77854789	
Fam221b	family with sequence similarity 221, member B	-34.92540636	
Amy2	amylase 2a5	-35.16797725	
Vmn1r185	vomeronasal 1 receptor 185	-35.19973743	
Reg3d	regenerating islet-derived 3 delta	-35.30307765	
Amy2a2	amylase 2a2	-35.60975479	
Gm44148	predicted gene, 44148	-36.11879713	
Gm49805	predicted gene, 49805	-36.73619962	
Olfr1204	olfactory receptor 1204	-36.73892889	
Gm42936	predicted gene 42936	-37.70861154	
Olfr653	olfactory receptor 653	-37.84536482	
Gm49750	predicted gene, 49750	-38.16841677	
5330416C01Rik	RIKEN cDNA 5330416C01 gene	-38.17105195	
Gm44341		-38.81531742	
Gm48094	predicted gene, 48094	-39.12164942	
Olfr1402	olfactory receptor 1402	-39.27592562	
AC140465.1	predicted gene 6332	-39.3266134	
Gm26412		-39.57109661	
Gm11693	predicted gene 11693	-40.64912205	
mt-Ts1	mitochondrially encoded tRNA serine 1	-40.73296459	
Gm50221	predicted gene, 50221	-41.29246081	
Gm43942	predicted gene, 43942	-41.52331815	
Gm46328	predicted gene, 46328	-42.16255503	
1700015F17Rik	PTTG1IP family member 2	-42.19532155	
Try5	trypsin 5	-42.26799528	
Gm44505	predicted readthrough transcript (NMD candidate), 44505	-42.64407267	
4930544I03Rik	RIKEN cDNA 4930544I03 gene	-44.56019235	
Gm6602	predicted gene 6602	-46.21215638	
D030018L15Rik	nuclear receptor coactivator 2 pseudogene	-47.05443328	
Gm16041	predicted gene 16041	-47.3109696	

Gm50092	predicted gene, 50092	-47.72916954	
Gm35808	predicted gene, 35808	-49.10700613	
AC157572.1	predicted gene, 49256	-49.66613531	
Olfr30	olfactory receptor 30	-49.89830058	
Gm47398	predicted gene, 47398	-50.41136551	
CT010467.1		-51.03872454	
Gm42650	predicted gene 42650	-51.25440194	
Gm13733	predicted gene 13733	-52.96912117	
Ifna7	interferon alpha 7	-56.56642881	
Gm15840	predicted gene 15840	-59.35511445	
Gm14651	predicted gene 14651	-60.50939827	
4930550C17Rik	RIKEN cDNA 4930550C17 gene	-61.40663887	
Mir151	microRNA 151	-61.87981893	
Gm29434	predicted gene 29434	-64.53849291	
Olfr643	olfactory receptor 643	-71.61691491	
Zfp935	zinc finger protein 935	-73.47204755	
Olfr1256	olfactory receptor 1256	-73.70108942	
1810018F18Rik	RIKEN cDNA 1810018F18 gene	-77.09716301	
Mir705	microRNA 705	-77.48495327	
Olfr1342	olfactory receptor 1342	-77.77857456	
Cabp2	calcium binding protein 2	-79.20806465	
Gm12124	predicted gene 12124	-82.60120521	
Gm22094		-84.39038977	
Gm15154	predicted gene 15154	-84.44426228	
Vmn1r191	vomeronasal 1 receptor 191	-85.559475	
Gm47854	predicted gene, 47854	-98.06092031	
Gm43701	predicted gene 43701	-104.1158195	
Aqp12	aquaporin 12	-109.7530169	
2210010C04Rik	RIKEN cDNA 2210010C04 gene	-116.1350488	
Gm12713	predicted gene 12713	-134.8170138	
AC139579.1		-139.4072038	
Gm27694		-145.100444	
1700061E18Rik	RIKEN cDNA 1700061E18 gene	-159.6717123	
Cpb1	carboxypeptidase B1 (tissue)	-210.2393333	
Gm12697	predicted gene 12697	-238.2960039	
Gm43738	predicted gene 43738	-238.3565507	
Cuzd1	CUB and zona pellucida-like domains 1	-246.0035901	
Ctrc	chymotrypsin C (caldecrin)	-293.942233	
Ctrl	chymotrypsin-like	-297.8760787	

Gm28006		-401.2769604	
Cela3a	chymotrypsin-like elastase family, member 3A	-415.8087665	
Cpa2	carboxypeptidase A2, pancreatic	-448.0966941	
Cela2a	chymotrypsin-like elastase family, member 2A	-533.6650046	
Pnlip	pancreatic lipase	-758.8556685	
Prss2	protease, serine 2	-841.6015881	
AC122546.1		-960.8824044	
Ctrb1	chymotrypsinogen B1	-1213.858884	
Cela3b	chymotrypsin-like elastase family, member 3B	-1866.90537	
Cpa1	carboxypeptidase A1, pancreatic	-4226.907133	

REFERENCES

1. Escherich, T. (1988). The intestinal bacteria of the neonate and breast-fed infant. 1884. *Rev Infect Dis*, *10*(6), 1220-1225.
2. Zimmer, C. (2012). *Microcosm: E-coli and the New Science of Life*. Random House.
3. Licitra, G. (2013). Etymologia: *Staphylococcus*. *Emerg Infect Dis.*, *19*(9), 1553.
4. Classics in infectious diseases. "On abscesses". Alexander Ogston (1844-1929). (1984). *Rev Infect Dis*, *6*(1), 122-128.
5. Goodwin CS, AJ, Chilvers T, Peters M, Collins MD, Sly L, McConnell W, Harper WES. (1989). Transfer of *Campylobacter pyloridis* and *Campylobacter mustelae* to *Helicobacter* gen. nov. as *Helicobacter pylori* comb. nov. and *Helicobacter mustelae* comb. nov., respectively. *International Journal of Systematic Bacteriology*(39), 397-405.
6. Blaser, MJ. (2005). An endangered species in the stomach. *Sci Am*, *292*(2), 38-45.
7. Konturek, JW. (2003). Discovery by Jaworski of *Helicobacter pylori* and its pathogenetic role in peptic ulcer, gastritis and gastric cancer. *J Physiol Pharmacol*, *54 Suppl 3*, 23-41.
8. Jaworski, W. (1899). Podrêcznik Chorób Zoladka (Handbook of Gastric Diseases). *Wydawnictwa Dziel Lekarskich Polskich: Krakow, Poland*, 30-47.
9. Doenges, JL. (1939). Spirochetes in the gastric glands of macacus rhesus and of man without related diseases. *Arch Pathol*, *27*, 469-477.
10. Freedberg A.S., BLE. (1940). The presence of spirochetes in human gastric mucosa. *Am. J. Dig. Dis.*, *7*, 443-445.
11. Palmer, ED. (1954). Investigation of the gastric mucosa spirochetes of the human. *Gastroenterology*, *27*(2), 218-220.
12. Warren, JR, & Marshall, B. (1983). Unidentified curved bacilli on gastric epithelium in active chronic gastritis. *Lancet*, *1*(8336), 1273-1275.
13. Marshall BJ, RH, Annear DI, Goodwin CS, Pearman J, Warren JR,, & J., A. (1984). Original isolation of *Campylobacter pyloridis* from human gastric mucosa. *Microbios Letters*(25), 83-88.
14. Achievement, AAo. (1998, May 23, 1998). *The Courage to Experiment: Interview with Barry Marshall* [Interview]. American Academy of Achievement.
15. Marshall, B. (2008). *Helicobacter pylori*--a Nobel pursuit? *Can J Gastroenterol*, *22*(11), 895-896.
16. Marshall, B, & Azad, M. (2014). Q&A: Barry Marshall. A bold experiment. *Nature*, *514*(7522), S6-7.
17. Marshall, BJ, J. A. Armstrong, D. B. McGechie, and R. J. Glancy. (1985). Attempt to fulfil Koch's postulates for pyloric *Campylobacter*. *Med J Aust*(142), 436-439.
18. Marshall, BJ, C. S. Goodwin, J. R. Warren, R. Murray, E. D. Blincow, S. J., & Blackbourn, MP, T. E. Waters, and C. R. Sanderson. (1988). Prospective double-blind trial of duodenal ulcer relapse after eradication of *Campylobacter pylori*. *Lancet*, *2*, 1437-1442.
19. Campylobacter pylori becomes *Helicobacter pylori*. (1989). *Lancet*, *2*(8670), 1019-1020.
20. Rauws, EA, & Tytgat, GN. (1990). Cure of duodenal ulcer associated with eradication of *Helicobacter pylori*. *Lancet*, *335*(8700), 1233-1235.
21. Suerbaum, S, & Josenhans, C. (2007). *Helicobacter pylori* evolution and phenotypic diversification in a changing host. *Nat Rev Microbiol*, *5*(6), 441-452.

22. Hooi, JKY, et al. (2017). Global Prevalence of *Helicobacter pylori* Infection: Systematic Review and Meta-Analysis. *Gastroenterology*, *153*(2), 420-429.
23. Falush, D, et al. (2003). Traces of human migrations in *Helicobacter pylori* populations. *Science*, *299*(5612), 1582-1585.
24. Moodley, Y, & Linz, B. (2009). *Helicobacter pylori* Sequences Reflect Past Human Migrations. *Genome Dyn*, *6*, 62-74.
25. Moodley, Y, et al. (2009). The peopling of the Pacific from a bacterial perspective. *Science*, *323*(5913), 527-530.
26. Wirth, T, et al. (2004). Distinguishing human ethnic groups by means of sequences from *Helicobacter pylori*: lessons from Ladakh. *Proc Natl Acad Sci U S A*, *101*(14), 4746-4751.
27. Maixner, F, et al. (2016). The 5300-year-old *Helicobacter pylori* genome of the Iceman. *Science*, *351*(6269), 162-165.
28. Lehours, P, & Yilmaz, O. (2007). Epidemiology of *Helicobacter pylori* infection. *Helicobacter*, *12 Suppl 1*, 1-3.
29. Malaty, HM, & Graham, DY. (1994). Importance of childhood socioeconomic status on the current prevalence of *Helicobacter pylori* infection. *Gut*, *35*(6), 742-745.
30. Yokota, S, et al. (2015). Intrafamilial, Preferentially Mother-to-Child and Intraspousal, *Helicobacter pylori* Infection in Japan Determined by Mutilocus Sequence Typing and Random Amplified Polymorphic DNA Fingerprinting. *Helicobacter*, *20*(5), 334-342.
31. Bruce, MG, & Maaroos, HI. (2008). Epidemiology of *Helicobacter pylori* infection. *Helicobacter*, *13 Suppl 1*, 1-6.
32. Peek, RM, Jr., & Blaser, MJ. (2002). *Helicobacter pylori* and gastrointestinal tract adenocarcinomas. *Nature Rev Cancer*, *2*(1), 28-37.
33. Peek, RM, Jr., & Crabtree, JE. (2006). *Helicobacter* infection and gastric neoplasia. *J Pathol*, *208*(2), 233-248.
34. Peterson, WL. (1991). *Helicobacter pylori* and peptic ulcer disease. *N Engl J Med*, *324*(15), 1043-1048.
35. Wroblewski, LE, et al. (2010). *Helicobacter pylori* and gastric cancer: factors that modulate disease risk. *Clin Microbiol Rev*, *23*(4), 713-739.
36. Kawanishi, S, et al. (2017). Crosstalk between DNA Damage and Inflammation in the Multiple Steps of Carcinogenesis. *Int J Mol Sci*, *18*(8).
37. Sung, H, et al. (2021). Global Cancer Statistics 2020: GLOBOCAN Estimates of Incidence and Mortality Worldwide for 36 Cancers in 185 Countries. *CA Cancer J Clin*, *71*(3), 209-249.
38. Kawahara, T, et al. (2001). Type I *Helicobacter pylori* lipopolysaccharide stimulates toll-like receptor 4 and activates mitogen oxidase 1 in gastric pit cells. *Infect Immun*, *69*(7), 4382-4389.
39. Mandell, L, et al. (2004). Intact gram-negative *Helicobacter pylori*, *Helicobacter felis*, and *Helicobacter hepaticus* bacteria activate innate immunity via toll-like receptor 2 but not toll-like receptor 4. *Infect Immun*, *72*(11), 6446-6454.
40. Smith, MF, Jr., et al. (2003). Toll-like receptor (TLR) 2 and TLR5, but not TLR4, are required for *Helicobacter pylori*-induced NF-kappa B activation and chemokine expression by epithelial cells. *J Biol Chem*, *278*(35), 32552-32560.
41. Lee, A, & Buck, F. (1996). Vaccination and mucosal responses to *Helicobacter pylori* infection. *Aliment Pharmacol Ther*, *10 Suppl 1*, 129-138.

42. D'Elios, MM, et al. (1997). T helper 1 effector cells specific for *Helicobacter pylori* in the gastric antrum of patients with peptic ulcer disease. *J Immunol*, *158*(2), 962-967.
43. Bimczok, D, et al. (2010). Human primary gastric dendritic cells induce a Th1 response to *H. pylori*. *Mucosal Immunol*, *3*(3), 260-269.
44. Eaton, KA, et al. (2001). The role of T cell subsets and cytokines in the pathogenesis of *Helicobacter pylori* gastritis in mice. *J Immunol*, *166*(12), 7456-7461.
45. Rolig, AS, et al. (2011). Bacterial chemotaxis modulates host cell apoptosis to establish a T-helper cell, type 17 (Th17)-dominant immune response in *Helicobacter pylori* infection. *Proc Natl Acad Sci U S A*, *108*(49), 19749-19754.
46. Zhuang, Y, et al. (2011). *Helicobacter pylori*-infected macrophages induce Th17 cell differentiation. *Immunobiology*, *216*(1-2), 200-207.
47. Castano-Rodriguez, N, et al. (2014). Pattern-recognition receptors and gastric cancer. *Front Immunol*, *5*, 336.
48. Horvath, DJ, Jr., et al. (2012). IL-23 Contributes to Control of Chronic *Helicobacter pylori* Infection and the Development of T Helper Responses in a Mouse Model. *Front Immunol*, *3*, 56.
49. Robinson, K, et al. (2007). The inflammatory and immune response to *Helicobacter pylori* infection. *Best Pract Res Clin Gastroenterol*, *21*(2), 237-259.
50. Atherton, JC. (2006). The pathogenesis of *Helicobacter pylori*-induced gastro-duodenal diseases. *Annu Rev Pathol*, *1*, 63-96.
51. Amieva, M, & Peek, RM, Jr. (2015). Pathobiology of *Helicobacter pylori*-induced Gastric Cancer. *Gastroenterology*.
52. Polk, DB, & Peek, RM, Jr. *Helicobacter pylori*: gastric cancer and beyond. *Nat Rev Cancer*, *10*(6), 403-414.
53. Gagnaire, A, et al. (2017). Collateral damage: insights into bacterial mechanisms that predispose host cells to cancer. *Nat Rev Microbiol*, *15*(2), 109-128.
54. Schistosomes, liver flukes and *Helicobacter pylori*. IARC Working Group on the Evaluation of Carcinogenic Risks to Humans. Lyon, 7-14 June 1994. (1994). *IARC Monogr Eval Carcinog Risks Hum*, *61*, 1-241.
55. Lauren, P. (1965). The Two Histological Main Types of Gastric Carcinoma: Diffuse and So-Called Intestinal-Type Carcinoma. An Attempt at a Histo-Clinical Classification. *Acta Pathol Microbiol Scand*, *64*, 31-49.
56. Plummer, M, et al. (2015). Global burden of gastric cancer attributable to *Helicobacter pylori*. *Int J Cancer*, *136*(2), 487-490.
57. Colquhoun, A, et al. (2015). Global patterns of cardia and non-cardia gastric cancer incidence in 2012. *Gut*, *64*(12), 1881-1888.
58. Sipponen, P, & Marshall, BJ. (2000). Gastritis and gastric cancer. Western countries. *Gastroenterol Clin North Am*, *29*(3), 579-592, v-vi.
59. Correa, P, et al. (1975). A model for gastric cancer epidemiology. *Lancet*, *2*(7924), 58-60.
60. Hu, B, et al. (2012). Gastric cancer: Classification, histology and application of molecular pathology. *J Gastrointest Oncol*, *3*(3), 251-261.
61. Malaty, HM, et al. (2002). Age at acquisition of *Helicobacter pylori* infection: a follow-up study from infancy to adulthood. *Lancet*, *359*(9310), 931-935.

62. Lee, YC, et al. (2016). Association Between *Helicobacter pylori* Eradication and Gastric Cancer Incidence: A Systematic Review and Meta-analysis. *Gastroenterology*, *150*(5), 1113-1124 e1115.
63. Amieva, M, & Peek, RM, Jr. (2016). Pathobiology of *Helicobacter pylori*-Induced Gastric Cancer. *Gastroenterology*, *150*(1), 64-78.
64. Castano-Rodriguez, N, et al. (2014). Genetic polymorphisms in the Toll-like receptor signalling pathway in *Helicobacter pylori* infection and related gastric cancer. *Hum Immunol*, *75*(8), 808-815.
65. Yaghoobi, M, et al. (2010). Family history and the risk of gastric cancer. *Br J Cancer*, *102*(2), 237-242.
66. Tay, SW, et al. (2021). Diet and cancer of the esophagus and stomach. *Curr Opin Gastroenterol*, *37*(2), 158-163.
67. Reibman, J, et al. (2008). Asthma is inversely associated with *Helicobacter pylori* status in an urban population. *PLoS One*, *3*(12), e4060.
68. Chen, Y, & Blaser, MJ. (2008). *Helicobacter pylori* colonization is inversely associated with childhood asthma. *J Infect Dis*, *198*(4), 553-560.
69. Blaser, MJ, et al. (2008). Does *Helicobacter pylori* protect against asthma and allergy? *Gut*, *57*(5), 561-567.
70. Chen, Y, & Blaser, MJ. (2007). Inverse associations of *Helicobacter pylori* with asthma and allergy. *Arch Intern Med*, *167*(8), 821-827.
71. Chow, WH, et al. (1998). An inverse relation between *cagA*+ strains of *Helicobacter pylori* infection and risk of esophageal and gastric cardia adenocarcinoma. *Cancer Res*, *58*(4), 588-590.
72. de Martel, C, et al. (2005). *Helicobacter pylori* infection and the risk of development of esophageal adenocarcinoma. *J Infect Dis*, *191*(5), 761-767.
73. Loffeld, RJ, et al. (2000). Colonization with *cagA*-positive *Helicobacter pylori* strains inversely associated with reflux esophagitis and Barrett's esophagus. *Digestion*, *62*(2-3), 95-99.
74. Vaezi, MF, et al. (2000). CagA-positive strains of *Helicobacter pylori* may protect against Barrett's esophagus. *Am J Gastroenterol*, *95*(9), 2206-2211.
75. Vicari, JJ, et al. (1998). The seroprevalence of *cagA*-positive *Helicobacter pylori* strains in the spectrum of gastroesophageal reflux disease. *Gastroenterology*, *115*(1), 50-57.
76. Luther, J, et al. (2011). *Helicobacter pylori* DNA decreases pro-inflammatory cytokine production by dendritic cells and attenuates dextran sodium sulphate-induced colitis. *Gut*, *60*(11), 1479-1486.
77. Owyang, SY, et al. (2012). *Helicobacter pylori* DNA's anti-inflammatory effect on experimental colitis. *Gut Microbes*, *3*(2), 168-171.
78. de Sablet, T, et al. (2011). Phylogeographic origin of *Helicobacter pylori* is a determinant of gastric cancer risk. *Gut*, *60*(9), 1189-1195.
79. Salama, N, et al. (2000). A whole-genome microarray reveals genetic diversity among *Helicobacter pylori* strains. *Proc Natl Acad Sci U S A*, *97*(26), 14668-14673.
80. Blaser, MJ, & Berg, DE. (2001). *Helicobacter pylori* genetic diversity and risk of human disease. *J Clin Invest*, *107*(7), 767-773.
81. Israel, DA, et al. (2001). *Helicobacter pylori* genetic diversity within the gastric niche of a single human host. *Proc Natl Acad Sci U S A*, *98*(25), 14625-14630.

82. McClain, MS, et al. (2009). Genome sequence analysis of *Helicobacter pylori* strains associated with gastric ulceration and gastric cancer. *BMC Genomics*, *10*, 3.
83. Linz, B, et al. (2007). An African origin for the intimate association between humans and *Helicobacter pylori*. *Nature*, *445*(7130), 915-918.
84. Ghose, C, et al. (2002). East Asian genotypes of *Helicobacter pylori* strains in Amerindians provide evidence for its ancient human carriage. *Proc Natl Acad Sci U S A*, *99*(23), 15107-15111.
85. Gressmann, H, et al. (2005). Gain and loss of multiple genes during the evolution of *Helicobacter pylori*. *PLoS Genet*, *1*(4), e43.
86. Tomb, JF, et al. (1997). The complete genome sequence of the gastric pathogen *Helicobacter pylori*. *Nature*, *388*(6642), 539-547.
87. Akopyants, NS, et al. (1998). Analyses of the *cag* pathogenicity island of *Helicobacter pylori*. *Mol Microbiol*, *28*(1), 37-53.
88. Alm, RA, et al. (1999). Genomic-sequence comparison of two unrelated isolates of the human gastric pathogen *Helicobacter pylori*. *Nature*, *397*(6715), 176-180.
89. Censini, S, et al. (1996). *cag*, a pathogenicity island of *Helicobacter pylori*, encodes type I-specific and disease-associated virulence factors. *Proc Natl Acad Sci U S A*, *93*(25), 14648-14653.
90. Blaser, MJ, et al. (1995). Infection with *Helicobacter pylori* strains possessing *cagA* is associated with an increased risk of developing adenocarcinoma of the stomach. *Cancer Res*, *55*(10), 2111-2115.
91. Kuipers, EJ, et al. (1995). *Helicobacter pylori* and atrophic gastritis: importance of the *cagA* status. *J Natl Cancer Inst*, *87*(23), 1777-1780.
92. Cover, TL, et al. (1990). Characterization of and human serologic response to proteins in *Helicobacter pylori* broth culture supernatants with vacuolizing cytotoxin activity. *Infect Immun*, *58*(3), 603-610.
93. Crabtree, JE, et al. (1991). Mucosal IgA recognition of *Helicobacter pylori* 120 kDa protein, peptic ulceration, and gastric pathology. *Lancet*, *338*(8763), 332-335.
94. Crabtree, JE, et al. (1993). Systemic and mucosal humoral responses to *Helicobacter pylori* in gastric cancer. *Gut*, *34*(10), 1339-1343.
95. Parsonnet, J, et al. (1997). Risk for gastric cancer in people with CagA positive or CagA negative *Helicobacter pylori* infection. *Gut*, *40*(3), 297-301.
96. Peek, RM, Jr., et al. (1995). Detection of *Helicobacter pylori* gene expression in human gastric mucosa. *J Clin Microbiol*, *33*(1), 28-32.
97. Peek, RM, Jr., et al. (1995). Heightened inflammatory response and cytokine expression *in vivo* to *cagA+ Helicobacter pylori* strains. *Lab Invest*, *73*(6), 760-770.
98. Queiroz, DM, et al. (1998). *cagA*-positive *Helicobacter pylori* and risk for developing gastric carcinoma in Brazil. *Int J Cancer*, *78*(2), 135-139.
99. Rudi, J, et al. (1997). Serum antibodies against *Helicobacter pylori* proteins VacA and CagA are associated with increased risk for gastric adenocarcinoma. *Dig Dis Sci*, *42*(8), 1652-1659.
100. Shimoyama, T, et al. (1998). CagA seropositivity associated with development of gastric cancer in a Japanese population. *J Clin Pathol*, *51*(3), 225-228.
101. Torres, J, et al. (1998). Infection with CagA+ *Helicobacter pylori* strains as a possible predictor of risk in the development of gastric adenocarcinoma in Mexico. *Int J Cancer*, *78*(3), 298-300.

102. Vorobjova, T, et al. (1998). CagA protein seropositivity in a random sample of adult population and gastric cancer patients in Estonia. *Eur J Gastroenterol Hepatol*, *10*(1), 41-46.
103. Covacci, A, et al. (1999). *Helicobacter pylori* virulence and genetic geography. *Science*, *284*(5418), 1328-1333.
104. Segal, ED, et al. (1999). Altered states: involvement of phosphorylated CagA in the induction of host cellular growth changes by *Helicobacter pylori*. *Proc Natl Acad Sci U S A*, *96*(25), 14559-14564.
105. Stein, M, et al. (2000). Tyrosine phosphorylation of the *Helicobacter pylori* CagA antigen after *cag*-driven host cell translocation. *Proc Natl Acad Sci U S A*, *97*(3), 1263-1268.
106. Odenbreit, S, et al. (2000). Translocation of *Helicobacter pylori* CagA into gastric epithelial cells by type IV secretion. *Science*, *287*(5457), 1497-1500.
107. Asahi, M, et al. (2000). *Helicobacter pylori* CagA protein can be tyrosine phosphorylated in gastric epithelial cells. *J Exp Med*, *191*(4), 593-602.
108. Backert, S, et al. (2000). Translocation of the *Helicobacter pylori* CagA protein in gastric epithelial cells by a type IV secretion apparatus. *Cell Microbiol*, *2*(2), 155-164.
109. Viala, J, et al. (2004). Nod1 responds to peptidoglycan delivered by the *Helicobacter pylori cag* pathogenicity island. *Nat Immunol*, *5*(11), 1166-1174.
110. Boughan, PK, et al. (2006). Nucleotide-binding oligomerization domain-1 and epidermal growth factor receptor: critical regulators of beta-defensins during *Helicobacter pylori* infection. *J Biol Chem*, *281*(17), 11637-11648.
111. Ferrero, RL. (2005). Innate immune recognition of the extracellular mucosal pathogen, *Helicobacter pylori*. *Mol Immunol*, *42*(8), 879-885.
112. Eberl, G, & Boneca, IG. (2010). Bacteria and MAMP-induced morphogenesis of the immune system. *Curr Opin Immunol*, *22*(4), 448-454.
113. Strober, W, et al. (2006). Signalling pathways and molecular interactions of NOD1 and NOD2. *Nat Rev Immunol*, *6*(1), 9-20.
114. Gall, A, et al. (2017). TIFA Signaling in Gastric Epithelial Cells Initiates the *cag* Type 4 Secretion System-Dependent Innate Immune Response to *Helicobacter pylori* Infection. *MBio*, *8*(4).
115. Stein, SC, et al. (2017). *Helicobacter pylori* modulates host cell responses by CagT4SS-dependent translocation of an intermediate metabolite of LPS inner core heptose biosynthesis. *PLoS Pathog*, *13*(7), e1006514.
116. Zimmermann, S, et al. (2017). ALPK1- and TIFA-Dependent Innate Immune Response Triggered by the *Helicobacter pylori* Type IV Secretion System. *Cell Rep*, *20*(10), 2384-2395.
117. Varga, MG, et al. (2016). Pathogenic *Helicobacter pylori* strains translocate DNA and activate TLR9 via the cancer-associated *cag* type IV secretion system. *Oncogene*, *35*(48), 6262-6269.
118. Varga, MG, & Peek, RM. (2017). DNA Transfer and Toll-like Receptor Modulation by *Helicobacter pylori*. *Curr Top Microbiol Immunol*, *400*, 169-193.
119. Varga, MG, et al. (2016). TLR9 activation suppresses inflammation in response to *Helicobacter pylori* infection. *Am J Physiol Gastrointest Liver Physiol*, *311*(5), G852-G858.

120. Camorlinga-Ponce, M, et al. (2004). Topographical localisation of *cagA* positive and *cagA* negative *Helicobacter pylori* strains in the gastric mucosa; an *in situ* hybridisation study. *J Clin Pathol*, *57*(8), 822-828.
121. Backert, S, et al. (2017). The *Helicobacter pylori* Type IV Secretion System Encoded by the *cag* Pathogenicity Island: Architecture, Function, and Signaling. *Curr Top Microbiol Immunol*, *413*, 187-220.
122. Fischer, W. (2011). Assembly and molecular mode of action of the *Helicobacter pylori* Cag type IV secretion apparatus. *FEBS J*, *278*(8), 1203-1212.
123. Frick-Cheng, AE, et al. (2016). Molecular and Structural Analysis of the *Helicobacter pylori cag* Type IV Secretion System Core Complex. *MBio*, *7*(1), e02001-02015.
124. Chandran, V, et al. (2009). Structure of the outer membrane complex of a type IV secretion system. *Nature*, *462*(7276), 1011-1015.
125. Fronzes, R, et al. (2009). Structure of a type IV secretion system core complex. *Science*, *323*(5911), 266-268.
126. Christie, PJ, & Cascales, E. (2005). Structural and dynamic properties of bacterial type IV secretion systems (review). *Mol Membr Biol*, *22*(1-2), 51-61.
127. Tanaka, J, et al. (2003). Structural definition on the surface of *Helicobacter pylori* type IV secretion apparatus. *Cell Microbiol*, *5*(6), 395-404.
128. Kwok, T, et al. (2007). *Helicobacter* exploits integrin for type IV secretion and kinase activation. *Nature*, *449*(7164), 862-866.
129. Haley, KP, et al. (2014). High resolution electron microscopy of the *Helicobacter pylori* Cag type IV secretion system pili produced in varying conditions of iron availability. *J Vis Exp*(93), e52122.
130. Noto, JM, et al. (2013). Iron deficiency accelerates *Helicobacter pylori*-induced carcinogenesis in rodents and humans. *J Clin Invest*, *123*(1), 479-492.
131. Gaddy, JA, et al. (2014). The host protein calprotectin modulates the *Helicobacter pylori cag* type IV secretion system via zinc sequestration. *PLoS Pathog*, *10*(10), e1004450.
132. Backert, S, et al. (2008). VirB2 and VirB5 proteins: specialized adhesins in bacterial type-IV secretion systems? *Trends Microbiol*, *16*(9), 409-413.
133. Chang, YW, et al. (2018). *In vivo* Structures of the *Helicobacter pylori cag* Type IV Secretion System. *Cell Rep*, *23*(3), 673-681.
134. Chung, JM, et al. (2019). Structure of the *Helicobacter pylori* Cag type IV secretion system. *Elife*, *8*.
135. Sheedlo, MJ, et al. (2020). Cryo-EM reveals species-specific components within the *Helicobacter pylori* Cag type IV secretion system core complex. *Elife*, *9*.
136. Hu, B, et al. (2019). In Situ Molecular Architecture of the *Helicobacter pylori* Cag Type IV Secretion System. *MBio*, *10*(3).
137. Barrozo, RM, et al. (2013). Functional Plasticity in the Type IV Secretion System of *Helicobacter pylori*. *PLOS Pathogens*, *9*(2), e1003189.
138. Delahay, RM, et al. (2008). The highly repetitive region of the *Helicobacter pylori* CagY protein comprises tandem arrays of an alpha-helical repeat module. *J Mol Biol*, *377*(3), 956-971.
139. Suarez, G, et al. (2017). Genetic Manipulation of *Helicobacter pylori* Virulence Function by Host Carcinogenic Phenotypes. *Cancer Res*, *77*(9), 2401-2412.

140. Sierra, JC, et al. (2019). alpha-Difluoromethylornithine reduces gastric carcinogenesis by causing mutations in *Helicobacter pylori cagY*. *Proc Natl Acad Sci U S A*, *116*(11), 5077-5085.
141. Cover, TL, et al. (1995). Serologic detection of infection with *cagA+ Helicobacter pylori* strains. *J Clin Microbiol*, *33*(6), 1496-1500.
142. Hatakeyama, M. (2004). Oncogenic mechanisms of the *Helicobacter pylori* CagA protein. *Nat Rev Cancer*, *4*(9), 688-694.
143. Stein, M, et al. (2002). c-Src/Lyn kinases activate *Helicobacter pylori* CagA through tyrosine phosphorylation of the EPIYA motifs. *Mol Microbiol*, *43*(4), 971-980.
144. Saadat, I, et al. (2007). *Helicobacter pylori* CagA targets PAR1/MARK kinase to disrupt epithelial cell polarity. *Nature*, *447*(7142), 330-333.
145. Amieva, MR, et al. (2008). Disruption of the epithelial apical-junctional complex by. *Helicobacter pylori*, *2003*(300), 1430-1434. (CagA. Science)
146. Franco, AT, et al. (2008). Regulation of gastric carcinogenesis by *Helicobacter pylori* virulence factors. *Cancer Res*, *68*(2), 379-387.
147. Bagnoli, F, et al. (2005). *Helicobacter pylori* CagA induces a transition from polarized to invasive phenotypes in MDCK cells. *Proc Natl Acad Sci U S A*, *102*(45), 16339-16344.
148. Murata-Kamiya, N, et al. (2007). *Helicobacter pylori* CagA interacts with E-cadherin and deregulates the beta-catenin signal that promotes intestinal transdifferentiation in gastric epithelial cells. *Oncogene*, *26*(32), 4617-4626.
149. Belogolova, E, et al. (2013). *Helicobacter pylori* outer membrane protein HopQ identified as a novel T4SS-associated virulence factor. *Cell Microbiol*, *15*(11), 1896-1912.
150. Sokolova, O, et al. (2013). *Helicobacter pylori* induces type 4 secretion system-dependent, but CagA-independent activation of IkappaBs and NF-kappaB/RelA at early time points. *Int J Med Microbiol*, *303*(8), 548-552.
151. Neumann, M, & Naumann, M. (2007). Beyond IkappaBs: alternative regulation of NF-kappaB activity. *FASEB J*, *21*(11), 2642-2654.
152. Hayakawa, Y, et al. (2013). Differential roles of ASK1 and TAK1 in *Helicobacter pylori*-induced cellular responses. *Infect Immun*, *81*(12), 4551-4560.
153. Sokolova, O, et al. (2014). MEKK3 and TAK1 synergize to activate IKK complex in *Helicobacter pylori* infection. *Biochim Biophys Acta*, *1843*(4), 715-724.
154. Hirata, Y, et al. (2006). MyD88 and TNF receptor-associated factor 6 are critical signal transducers in *Helicobacter pylori*-infected human epithelial cells. *J Immunol*, *176*(6), 3796-3803.
155. Naumann, M, et al. (2017). *Helicobacter pylori*: A Paradigm Pathogen for Subverting Host Cell Signal Transmission. *Trends Microbiol*, *25*(4), 316-328.
156. Milivojevic, M, et al. (2017). ALPK1 controls TIFA/TRAF6-dependent innate immunity against heptose-1,7-bisphosphate of gram-negative bacteria. *PLoS Pathog*, *13*(2), e1006224.
157. Lee, J, et al. (2006). Maintenance of colonic homeostasis by distinctive apical TLR9 signalling in intestinal epithelial cells. *Nat Cell Biol*, *8*(12), 1327-1336.
158. Alvarez-Arellano, L, et al. (2014). TLR9 and NF-kappaB are partially involved in activation of human neutrophils by *Helicobacter pylori* and its purified DNA. *PLoS One*, *9*(7), e101342.

159. Kaparakis, M, et al. (2009). Bacterial membrane vesicles deliver peptidoglycan to NOD1 in epithelial cells. *Cell Microbiol*.
160. Suarez, G, et al. (2019). Nod1 Imprints Inflammatory and Carcinogenic Responses toward the Gastric Pathogen *Helicobacter pylori*. *Cancer Res*, *79*(7), 1600-1611.
161. Philpott, DJ, et al. (2014). NOD proteins: regulators of inflammation in health and disease. *Nat Rev Immunol*, *14*(1), 9-23.
162. Sorbara, MT, et al. (2013). The protein ATG16L1 suppresses inflammatory cytokines induced by the intracellular sensors Nod1 and Nod2 in an autophagy-independent manner. *Immunity*, *39*(5), 858-873.
163. Gresnigt, MS, et al. (2017). The Absence of NOD1 Enhances Killing of Aspergillus fumigatus Through Modulation of Dectin-1 Expression. *Front Immunol*, *8*, 1777.
164. Takahashi, Y, et al. (2006). Up-regulation of NOD1 and NOD2 through TLR4 and TNF-alpha in LPS-treated murine macrophages. *J Vet Med Sci*, *68*(5), 471-478.
165. Juarez, E, et al. (2014). Nucleotide-oligomerizing domain-1 (NOD1) receptor activation induces pro-inflammatory responses and autophagy in human alveolar macrophages. *BMC Pulm Med*, *14*, 152.
166. Watanabe, T, et al. (2010). NOD1 contributes to mouse host defense against *Helicobacter pylori* via induction of type I IFN and activation of the ISGF3 signaling pathway. *J Clin Invest*, *120*(5), 1645-1662.
167. Raju, D, et al. (2012). Vacuolating cytotoxin and variants in Atg16L1 that disrupt autophagy promote *Helicobacter pylori* infection in humans. *Gastroenterology*, *142*(5), 1160-1171.
168. He, JQ, et al. (2007). TRAF3 and its biological function. *Adv Exp Med Biol*, *597*, 48-59.
169. Zarnegar, B, et al. (2008). Control of canonical NF-kappaB activation through the NIK-IKK complex pathway. *Proc Natl Acad Sci U S A*, *105*(9), 3503-3508.
170. Gorrell, RJ, et al. (2013). A novel NOD1- and CagA-independent pathway of interleukin-8 induction mediated by the *Helicobacter pylori* type IV secretion system. *Cell Microbiol*, *15*(4), 554-570.
171. Cover, TL, et al. (1994). Divergence of genetic sequences for the vacuolating cytotoxin among *Helicobacter pylori* strains. *J Biol Chem*, *269*(14), 10566-10573.
172. Cover, TL, & Blanke, SR. (2005). *Helicobacter pylori* VacA, a paradigm for toxin multifunctionality. *Nat Rev Microbiol*, *3*(4), 320-332.
173. Backert, S, & Tegtmeyer, N. (2010). the versatility of the *Helicobacter pylori* vacuolating cytotoxin vacA in signal transduction and molecular crosstalk. *Toxins (Basel)*, *2*(1), 69-92.
174. Argent, RH, et al. (2008). Functional association between the *Helicobacter pylori* virulence factors VacA and CagA. *J Med Microbiol*, *57*(Pt 2), 145-150.
175. Javed, S, et al. (2019). Impact of *Helicobacter pylori* Virulence Factors on the Host Immune Response and Gastric Pathology. *Curr Top Microbiol Immunol*, *421*, 21-52.
176. Alm, RA, et al. (2000). Comparative genomics of *Helicobacter pylori*: analysis of the outer membrane protein families. *Infect Immun*, *68*(7), 4155-4168.
177. Boren, T, et al. (1993). Attachment of *Helicobacter pylori* to human gastric epithelium mediated by blood group antigens. *Science*, *262*(5141), 1892-1895.
178. Ilver, D, et al. (1998). *Helicobacter pylori* adhesin binding fucosylated histo-blood group antigens revealed by retagging. *Science*, *279*(5349), 373-377.

179. Aspholm-Hurtig, M, et al. (2004). Functional adaptation of BabA, the *H. pylori* ABO blood group antigen binding adhesin. *Science*, *305*(5683), 519-522.
180. Benktander, J, et al. (2012). Redefinition of the carbohydrate binding specificity of *Helicobacter pylori* BabA adhesin. *J Biol Chem*, *287*(38), 31712-31724.
181. Backstrom, A, et al. (2004). Metastability of *Helicobacter pylori bab* adhesin genes and dynamics in Lewis b antigen binding. *Proc Natl Acad Sci U S A*, *101*(48), 16923-16928.
182. Solnick, JV, et al. (2004). Modification of *Helicobacter pylori* outer membrane protein expression during experimental infection of rhesus macaques. *Proc Natl Acad Sci U S A*, *101*(7), 2106-2111.
183. Styer, CM, et al. (2010). Expression of the BabA adhesin during experimental infection with *Helicobacter pylori*. *Infect Immun*, *78*(4), 1593-1600.
184. Rad, R, et al. (2002). The *Helicobacter pylori* blood group antigen-binding adhesin facilitates bacterial colonization and augments a nonspecific immune response. *J Immunol*, *168*(6), 3033-3041.
185. Ishijima, N, et al. (2011). BabA-mediated adherence is a potentiator of the *Helicobacter pylori* type IV secretion system activity. *J Biol Chem*, *286*(28), 25256-25264.
186. Gerhard, M, et al. (1999). Clinical relevance of the *Helicobacter pylori* gene for blood-group antigen-binding adhesin. *Proc Natl Acad Sci U S A*, *96*(22), 12778-12783.
187. Matsuo, Y, et al. (2017). *Helicobacter pylori* Outer Membrane Protein-Related Pathogenesis. *Toxins (Basel)*, *9*(3).
188. Javaheri, A, et al. (2016). *Helicobacter pylori* adhesin HopQ engages in a virulence-enhancing interaction with human CEACAMs. *Nat Microbiol*, *2*, 16189.
189. Bonsor, DA, et al. (2018). The *Helicobacter pylori* adhesin protein HopQ exploits the dimer interface of human CEACAMs to facilitate translocation of the oncoprotein CagA. *EMBO J*, *37*(13).
190. Moonens, K, et al. (2018). *Helicobacter pylori* adhesin HopQ disrupts trans dimerization in human CEACAMs. *EMBO J*, *37*(13).
191. Mahdavi, J, et al. (2002). *Helicobacter pylori* SabA adhesin in persistent infection and chronic inflammation. *Science*, *297*(5581), 573-578.
192. Marcos, NT, et al. (2008). *Helicobacter pylori* induces beta3GnT5 in human gastric cell lines, modulating expression of the SabA ligand sialyl-Lewis x. *J Clin Invest*, *118*(6), 2325-2336.
193. Goodwin, AC, et al. (2008). Expression of the *Helicobacter pylori* adhesin SabA is controlled via phase variation and the ArsRS signal transduction system. *Microbiology (Reading)*, *154*(Pt 8), 2231-2240.
194. Sheu, BS, et al. (2006). Interaction between host gastric Sialyl-Lewis X and *H. pylori* SabA enhances *H. pylori* density in patients lacking gastric Lewis B antigen. *Am J Gastroenterol*, *101*(1), 36-44.
195. Talarico, S, et al. (2012). Regulation of *Helicobacter pylori* adherence by gene conversion. *Mol Microbiol*, *84*(6), 1050-1061.
196. Cao, P, & Cover, TL. (2002). Two different families of *hopQ* alleles in *Helicobacter pylori*. *J Clin Microbiol*, *40*(12), 4504-4511.
197. Cao, P, et al. (2005). Analysis of *hopQ* alleles in East Asian and Western strains of *Helicobacter pylori*. *FEMS Microbiol Lett*, *251*(1), 37-43.
198. Loh, JT, et al. (2008). *Helicobacter pylori* HopQ outer membrane protein attenuates bacterial adherence to gastric epithelial cells. *FEMS Microbiol Lett*, *289*(1), 53-58.

199. Dooyema, SDR, et al. (2021). *Helicobacter pylori*-Induced TLR9 Activation and Injury Are Associated With the Virulence-Associated Adhesin HopQ. *J Infect Dis*, *224*(2), 360-365.
200. Koniger, V, et al. (2016). *Helicobacter pylori* exploits human CEACAMs via HopQ for adherence and translocation of CagA. *Nat Microbiol*, *2*, 16188.
201. Zhao, Q, et al. (2018). Integrin but not CEACAM receptors are dispensable for *Helicobacter pylori* CagA translocation. *PLoS Pathog*, *14*(10), e1007359.
202. Tegtmeyer, N, et al. (2019). Expression of CEACAM1 or CEACAM5 in AZ-521 cells restores the type IV secretion deficiency for translocation of CagA by *Helicobacter pylori*. *Cell Microbiol*, *21*(1), e12965.
203. Tegtmeyer, N, et al. (2017). *Helicobacter pylori* Employs a Unique Basolateral Type IV Secretion Mechanism for CagA Delivery. *Cell Host Microbe*, *22*(4), 552-560 e555.
204. Wessler, S, & Backert, S. (2017). A novel basolateral type IV secretion model for the CagA oncoprotein of *Helicobacter pylori*. *Microb Cell*, *5*(1), 60-62.
205. El-Omar, EM, et al. (2000). Interleukin-1 polymorphisms associated with increased risk of gastric cancer. *Nature*, *404*(6776), 398-402.
206. El-Omar, EM, et al. (2003). Increased risk of noncardia gastric cancer associated with proinflammatory cytokine gene polymorphisms. *Gastroenterology*, *124*(5), 1193-1201.
207. Machado, JC, et al. (2001). Interleukin 1B and interleukin 1RN polymorphisms are associated with increased risk of gastric carcinoma. *Gastroenterology*, *121*(4), 823-829.
208. Figueiredo, C, et al. (2002). *Helicobacter pylori* and interleukin 1 genotyping: an opportunity to identify high-risk individuals for gastric carcinoma. *J Natl Cancer Inst*, *94*(22), 1680-1687.
209. Gorouhi, F, et al. (2008). Tumour-necrosis factor-A polymorphisms and gastric cancer risk: a meta-analysis. *Br J Cancer*, *98*(8), 1443-1451.
210. Wang, J, et al. (2012). Association of *IL-6* polymorphisms with gastric cancer risk: evidences from a meta-analysis. *Cytokine*, *59*(1), 176-183.
211. Yin, YW, et al. (2012). Association between interleukin-6 gene -174 G/C polymorphism and the risk of coronary heart disease: a meta-analysis of 20 studies including 9619 cases and 10,919 controls. *Gene*, *503*(1), 25-30.
212. Xue, H, et al. (2012). A meta-analysis of interleukin-8 -251 promoter polymorphism associated with gastric cancer risk. *PLoS One*, *7*(1), e28083.
213. Ni, P, et al. (2012). A meta-analysis of interleukin-10-1082 promoter polymorphism associated with gastric cancer risk. *DNA Cell Biol*, *31*(4), 582-591.
214. Yu, Z, et al. (2013). The interleukin 10 -819C/T polymorphism and cancer risk: a HuGE review and meta-analysis of 73 studies including 15,942 cases and 22,336 controls. *OMICS*, *17*(4), 200-214.
215. Yuzhalin, AE, & Kutikhin, AG. (2012). Interleukin-12: clinical usage and molecular markers of cancer susceptibility. *Growth Factors*, *30*(3), 176-191.
216. Haghshenas, MR, et al. (2009). IL-18 serum level and *IL-18* promoter gene polymorphism in Iranian patients with gastrointestinal cancers. *J Gastroenterol Hepatol*, *24*(6), 1119-1122.
217. Yuzhalin, A. (2011). The role of interleukin DNA polymorphisms in gastric cancer. *Hum Immunol*, *72*(11), 1128-1136.
218. Allison, CC, et al. (2009). *Helicobacter pylori* induces MAPK phosphorylation and AP-1 activation via a NOD1-dependent mechanism. *J Immunol*, *183*(12), 8099-8109.

219. Kupcinskas, J, et al. (2011). Lack of association between gene polymorphisms of Angiotensin converting enzyme, Nod-like receptor 1, Toll-like receptor 4, FAS/FASL and the presence of *Helicobacter pylori*-induced premalignant gastric lesions and gastric cancer in Caucasians. *BMC Med Genet*, *12*, 112.
220. Rosenstiel, P, et al. (2006). Influence of polymorphisms in the NOD1/CARD4 and NOD2/CARD15 genes on the clinical outcome of *Helicobacter pylori* infection. *Cell Microbiol*, *8*(7), 1188-1198.
221. Wang, P, et al. (2012). Association of *NOD1* and *NOD2* genes polymorphisms with *Helicobacter pylori* related gastric cancer in a Chinese population. *World J Gastroenterol*, *18*(17), 2112-2120.
222. Kim, EJ, et al. (2013). Association between genetic polymorphisms of *NOD 1* and *Helicobacter pylori*-induced gastric mucosal inflammation in healthy Korean population. *Helicobacter*, *18*(2), 143-150.
223. Yang, CA, et al. (2013). A frequent Toll-like receptor 1 gene polymorphism affects NK- and T-cell IFN-gamma production and is associated with *Helicobacter pylori*-induced gastric disease. *Helicobacter*, *18*(1), 13-21.
224. Zeng, HM, et al. (2011). Genetic variants of toll-like receptor 2 and 5, *Helicobacter pylori* infection, and risk of gastric cancer and its precursors in a Chinese population. *Cancer Epidemiol Biomarkers Prev*, *20*(12), 2594-2602.
225. Castano-Rodriguez, N, et al. (2013). The role of TLR2, TLR4 and CD14 genetic polymorphisms in gastric carcinogenesis: a case-control study and meta-analysis. *PLoS One*, *8*(4), e60327.
226. de Oliveira, JG, et al. (2013). Profiles of gene polymorphisms in cytokines and Toll-like receptors with higher risk for gastric cancer. *Dig Dis Sci*, *58*(4), 978-988.
227. Hold, GL, et al. (2007). A functional polymorphism of toll-like receptor 4 gene increases risk of gastric carcinoma and its precursors. *Gastroenterology*, *132*(3), 905-912.
228. Huang, L, et al. (2014). Polymorphisms of the *TLR4* gene and risk of gastric cancer. *Gene*, *537*(1), 46-50.
229. Kim, J, et al. (2013). Effects of polymorphisms of innate immunity genes and environmental factors on the risk of noncardia gastric cancer. *Cancer Res Treat*, *45*(4), 313-324.
230. Loganathan, R, et al. (2017). Genetic variants of *TLR4* and *TLR9* are risk factors for chronic *Helicobacter pylori* infection in South Indian Tamils. *Human Immunology*, *78*(2), 216-220.
231. Neish, AS. (2002). The gut microflora and intestinal epithelial cells: a continuing dialogue. *Microbes Infect*, *4*(3), 309-317.
232. Fitzgerald, KA, & Kagan, JC. (2020). Toll-like Receptors and the Control of Immunity. *Cell*, *180*(6), 1044-1066.
233. Cui, J, et al. (2014). Mechanisms and pathways of innate immune activation and regulation in health and cancer. *Hum Vaccin Immunother*, *10*(11), 3270-3285.
234. Motshwene, PG, et al. (2009). An oligomeric signaling platform formed by the Toll-like receptor signal transducers MyD88 and IRAK-4. *J Biol Chem*, *284*(37), 25404-25411.
235. Coussens, LM, & Werb, Z. (2002). Inflammation and cancer. *Nature*, *420*(6917), 860-867.

236. Schmausser, B, et al. (2005). Toll-like receptors TLR4, TLR5 and TLR9 on gastric carcinoma cells: an implication for interaction with *Helicobacter pylori*. *Int J Med Microbiol*, *295*(3), 179-185.
237. Peek, RM, Jr., et al. (2010). Role of innate immunity in *Helicobacter pylori*-induced gastric malignancy. *Physiol Rev*, *90*(3), 831-858.
238. Pachathundikandi, SK, & Backert, S. (2016). Differential Expression of Interleukin 1beta During *Helicobacter pylori* Infection of Toll-like Receptor 2 (TLR2)- and TLR10-Expressing HEK293 Cell Lines. *J Infect Dis*, *214*(1), 166-167.
239. Nagashima, H, et al. (2015). Toll-like Receptor 10 in *Helicobacter pylori* Infection. *J Infect Dis*, *212*(10), 1666-1676.
240. Nogueira, AM, et al. (2004). Lewis antigen expression in gastric mucosa of children: relationship with *Helicobacter pylori* infection. *J Pediatr Gastroenterol Nutr*, *38*(1), 85-91.
241. Kobayashi, K, et al. (1993). Lewis blood group-related antigen expression in normal gastric epithelium, intestinal metaplasia, gastric adenoma, and gastric carcinoma. *Am J Gastroenterol*, *88*(6), 919-924.
242. Monteiro, MA. (2001). *Helicobacter pylori*: a wolf in sheep's clothing: the glycotype families of *Helicobacter pylori* lipopolysaccharides expressing histo-blood groups: structure, biosynthesis, and role in pathogenesis. *Adv Carbohydr Chem Biochem*, *57*, 99-158.
243. Cullen, TW, et al. (2011). *Helicobacter pylori* versus the host: remodeling of the bacterial outer membrane is required for survival in the gastric mucosa. *PLoS Pathog*, *7*(12), e1002454.
244. Perez-Perez, GI, et al. (1995). Activation of human THP-1 cells and rat bone marrow-derived macrophages by *Helicobacter pylori* lipopolysaccharide. *Infect Immun*, *63*(4), 1183-1187.
245. Hajjar, AM, et al. (2002). Human Toll-like receptor 4 recognizes host-specific LPS modifications. *Nat Immunol*, *3*(4), 354-359.
246. King, JD, et al. (2009). Review: Lipopolysaccharide biosynthesis in *Pseudomonas aeruginosa*. *Innate Immun*, *15*(5), 261-312.
247. Li, H, et al. (2016). Lipopolysaccharide structure and biosynthesis in *Helicobacter pylori*. *Helicobacter*.
248. Ogawa, T, et al. (1997). Immunobiological activities of chemically defined lipid A from *Helicobacter pylori* LPS in comparison with *Porphyromonas gingivalis* lipid A and *Escherichia coli*-type synthetic lipid A (compound 506). *Vaccine*, *15*(15), 1598-1605.
249. Su, B, et al. (2003). *Helicobacter pylori* activates Toll-like receptor 4 expression in gastrointestinal epithelial cells. *Infect Immun*, *71*(6), 3496-3502.
250. Backhed, F, et al. (2003). Gastric mucosal recognition of *Helicobacter pylori* is independent of Toll-like receptor 4. *J Infect Dis*, *187*(5), 829-836.
251. Ishihara, S, et al. (2004). Essential role of MD-2 in TLR4-dependent signaling during *Helicobacter pylori*-associated gastritis. *J Immunol*, *173*(2), 1406-1416.
252. Lepper, PM, et al. (2005). Lipopolysaccharides from *Helicobacter pylori* can act as antagonists for Toll-like receptor 4. *Cell Microbiol*, *7*(4), 519-528.
253. Yokota, S, et al. (2010). *Helicobacter pylori* lipopolysaccharides upregulate toll-like receptor 4 expression and proliferation of gastric epithelial cells via the MEK1/2-ERK1/2 mitogen-activated protein kinase pathway. *Infect Immun*, *78*(1), 468-476.

254. Yokota, S, et al. (2007). Highly-purified *Helicobacter pylori* LPS preparations induce weak inflammatory reactions and utilize Toll-like receptor 2 complex but not Toll-like receptor 4 complex. *FEMS Immunol Med Microbiol*, *51*(1), 140-148.
255. Rad, R, et al. (2009). Extracellular and intracellular pattern recognition receptors cooperate in the recognition of *Helicobacter pylori*. *Gastroenterology*, *136*(7), 2247-2257.
256. Panthel, K, et al. (2003). Colonization of C57BL/6J and BALB/c wild-type and knockout mice with *Helicobacter pylori*: effect of vaccination and implications for innate and acquired immunity. *Infect Immun*, *71*(2), 794-800.
257. Amedei, A, et al. (2006). The neutrophil-activating protein of *Helicobacter pylori* promotes Th1 immune responses. *J Clin Invest*, *116*(4), 1092-1101.
258. Zhao, Y, et al. (2007). *Helicobacter pylori* heat-shock protein 60 induces interleukin-8 via a Toll-like receptor (TLR)2 and mitogen-activated protein (MAP) kinase pathway in human monocytes. *J Med Microbiol*, *56*(Pt 2), 154-164.
259. Lindgren, A, et al. (2011). Interferon-gamma secretion is induced in IL-12 stimulated human NK cells by recognition of *Helicobacter pylori* or TLR2 ligands. *Innate Immun*, *17*(2), 191-203.
260. Koch, KN, et al. (2015). *Helicobacter* urease-induced activation of the TLR2/NLRP3/IL-18 axis protects against asthma. *J Clin Invest*, *125*(8), 3297-3302.
261. Smith, KD, et al. (2003). Toll-like receptor 5 recognizes a conserved site on flagellin required for protofilament formation and bacterial motility [10.1038/ni1011]. *Nat Immunol*, *4*(12), 1247-1253.
262. Andersen-Nissen, E, et al. (2005). Evasion of Toll-like receptor 5 by flagellated bacteria. *Proc Natl Acad Sci U S A*, *102*(26), 9247-9252.
263. Gewirtz, AT, et al. (2004). *Helicobacter pylori* flagellin evades toll-like receptor 5-mediated innate immunity. *J Infect Dis*, *189*(10), 1914-1920.
264. Lee, SK, et al. (2003). *Helicobacter pylori* flagellins have very low intrinsic activity to stimulate human gastric epithelial cells via TLR5. *Microbes Infect*, *5*(15), 1345-1356.
265. Schroder, K, & Tschopp, J. (2010). The inflammasomes. *Cell*, *140*(6), 821-832.
266. Kelley, N, et al. (2019). The NLRP3 Inflammasome: An Overview of Mechanisms of Activation and Regulation. *Int J Mol Sci*, *20*(13).
267. Swanson, KV, et al. (2019). The NLRP3 inflammasome: molecular activation and regulation to therapeutics. *Nat Rev Immunol*, *19*(8), 477-489.
268. Pachathundikandi, SK, et al. (2016). Inflammasome Activation by *Helicobacter pylori* and Its Implications for Persistence and Immunity. *Curr Top Microbiol Immunol*, *397*, 117-131.
269. Koch, KN, & Muller, A. (2015). *Helicobacter pylori* activates the TLR2/NLRP3/caspase-1/IL-18 axis to induce regulatory T-cells, establish persistent infection and promote tolerance to allergens. *Gut Microbes*, *6*(6), 382-387.
270. Kim, DJ, et al. (2013). The Cag pathogenicity island and interaction between TLR2/NOD2 and NLRP3 regulate IL-1beta production in *Helicobacter pylori* infected dendritic cells. *Eur J Immunol*, *43*(10), 2650-2658.
271. Semper, RP, et al. (2014). *Helicobacter pylori*-induced IL-1beta secretion in innate immune cells is regulated by the NLRP3 inflammasome and requires the *cag* pathogenicity island. *J Immunol*, *193*(7), 3566-3576.

272. Suarez, G, et al. (2015). Modification of *Helicobacter pylori* peptidoglycan enhances NOD1 activation and promotes cancer of the stomach. *Cancer research*, *75*(8), 1749-1759.
273. Wang, G, et al. (2009). Oxidative stress-induced peptidoglycan deacetylase in *Helicobacter pylori*. *J Biol Chem*, *284*(11), 6790-6800.
274. Wang, G, et al. Peptidoglycan deacetylation in *Helicobacter pylori* contributes to bacterial survival by mitigating host immune responses. *Infect Immun*.
275. Boneca, IG, et al. (2007). A critical role for peptidoglycan N-deacetylation in Listeria evasion from the host innate immune system. *Proc Natl Acad Sci U S A*, *104*(3), 997-1002.
276. Onoguchi, K, et al. (2011). Retinoic acid-inducible gene-I-like receptors. *J Interferon Cytokine Res*, *31*(1), 27-31.
277. Brisse, M, & Ly, H. (2019). Comparative Structure and Function Analysis of the RIG-I-Like Receptors: RIG-I and MDA5. *Front Immunol*, *10*, 1586.
278. Tatsuta, T, et al. (2012). Expression of melanoma differentiation associated gene 5 is increased in human gastric mucosa infected with *Helicobacter pylori*. *J Clin Pathol*, *65*(9), 839-843.
279. Hemmi, H, et al. (2000). A Toll-like receptor recognizes bacterial DNA. *Nature*, *408*(6813), 740-745.
280. Wagner, H. (2008). The sweetness of the DNA backbone drives Toll-like receptor 9. *Curr Opin Immunol*, *20*(4), 396-400.
281. Ohto, U, et al. (2015). Structural basis of CpG and inhibitory DNA recognition by Toll-like receptor 9. *Nature*, *520*(7549), 702-705.
282. Haas, T, et al. (2008). The DNA sugar backbone 2' deoxyribose determines toll-like receptor 9 activation. *Immunity*, *28*(3), 315-323.
283. Barton, GM, et al. (2006). Intracellular localization of Toll-like receptor 9 prevents recognition of self DNA but facilitates access to viral DNA. *Nat Immunol*, *7*(1), 49-56.
284. Mouchess, ML, et al. (2011). Transmembrane mutations in Toll-like receptor 9 bypass the requirement for ectodomain proteolysis and induce fatal inflammation. *Immunity*, *35*(5), 721-732.
285. Sinha, SS, et al. (2016). Complex Negative Regulation of TLR9 by Multiple Proteolytic Cleavage Events. *J Immunol*, *197*(4), 1343-1352.
286. Fukui, R, et al. (2018). Cleavage of Toll-Like Receptor 9 Ectodomain Is Required for *In vivo* Responses to Single Strand DNA. *Front Immunol*, *9*, 1491.
287. Collins, B, & Wilson, IA. (2014). Crystal structure of the C-terminal domain of mouse TLR9. *Proteins*, *82*(10), 2874-2878.
288. Ewald, SE, et al. (2008). The ectodomain of Toll-like receptor 9 is cleaved to generate a functional receptor. *Nature*, *456*(7222), 658-662.
289. Latz, E, et al. (2004). TLR9 signals after translocating from the ER to CpG DNA in the lysosome. *Nat Immunol*, *5*(2), 190-198.
290. Guiducci, C, et al. (2006). Properties regulating the nature of the plasmacytoid dendritic cell response to Toll-like receptor 9 activation. *J Exp Med*, *203*(8), 1999-2008.
291. Honda, K, et al. (2005). IRF-7 is the master regulator of type-I interferon-dependent immune responses. *Nature*, *434*(7034), 772-777.
292. Kim, YM, et al. (2008). UNC93B1 delivers nucleotide-sensing toll-like receptors to endolysosomes. *Nature*, *452*(7184), 234-238.

293. Leifer, CA, et al. (2004). TLR9 is localized in the endoplasmic reticulum prior to stimulation. *J Immunol*, *173*(2), 1179-1183.
294. Akira, S, & Takeda, K. (2004). Toll-like receptor signalling. *Nat Rev Immunol*, *4*(7), 499-511.
295. Sasai, M, et al. (2010). Bifurcation of Toll-like receptor 9 signaling by adaptor protein 3. *Science*, *329*(5998), 1530-1534.
296. Wang, TR, et al. (2014). *Helicobacter pylori* regulates TLR4 and TLR9 during gastric carcinogenesis. *Int J Clin Exp Pathol*, *7*(10), 6950-6955.
297. Schmausser, B, et al. (2004). Expression and subcellular distribution of toll-like receptors TLR4, TLR5 and TLR9 on the gastric epithelium in *Helicobacter pylori* infection. *Clin Exp Immunol*, *136*(3), 521-526.
298. Gupta, RA, & Dubois, RN. (2001). Colorectal cancer prevention and treatment by inhibition of cyclooxygenase-2. *Nat Rev Cancer*, *1*(1), 11-21.
299. Williams, CS, et al. (1997). Aspirin use and potential mechanisms for colorectal cancer prevention. *J Clin Invest*, *100*(6), 1325-1329.
300. Fu, S, et al. (1999). Increased expression and cellular localization of inducible nitric oxide synthase and cyclooxygenase 2 in *Helicobacter pylori* gastritis. *Gastroenterology*, *116*(6), 1319-1329.
301. Ristimaki, A, et al. (1997). Expression of cyclooxygenase-2 in human gastric carcinoma. *Cancer Res*, *57*(7), 1276-1280.
302. Sawaoka, H, et al. (1998). *Helicobacter pylori* infection induces cyclooxygenase-2 expression in human gastric mucosa. *Prostaglandins Leukot Essent Fatty Acids*, *59*(5), 313-316.
303. Sung, JJ, et al. (2000). Cyclooxygenase-2 expression in *Helicobacter pylori*-associated premalignant and malignant gastric lesions. *Am J Pathol*, *157*(3), 729-735.
304. Sierra, JC, et al. (2013). Induction of COX-2 expression by *Helicobacter pylori* is mediated by activation of epidermal growth factor receptor in gastric epithelial cells. *Am J Physiol Gastrointest Liver Physiol*, *305*(2), G196-203.
305. Chang, YJ, et al. (2005). *Helicobacter pylori*-Induced invasion and angiogenesis of gastric cells is mediated by cyclooxygenase-2 induction through TLR2/TLR9 and promoter regulation. *J Immunol*, *175*(12), 8242-8252.
306. Chang, YJ, et al. (2004). Induction of cyclooxygenase-2 overexpression in human gastric epithelial cells by *Helicobacter pylori* involves TLR2/TLR9 and c-Src-dependent nuclear factor-kappaB activation. *Mol Pharmacol*, *66*(6), 1465-1477.
307. Kauppila, JH, et al. (2013). Short DNA sequences and bacterial DNA induce esophageal, gastric, and colorectal cancer cell invasion. *APMIS*, *121*(6), 511-522.
308. Christie, PJ, et al. (2014). Mechanism and structure of the bacterial type IV secretion systems. *Biochim Biophys Acta*, *1843*(8), 1578-1591.
309. Otani, K, et al. (2012). Toll-like receptor 9 signaling has anti-inflammatory effects on the early phase of *Helicobacter pylori*-induced gastritis. *Biochemical and Biophysical Research Communications*, *426*(3), 342-349.
310. Yu, L, & Liu, P. (2021). Cytosolic DNA sensing by cGAS: regulation, function, and human diseases. *Signal Transduct Target Ther*, *6*(1), 170.
311. Ahn, J, & Barber, GN. (2019). STING signaling and host defense against microbial infection. *Exp Mol Med*, *51*(12), 1-10.

312. Kwon, J, & Bakhoum, SF. (2020). The Cytosolic DNA-Sensing cGAS-STING Pathway in Cancer. *Cancer Discov*, *10*(1), 26-39.
313. Hornung, V, et al. (2009). AIM2 recognizes cytosolic dsDNA and forms a caspase-1-activating inflammasome with ASC. *Nature*, *458*(7237), 514-518.
314. Burckstummer, T, et al. (2009). An orthogonal proteomic-genomic screen identifies AIM2 as a cytoplasmic DNA sensor for the inflammasome. *Nat Immunol*, *10*(3), 266-272.
315. Fernandes-Alnemri, T, et al. (2009). AIM2 activates the inflammasome and cell death in response to cytoplasmic DNA. *Nature*, *458*(7237), 509-513.
316. Unterholzner, L, et al. (2010). IFI16 is an innate immune sensor for intracellular DNA. *Nat Immunol*, *11*(11), 997-1004.
317. Ding, Y, et al. (2004). Antitumor activity of IFIX, a novel interferon-inducible HIN-200 gene, in breast cancer. *Oncogene*, *23*(26), 4556-4566.
318. Briggs, JA, et al. (1992). Cloning and expression of the human myeloid cell nuclear differentiation antigen: regulation by interferon alpha. *J Cell Biochem*, *49*(1), 82-92.
319. Takaoka, A, et al. (2007). DAI (DLM-1/ZBP1) is a cytosolic DNA sensor and an activator of innate immune response. *Nature*, *448*(7152), 501-505.
320. Yang, P, et al. (2010). The cytosolic nucleic acid sensor LRRFIP1 mediates the production of type I interferon via a beta-catenin-dependent pathway. *Nat Immunol*, *11*(6), 487-494.
321. Chiu, YH, et al. (2009). RNA polymerase III detects cytosolic DNA and induces type I interferons through the RIG-I pathway. *Cell*, *138*(3), 576-591.
322. Ablasser, A, et al. (2009). RIG-I-dependent sensing of poly(dA:dT) through the induction of an RNA polymerase III-transcribed RNA intermediate. *Nat Immunol*, *10*(10), 1065-1072.
323. Zhang, X, et al. (2011). Cutting edge: Ku70 is a novel cytosolic DNA sensor that induces type III rather than type I IFN. *J Immunol*, *186*(8), 4541-4545.
324. Sui, H, et al. (2017). STING is an essential mediator of the Ku70-mediated production of IFN-lambda1 in response to exogenous DNA. *Sci Signal*, *10*(488).
325. Zhang, Z, et al. (2011). The helicase DDX41 senses intracellular DNA mediated by the adaptor STING in dendritic cells. *Nat Immunol*, *12*(10), 959-965.
326. Kondo, T, et al. (2013). DNA damage sensor MRE11 recognizes cytosolic double-stranded DNA and induces type I interferon by regulating STING trafficking. *Proc Natl Acad Sci U S A*, *110*(8), 2969-2974.
327. Rathinam, VA, & Fitzgerald, KA. (2011). Innate immune sensing of DNA viruses. *Virology*, *411*(2), 153-162.
328. Keating, SE, et al. (2011). Cytosolic DNA sensors regulating type I interferon induction. *Trends Immunol*, *32*(12), 574-581.
329. Sun, L, et al. (2013). Cyclic GMP-AMP synthase is a cytosolic DNA sensor that activates the type I interferon pathway. *Science*, *339*(6121), 786-791.
330. Wu, X, et al. (2014). Molecular evolutionary and structural analysis of the cytosolic DNA sensor cGAS and STING. *Nucleic Acids Res*, *42*(13), 8243-8257.
331. Civril, F, et al. (2013). Structural mechanism of cytosolic DNA sensing by cGAS. *Nature*, *498*(7454), 332-337.

332. Barnett, KC, et al. (2019). Phosphoinositide Interactions Position cGAS at the Plasma Membrane to Ensure Efficient Distinction between Self- and Viral DNA. *Cell*, *176*(6), 1432-1446 e1411.
333. Sun, H, et al. (2021). A Nuclear Export Signal Is Required for cGAS to Sense Cytosolic DNA. *Cell Rep*, *34*(1), 108586.
334. Li, X, et al. (2013). Cyclic GMP-AMP synthase is activated by double-stranded DNA-induced oligomerization. *Immunity*, *39*(6), 1019-1031.
335. Lahaye, X, et al. (2018). NONO Detects the Nuclear HIV Capsid to Promote cGAS-Mediated Innate Immune Activation. *Cell*, *175*(2), 488-501 e422.
336. Zhang, X, et al. (2014). The cytosolic DNA sensor cGAS forms an oligomeric complex with DNA and undergoes switch-like conformational changes in the activation loop. *Cell Rep*, *6*(3), 421-430.
337. Ishikawa, H, et al. (2009). STING regulates intracellular DNA-mediated, type I interferon-dependent innate immunity. *Nature*, *461*(7265), 788-792.
338. Shang, G, et al. (2019). Cryo-EM structures of STING reveal its mechanism of activation by cyclic GMP-AMP. *Nature*, *567*(7748), 389-393.
339. Ergun, SL, et al. (2019). STING Polymer Structure Reveals Mechanisms for Activation, Hyperactivation, and Inhibition. *Cell*, *178*(2), 290-301 e210.
340. Saitoh, T, et al. (2009). Atg9a controls dsDNA-driven dynamic translocation of STING and the innate immune response. *Proc Natl Acad Sci U S A*, *106*(49), 20842-20846.
341. Dobbs, N, et al. (2015). STING Activation by Translocation from the ER Is Associated with Infection and Autoinflammatory Disease. *Cell Host Microbe*, *18*(2), 157-168.
342. Mukai, K, et al. (2016). Activation of STING requires palmitoylation at the Golgi. *Nat Commun*, *7*, 11932.
343. Ergun, SL, & Li, L. (2020). Structural Insights into STING Signaling. *Trends Cell Biol*, *30*(5), 399-407.
344. Zheng, C. (2020). Protein Dynamics in Cytosolic DNA-Sensing Antiviral Innate Immune Signaling Pathways. *Front Immunol*, *11*, 1255.
345. Zhang, C, et al. (2019). Structural basis of STING binding with and phosphorylation by TBK1. *Nature*, *567*(7748), 394-398.
346. Zhao, B, et al. (2019). A conserved PLPLRT/SD motif of STING mediates the recruitment and activation of TBK1. *Nature*, *569*(7758), 718-722.
347. Liu, S, et al. (2015). Phosphorylation of innate immune adaptor proteins MAVS, STING, and TRIF induces IRF3 activation. *Science*, *347*(6227), aaa2630.
348. Tao, J, et al. (2016). cGAS-cGAMP-STING: The three musketeers of cytosolic DNA sensing and signaling. *IUBMB Life*, *68*(11), 858-870.
349. Ivashkiv, LB, & Donlin, LT. (2014). Regulation of type I interferon responses. *Nat Rev Immunol*, *14*(1), 36-49.
350. Abe, T, & Barber, GN. (2014). Cytosolic-DNA-mediated, STING-dependent proinflammatory gene induction necessitates canonical NF-κB activation through TBK1. *J Virol*, *88*(10), 5328-5341.
351. Gui, X, et al. (2019). Autophagy induction via STING trafficking is a primordial function of the cGAS pathway. *Nature*, *567*(7747), 262-266.
352. Song, S, et al. (2017). Decreased expression of STING predicts poor prognosis in patients with gastric cancer. *Sci Rep*, *7*, 39858.

353. Hansen, K, et al. (2014). Listeria monocytogenes induces IFNbeta expression through an IFI16-, cGAS- and STING-dependent pathway. *EMBO J*, *33*(15), 1654-1666.
354. Moretti, J, et al. (2017). STING Senses Microbial Viability to Orchestrate Stress-Mediated Autophagy of the Endoplasmic Reticulum. *Cell*, *171*(4), 809-823 e813.
355. Burdette, DL, et al. (2011). STING is a direct innate immune sensor of cyclic di-GMP. *Nature*, *478*(7370), 515-518.
356. Whiteley, AT, et al. (2019). Bacterial cGAS-like enzymes synthesize diverse nucleotide signals. *Nature*, *567*(7747), 194-199.
357. Archer, KA, et al. (2014). STING-dependent type I IFN production inhibits cell-mediated immunity to Listeria monocytogenes. *PLoS Pathog*, *10*(1), e1003861.
358. Lau, L, et al. (2015). DNA tumor virus oncogenes antagonize the cGAS-STING DNA-sensing pathway. *Science*, *350*(6260), 568-571.
359. Eaglesham, JB, & Kranzusch, PJ. (2020). Conserved strategies for pathogen evasion of cGAS-STING immunity. *Curr Opin Immunol*, *66*, 27-34.
360. Huang, J, et al. (2018). Herpes Simplex Virus 1 Tegument Protein VP22 Abrogates cGAS/STING-Mediated Antiviral Innate Immunity. *J Virol*, *92*(15).
361. Biolatti, M, et al. (2018). Human Cytomegalovirus Tegument Protein pp65 (pUL83) Dampens Type I Interferon Production by Inactivating the DNA Sensor cGAS without Affecting STING. *J Virol*, *92*(6).
362. Zhang, J, et al. (2018). Species-Specific Deamidation of cGAS by Herpes Simplex Virus UL37 Protein Facilitates Viral Replication. *Cell Host Microbe*, *24*(2), 234-248 e235.
363. Huang, ZF, et al. (2018). Human Cytomegalovirus Protein UL31 Inhibits DNA Sensing of cGAS to Mediate Immune Evasion. *Cell Host Microbe*, *24*(1), 69-80 e64.
364. Fu, YZ, et al. (2019). Human cytomegalovirus protein UL42 antagonizes cGAS/MITA-mediated innate antiviral response. *PLoS Pathog*, *15*(5), e1007691.
365. Wu, JJ, et al. (2015). Inhibition of cGAS DNA Sensing by a Herpesvirus Virion Protein. *Cell Host Microbe*, *18*(3), 333-344.
366. Zhang, G, et al. (2016). Cytoplasmic isoforms of Kaposi sarcoma herpesvirus LANA recruit and antagonize the innate immune DNA sensor cGAS. *Proc Natl Acad Sci U S A*, *113*(8), E1034-1043.
367. Kim, JE, et al. (2017). Human Cytomegalovirus IE2 86 kDa Protein Induces STING Degradation and Inhibits cGAMP-Mediated IFN-beta Induction. *Front Microbiol*, *8*, 1854.
368. Yi, G, et al. (2016). Hepatitis C Virus NS4B Can Suppress STING Accumulation To Evade Innate Immune Responses. *J Virol*, *90*(1), 254-265.
369. Sun, L, et al. (2012). Coronavirus papain-like proteases negatively regulate antiviral innate immune response through disruption of STING-mediated signaling. *PLoS One*, *7*(2), e30802.
370. Fu, YZ, et al. (2017). Human Cytomegalovirus Tegument Protein UL82 Inhibits STING-Mediated Signaling to Evade Antiviral Immunity. *Cell Host Microbe*, *21*(2), 231-243.
371. Ma, Z, et al. (2015). Modulation of the cGAS-STING DNA sensing pathway by gammaherpesviruses. *Proc Natl Acad Sci U S A*, *112*(31), E4306-4315.
372. Li, K, et al. (2019). Avian oncogenic herpesvirus antagonizes the cGAS-STING DNA-sensing pathway to mediate immune evasion. *PLoS Pathog*, *15*(9), e1007999.
373. Christensen, MH, et al. (2016). HSV-1 ICP27 targets the TBK1-activated STING signalsome to inhibit virus-induced type I IFN expression. *EMBO J*, *35*(13), 1385-1399.

374. Eaglesham, JB, et al. (2019). Viral and metazoan poxins are cGAMP-specific nucleases that restrict cGAS-STING signalling. *Nature*, *566*(7743), 259-263.
375. Dey, RJ, et al. (2017). Inhibition of innate immune cytosolic surveillance by an M. tuberculosis phosphodiesterase. *Nat Chem Biol*, *13*(2), 210-217.
376. Li, A, et al. (2019). Activating cGAS-STING pathway for the optimal effect of cancer immunotherapy. *J Hematol Oncol*, *12*(1), 35.
377. Dou, Z, et al. (2017). Cytoplasmic chromatin triggers inflammation in senescence and cancer. *Nature*, *550*(7676), 402-406.
378. Fuertes, MB, et al. (2013). Type I interferon response and innate immune sensing of cancer. *Trends Immunol*, *34*(2), 67-73.
379. Khoo, LT, & Chen, LY. (2018). Role of the cGAS-STING pathway in cancer development and oncotherapeutic approaches. *EMBO Rep*, *19*(12).
380. Vanpouille-Box, C, et al. (2018). Cytosolic DNA Sensing in Organismal Tumor Control. *Cancer Cell*, *34*(3), 361-378.
381. Hsu, YA, et al. (2016). The anti-proliferative effects of type I IFN involve STAT6-mediated regulation of SP1 and BCL6. *Cancer Lett*, *375*(2), 303-312.
382. Xia, T, et al. (2016). Recurrent Loss of STING Signaling in Melanoma Correlates with Susceptibility to Viral Oncolysis. *Cancer Res*, *76*(22), 6747-6759.
383. Xia, T, et al. (2016). Deregulation of STING Signaling in Colorectal Carcinoma Constrains DNA Damage Responses and Correlates With Tumorigenesis. *Cell Rep*, *14*(2), 282-297.
384. Konno, H, et al. (2018). Suppression of STING signaling through epigenetic silencing and missense mutation impedes DNA damage mediated cytokine production. *Oncogene*, *37*(15), 2037-2051.
385. Takashima, K, et al. (2016). STING in tumor and host cells cooperatively work for NK cell-mediated tumor growth retardation. *Biochem Biophys Res Commun*, *478*(4), 1764-1771.
386. Ho, SS, et al. (2016). The DNA Structure-Specific Endonuclease MUS81 Mediates DNA Sensor STING-Dependent Host Rejection of Prostate Cancer Cells. *Immunity*, *44*(5), 1177-1189.
387. Yang, H, et al. (2017). cGAS is essential for cellular senescence. *Proc Natl Acad Sci U S A*, *114*(23), E4612-E4620.
388. Zhao, Q, et al. (2019). STING signalling protects against chronic pancreatitis by modulating Th17 response. *Gut*, *68*(10), 1827-1837.
389. Chen, X, et al. (2019). IL-17R-EGFR axis links wound healing to tumorigenesis in Lrig1(+) stem cells. *J Exp Med*, *216*(1), 195-214.
390. Lotti, F, et al. (2013). Chemotherapy activates cancer-associated fibroblasts to maintain colorectal cancer-initiating cells by IL-17A. *J Exp Med*, *210*(13), 2851-2872.
391. Zhang, Y, et al. (2018). Immune Cell Production of Interleukin 17 Induces Stem Cell Features of Pancreatic Intraepithelial Neoplasia Cells. *Gastroenterology*, *155*(1), 210-223 e213.
392. Shiomi, S, et al. (2008). IL-17 is involved in *Helicobacter pylori*-induced gastric inflammatory responses in a mouse model. *Helicobacter*, *13*(6), 518-524.
393. Dixon, B, et al. (2019). Th17 Cells in *Helicobacter pylori* Infection: a Dichotomy of Help and Harm. *Infect Immun*, *87*(11).

394. Kim, JY, et al. (2017). Cytokine expression associated with *Helicobacter pylori* and Epstein-Barr virus infection in gastric carcinogenesis. *APMIS*, *125*(9), 808-815.
395. Wang, Y, et al. (2014). Interleukin 17A promotes gastric cancer invasiveness via NF-kappaB mediated matrix metalloproteinases 2 and 9 expression. *PLoS One*, *9*(6), e96678.
396. Arisawa, T, et al. (2007). Genetic polymorphisms of molecules associated with inflammation and immune response in Japanese subjects with functional dyspepsia. *Int J Mol Med*, *20*(5), 717-723.
397. Kimang'a, A, et al. (2010). IL-17A and IL-17F gene expression is strongly induced in the mucosa of *H. pylori*-infected subjects from Kenya and Germany. *Scand J Immunol*, *72*(6), 522-528.
398. Miao, L, et al. (2020). Targeting the STING pathway in tumor-associated macrophages regulates innate immune sensing of gastric cancer cells. *Theranostics*, *10*(2), 498-515.
399. Yang, KS, et al. (2021). Identification and validation of the prognostic value of cyclic GMP-AMP synthase-stimulator of interferon (cGAS-STING) related genes in gastric cancer. *Bioengineered*, *12*(1), 1238-1250.
400. Hong, S, et al. (2020). Radiation therapy enhanced therapeutic efficacy of anti-PD1 against gastric cancer. *J Radiat Res*, *61*(6), 851-859.
401. Peek, RM, Jr., et al. (2000). Quantitative detection of *Helicobacter pylori* gene expression *in vivo* and relationship to gastric pathology. *Infect Immun*, *68*(10), 5488-5495.
402. Loh, JT, et al. (2018). High-Salt Conditions Alter Transcription of *Helicobacter pylori* Genes Encoding Outer Membrane Proteins. *Infect Immun*, *86*(3).
403. Yokoyama, K, et al. (2005). Functional antagonism between *Helicobacter pylori* CagA and vacuolating toxin VacA in control of the NFAT signaling pathway in gastric epithelial cells. *Proc Natl Acad Sci U S A*, *102*(27), 9661-9666.
404. Loganathan, R, et al. (2017). Genetic variants of TLR4 and TLR9 are risk factors for chronic *Helicobacter pylori* infection in South Indian Tamils. *Hum Immunol*, *78*(2), 216-220.
405. Qin, XR, et al. (2019). DNA promotes cellular proliferation, migration, and invasion of gastric cancer by activating toll-like receptor 9. *Saudi J Gastroenterol*, *25*(3), 181-187.
406. Varga, MG, et al. (2016). TLR9 activation suppresses inflammation in response to. *Helicobacter pylori. infection*. (American Journal of Physiology-Gastrointestinal and Liver Physiology)
407. Chow, J, et al. (2011). Pathobionts of the gastrointestinal microbiota and inflammatory disease. *Curr Opin Immunol*, *23*(4), 473-480.
408. Schumacher, MA, et al. (2012). Gastric Sonic Hedgehog acts as a macrophage chemoattractant during the immune response to *Helicobacter pylori*. *Gastroenterology*, *142*(5), 1150-1159 e1156.
409. Salama, N, et al. (2000). A whole-genome microarray reveals genetic diversity among *Helicobacter pylori* strains. *Proc Natl Acad Sci U S A*, *97*(26), 14668-14673.
410. Parsonnet, J, et al. (1997). Risk for gastric cancer in people with CagA positive or CagA negative *Helicobacter pylori* infection [see comments]. *Gut*, *40*(3), 297-301.
411. Tammer, I, et al. (2007). Activation of Abl by *Helicobacter pylori*: a novel kinase for CagA and crucial mediator of host cell scattering. *Gastroenterology*, *132*(4), 1309-1319.
412. Balka, KR, et al. (2020). TBK1 and IKKε Act Redundantly to Mediate STING-Induced NF-κB Responses in Myeloid Cells. *Cell Rep*, *31*(1), 107492.

413. Bertaux-Skeirik, N, et al. (2015). CD44 plays a functional role in *Helicobacter pylori*-induced epithelial cell proliferation. *PLoS Pathog*, *11*(2), e1004663.
414. Franco, AT, et al. (2005). Activation of beta-catenin by carcinogenic *Helicobacter pylori*. *Proc Natl Acad Sci U S A*, *102*(30), 10646-10651.
415. Kashyap, D, et al. (2020). Oral rinses in growth inhibition and treatment of *Helicobacter pylori* infection. *BMC Microbiol*, *20*(1), 45.
416. Leal, MF, et al. (2014). Deregulated expression of Nucleophosmin 1 in gastric cancer and its clinicopathological implications. *BMC Gastroenterol*, *14*, 9.
417. Holokai, L, et al. (2019). Increased Programmed Death-Ligand 1 is an Early Epithelial Cell Response to *Helicobacter pylori* Infection. *PLoS Pathog*, *15*(1), e1007468.
418. Wroblewski, LE, et al. (2019). Targeted mobilization of Lrig1. *Proc Natl Acad Sci U S A*, *116*(39), 19652-19658.
419. Teal, E, et al. (2018). Establishment of Human- and Mouse-Derived Gastric Primary Epithelial Cell Monolayers from Organoids. *Methods Mol Biol*, *1817*, 145-155.
420. Robinson, MD, et al. (2010). edgeR: a Bioconductor package for differential expression analysis of digital gene expression data. *Bioinformatics*, *26*(1), 139-140.
421. McCarthy, DJ, et al. (2012). Differential expression analysis of multifactor RNA-Seq experiments with respect to biological variation. *Nucleic Acids Res*, *40*(10), 4288-4297.
422. Barker, N, et al. (2010). Lgr5(+ve) stem cells drive self-renewal in the stomach and build long-lived gastric units *in vitro*. *Cell Stem Cell*, *6*(1), 25-36.
423. Schlaermann, P, et al. (2016). A novel human gastric primary cell culture system for modelling *Helicobacter pylori* infection *in vitro*. *Gut*, *65*(2), 202-213.
424. Yamashiro, LH, et al. (2020). Interferon-independent STING signaling promotes resistance to HSV-1 *in vivo*. *Nat Commun*, *11*(1), 3382.
425. Halder, P, et al. (2015). The secreted antigen, HP0175, of *Helicobacter pylori* links the unfolded protein response (UPR) to autophagy in gastric epithelial cells. *Cell Microbiol*, *17*(5), 714-729.
426. Terebiznik, MR, et al. (2009). Effect of *Helicobacter pylori*'s vacuolating cytotoxin on the autophagy pathway in gastric epithelial cells. *Autophagy*, *5*(3), 370-379.
427. Dixon, MF, et al. (1996). Classification and grading of gastritis. The updated Sydney System. International Workshop on the Histopathology of Gastritis, Houston 1994. *Am J Surg Pathol*, *20*(10), 1161-1181.
428. Algood, HM, et al. (2009). Regulation of gastric B cell recruitment is dependent on IL-17 receptor A signaling in a model of chronic bacterial infection. *J Immunol*, *183*(9), 5837-5846.
429. Mizuno, T, et al. (2005). Interleukin-17 levels in *Helicobacter pylori*-infected gastric mucosa and pathologic sequelae of colonization. *World J Gastroenterol*, *11*(40), 6305-6311.
430. Di Rienzo, M, et al. (2020). TRIM proteins in autophagy: selective sensors in cell damage and innate immune responses. *Cell Death Differ*, *27*(3), 887-902.
431. Tocchini, C, & Ciosk, R. (2015). TRIM-NHL proteins in development and disease. *Semin Cell Dev Biol*, *47-48*, 52-59.
432. Yang, W, et al. (2020). To TRIM the Immunity: From Innate to Adaptive Immunity. *Front Immunol*, *11*, 02157.

433. Lu, M, et al. (2019). E3 ubiquitin ligase tripartite motif 7 positively regulates the TLR4-mediated immune response via its E3 ligase domain in macrophages. *Mol Immunol*, *109*, 126-133.
434. Shen, Y, et al. (2021). Riok3 inhibits the antiviral immune response by facilitating TRIM40-mediated RIG-I and MDA5 degradation. *Cell Rep*, *35*(12), 109272.
435. Wang, Y, et al. (2015). TRIM30α Is a Negative-Feedback Regulator of the Intracellular DNA and DNA Virus-Triggered Response by Targeting STING. *PLoS Pathog*, *11*(6), e1005012.
436. Shi, M, et al. (2008). TRIM30 alpha negatively regulates TLR-mediated NF-kappa B activation by targeting TAB2 and TAB3 for degradation. *Nat Immunol*, *9*(4), 369-377.
437. Lee, JJ, et al. (2021). HMGB1 orchestrates STING-mediated senescence via TRIM30α modulation in cancer cells. *Cell Death Discov*, *7*(1), 28.
438. Li, Q, et al. (2018). TRIM29 negatively controls antiviral immune response through targeting STING for degradation. *Cell Discov*, *4*, 13.
439. Qiu, F, et al. (2015). *TRIM29* functions as an oncogene in gastric cancer and is regulated by miR-185. *Int J Clin Exp Pathol*, *8*(5), 5053-5061.
440. Zhao, MX, et al. (2012). Predicative value of expression of TrkB and TRIM29 in biopsy tissues from preoperative gastroscopy in lymph node metastasis of gastric cancer. *Zhonghua Yi Xue Za Zhi*, *92*(6), 376-379.
441. Guo, M, et al. (2021). TRIM10 binds to IFN-alpha/beta receptor 1 to negatively regulate type I IFN signal transduction. *Eur J Immunol*, *51*(7), 1762-1773.
442. Lin, Y, et al. (2021). Global Patterns and Trends in Gastric Cancer Incidence Rates (1988-2012) and Predictions to 2030. *Gastroenterology*, *161*(1), 116-127 e118.
443. Graham, DY, & Liou, JM. (2021). Primer for Development of Guidelines for *Helicobacter pylori* Therapy Using Antimicrobial Stewardship. *Clin Gastroenterol Hepatol*.
444. Taxauer, K, et al. (2021). Engagement of CEACAM1 by *Helicobacter pylori* HopQ Is Important for the Activation of Non-Canonical NF-kappaB in Gastric Epithelial Cells. *Microorganisms*, *9*(8).
445. Lin, AS, et al. (2020). Bacterial Energetic Requirements for *Helicobacter pylori* Cag Type IV Secretion System-Dependent Alterations in Gastric Epithelial Cells. *Infect Immun*, *88*(2).
446. Fischer, W, et al. (2001). Systematic mutagenesis of the *Helicobacter pylori cag* pathogenicity island: essential genes for CagA translocation in host cells and induction of interleukin-8. *Mol Microbiol*, *42*(5), 1337-1348.
447. Terradot, L, & Waksman, G. (2011). Architecture of the *Helicobacter pylori* Cag-type IV secretion system. *FEBS J*, *278*(8), 1213-1222.
448. Jurik, A, et al. (2010). The coupling protein Cagbeta and its interaction partner CagZ are required for type IV secretion of the *Helicobacter pylori* CagA protein. *Infect Immun*, *78*(12), 5244-5251.
449. Cascales, E, & Christie, PJ. (2004). Definition of a bacterial type IV secretion pathway for a DNA substrate. *Science*, *304*(5674), 1170-1173.
450. Christie, PJ, et al. (2017). Biological Diversity and Evolution of Type IV Secretion Systems. *Curr Top Microbiol Immunol*, *413*, 1-30.
451. Redzej, A, et al. (2017). Structure of a VirD4 coupling protein bound to a VirB type IV secretion machinery. *EMBO J*, *36*(20), 3080-3095.

452. Waksman, G. (2019). From conjugation to T4S systems in Gram-negative bacteria: a mechanistic biology perspective. *EMBO Rep*, *20*(2).
453. Grohmann, E, et al. (2018). Type IV secretion in Gram-negative and Gram-positive bacteria. *Mol Microbiol*, *107*(4), 455-471.
454. Shaffer, CL, et al. (2011). *Helicobacter pylori* Exploits a Unique Repertoire of Type IV Secretion System Components for Pilus Assembly at the Bacteria-Host Cell Interface. *PLOS Pathogens*, *7*(9), e1002237.
455. Johnson, EM, et al. (2014). Genes required for assembly of pili associated with the *Helicobacter pylori cag* type IV secretion system. *Infect Immun*, *82*(8), 3457-3470.
456. Rohrer, S, et al. (2012). Multiple pathways of plasmid DNA transfer in *Helicobacter pylori*. *PLoS One*, *7*(9), e45623.
457. Cendron, L, et al. (2004). Crystal structure of CagZ, a protein from the *Helicobacter pylori* pathogenicity island that encodes for a type IV secretion system. *J Mol Biol*, *340*(4), 881-889.
458. Bijlsma, JJ, et al. (1999). Identification of virulence genes of *Helicobacter pylori* by random insertion mutagenesis. *Infect Immun*, *67*(5), 2433-2440.
459. Linz, B, et al. (2014). A mutation burst during the acute phase of *Helicobacter pylori* infection in humans and rhesus macaques. *Nat Commun*, *5*, 4165.
460. Vallese, F, et al. (2015). The crystal structure of *Helicobacter pylori* HP1029 highlights the functional diversity of the sialic acid-related DUF386 family. *FEBS J*, *282*(17), 3311-3322.
461. Teplyakov, A, et al. (2005). Crystal structure of the bacterial YhcH protein indicates a role in sialic acid catabolism. *J Bacteriol*, *187*(16), 5520-5527.
462. McClain, MS, et al. (2020). Lipoprotein Processing and Sorting in *Helicobacter pylori*. *MBio*, *11*(3).
463. van Gent, M, et al. (2018). TRIM Proteins and Their Roles in Antiviral Host Defenses. *Annu Rev Virol*, *5*(1), 385-405.
464. Giraldo, MI, et al. (2020). TRIM Proteins in Host Defense and Viral Pathogenesis. *Curr Clin Microbiol Rep*, 1-14.
465. Davila-Collado, R, et al. (2020). Epstein-Barr Virus and *Helicobacter pylori* Co-Infection in Non-Malignant Gastroduodenal Disorders. *Pathogens*, *9*(2).
466. Martinez-Lopez, JL, et al. (2014). Evidence of Epstein-Barr virus association with gastric cancer and non-atrophic gastritis. *Viruses*, *6*(1), 301-318.
467. Zong, L, & Seto, Y. (2014). CpG island methylator phenotype, *Helicobacter pylori*, Epstein-Barr virus, and microsatellite instability and prognosis in gastric cancer: a systematic review and meta-analysis. *PLoS One*, *9*(1), e86097.
468. Xing, J, et al. (2017). TRIM29 promotes DNA virus infections by inhibiting innate immune response. *Nat Commun*, *8*(1), 945.
469. Higgs, R, et al. (2008). The E3 ubiquitin ligase Ro52 negatively regulates IFN-beta production post-pathogen recognition by polyubiquitin-mediated degradation of IRF3. *J Immunol*, *181*(3), 1780-1786.
470. Higgs, R, et al. (2010). Self protection from anti-viral responses--Ro52 promotes degradation of the transcription factor IRF7 downstream of the viral Toll-Like receptors. *PLoS One*, *5*(7), e11776.
471. Zhang, Z, et al. (2013). The E3 ubiquitin ligase TRIM21 negatively regulates the innate immune response to intracellular double-stranded DNA. *Nat Immunol*, *14*(2), 172-178.

472. Zhang, J, et al. (2012). TRIM32 protein modulates type I interferon induction and cellular antiviral response by targeting MITA/STING protein for K63-linked ubiquitination. *J Biol Chem*, *287*(34), 28646-28655.
473. Tsuchida, T, et al. (2010). The ubiquitin ligase TRIM56 regulates innate immune responses to intracellular double-stranded DNA. *Immunity*, *33*(5), 765-776.
474. Hu, Y, et al. (2010). Tripartite-motif protein 30 negatively regulates NLRP3 inflammasome activation by modulating reactive oxygen species production. *J Immunol*, *185*(12), 7699-7705.
475. Liu, X, et al. (2020). TRIM58 suppresses the tumor growth in gastric cancer by inactivation of beta-catenin signaling via ubiquitination. *Cancer Biol Ther*, *21*(3), 203-212.
476. Eyking, A, et al. (2019). TRIM58 Restrains Intestinal Mucosal Inflammation by Negatively Regulating TLR2 in Myeloid Cells. *J Immunol*, *203*(6), 1636-1649.
477. Chen, W, et al. (2018). TRIM15 Exerts Anti-Tumor Effects Through Suppressing Cancer Cell Invasion in Gastric Adenocarcinoma. *Med Sci Monit*, *24*, 8033-8041.
478. Zhou, W, et al. (2021). High Expression of TRIM15 Is Associated with Tumor Invasion and Predicts Poor Prognosis in Patients with Gastric Cancer. *J Invest Surg*, *34*(8), 853-861.
479. Zhang, L, et al. (2021). Knockdown of TRIM15 inhibits the proliferation, migration and invasion of esophageal squamous cell carcinoma cells through inactivation of the Wnt/beta-catenin signaling pathway. *J Bioenerg Biomembr*, *53*(2), 213-222.
480. Lascano, J, et al. (2016). TRIM5 Retroviral Restriction Activity Correlates with the Ability To Induce Innate Immune Signaling. *J Virol*, *90*(1), 308-316.
481. Chang, TH, et al. (2015). Tripartite Motif (TRIM) 12c, a Mouse Homolog of TRIM5, Is a Ubiquitin Ligase That Stimulates Type I IFN and NF-kappaB Pathways along with TNFR-Associated Factor 6. *J Immunol*, *195*(11), 5367-5379.
482. Han, QY, et al. (2015). Circulating E3 ligases are novel and sensitive biomarkers for diagnosis of acute myocardial infarction. *Clin Sci (Lond)*, *128*(11), 751-760.
483. Fu, H, et al. (2018). Exosomal TRIM3 is a novel marker and therapy target for gastric cancer. *J Exp Clin Cancer Res*, *37*(1), 162.
484. Farhadi, J, et al. (2021). Decreased expression of TRIM3 gene predicts a poor prognosis in gastric cancer. *J Gastrointest Cancer*.
485. Lan, Q, et al. (2021). TRIM11 Promotes Proliferation, Migration, Invasion and EMT of Gastric Cancer by Activating beta-Catenin Signaling. *Onco Targets Ther*, *14*, 1429-1440.
486. Wang, F, et al. (2018). TRIM14 promotes the migration and invasion of gastric cancer by regulating epithelialtomesenchymal transition via activation of AKT signaling regulated by miR1955p. *Oncol Rep*, *40*(6), 3273-3284.
487. Xiao, F, et al. (2020). Trim14 promotes autophagy and chemotherapy resistance of gastric cancer cells by regulating AMPK/mTOR pathway. *Drug Dev Res*, *81*(5), 544-550.
488. Yao, Y, et al. (2018). Elevated TRIM23 expression predicts poor prognosis in Chinese gastric cancer. *Pathol Res Pract*, *214*(12), 2062-2068.
489. Fang, Z, et al. (2017). TRIM24 promotes the aggression of gastric cancer via the Wnt/beta-catenin signaling pathway. *Oncol Lett*, *13*(3), 1797-1806.
490. Zhu, Z, et al. (2016). TRIM25 blockade by RNA interference inhibited migration and invasion of gastric cancer cells through TGF-beta signaling. *Sci Rep*, *6*, 19070.

491. Gack, MU, et al. (2007). TRIM25 RING-finger E3 ubiquitin ligase is essential for RIG-I-mediated antiviral activity. *Nature*, *446*(7138), 916-920.
492. Sugiura, T. (2011). The cellular level of TRIM31, an RBCC protein overexpressed in gastric cancer, is regulated by multiple mechanisms including the ubiquitin-proteasome system. *Cell Biol Int*, *35*(7), 657-661.
493. Sugiura, T, & Miyamoto, K. (2008). Characterization of TRIM31, upregulated in gastric adenocarcinoma, as a novel RBCC protein. *J Cell Biochem*, *105*(4), 1081-1091.
494. Wang, C, et al. (2018). TRIM32 promotes cell proliferation and invasion by activating beta-catenin signalling in gastric cancer. *J Cell Mol Med*, *22*(10), 5020-5028.
495. Man, Z, et al. (2019). High expression of TRIM36 is associated with radiosensitivity in gastric cancer. *Oncol Lett*, *17*(5), 4401-4408.
496. Chen, D, et al. (2018). TRIM37 promotes cell invasion and metastasis by regulating SIP1-mediated epithelial-mesenchymal transition in gastric cancer. *Onco Targets Ther*, *11*, 8803-8813.
497. Zhu, H, et al. (2020). Knockdown of TRIM37 Promotes Apoptosis and Suppresses Tumor Growth in Gastric Cancer by Inactivation of the ERK1/2 Pathway. *Onco Targets Ther*, *13*, 5479-5491.
498. Kashimoto, K, et al. (2012). Overexpression of TRIM44 contributes to malignant outcome in gastric carcinoma. *Cancer Sci*, *103*(11), 2021-2026.
499. Xia, Y, et al. (2021). Trim47 overexpression correlates with poor prognosis in gastric cancer. *Neoplasma*, *68*(2), 307-316.
500. Zhou, Z, et al. (2014). TRIM59 is up-regulated in gastric tumors, promoting ubiquitination and degradation of p53. *Gastroenterology*, *147*(5), 1043-1054.